DEVELOPMENT AND EVALUATION OF HIGH-PERFORMANCE RULE-BASED SEQUENCES OF OPERATION FOR VARIABLE AIR VOLUME SYSTEMS

A Dissertation

by

XING LU

Submitted to the Graduate and Professional School of
Texas A&M University
In partial fulfillment of the requirements for the degree of

DOCTOR OF PHILOSOPHY

Chair of Committee,	Zheng O'Neill
Committee Members,	Bryan Rasmussen
	Charles Culp
	David Claridge
Head of Department,	Guillermo Aguilar

May 2022

Major Subject: Mechanical Engineering

ABSTRACT

Commercial buildings account for 35 percent of electricity consumption in the U.S., of which 30 percent is used by the heating, ventilation, and air conditioning (HVAC) system. Despite the significant role of the HVAC control systems in energy efficiency, its design, commissioning, and retrofit have long been an intricate and complicated issue, considering that only diffuse and fragmented information on system operation is available for decision making in most of the scenarios. Due to this limitation, designers and control contractors can only rely on ad-hoc control sequences for system operation in practice, which is one of the major reasons why buildings are operated sub-optimally. To provide standardized and high-performance rule-based HVAC control sequences, the American Society of Heating, Refrigerating and Air-Conditioning Engineers (ASHRAE) has developed the Guideline 36 (GDL36) High Performance Sequences of Operation (SOO) for HVAC Systems to maximize energy efficiency. Although GDL36 was considered the most advanced rule-based HVAC control sequences in this era, most of the proposed controls are still under development and its actual performance remains largely unknown. Up till now, only a few field studies have been conducted to verify the overall effectiveness of GDL36 after its publication, and these studies only focused on the energy saving potential. There is a practical need to benchmark the SOO in GDL36 in different aspects.

To address these gaps, this research aims at enhancing the existing standardized high-performance control sequences (GDL36) by conducting a comprehensive evaluation in terms of energy efficiency, fault robustness, ventilation performance, and grid ancillary service compatibility. The target HVAC systems in this research are multi-zone variable air volume

(VAV) systems, which are one of the most popular HVAC system configurations in U.S. commercial buildings.

First, a Modelica model of a five-zone VAV system that follows both airside and waterside SOO was developed and verified. This building model serves as the virtual testbed for the following intelligent controller evaluation and comprehensive fault impact analysis.

Second, the energy saving potential of the high-performance rule-based controls was compared with that of the state-of-the-art intelligent controls (deep reinforcement learning (DRL)-based control (DRLC) and optimization-based control (OBC)) in two typical cooling weeks. Two supervisory control loops in the airside GDL36 SOO (e.g., supply air temperature and duct static pressure) were replaced by DRL and OBC controller. The results show that the GDL36 has a comparable energy performance (within a 3% deviation) with DRLC in scenarios under both high and mild cooling loads. GDL36 also has a comparable energy performance (within a 3% deviation) with OBC in scenarios with high cooling load, but it consumed 7% more energy in the shoulder week. In terms of thermal comfort, the GDL36 was found to have slightly more zone air temperature violation in all scenarios compared to the other two intelligent controllers (i.e., DRLC and OBC).

Third, a comprehensive fault impact analysis of the GDL36 was conducted to assess its fault robustness. How these sequences handle and adapt to various types of common faults was evaluated through a large-scale fault simulation. The results show that a vast majority (~90%) of fault scenarios have a fault impact ratio (FIR) of less than 6% for energy consumption and energy cost. Besides, the results of FIR distributions also indicate that GDL36 SOO only has limited influence on key performance indexes (KPIs) such as the supply air temperature control quality, thermal comfort, ventilation performance, and peak power load.

Fourth, considering that the HVAC system configuration of multiple zone VAV systems with multiple recirculation paths has long been neglected in literature, a CO_2-based demand control ventilation (DCV) was developed and quantitatively investigated in this study in terms of energy and ventilation performance. The proposed DCV control sequences were tested in four typical ASHRAE climate zones and proved to achieve considerable energy savings while maintaining an acceptable indoor air quality compliant with ASHRAE Standard 62.1.

Lastly, an experimentally validated frequency regulation (FR) control scheme was integrated with the GDL36 SOO for air handling unit (AHU) fans from the perspective of the building providing ancillary service in the future. The impacts on the energy efficiency and thermal comfort were assessed and potential control conflict was identified when the VAV system provides frequency regulation using the GDL36 SOO.

In summary, this dissertation developed a Modelica-based virtual testbed and evaluated the GDL36 SOO for multi-zone VAV systems in a holistic view. For energy efficiency, the GDL36 SOO achieved a comparable performance in terms of energy efficiency and thermal comfort with two intelligent supervisory controls in both high and mild cooling load conditions. For the fault robustness, it demonstrated that there were only minor fault impacts over different KPIs for the system with GDL36 SOO through a large fault simulation. From the ventilation aspect, the proposed DCV SOO for multi-zone recirculating path systems showed its energy efficiency and ventilation compliance and could be readily merged into GDL36. Lastly, when the AHU fan provides the FR service, the FR control could be integrated with GDL36 SOO with limited impacts on the HVAC system. Following prerequisites need to be met. First, the time-varying FR capacity must be correctly estimated. Second, an anti-saturation control scheme needs to be developed to avoid the fan power surge and ensure a smooth transition to post-FR operation.

DEDICATION

This dissertation is dedicated to my parent and sister, whose love, encouragement, support, and sacrifice made it possible for me to complete this degree.

ACKNOWLEDGEMENTS

I would like to express my deep gratitude to my advisor Prof. Zheng O'Neill for her consistent help and inspiration along this journey. I am so lucky to be her student. She is always kind, warmhearted, and insightful. Her rigorous attitude towards research and easygoing personality will impact my future endeavors. I would like to recognize and extend appreciation to the rest of my dissertation committee: Prof. Bryan Rasmussen, Prof. Charles Culp, Prof. David Claridge, and Dr. Veronica Adetola, for their insightful comments, which bring my research to the current depth.

I would like to thank all the collaborators for providing support, data, help, and advice for my work. They include Dr. Yangyang Fu from Texas A&M University, Dr. Wen Jin from Drexel University, Ojas Pradhan from Drexel University, Dr. Teresa Wu from Arizona University, and Dr. Xiaohui (Joe) Zhou from SlipStream. This dissertation is partially supported by National Science Foundation under Award No. IIS- 2050509 and by ASHRAE (The American Society of Heating, Refrigerating and Air-Conditioning Engineers) under RP-1819.

I would also like to thank all of the former and current students in Building Energy and HVAC & R Research Group. I usually spoke with them when I had questions. Among them are Dr. Yanfei Li, Dr. Yangyang Fu, Dr. Zhiyao Yang, Tao Yang, Fan Feng, Zhihong Pang, Caleb Calfa, and Guowen Li.

Last but not the least, I would like to thank all of my family members for their unconditional love and support.

CONTRIBUTORS AND FUNDING SOURCES

Contributors

This work was supported by a dissertation committee consisting of Professor Bryan Rasmussen, Professor David Claridge, and Professor Zheng O'Neill of the Department of Mechanical Engineering; Professor Charles Culp of the Department of Architecture; and Dr. Veronica Adetola from Pacific Northwest National Laboratory.

The virtual testbed in CHAPTER II was co-developed with Dr. Yangyang Fu. All the other work included in this dissertation was completed by the student independently.

Funding Sources

Graduate study was supported by research projects from ASHRAE RP-1819 and National Science Foundation under Award No. IIS- 2050509.

TABLE OF CONTENTS

Page

LIST OF FIGURES

Page

LIST OF TABLES

Page

NOMENCLATURE

ACE	Area Control Error.
AGC	Automatic Generation Control.
AHU	Air Handling Unit.
ASHRAE	The American Society of Heating, Refrigerating and Air-Conditioning Engineers.
BAS:	Building Automation System.
CDL	Control Description Language.
COP	Coefficient of Performance.
CQF	Control Quality Factor.
CV-RMSE	Root Mean Square Error.
DCV	Demand Control Ventilation.
DOE	U.S. Department of Energy.
DRL	Deep Reinforcement Learning.
DRLC:	DRL-based Controller.
DQN	Deep-Q neural Network.
ERS	Iowa Energy Center Energy Resource Station.
DSP	Duct Static Pressure.
EWMA	Exponentially Weighted Moving Average.
FDD:	Fault Detection and Diagnosis.
FI	Fault Intensity.
FIR	Fault Impact Ratio.
FPTU	Fan-Powered Terminal Unit.

FR:	Frequency Regulation.
FRC	Frequency Regulation Controller.
GDL36	Guideline 36.
HVAC:	Heating, Ventilation, and Air-Conditioning.
KPI	Key Performance Index.
MDP	Markov Decision Processes.
MPC	Model Predictive Control.
NMBE	Normalized Mean Bias Error.
OA	Outdoor Air.
OAR	Outdoor Air Ratio.
OAT	Outdoor Air Temperature.
OBC	Optimization-based Controller.
PFPTU	Parallel Fan-Powered Terminal Unit.
PI	Proportional–Integral.
PID	Proportional–Integral- Derivative.
PLR	Part Load Ratio.
PPO	Proximal Policy Optimization.
PJM	Pennsylvania, Jersey, Maryland Regional Transmission Organization.
PMV:	Predicted Mean Vote.
PPD	Predicted Percentage of Dissatisfied.
RA	Return Air.
Reg	Regulation Signal.
RMSE	Root Mean Square Error.

ROC	Real-time Optimal Control.
R2	Coefficient of Determination.
RL:	Reinforcement Learning.
RP	Research Project.
RTE:	Round-Trip Efficiency.
SFPTU	Series Fan-Powered Terminal Unit.
SAT	Supply Air Temperature.
SPT	Setpoint.
SOO	Sequences of Operation
SRC	Symmetric Regulation Capacity.
VAV	Variable Air Volume.
T&R	Trim and Respond.
VAV	Variable Air Volume.
VFD	Variable Frequency Drive.
VRP	Ventilation Rate Procedure.
ZAT	Zone Air Temperature

CHAPTER I INTRODUCTION

Commercial buildings accounted for 35 percent of electricity consumption in the U.S., of which heating, ventilation, and air conditioning (HVAC) system was responsible for more than 30 percent in [1] Considering large contributions of the HVAC system energy consumption, different building energy efficiency measures are adopted to reduce energy use. The design, commissioning, and retrofit of building HVAC control systems are some of the important measures for energy efficiency but are often neglected. To be specific, the HVAC system control design is often done sequentially at the end of the design process with a limited time and budget spent. Due to the high requirement of the control design and the lack of standardized "sequences of operation" (SOO), which coordinates the operation of the whole building HVAC systems, the design engineers usually apply ad-hoc control sequences by their own experience. In addition, the control contractors often apply custom software they have developed to program the sequence and mimic the design SOO. Therefore, the energy efficiency of the SOO largely depends on the professional knowledge and experience of the control designers and operators. ASHRAE Guideline 36 (hereinafter referred to GDL36) [2], High Performance Sequences of Operation for HVAC Systems, is thus developed to provide standardized and high-performance rule-based SOO with the focus of maximizing the energy efficiency performance, providing control stability, and allowing for real-time fault detection and diagnostics.

The High Performance Sequences of Operation for HVAC Systems, GDL36, aims at publishing and maintaining the best-in-class sequences for various HVAC system types. The 2018 version largely depends on the ASHRAE project RP-1455 [3] and covers mostly the airside systems [4], e.g., variable air volume (VAV) systems, dual duct systems, zone terminal boxes, etc.

It will be continuously developed with state-of-the-art research on the high-performance rule-based SOO for HVAC systems and expand the coverage to the whole building systems and configurations. Figure 1-1 shows the timeline of the development of the GDL36 and associated ASHRAE projects in the past, present, and future. The GDL36 adapted the work in the past, such as the ASHRAE projects on the CO_2-based Demand Control Ventilation (DCV) control strategies [5, 6], the VAV terminal box control at the low flow rates [7], and the control loop assessment [8], etc. In the most recent update, the high-performance waterside SOO was integrated to ASHRAE Guideline36-2021 [2] from the completed ASHRAE project RP-1711 [9]. The added SOO includes the control sequences from the chilled water plant, the hot water plant, and the fan-coil unit. The advanced SOO for the dedicated outdoor air system from the ongoing ASHRAE RP-1865 will be reflected in GDL36 in the future.

The current GDL36 consists of four parts, the information part, the list of the hardwired points, the sequences of operations (SOO), and the control diagrams. The information part includes the information from the designer and the information from the test & balance contractor. The list of the hardwired points includes a list of the minimum points required for various equipment in order to implement the sequences as written. Compared to the old ASHRAE control guidance, Sequences of Operation for Common HVAC Systems (i.e., conventional SOO) [10] published in 2006, the featured SOO in GDL36 includes [11, 12]: (1) Dual maximum VAV box control sequences with airflow minimums reset to reduce cooling, fan energy and reheat; (2) Demand-based supply air temperature and duct static pressure resets enabled by the Trim & Respond (T&R) logic; (3) Demand-controlled ventilation and rogue zone detection to help maintain the effectiveness of demand-based resets; (4) Series-sequenced outdoor air (OA) and return air (RA)

dampers (as opposed to the more conventional parallel sequencing) to reduce fan energy; (5) Feature zone groups (aka isolation areas) to allow for individual scheduling of zone groups.

In the future, the high-performance rule-based SOO will cover more system configurations such as dedicated outdoor air systems, radiant heating, and cooling systems, etc. The SOO will be kept up to date by processing recommendations from different stakeholders to further improve the system performance or fix bugs. New tools and procedures are under development to better design, test, and commissioning of high-performance rule-based SOO. Control description language (CDL) [13, 14], a standard for digitized representation of control logic, was proposed and created to support the specification, simulation, documentation, and implementation through the machine-to-machine translation of the GDL36 SOO. The development of the CDL allows for the testing of the GDL36 SOO in an energy model, documenting the SOO with a verbose sequence description, and transmitting the sequences to the control contractor which eliminates the need to interpret the sequence and develop the control programming. In addition, the control design will be concurrent with the HVAC system design. The system design parameters (e.g., number of equipment, equipment type, equipment capacity, equipment performance parameters, number and location of sensors) and the parameters of the controllers in GDL36 will be adjusted simultaneously to optimize metrics such as system efficiency, load flexibility, total energy cost, and system life-cycle cost. Designing controls iteratively with systems also opens more opportunities and functionalities of high-performance rule-based SOO, such as demand flexibility and grid service provision. The future high-performance rule-based SOO is envisioned as follows: (1) Experts and engineers create and maintain advanced GDL36 SOO; (2) Control vendors and contractors program, test, and debug all the sequences from GDL36 using the control design tools; (3) Commissioning agents use the

functional performance tests included within GDL36. (4) Building operators manage the HVAC system according to the alarm and AFDD rules from GDL36.

Apart from the demonstrated solid foundation and strong vision, the success of GDL36 cannot live without the competitive benchmarking and performance evaluation in various aspects, such as the energy efficiency, the robustness of the control to uncertainties and faults, etc. The ambiguity of the achievable benefits would slow down the adoption and promotion of the high-performance rule-based SOO in real applications. Therefore, the continuous development and comprehensive evaluation of the new high-performance rule-based SOO are critical to facilitate the wide adoption of the technology. The following sections are the literature review regarding the development and comprehensive evaluation of the high-performance rule-based SOO.

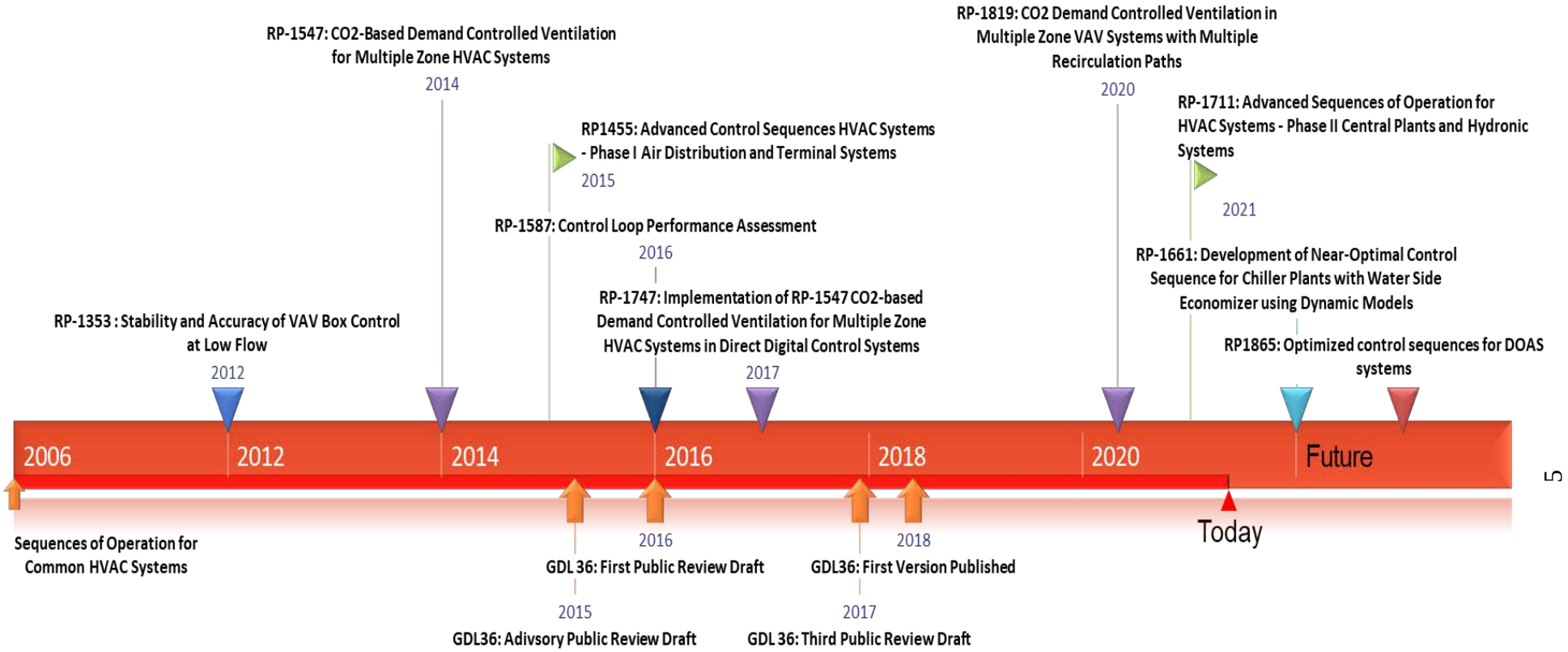

Figure 1-1 Timeline for the development of the GDL36 and its associated ASHRAE projects

1.1 Literature Review

1.1.1 Evaluation of GDL36 SOO in Different Aspects

1.1.1.1 Energy Efficiency

The energy efficiency performance of GDL36 has been demonstrated by limited lab/field tests and simulation-based studies [15-17], as tabulated in Table 1-1. Rodriguez [18] conducted an experiment in a commercial building air handling unit (AHU) and showed that more outside air was used and building cooling energy use was reduced after GDL36 was implemented. In the first year of the testing, 15% of whole building electricity use and 56% of natural gas use were saved with a retrofitted building automation system (BAS) using the GDL36 airside SOO in 555 County Center, a five-story office building in California [12]. A medium building in Vallejo, California, was retrofitted by implementing GDL36 SOO. The control sequence retrofits reduced annual energy bills by over $200,000 and heating energy use by more than 55% [19]. These two field demonstrations showed a simple payback year of 6.7 and 8.9 years, respectively.

Wetter et al. [17] implemented the airside GDL36 SOO in a single-floor medium office building model and reported a 30% annual site energy usage saving for the HVAC system with acceptable thermal comfort compared to the old SOO published in 2006 by ASHRAE [10]. Zhang et al. [20] implemented and verified both airside and waterside control sequences in a Modelica-based simulation environment for a single-zone VAV system. Their simulation results showed that the GDL36 yielded 17.3 % of annual HVAC energy saving compared to the conventional baseline control strategy. In a follow-up study [21], they estimated the energy saving of the control retrofit for multi-zone variable air volume systems using Spawn of EnergyPlus. The results showed the GDL36 SOO could provide a wide range of HVAC energy savings with an average savings of 31% in different climates, internal loads, and HVAC system operation periods. Overall, the energy

saving potential from retrofitting existing controls to the GDL36 SOO had yet to be shown for a wide range of cases [21].

Table 1-1 Summary of existing evaluation studies of GDL36 SOO on energy efficiency

Study	Approach	Test Conditions	Baseline	Results
[17]	Simulation	Modelica-based single-floor five-zone medium office VAV system (airside)	Typical rule-based	- 30% annual site energy use of the HVAC system with acceptable thermal comfort.
[20]	Simulation	Modelica-based single-zone system (plant & airside)	Typical rule-based	- 17.3% of annual HVAC energy saving with acceptable thermal comfort.
[21]	Simulation	21-zone VAV system (airside)	Typical rule-based	- an average of 31% HVAC energy saving
[18]	Field test	AHU in a commercial building	Not mentioned	- More outside air was used and building cooling energy use was reduced.
[12]	Field test	555 County Center, five-story office building, CA (Airside)	Not mentioned	- In the first year, 15% of whole building electricity use and 56% of natural gas use. - Estimated payback period was 6.7 years.
[19]	Field test	A medium hospital building in Vallejo, CA (Airside & Waterside)	Not mentioned	- Reduced annual energy bills by over $200,000 and heating energy use by more than 55%. - Estimated payback period was 8.9 years.

1.1.1.2 Uncertainty and Fault Handling

Apart from energy efficiency evaluation, uncertainties analysis was also conducted on GDL36. Haleem et al. [22] investigated the performance of the GDL36 in handling uncertainties of sensors and actuators in energy use and indoor environmental quality. They concluded that using low-grade sensors and actuators instead of the standard tier would significantly degrade the system performance for the GDL36 SOO. Through a sensitivity analysis, they also stated that the

inaccuracy in temperature sensors such as supply air temperature and zone air temperature sensors produced the most degradation compared to the AHU economizer dampers, terminal unit heating valves, and the fan loop components. They also assessed the impact of the untuned local control loop on the whole system performance [23].

Due to more comprehensive setpoint reset rules and more advanced control logic than typical HVAC systems, it is thus critical to understand how different faults might affect the HVAC energy system performance under GDL36 SOO and whether fault detection and diagnosis (FDD) strategies could be applied even for systems with such comprehensive control sequences. A hierarchical alarm suppression framework was adopted in GDL36 to avoid too many false alarms or too few alarms [24]. The automated fault detection and diagnostic (AFDD) rules, mostly based on the National Institute of Standards and Technology (NIST) air handling unit (AHU) FDD work, were also included in GDL36 to provide automatic alerts to building operators of potential equipment issues. The control diagram includes a selection of the equipment configurations in the current GDL36, which covers the VAV terminal unit, fan-powered terminal unit, dual duct terminal unit, single/multiple zone VAV AHU, and dual fan dual duct heating VAV AHU. In another recent work, Ojas et al. [25] developed a Dynamic Bayesian Network-based approach in diagnosing and isolating the root fault causes for HVAC systems that are controlled based on the GDL36 SOO.

1.1.1.3 Ventilation Compliance

Building HVAC system controls should fulfill the ventilation compliance requirements while achieving energy efficiency. Demand control ventilation (DCV) is therefore mandatory in many building standards and codes where CO_2 is often used as the ventilation indicator. In the GDL36-2021 SOO [2], the CO_2 DCV strategy follows the strategy in ASHRAE Guideline 62.1

[26]. The zone primary airflow and population component of the breathing zone outdoor airflow are adjusted based on the CO_2 concentration. The minimum outdoor airflow setpoint is changed accordingly in tandem with the zone DCV response based on the dynamic implementation of the Standard 62.1 Multiple Spaces Equation. However, it is noted that this approach might not be strictly adherent to Standard 62.1 [2]. In addition, there exists a few research studies [27-30] on developing and evaluating the technically rigorous DCV approach.

Lin et al. [28, 29] proposed SOO to dynamically reset the zone minimum primary airflow rate for the single-duct multi-zone VAV system. The control logic is referred to as the ASHRAE RP-1547 Logic. Simulation results have shown that this type of control strategy could achieve significant energy savings in the climate zone that is favorable for economizer operation since the zone minimum primary airflow setpoint could be lowered during operations with the economizer mode. The simulation results for a classroom building showed that the annual monetary saving ratios were 24.1% for Fairbanks, AK, and 46.2% for San Francisco, CA.

Despite the advantages, the ASHRAE RP-1547 Logic also suffers from some limitations, e.g., the control is too complex to comprehend, the iterations used in the algorithm cannot be implemented in real control systems, etc. To address such limitation, O'Neill et al. [30] developed a new control sequence based on the ASHRAE RP-1547 Logic. This new control sequence is practical and implementable in typical single-duct multi-zone VAV systems with direct digital control (DDC) systems. Their logic is referred to as the ASHRAE RP-1747 Logic. O'Neill et al. [27] tested the proposed logic in realistic simulations that accounted for dynamic occupant behaviors and concurrent cooling loads. The simulation results demonstrate that the RP-1747 DCV control logic achieved good compliance with the ventilation requirements in Standard 62.1 and save 9% to 33% HVAC energy consumption compared to the baseline. In addition, they also

implemented and assessed the stability of the proposed sequence in a well-instrumented test facility in Iowa [6]. These SOO have the potential to be merged into GDL36 pending further confirmation of their stability and performance in real applications.

1.1.1.4 Control Functional Test

Control functional tests were conducted to verify the control performance of the subroutines in GDL36 SOO. A functional test framework that checked the programming of GDL36 was developed and demonstrated by testing the VAV-box sequence from GDL36 [16]. In another work, Ferretti et al. [31] used the HVAC-Cx Functional Performance Test Module in NIST to conduct the functional performance tests of GDL36 SOO, including the supply air temperature control and T&R static pressure reset logic for VAV AHUs.

1.1.2 Simulation Testbeds for GDL36 SOO

As mentioned earlier in Section 1.1.1.1, there exist only a few lab experiment resources and field testbeds for the development and efficacy evaluations of GDL36 SOO. Due to the complexity and myriads of control subroutines in the SOO, it is very cost-intensive to conduct the field test for verifying SOO. In contrast, the simulation is a cost-effective way for the control verification for GDL36 SOO.

For the simulation tools, EnergyPlus [32], Modelica [33], and Spawn of EnergyPlus [34] stand out as the mainstream simulation platforms to be used for modeling the HVAC system SOO. It is also noted that TRNSYS and HVACSIM+ could serve as research testbeds for the development, evaluation, and demonstration of SOO, which has been demonstrated in a small number of studies [25, 35].

1.1.2.1 EnergyPlus-based

EnergyPlus has built-in modules to model many SOO in GDL36, such as the dual maximum VAV control and the CO_2-based DCV [36]. For the complex rule-based SOO, the control sequence can be coded with the built-in Energy Management System (EMS) module, which provides a high-level and supervisory control to override selected aspects of EnergyPlus modeling (i.e., zone minimum airflow rate, system minimum OA flow rate). A Python application interface was developed to allow users to write EMS program in Python for better flexibility [37]. To capture the pressure drop in the thermal-fluid network, the built-in airflow network module could be used to realistically model these effects. Although the EnergyPlus-based simulation provides good fidelity in terms of the building envelope and the mimic of building controls, it still has the limitations for simulating the dynamic behavior of the local controls. Furthermore, it is hard to reflect the realistic airflow distribution in EnergyPlus if the airflow network module is not used, which may influence the modeling results.

1.1.2.2 Modelica-based

These limitations related to simulations of controls could be properly addressed using Modelica [33]. Modelica is an equation-based, object-oriented language to model complex engineered systems that are described by coupled systems of differential, algebraic and discrete equations. The Modelica Buildings Library [38] is a free open-source library with dynamic building simulation, which enables the rapid prototyping, design, and analysis of new building and district energy and control systems. The Buildings library contains a model *Guideline36. mo (GDL36)* that includes both system-level and zone-level airside SOO for a multi-zone VAV system. Furthermore, Wetter et al. [14] developed a Control Description Language (CDL) that allows expressing GDL36 SOO in a digital, machine-readable language. They demonstrated that

with CDL-conforming control sequences, coupled with Modelica models, these energy savings could be quantified, allowing to compare different control strategies. Blum et al. [39] developed Building Optimization Testing Framework (BOPTEST) and associated software for Modelica-simulation-based benchmarking of building HVAC SOO. Despite the great flexibility of modeling the dynamics of the HVAC control systems using Modelica, it is worth mentioning that modeling with Modelica usually takes great modeling efforts and computational time, especially for the annual performance evaluation. In addition, it has limited libraries that support the fast prototyping and high-fidelity modeling of complex building geometry.

1.1.2.3 Spawn of EnergyPlus

To leverage the respective advantages from EnergyPlus and Modelica, the Spawn of EnergyPlus (SOEP) [34], a next-generation simulation engine for building and energy systems, was developed by the U.S. DOE labs. SOEP allows explicit modeling of the control sequences and HVAC system operation using the CDL. Zhang et al. [21] used SOEP to model a single-floor 21-zone VAV system and evaluated the energy savings from the GDL36 retrofit. To be specific, SOEP uses EnergyPlus for the building envelope with detailed zoning scenarios, and Modelica for the pressure-flow network of the airside HVAC system. The baselines in their study are the combination of conventional rule-based control subroutines. They studied the impact of the climate, internal load, and operating time on the final results. The simulation results showed a wide range of energy saving potential from 2% to 75% with an average of 31% for the GDL36 SOO. It is noted that the waterside system is simplified and modeled using a fixed coefficient of performance (COP), which makes the plant energy calculation not accurate. In addition, the baseline is conventional rule-based control subroutines, which are not energy-efficient (e.g., fixed setpoint schedules).

1.2 Research Objectives

The reviewed literature indicates the design and commissioning of the HVAC system control sequences could have a substantial impact on the building energy efficiency. The airside control retrofits following high-performance SOO could achieve energy savings up to 30% and more compared to the conventional rule-based control. However, achievable savings from the high-performance SOO in other HVAC system parts are still unknown (e.g., airside controls together with waterside controls). In addition, the energy saving potential of high-performance SOO compared to the state-of-the-art intelligent controls as the benchmark is also unclear. Apart from the energy efficiency, there are other key performance indexes we should look at, such as the robustness to the uncertainties and faults, ventilation performance, etc. The ambiguity of the achievable savings would slow down the adoption and prevalence of the high-performance SOO in real applications. Therefore, the continuous development and comprehensive evaluation of the new high-performance SOO are critical to facilitate the wide adoption of the technology.

To this end, this research aims at enhancing the existing standardized high-performance control sequences (GDL36) by conducting a comprehensive evaluation in terms of energy saving potential, fault robustness, ventilation compliance, and grid service compatibility. We propose to use a simulation-based approach to conduct the aforementioned evaluations. To begin with, a five-zone VAV system testbed in the Modelica-environment with the implementation of GDL36 SOO were first developed and used to answer the following research questions, as listed in Table 1-2.

Table 1-2 Research questions and the method to be used in this research

Research Questions	Overview of the Research Method
1. Since the energy saving performance of GDL36 has the edge over the conventional rule-based SOO, what is the performance regarding the energy efficiency compared to the advanced intelligent controllers?	The advance intelligent controllers, including DRL and OBC, were formulated and tested in the five-zone VAV system Modelica testbed. Apples-to-apples comparison will be conducted to assess the energy and thermal comfort performance between the GDL36 and intelligent controllers in the cooling season.
2. How robust GDL36 is towards various faults in HVAC systems? What are the most influential faults with negative impacts?	A comprehensive fault impact and robustness analysis were conducted by injecting faults systematically into the five-zone VAV system Modelica testbed. A total of 359 fault scenarios were simulated deterministically in three different seasonal operating conditions
3. CO_2-based demand control ventilation strategies that could potentially be merged into GDL36 have been developed to single-path multi-zone VAV systems. Can similar CO_2-based DCV strategies be applied to the multi-zone VAV system with multiple recirculating paths? What are the energy saving and ventilation performance?	Theoretical equations were developed to use CO_2 concentration as an indicator of occupant-related pollutant concentration for multiple zone VAV systems with recirculating paths. The proposed CO_2-based DCV SOO for the new systems were evaluated in the office building by co-simulation of EnergyPlus and CONTAM.
4. The GDL36 SOO will probably add a new feature of grid service provision in its future version. One of the fundamental questions is: what are the impacts of the HVAC system when it provides the frequency regulation? Are there any conflicts between the frequency regulation scheme and GDL36 SOO?	The experimentally verified frequency regulation control was developed into the five-zone VAV system Modelica testbed. 832 case studies with and without FR were simulated considering different regulation capacities (demand levels), standardized FR test signals, and building load profiles in 16 U.S. climate zones.

1.3 Contributions

The contributions of the research are outlined as follows:

- First, the virtual testbed of a multi-zone VAV system was developed in Modelica, which consists of the high-performance rule-based SOO for both the airside and waterside system. This open-source testbed could be used in future research for control verification and performance evaluation.
- Second, two intelligent controllers (i.e., optimization-based controller and deep reinforcement learning-based controller) were formulated and applied to the virtual testbed. The energy efficiency and thermal comfort metrics were compared with those from the case with GDL36 SOO. The comparison results contribute to a more convinced benchmarking regarding energy efficiency.
- Third, the fault impact analysis of the GDL36 was conducted to assess its fault robustness. The Modelica virtual testbed was further developed with functions of faults injection and fault modeling. Different from the idealization of the control sequences in most existing fault modeling studies, this testbed captures the fast-dynamic effects of the faults on the control sequences performance for the airside, waterside, and zone systems. Instead of only considering limited types of physical faults in the open literature, this work performs a comprehensive fault impact analysis including the faults from sensors, duct & pipes, dampers & valves, HVAC equipment, control-related elements, building envelope, system scheduling, and design and construction aspects.
- Fourth, the theoretical equations were developed to use CO_2 concentration as an indicator of occupant-related pollutant concentration for multiple zone VAV systems with recirculating paths. The developed practical CO_2-based DCV sequences are ready

to be merged in GDL36 with verified energy and ventilation performance in realistic models.

- Fifth, a holistic analysis was conducted to assess the performance of airside GDL36 SOO when the AHU fan is providing the FR, using dynamic HVAC models instead of quasi-steady-state models used in the literature.

1.4 Organization

This dissertation is organized as follows. CHAPTER II describes the work on the development of a Modelica-based virtual testbed for a multi-zone VAV system for GDL36 SOO. In CHAPTER III, the energy efficiency and thermal comfort performance of airside GDL36 SOO are compared with the state-of-the-art intelligent controllers (i.e., DRL and OBC). CHAPTER IV presents the work on the fault impact analysis of the GDL36 SOO. CHAPTER V describes the work on the development of the CO_2-based DCV for the multi-zone VAV system with recirculating path. CHAPTER VI details the work on the impact analysis of the HVAC system performance when it provides the FR under the GDL36 SOO. CHAPTER VII summarizes the outcome and limitations of the above work.

1.5 References

[1] The U.S. Energy Information Administration (EIA). Annual Energy Outlook 2021. 2021.

[2] ASHRAE. ASHRAE Guideline 36-2021 High Performance Sequences of Operation for HVAC Systems. 2021.

[3] Hydeman M, Eubanks B. ASHRAE RP-1455: Advanced Control Sequences for HVAC Systems Phase I, Air Distribution and Terminal Systems The American Society of Heating, Refrigerating and Air-Conditioning Engineers (ASHRAE); 2014.

[4] Hydeman M, Taylor ST, Eubanks B. Control sequences & controller programming. ASHRAE Journal. 2015;57:58-62.

[5] Lin X, Lau J, Yuill G. ASHRAE 1547-RP. CO2-Based Demand Controlled Ventilation for Multiple Zone HVAC Systems. 2013.

[6] O'Neill ZD, Li Y, Cheng HC, Zhou X, Taylor ST. ASHRAE 1747-RP. Implementation of RP-1547 CO2-based Demand Controlled Ventilation for Multiple Zone HVAC Systems in Direct Digital Control Systems. 2017.

[7] Liu R, Wen J, Regnier A, Zhou X, Klaassen C. RP-1353: Stability and Accuracy of VAV Box Control at Low Flows. The American Society of Heating, Refrigerating and Air-Conditioning Engineers (ASHRAE); 2012.

[8] O'Neill; Z, Williams; K, Li; Y, Henry; A, Liu; R, Zhou X. RP-1587: Control Loop Performance Assessment. The American Society of Heating, Refrigerating and Air-Conditioning Engineers (ASHRAE); 2015.

[9] Taylor Engineering. RP-1711 Advanced Sequences of Operation for HVAC Systems – Phase II Central Plants and Hydronic Systems. The American Society of Heating, Refrigerating and Air-Conditioning Engineers (ASHRAE); 2017.

[10] ASHRAE. Sequences of Operation for Common HVAC Systems: American Society of Heating Refrigerating and Air-Conditioning Engineers; 2005.

[11] Kiriu R, Stein J. Medical Office Building Thrives With Advanced Control Sequences. ASHRAE Journal. 2021.

[12] Talyor Engineering. Case Study: Advanced HVAC Controls. 2020.

[13] Wetter M, Grahovac M, Hu J. Control description language. Proceedings of The American Modelica Conference 2018, October 9-10, Somberg Conference Center, Cambridge MA, USA: Linköping University Electronic Press; 2019. p. 17-26.

[14] Wetter M, Ehrlich P, Gautier A, Grahovac M, Haves P, Hu J, et al. OpenBuildingControl: Digitizing the control delivery from building energy modeling to specification, implementation and formal verification. 2022;238:121501.

[15] Paliaga G, Singla R, Snaith C, Lipp S, Mangalekar D, Cheng H, et al. Re-Envisioning RCx: Achieving Max Potential HVAC Controls Retrofits through Modernized BAS Hardware and Software. 2020.

[16] Pritoni M, Prakash A, Blum D, Zhang K, Tang R, Granderson J, et al. Advanced control sequences and FDD technology. Just shiny objects, or ready for scale? 2020.

[17] Wetter M, Hu J, Grahovac M, Eubanks B, Haves P. OpenBuildingControl: Modeling feedback control as a step towards formal design, specification, deployment, and verification of building control sequences. Building Performance Modeling Conference and SimBuild2018.

[18] Rodriguez A. Utilizing ASHRAE G36 for Free Outside Air Cooling (Economizer): The George Washington University; 2019.

[19] Kiriu R, Stein JJAJ. Medical Office Building Thrives With Advanced Control Sequences. 2021;63:62-7.

[20] Zhang K, Blum DH, Grahovac M, Hu J, Granderson J, Wetter M. Development and Verification of Control Sequences for Single-Zone Variable Air Volume System Based on ASHRAEGuideline 36. Lawrence Berkeley National Lab.(LBNL), Berkeley, CA (United States); 2020.

[21] Zhang K, Blum D, Cheng H, Paliaga G, Wetter M, Granderson JJJoBPS. Estimating ASHRAE Guideline 36 energy savings for multi-zone variable air volume systems using Spawn of EnergyPlus. 2022;15:215-36.

[22] Haleem SMA, Pavlak GS, Bahnfleth WP. Performance of advanced control sequences in handling uncertainty in energy use and indoor environmental quality using uncertainty and sensitivity analysis for control components. Energy and Buildings. 2020;225:110308.

[23] Abdel Haleem S. Impact of Component Uncertainty and Control Loop on Performance in HVAC Systems with Advanced Sequences of Operation [Doctoral thesis]: The Pennsylvania State University; 2020.

[24] Hydeman M, Taylor ST, Eubanks B. Control sequences & controller programming. ASHRAE Journal. 2015;57:58-62.

[25] Pradhan O. Development and Validation of a Simulation Testbed for the Intelligent Building Agents Laboratory (IBAL) using TRNSYS. ASHRAE Transactions. 2020;126:458-66.

[26] ASHRAE. ANSI/ASHRAE Standard 62.1-2019 Ventilation for Acceptable Indoor Air Quality 2019.

[27] O'Neill ZD, Le YF, Cheng HC, Zhou XH, Taylor ST. Energy savings and ventilation performance from CO2-based demand controlled ventilation: Simulation results from ASHRAE RP-1747 (ASHRAE RP-1747). Sci Technol Built Environ. 2020;26:257-81.

[28] Lin X, Lau J. Demand-controlled ventilation for multiple-zone HVAC systems—Part 2: CO2-based dynamic reset with zone primary airflow minimum set-point reset (RP-1547). Science and Technology for the Built Environment. 2015;21:1100-8.

[29] Lin X, Lau J. Demand controlled ventilation for multiple zone HVAC systems: CO2-based dynamic reset (RP 1547). Hvac & R Research. 2014;20:875-88.

[30] O'Neill ZD, Li Y, Cheng HC, Zhou X, Taylor ST. Energy Savings and Ventilation Performance from CO2-based Demand Controlled Ventilation: Simulation Results from ASHRAE RP-1747 (ASHRAE RP-1747). Science and Technology for the Built Environment. 2019:257-81.

[31] Ferretti NM, Milesi-Ferretti N, Galler MA, Bushby ST, Sorra J. Commissioning ASHRAE High-performance Sequences of Operation for Multiple-zone Variable Air Volume Air Handling Units: US Department of Commerce, National Institute of Standards and Technology; 2019.

[32] Crawley DB, Lawrie LK, Pedersen CO, Winkelmann FCJAj. Energy plus: energy simulation program. 2000;42:49-56.

[33] Mattsson SE, Elmqvist H, Otter MJCEP. Physical system modeling with Modelica. 1998;6:501-10.

[34] Wetter M, Nouidui TS, Lorenzetti D, Lee EA, Roth A. Prototyping the next generation energyplus simulation engine. Proceedings of the 3rd IBPSA Conference, Jeju island, South Korea2015. p. 27-9.

[35] Chen Z. Advanced Solver Development for Large-scale Dynamic Building System Simulation: Drexel University; 2019.

[36] Chenari B, Lamas FB, Gaspar AR, Manuel Carlos GdS. Development of a new CO2-based Demand-controlled Ventilation Strategy Using EnergyPlus. Energy for Sustainability International Conference: Designing Cities Communities for the Future Funchal, 8–10 February2017.

[37] Office of Energy Efficiency &Renewable Energy, U.S. DOE. Python EMS: A Unique EnergyPlus Feature Gets a Serious Upgrade. 2020.

[38] Wetter M, Zuo W, Nouidui TS, Pang X. Modelica buildings library. Journal of Building Performance Simulation. 2014;7:253-70.

[39] Blum D, Arroyo J, Huang S, Drgoňa J, Jorissen F, Walnum HT, et al. Building optimization testing framework (BOPTEST) for simulation-based benchmarking of control strategies in buildings. 2021;14:586-610.

CHAPTER II DEVELOPMENT OF A VIRTUAL TESTBED FOR A MULTI-ZONE VAV SYSTEM FOLLOWING GDL36 SOO

2.1 Introduction

The potential benefits of retrofitting existing controls to the GDL36 SOO have yet to be demonstrated for a wide range of cases. The simulation-based testbed could provide a cost-effective solution for the performance evaluation of the GDL36 SOO. Recently, the ASHRAE Guideline 36-2021 has merged the waterside high-performance rule-based SOO from ASHRAE RP-1711 [1]. However, there exists no existing multi-zone building testbed that integrates the SOO from both the airside and waterside systems. Zhang et al. [2] developed a Modelica virtual testbed for the single-zone VAV system and assessed the energy saving potential of the airside and waterside control retrofit. In another work [3], they applied the same method in a multi-zone VAV system for the retrofit energy saving analysis. However, the waterside system in their model was simplified and calculated using the coil load and a fixed COP. To this context, a virtual testbed for a multi-zone VAV system following both airside and waterside SOO was developed to fulfill the research gap. This testbed also serves as the platform in the following CHAPTER III and CHAPTER IV. In the following sections, the virtual testbed is validated by the comparison verification with the counterpart simulator and by the expected system behavior from domain knowledge.

2.2 System Configuration

The simulation testbed was developed based on a five-zone airside VAV system model Guideline36.mo (GDL36*)* in Modelica Buildings Library 7.0.0 [4, 5]. This GDL36 model consists of a model of a VAV system with terminal reheat units, a building envelope model, and a model

for leakage airflow through building envelopes and open doors. On top of that, in this study, a chilled water plant system and a boiler hot water system are added to the GDL36 model following the waterside high-performance control sequences in the latest GDL36-2021 [6] (which come from ASHRAE RP-1711 [1]). The developed virtual testbed schematics are shown in Figure 2-1. The testbed consists of four perimeter zones and one core zone, which is representative of one mid-floor of the new construction medium office building, as described in the set of the U.S. Department of Energy (DOE) Commercial Prototype Building Models [7]. Heating and cooling are delivered by a single-duct multi-zone VAV system. One AHU connected with five VAV terminal boxes serves five zones (four exterior zones and one interior zone, respectively) on one floor. The chilled water is supplied by a central chiller plant which consists of a chiller, a waterside economizer, a cooling tower, one chilled water pump, and one cooling water pump. A boiler, fed by natural gas, supplies the hot water to the AHU heating coil. The reheat coils in the VAV terminals are electric resistance coils.

The modeled HVAC system follows the state-of-the-art SOO in ASHRAE Guideline 36-2018 for the airside SOO [8] and ASHRAE project RP-1711 report for the waterside SOO [9] (Note: the latest ASHRAE Guideline 36-2021 [6] includes both airside and waterside SOO). Both airside and waterside high-performance operation sequences implemented in the virtual testbed are summarized in Table 2-1. Appendix A.1 lists the detailed sequences for each local and supervisory control. The waterside controls were implemented using the Control Description Language (CDL) [5] and verified in the open-loop tests before being integrated into the system [10]. Figure 2-2 depicts the virtual testbed in Dymola.

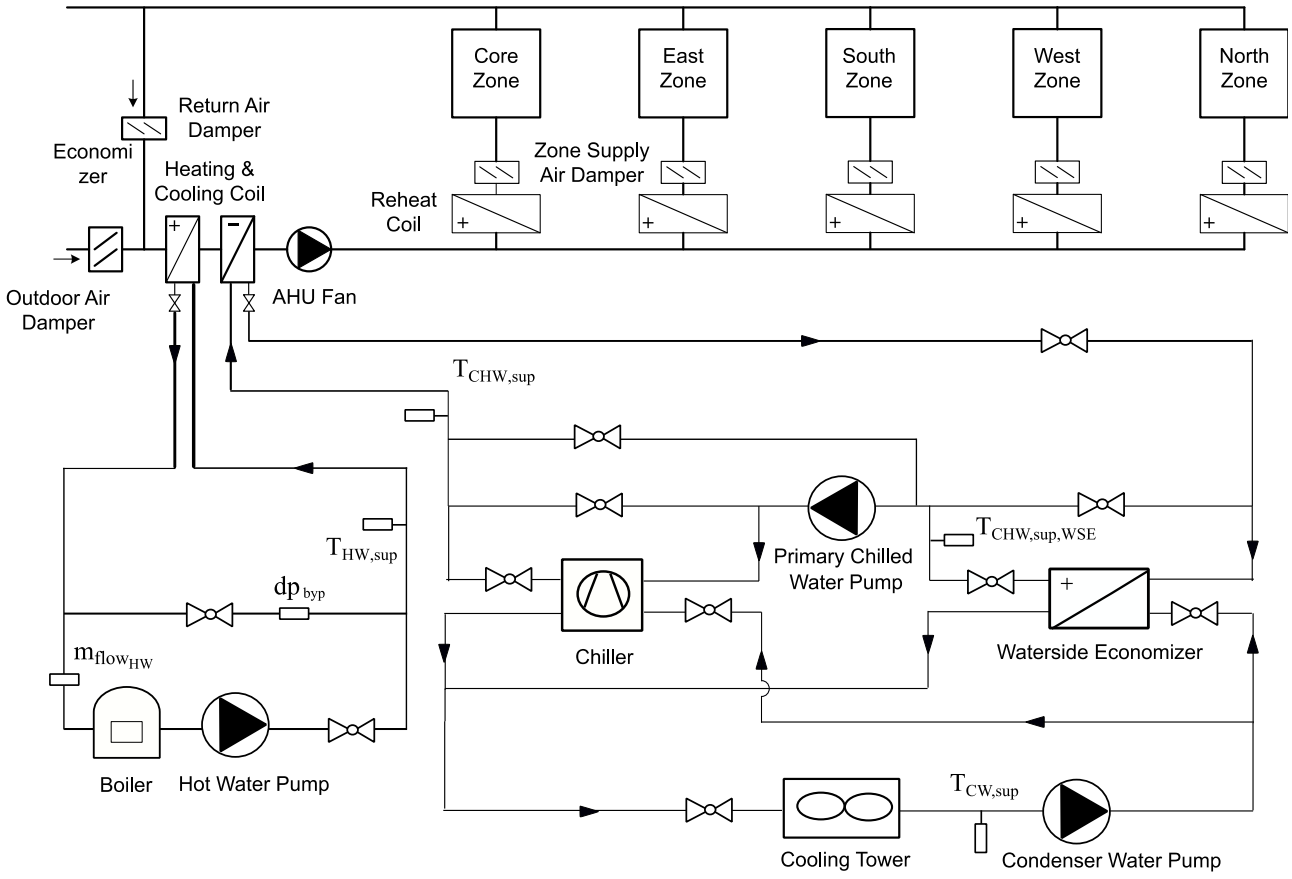

Figure 2-1 Schematics of the HVAC system in the virtual testbed

Table 2-1 Summary of the implemented control sequences in both airside and waterside

Category		Control Sequences
Airside	Air handling unit	• Fan speed control • Economizer damper control • Minimum outdoor air control • Supply air temperature control
	Zone VAV Terminal	• Zone air temperature control • VAV box airflow and reheat coil control
	Supervisory	• AHU and zone mode control

Waterside	Chiller	• Chiller staging control • Minimum flow bypass valve control • Chilled water supply temperature reset control
	Cooling tower	• Cooling tower fan speed
	Pump	• Chilled water pump speed control • Hot water pump speed control
	Boiler	• Boiler staging and heating power control • Minimum flow bypass valve control • Hot water supply temperature reset control
	Supervisory	• Chiller/boiler plant enable/disable control • Cooling mode control

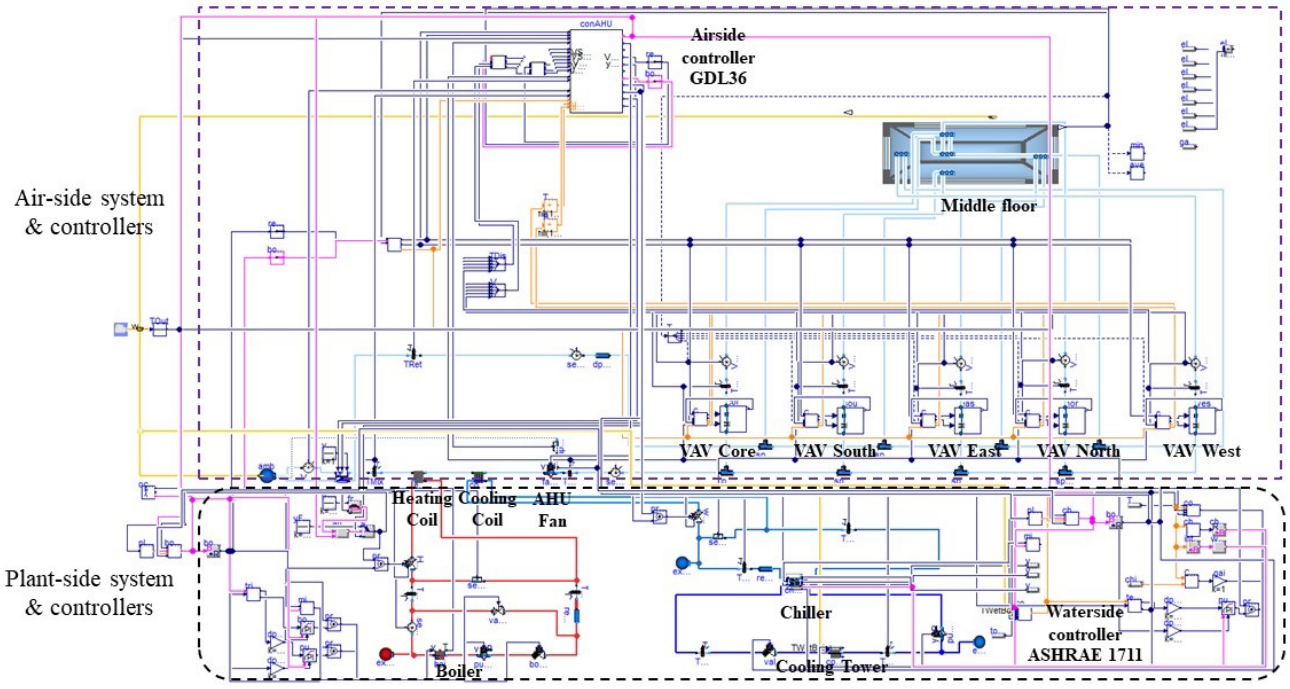

Figure 2-2 Schematics of the virtual testbed in Dymola

2.3 Model Setup and Verification

2.3.1 System Sizing

The system is sized under the ASHRAE climate zone 5A Chicago, IL. The Modelica system model is set up according to the middle floor of the EnergyPlus prototype medium office model [7]. The air loop of the Modelica system model is sized as the middle floor in the EnergyPlus model. Table 2-2 shows peak load and sizing comparisons between the EnergyPlus prototype medium office model with the Modelica system model. The peak cooling load is similar between these two models. The design airflow rate in our model, which is the default value from the original GDL36 model in Modelica Buildings Library, is slightly larger than that in the EnergyPlus prototype model. The air handling unit (AHU) fan head is sized similarly to the EnergyPlus prototype model. Both fan hydraulic efficiency and motor efficiency are chosen as 0.7, while the EnergyPlus prototype model has a fan with an overall efficiency of 0.6. Such efficiency difference makes AHU fan rated electric power in the Modelica system model higher than that in the EnergyPlus model.

Since the EnergyPlus prototype medium office model uses the packaged air conditioning unit with a gas furnace, its waterside sizing has little reference value. Therefore, the waterside equipment is sized based on the HVAC engineering knowledge using the following assumptions:

- Chilled Water Pump Head Calculation: Chiller evaporator: 6m H2O; Cooling coil: 6m H2O; Return chilled water filter: 4m H2O; Water loop frictional head loss and local head loss: 10m H2O; In total ~26m H2O (255,000 Pa).
- Cooling Water Pump Head Calculation: Chiller condenser: 5m H2O; Cooling tower: 5m H2O; Return cooling water filter: 4m H2O; Water loop frictional head loss and local head loss: 8m H2O; In total 22m H2O; (215,700 Pa).

- Hot Water Pump Head Calculation: Boiler: 6m H2O; Return hot water filter: 4 m H2O; Water loop frictional head loss and local head loss: 6m H2O; In total ~18m H2O; (157,000Pa).

Appendix Table A-1 shows a summary of the HVAC equipment sizing parameters in the system model.

Table 2-2 Comparison between the EnergyPlus prototype with the Modelica system model

Item	**EnergyPlus Midfloor_Plenum**	**Modelica**
Area [m^2]	1,660.7	1,662.7
AHU Fan Design Flow Rate [m^3/s]	4.2	4.8
AHU Fan Head [Pa]	1,389	1,381
Overall Efficiency	0.6	0.49
AHU Fan Rated Electric Power [W]	9,685	13,530
Cooling Coil Capacity [W]	95,438	100,711
Heating Coil Capacity [W]	34,995	40,526
Chilled Water Pump Head [W]	Not applicable	255,000
Chilled Water Pump Flow [m^3/s]		0.004
Cooling Water Pump Head [W]		215,700
Cooling Water Pump Flow [m^3/s]		0.0043
Hot Water Pump Head [W]		157,000
Hot Water Pump Flow [m^3/s]		0.00132
Cooling Tower Fan Power [W]		4,300

2.3.2 System Behavior Verification

Apart from the system sizing comparison with the EnergyPlus counterpart, the whole system, and different subsystems are well-tuned by adjusting various control parameters (e.g., parameters in various PID loops, T&R loop, etc.). Although there is no experiment or real data available to support the validation of the system model, a thorough quality check was conducted in different subsystems to make sure that the system behaves as expected from the control SOO and domain knowledge. In the following sections, the detailed whole system and subsystem results are reported for a typical summer week from Day 204 to Day 211.

2.3.2.1 AHU

The supply air temperature is reset to 12 ℃ (the lowest value) during the occupied period due to the high outdoor air temperature. The oscillations of the supply air temperature are due to the pressure and temperature resets from the T&R Control in the chilled water plant. Since the system was operated in the part a load condition, the supply fan works at around 70% of its nominal speed to track the static pressure setpoint as shown in Figure 2-3.

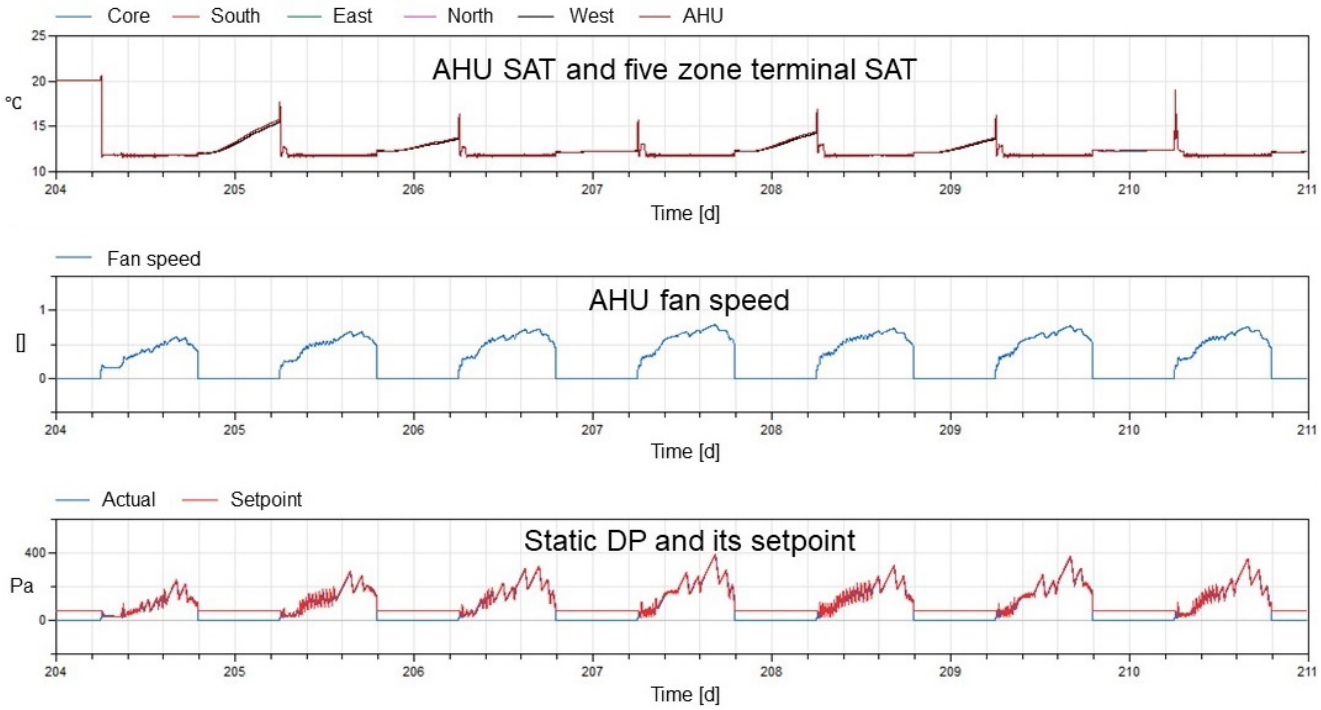

Figure 2-3 Time series data for AHU

2.3.2.2 Zone Terminals and Zones

The cooling load of each zone is shown in the bottom subplot of Figure 2-4. Core zone has the largest cooling load, but it is only around 22% of its design cooling load. All zone temperatures are controlled at 24 ℃ during the occupied period for cooling. By tuning the parameters of T&R Logic used for fan speed and supply air temperature control, the zone temperatures deviate from the setpoint within 0.7℃.

The temperature of the core zone and north zone is well controlled within 24 ± 0.3℃, while temperatures in the east, south, and west zones have relatively larger deviations. The core zone and north zone have a small cooling load, which is around 22% and 50% of their design cooling load, respectively. East, south, and west zones have a 62%, 75%, and 88% of their design cooling load, respectively. The uneven cooling demands among different zones lead to the starving of VAV damper when the cooling load is large in the east, south, and west zones, as suggested in the bottom subplot of Figure 2-4. It eventually leads to the deviation of air flow rates from their setpoints and leads to the rise of zone temperatures. As mentioned earlier, the control parameters were tuned to ensure the largest temperature violation within 0.7℃, which is rational in the real world.

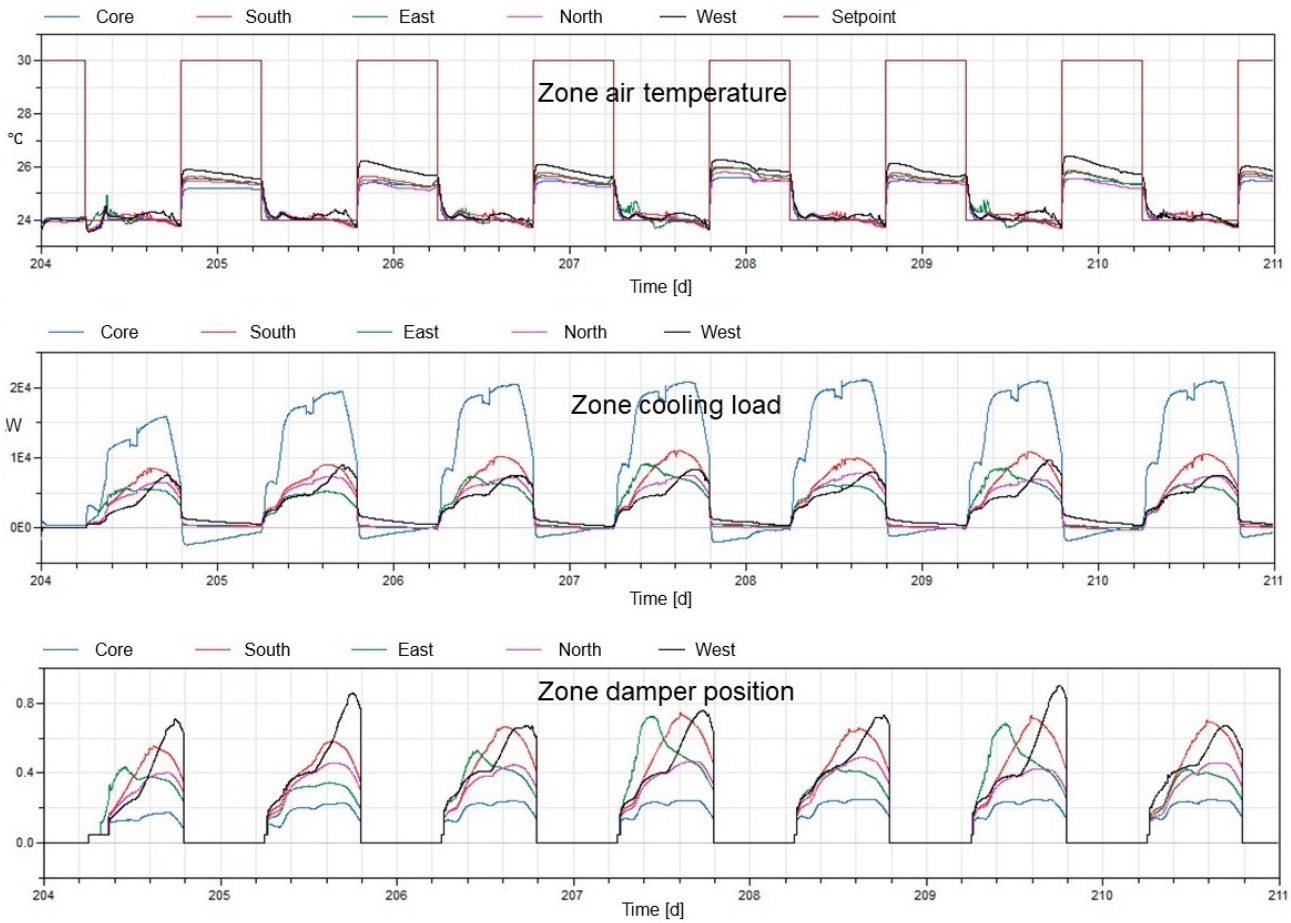

Figure 2-4 Time series data for zone temperature and cooling load

2.3.2.3 Waterside

Figure 2-5(a) shows the HVAC system operation status. The second subplot depicts the cooling mode signal and the chiller/boiler on/off signal. The latter one shows the cooling coil valve position. From these figures, we can see that the chiller plant is called on as soon as the AHU is operated, and the cooling coil valve position is larger than 0.95. The observed fluctuation is due to the 2-min sampling period in the T&R control. The cooling mode controller decides the operation mode of the cooling plant (i.e., 4 – off, 3 – full mechanical, 2 – partial mechanical, 1 – free cooling). In this simulation period, the chiller plant only works in two modes, i.e., full mechanical mode and off mode.

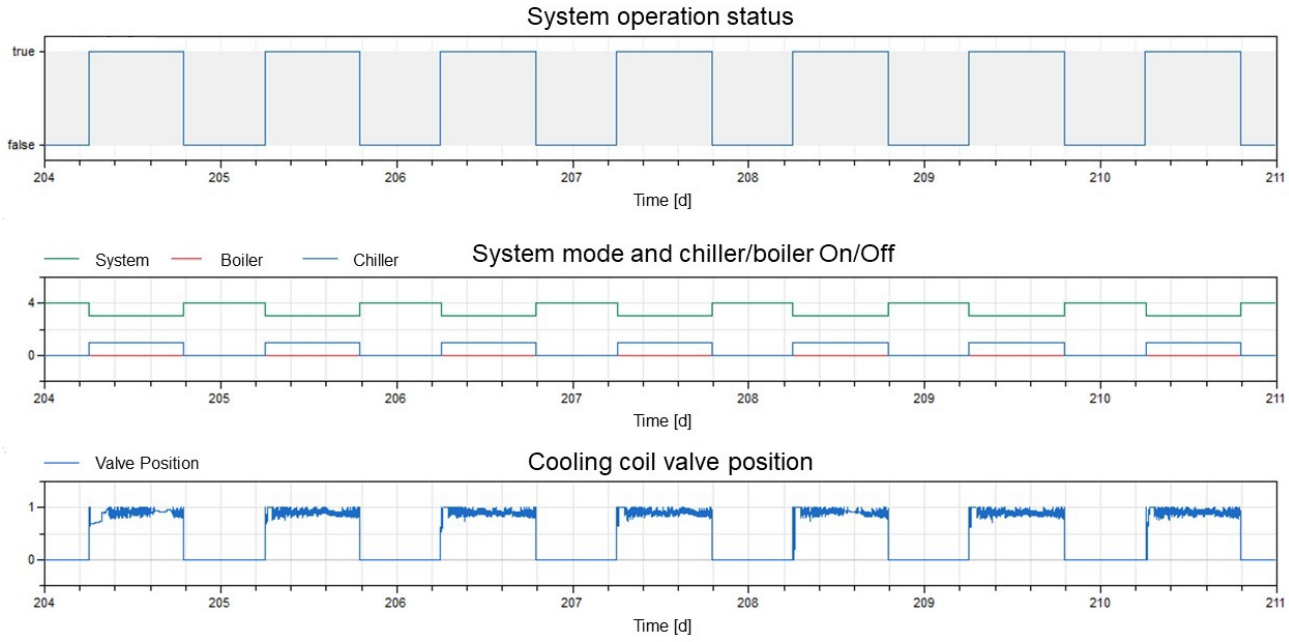

Figure 2-5 Time series data for waterside operation status and cooling coil valve position

Figure 2-6 shows the dynamic reset of the chiller supply temperature setpoint and differential pressure. The differential pressure (DP) setpoint of the chilled water loop was first reset with a larger value to increase the chilled water mass flow rate. If the DP setpoint reaches its

maximum value and more cooling is still needed, the chilled supply water temperature setpoint is reduced until it reaches its minimal.

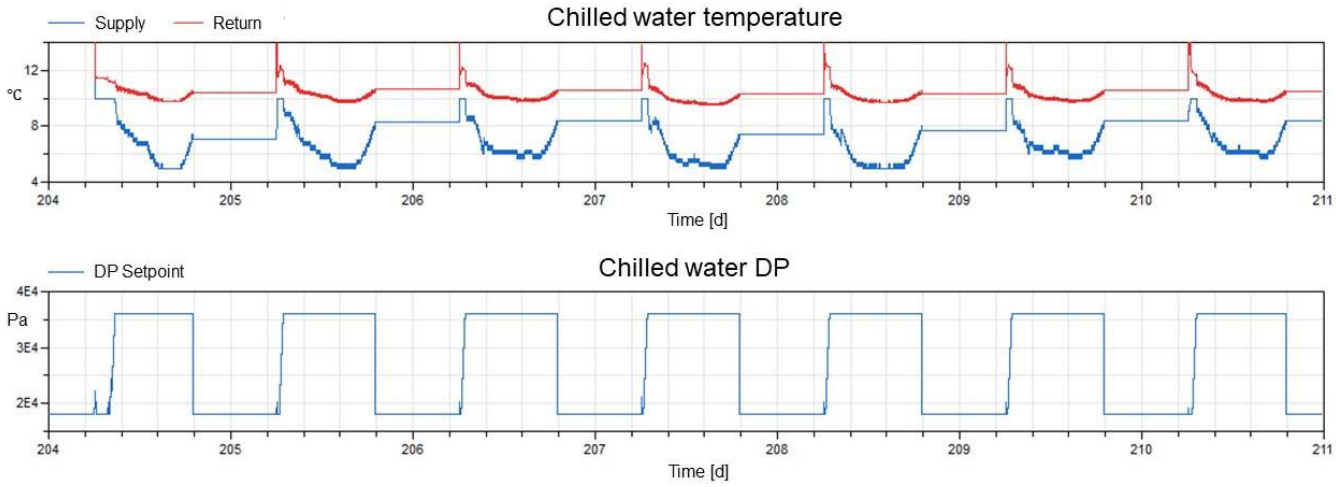

Figure 2-6 Time series data for chilled water temperature and DP

2.4 Numerical Performance

The simulation is conducted using the *cvode* solver [11], a variable time step solver in Dymola. The simulation is time-consuming because the system model is massive in terms of the number of mathematical equations. There are 20,925 numerical equations in total. In addition, there are samplers used to sample the control signal at an interval of 2 minutes. These characteristics lead to a long simulation time. To speed up the simulation, the accuracy is sacrificed by resetting the solver tolerance to 10^{-4} as defaulted by Dymola instead of 10^{-6} as recommended by the Modelica Buildings Library. The example of a one-week simulation takes around 90 seconds using Dymola 2021 on a Windows machine with Intel® Core™ i5-9500 @3.00 GHz CPU and a 16 GB RAM.

2.5 Conclusions

In this chapter, a five-zone VAV system that follows the latest version GDL36 was developed in Modelica. By leveraging the existing airside five-zone model in Modelica Buildings

Library, we added the detailed waterside SOO based on ASHRAE project 1711. The waterside controls were implemented using the CDL and verified in the open-loop tests before being integrated into the system. This Modelica-based testbed is sized for Climate Zone 5A (Chicago, IL) and the sizing results are within a similar range with the EnergyPlus counterpart. The rule-based SOO was fine-tuned and the system behaves as expected from the control logic and domain knowledge. This virtual testbed was used in the following CHAPTER III and CHAPTER IV.

2.6 References

[1] Taylor Engineering. RP-1711 Advanced Sequences of Operation for HVAC Systems – Phase II Central Plants and Hydronic Systems. The American Society of Heating, Refrigerating and Air-Conditioning Engineers (ASHRAE); 2017.

[2] Zhang K, Blum DH, Grahovac M, Hu J, Granderson J, Wetter M. Development and Verification of Control Sequences for Single-Zone Variable Air Volume System Based on ASHRAEGuideline 36. Lawrence Berkeley National Lab.(LBNL), Berkeley, CA (United States); 2020.

[3] Zhang K, Blum D, Cheng H, Paliaga G, Wetter M, Granderson JJJoBPS. Estimating ASHRAE Guideline 36 energy savings for multi-zone variable air volume systems using Spawn of EnergyPlus. 2022;15:215-36.

[4] Wetter M, Zuo W, Nouidui TS, Pang X. Modelica buildings library. Journal of Building Performance Simulation. 2014;7:253-70.

[5] Wetter M, Hu J, Grahovac M, Eubanks B, Haves P. OpenBuildingControl: Modeling feedback control as a step towards formal design, specification, deployment, and verification of building control sequences. Building Performance Modeling Conference and SimBuild2018.

[6] ASHRAE. ASHRAE Guideline 36-2021 High Performance Sequences of Operation for HVAC Systems. 2021.

[7] The U.S. Department of Energy (DOE). DOE Commercial Prototype Building Models. Building Energy Codes Program2020.

[8] ASHRAE Guideline 36. High Performance Sequences of Operation for HVAC Systems. American Society of Heating, Refrigerating, and Air-conditioning Engineers (ASHRAE); 2018.

[9] Talyor Engineering. Best-In-Class: Demonstrating Scalable Operational Efficiency through Optimized Controls Sequences and Plug-and-Play Solutions. California Energy Commission; 2017.

[10] Fu Y, Lu X, Zuo W. Modelica models for the control evaluations of the chilled water system with waterside economizer. Proceedings of the 13th International Modelica Conference, Regensburg, Germany, March 4–6, 2019: Linköping University Electronic Press; 2019.

[11] Cohen SD, Hindmarsh AC, Dubois PFJCip. CVODE, a stiff/nonstiff ODE solver in C. 1996;10:138-43.

CHAPTER III ENERGY PERFORMANCE COMPARISON OF INTELLIGENT CONTROLLERS AND GDL36 SOO

3.1 Introduction

Innovations in building controls at the supervisory level have great potential to achieve the whole-building level energy savings on the order of 30% and higher [1]. Generally, there are three categories of building controls [2]. The first category is the prescriptive and feedback-based reactive control strategies. In this type of control, different setpoints or schedules are determined at the supervisory level based on the heuristic rules and then the Proportional-Integral-Derivative (PID) local controls are used to track the setpoints. ASHRAE Guideline 36 (GDL36), which collects these best-in-class rules, falls into this category. GDL36's high performance in terms of energy efficiency has been demonstrated when compared with the counterparts within this category [3]. Despite its simplicity and ease of implementation, the rule-based controls might not be optimal because the control sequences are reactive and do not consider the predictive information.

The other two types belong to the intelligent building controllers. The first is the optimization-based controllers, which consider the real-time or predictive information and thus be able to adapt to the changing building climate conditions, occupancy, etc. Model Predictive Control (MPC) represents the state of the art of this real-time optimal control in practice. The other type is the learning-based method, e.g., the reinforcement learning-based controller. Although the latter two intelligent building control methods can notably reduce the energy use (e.g., building systems integrated with storage systems or distributed energy resources), the high computational requirements and scalability issues have been imposed on the widespread adoption [4].

Given the common pros and cons of different building controls, it is imperative to conduct an apples-to-apples comparison of these building controls to justify the respective energy saving benefits.

3.2 Literature Review

3.3 Optimization-based Controllers

The optimization-based controllers (e.g., real-time optimal control (ROC) and model predictive control (MPC)) have attracted broad attention in research academia for optimal building operations. These research studies included the optimal control strategies of multi-zone VAV systems [5, 6], single-zone VAV systems [7], chilled water systems [8], cooling water systems [9], and building energy storage [10].

For the real-time optimal controls, optimization actions are conducted under a fixed frequency or a predefined timetable during the operation of HVAC systems. For example, Nassif et al. [11] employed a bi-objective genetic scheme where the supervisory level control setpoints were optimized every 30 minutes with respect to energy use and thermal comfort. However, the time-based real-time optimal control may not effectively respond to the changing building operating conditions such as the weather and occupant behavior [12]. Furthermore, there is a potential computational waste under the time period when the operating conditions are stable, and optimization is not needed. Therefore, in the last decade, MPCs have been widely studied for the optimal control of building systems.

MPC can be explained literally by the composed three words: model, predictive, control. The system mathematical “model” (together with the current measurements) and “predictive” information, are used to optimize the “control” inputs by minimizing a given objective function over a finite prediction horizon [13]. MPC has demonstrated its energy saving potential in

simulations and also several experimental field testing in real buildings [14-16]. However, the major challenge lies in its complexity regarding the MPC design and controller tuning. It is not only labor-intensive but also requires expertise for control design and commissioning. Huang et al. [17] investigated several critical settings, including the model interval, control sampling interval, and prediction horizon in MPC for building controls. Drgona et al. [18] outlined current bottlenecks and challenges for the wide adoption of MPC in real buildings. They predicted that the large-scale market penetration of MPC can be expected to happen within the next decade with a few optimistic conditions.

There exist several studies on developing optimization-based control strategies for commercial building VAV systems. Koehler et al. [19] proposed an explicit MPC and compared its performance with the T&R control schemes for a multi-zone VAV system. The simulation results of both control schemes are similar. Liang et al. [20] designed an auto-regressive moving average exogenous (ARMAX)-based MPC scheme for optimizing the supply air temperature (SAT), the outside air flow rate, and the recirculation air damper ratio. Compared to the original rule-based supervisory controls, the simulation results showed that a 27.8% energy saving on average could be achieved. Raman et al. [21] proposed a hierarchical MPC for multi-zone VAV systems with a high-level controller deciding the AHU-level control commands based on low-resolution large meta-zone models and a projection-based low-level controller using not only what the MPC computes but also feedback from zones. The proposed controller significantly reduced energy use compared to the baseline controller, which used fixed air temperatures and fixed outdoor air flow rates for AHU commands and dual-maximum VAV box control for zone-level commands.

3.3.1 Reinforcement learning-based Controllers

Reinforcement learning (RL) has attracted tremendous research interests in solving high-dimensional complex control and optimization problems due to the vast development of deep learning and RL algorithms in the last decade. Optimal building controls are one of the complicated problems due to the multivariant actions and dynamic energy demand.

RL is a category of machine learning algorithms that aims to learn an optimal control policy from the direct interaction between the agent and the environment. The agent will perform empirical learning and decide on the action to drive the environment towards a favorable trajectory according to a predefined reward function.

In mathematics, RL problems could be formalized as Markov decision processes (MDP), in which the agent and the environment interact at a sequence of discrete time steps. Figure 3-1 depicts the interaction process. For time step t, the agent receives representation information of the environment named state S_t. In turn, the agent computes based on the current control policy π and send back to the environment a control action A_t. Policy π maps states to actions which represents the probability that the agent will take action A_t under the state S_t. One time step later, the agent observes a new state S_{t+1} from the environment along with its reward R_{t+1}, which indicates the feedback from the environment after taking action A_t. During this interaction, the RL agent aims to find an optimal policy π^* as shown in Eq. (3-1) based on various RL algorithms. For the model-based RL algorithms, the optimal policy π^* could be obtained by Dynamic Programming while in the model-free RL the agent learns the optimal policy π^* through the interaction with the environment [22].

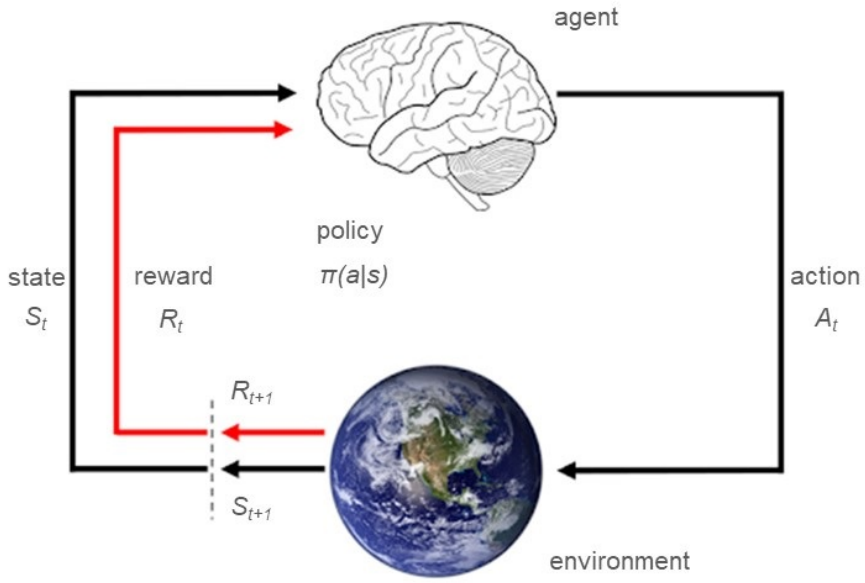

Figure 3-1 Schematics of the reinforcement learning

$$\pi^* \in \arg\max_{\pi} J(\pi) = \mathbb{E}_{s_0 \sim \mu_0} \mathbb{E}_{\pi} \sum_{t=0}^{\infty} \gamma^t r(s_t, a_t), \tag{3-1}$$

where $\mathbb{E}_{\pi}$ is the expectation that the action a_t is taken based on the policy. γ is the discount factor that normalizes the future reward.

Compared to the model-based RL, the model-free RL is more appealing to the building application because every building is different, and it is hard to learn a detailed physical model. The model-free RL could be further divided into value-based and policy-based methods. As a conventional valued-based method, Q-learning is a table-based algorithm. The Q-value table will decide the next action based on the current state and the algorithm will continuously update the Q-table. With the development of the deep learning methods, the Q-table is replaced by a deep neural network (DNN) that belongs to the deep-Q neural network (DQN) algorithm, especially for the case that has large dimensions of states and agents. In that case the Q-learning approach becomes no longer efficient. For the policy-based RL algorithms, the optimal policy in Eq. (3-1) is parameterized as π_θ with regards to θ and RL formulation becomes Eq. (3-2) to find the optimal

policy θ^*. The policy gradient theorem is employed to update the policy θ. The popular policy-based algorithms include the actor-critic algorithm [23] and the Proximal Policy Optimization (PPO) [24].

$$\theta^* \in \arg\max_{\theta \in \Theta} J(\theta), \tag{3-2}$$

Different researchers have investigated the application of model-free RL controllers in building systems, including single air-conditioning units [25, 26], VAV systems [27-31], radiant heating systems [32, 33], building envelope[34], and whole HVAC systems [35-38]. Despite the reported benefits after the successful controller tuning, the model-free RL controllers are subject to the issues such as the long training period and stability issues.

There exist several studies on developing the RL strategies for the commercial building VAV systems. Yuan et al. [29] applied the Q-learning-based RL in both single-zone and multi-zone VAV systems to optimize the supply airflow rate. Despite the achieved energy saving over the baseline control, details on the baseline control are unclear. In addition, it is not clear whether the control design of the AHU-level control loops is considered or not. Wei et al. [39] used deep Q network (DQN) algorithms for the optimal airflow control of the multi-zone VAV systems. The simulation experiments demonstrated the DRL-based algorithm was more effective in an energy cost reduction compared with the rule-based controllers. Hanumaiah et al. [40] proposed a distributed multi-agent DRL framework for the optimal control of multi-zone systems. The impact of the reward ratio and the weather on different model-free RL performances was discussed. Ding et al. developed a model-based RL with a model predictive path integral control method to the multi-zone VAV. The results showed that the proposed controller could achieve 10.65% more energy savings compared to the rule-based benchmark while maintaining similar thermal comfort.

Furthermore, the training time was reduced significantly compared to the model-free RL benchmark.

Although the aforementioned literature review demonstrates the energy saving potential of the intelligent control strategies, there exist few studies that compare the performance of intelligent controllers with the high-performance rule-based control sequences of operation, i.e., ASHRAE Guideline 36. In addition, the benchmark control strategies in most existing evaluation studies are the PID, bang-bang, and ON/OFF controllers, which are not worthy of comparison. For example, the benchmark rule-based controller for the zone air temperature (ZAT) controller is the on-off control in Ref. [39], which makes the reported high energy savings from the DRL controller inconvincible. Essentially speaking, the GLD36 SOO is much simpler compared to the OBC and RL controllers. The heuristic rules in GLD36 could improve the energy efficiency; however, the improvement may be constrained by the incapability of predictive and adaptive learning. OBC and RL controllers have their own obvious challenges and limitations, which prevent their wide applications in the field at the current stage.

In this context, this study presents an energy performance comparison of GDL36 SOO and two types of intelligent controllers within the same building virtual testbed. This chapter is organized as follows. Section 3.3 describes the case study description and the experiment testbed. Section 3.4 details the formulation and implementation of the optimization-based controller (OBC) and deep reinforcement learning-based controller (DRLC). Section 3.5 discusses the energy efficiency comparison results of these two intelligent controllers and the ASHRAE Guideline 36.

3.4 Description of Case Study

This case study aims to compare the energy efficiency and thermal comfort performance of the intelligent controllers with ASHRAE Guideline 36 for a multi-zone VAV cooling system,

which is a typical HVAC system configuration in commercial buildings. The energy efficiency is reflected by the cooling energy use for the whole HVAC system and the total ZAT violation during the system operation hours (i.e., 7 am – 7 pm).

$$E_{Coo,tot} = \sum_{t_0}^{t_N} E_{HVAC}(t_i) = \sum_{t_0}^{t_N} E_{Fan}(t_i) + \sum_{t_0}^{t_N} E_{Plant}(t_i) \tag{3-3}$$

$$dt_{tot}(t_0, t_N) = \sum_{z \in Z} \sum_{t_0}^{t_N} |s_z(t_i)| \tag{3-4}$$

where N is the sampling number for each operation time step point t. E_{Fan} and E_{Plant} are the energy use for the AHU fan and the plant system. z is the zone index for the set of zones, and s_z is the deviation from the lower and upper setpoint temperatures. The zone air cooling temperature setpoint is 24 ℃, and the allowable deviation in this study is ± 0.5 ℃ from the setpoint.

Since the published version of GDL36-2018 only contains the control sequences on the airside systems, this study focuses on the comparison of the rule-based airside high-performance sequences with the intelligent controllers. Another assumption is that the comparison is conducted at the supervisory level, which is the overall control of the local subsystems [41]. For the airside control SOO of multi-zone VAV systems in GDL36, there exist several critical supervisory level controls, e.g., AHU supply air temperature (SAT) reset and static differential pressure (DP) setpoint reset, and economizer damper controls. In this comparison study, the first two controls are replaced by the counterpart in two intelligent controllers. For the AHU SAT reset, as shown in Figure 3-2(a), the SAT is reset based on the outdoor air temperature (OAT) and the setpoint request from the zone terminal units to find a balance between the fan energy and cooling energy. To be specific, the setpoint shall be reset from minimum cooling SAT (*Min_ClgSAT*) when the outdoor air temperature is maximum OAT (*OAT_Max*) and above, proportionally up to maximum SAT (*T-max*) when the outdoor air temperature is minimum OAT (*OAT_Min*) and below. *T-max* is reset

using T&R logic based on the zone-level reset requests between *Min_ClgSAT* and maximum cooling SAT (*Max_ClgSAT*).

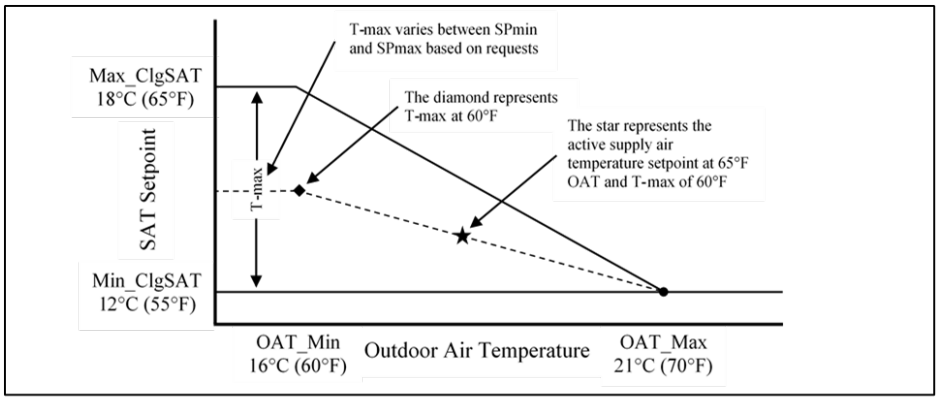

(a)

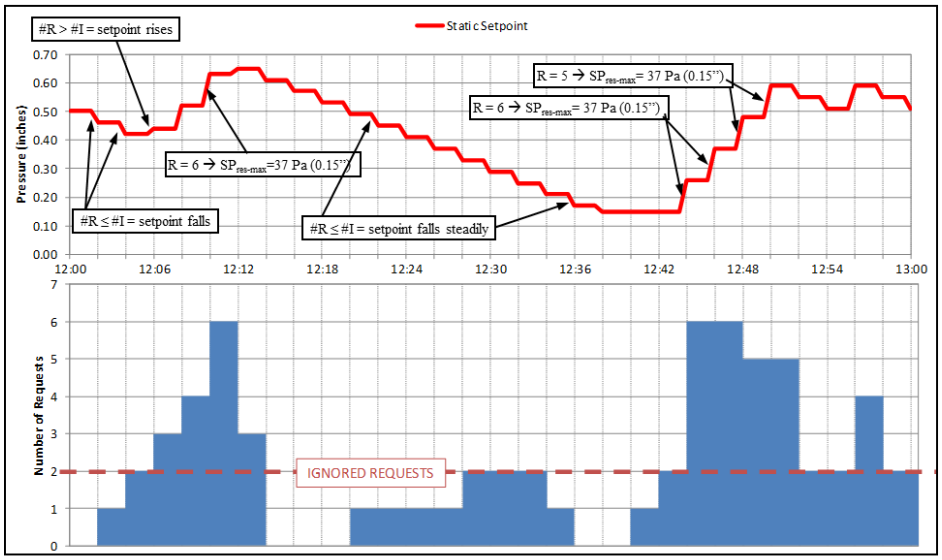

(b)

Figure 3-2 Schematics of the principle of (a) SAT reset (b) Static DP reset in GDL36 (excerpt from GDL36-2021)

Figure 3-2(b) depicts the principle of the static DP reset from the T&R logic. Under this control logic, the system will tend towards minimum static pressure but respond to the increasing demand from the zone terminal units. The red cyclic pattern, as shown in Figure 3-2(b) is a general characteristic of a robust T&R loop, and the setpoint is not expected to remain static except at its minimum and maximum values.

Compared to the high-performance SOO in GDL36, the SAT and the static DP will be determined by the optimization in OBC and the control policy in DRLC. To ensure an apples-to-apples comparison, the local controls (e.g., zone-level PID controls) remain the same for the three controllers. Table 3-1 lists the differences of SOO between the three controller types.

Table 3-1 Difference between three controller types.

Supervisory control loop name	**GDL36**	**OBC**	**DRLC**
SAT setpoint reset	Rule-based, i.e., determined by the OAT and zone requests	Determined by the optimization at different control intervals	Determined by the optimal control policy after the training
Static DP reset	Rule-based, i.e., determined from zone requests		

The simulation experiment was for Chicago, IL, USA (ASHRAE climate zone 5A) in two typical weeks of different cooling loads, i.e., a cooling week (07/24-07/31) and a shoulder week (06/09-06/16). The cooling week has a high average outdoor air temperature, and the shoulder week has a mild cooling load which enables a long operation period of the airside economizer. The simulated building was the single-floor five-zone VAV system as described in CHAPTER II under both airside and waterside control sequences of GDL36 [42]. The original model was developed from the GDL36 model in Modelica Buildings Library 7.0.0 [43]. To ease the computational cost, the detailed waterside model was replaced by the data-driven regression model for both the cooling season and the shoulder season, respectively, as shown in Eq. (3-5) and (3-6).

$$P_{pla} = 11188 + 0.18 \cdot \mathrm{Q_{coo}} + 24.24 \cdot \mathrm{T_{db}} - 44.44 \cdot \mathrm{T_{wb}} - 0.05, \quad (3\text{-}5)$$

$$P_{pla} = 726656 + 4.12 \cdot Q_{coo} - 2816.1 \cdot T_{db} - 2638.7 \cdot T_{wb} + 26.2 \cdot H_{gh} -$$
$$0.0037 Q_{coo} \cdot T_{db} - 0.0097 Q_{coo} \cdot T_{wb} + 2.01 \cdot 10^{-5} \cdot Q_{coo} \cdot H_{gh} + 10.2 \cdot T_{db}\, T_{wb} + \quad (3\text{-}6)$$
$$0.16 \cdot T_{db} \cdot H_{gh} - 0.25 \cdot T_{wb} \cdot H_{gh},$$

where Q_{coo} is the cooling load at the cooling coil, T_{db} is the dry bulb outdoor air temperature, T_{wb} is the wet bulb outdoor air temperature and H_{gh} is the global horizontal solar radiation. Table 3-2 shows the statistical metrics of the regression model. The coefficient of determination (R2), root mean square error (CV-RMSE), and normalized mean bias error (NMBE) both indicate the high accuracy of the regression models. As mentioned earlier, the system is sized under the ASHRAE climate zone 5A Chicago, IL [44, 45].

Table 3-2 Regression model accuracy statistical results

Regression model	Model type	R2	CV-RMSE	NMBE
Cooling season model	Linear	0.99	2.1%	1.3%
Shoulder season model	Interactions linear	0.99	3.2%	2.3%

3.5 Controller Formulation and Implementation

The formulation and implementation of OBC are described in Section 3.4.1. In Section 3.4.2, the experimental setups of DRLC are illustrated.

3.5.1 OBC

The OBC in this study was formulated as a set of bi-objective optimization problems to minimize the HVAC total energy consumption while maintaining the ZAT within the comfort bound. Let Γ be the experiment time (1 week in this case), and *N* be the number of optimization intervals. Within the i^{th} optimization interval ($i \in [0,1\ldots, N\text{-}1]$), the objective function (i.e., a given

function that results in the minimum or maximum output from the function) is represented in Eq. (3-7).

$$\boldsymbol{J_i} \min_{u} \; E_{HVAC,i}(u,x) + \alpha \cdot dT_{vio,i}(u,x), \tag{3-7}$$

where $\boldsymbol{J_i}$ is the control objective as a function of both system state vector x and control input vector u at the i^{th} optimization period. Control inputs u are the AHU SAT setpoint and the static DP setpoint, which are bounded within [12 ℃,18 ℃] and [25 Pa,410 Pa], respectively. $E_{HVAC,i}(\cdot)$ and $dT_{vio,i}(\cdot)$ are the functions of HVAC energy consumption and ZAT violation. α is the penalty coefficient, which prioritizes reducing energy consumption versus maintaining thermal comfort. In this study, we assume a perfect model prediction in OBC and use the same model as discussed in Section 3.3 to calculate power consumption and temperature deviations. The optimal control setpoints in the experiment are thus determined through OBC.

For the implementation, Dymola Optimization library version 2.2.4 was leveraged, which was a commercial package that provides tools for the multi-objective optimization of modeled Modelica systems in Dymola. The simplex method was adopted as the optimization algorithm due to its fast computation speed as a local method. This method was explored with an acceptable performance in similar optimal control problems of HVAC systems [46, 47].

Figure 3-3 depicts the workflow of the OBC in Dymola and associated pseudo code. For the i^{th} optimization interval, the optimized setpoints are obtained through running the Optimization Library. Then the system states are rolled back and the Dymola model is simulated with the optimized setpoints. After that, the states at that time step are saved. This procedure is iterated until the end of the experiment. In this study, different lengths of the optimization interval (also control interval) are studied: 15 minutes, 30 minutes, 1 hour, 2 hours, and 4 hours.

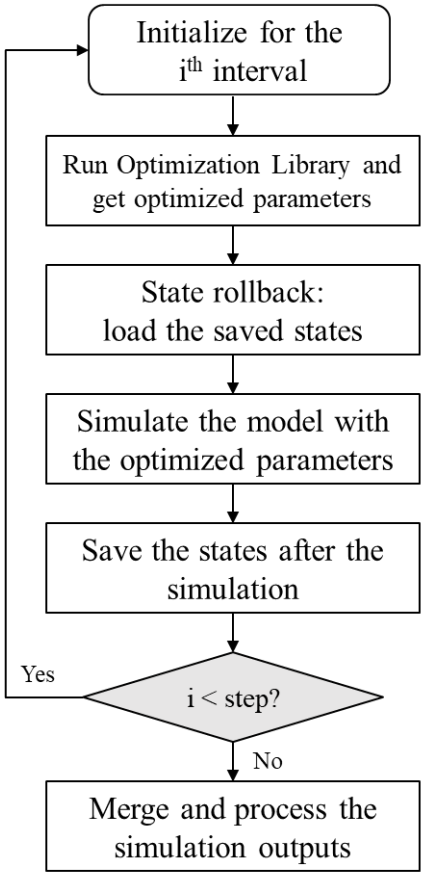

(a)

```
for i in 1:steps loop

  Optimization.Airside.GDL36 (startTime, stopTime);
  Lines=Modelica.Utilities.Streams.readFile("Optimizatio
  nBest.txt"); TSuplin=Lines[4];
  TSupopt=Modelica.Utilities.Strings.scanReal(TSuplin);
  dpStalin=Lines[5];
  dpStaopt=Modelica.Utilities.Strings.scanReal(dpStalin);

  importInitial("dsfinal_"+String(i-1)+".txt")


  simulateExtendedModel("VAVReheat.Guideline36MPC",
  initialNames={"conAHU.TSupSetOcc","conAHU.dpStaS
  et"}, initialValues = {TSupopt,dpStaopt},
  startTime,stopTime, method="Cvode",
  tolerance=1e-6,resultFile = "dsres"+String(i));

  system("copy dsfinal.txt dsfinal_"+String(i)+".txt");


end for;
```

(b)

Figure 3-3 (a) Workflow (b) Pseudo codes of OBC implementation in Dymola

3.5.2 DRLC

Similarly, the DRLC is formulated to minimize the HVAC total energy consumption while mitigating the ZAT violation by adjusting the AHU SAT setpoint and the AHU static pressure setpoint. Figure 3-4 depicts the DRLC formulation. The reward R for the DRL is shown in Eq. (3-8), similar to the objective function for OBC in Eq. (3-7).

$$R_i = E_{HVAC,i} + \alpha \cdot dT_{vio,i}\ , \tag{3-8}$$

where $E_{HVAC,i}$ are the HVAC energy consumption and $dT_{vio,\mathrm{i}}$ are and ZAT violation at the i^{th} control interval (i.e., 15 minute each). α is the penalty coefficient that balances the energy consumption and thermal comfort.

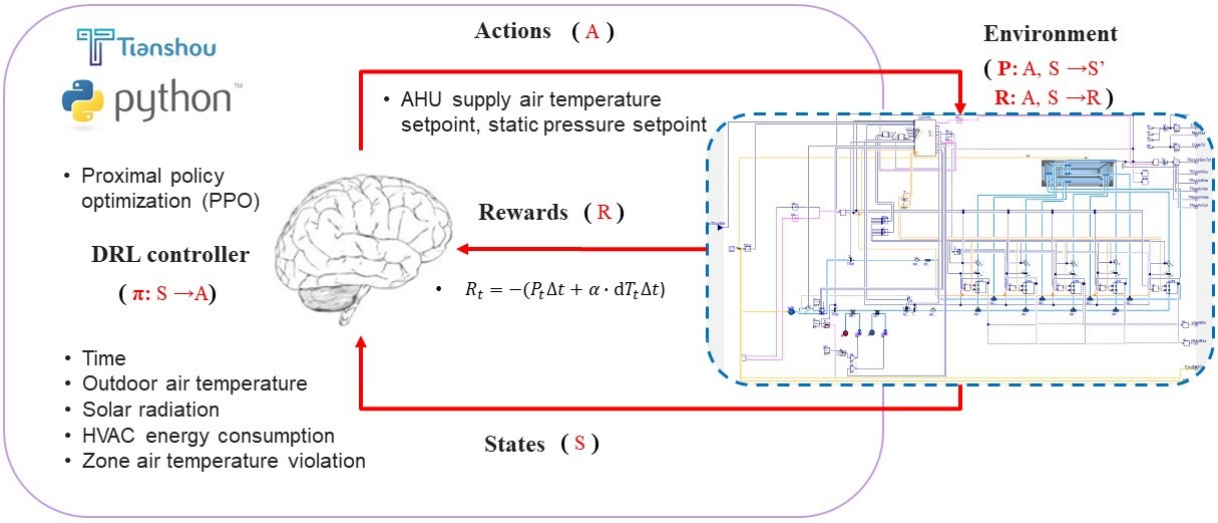

Figure 3-4 Schematics of DRLC formulation and implementation

The control actions are bidimensional and the action space is a continuous space to avoid the curse of the dimension in the discretized action space. The states are determined based on HVAC engineering knowledge. We consider three different state spaces, as shown in Table 3-3. The commonly used states are time, outdoor air temperature, solar radiation, HVAC energy consumption, and ZAT violation. The simulation environment is the same GDL36 model as described in Section 3.3 which provides the reward value (*R*) and next observations (*S'*) during the interaction with the DRLC.

Table 3-3 Summary of different state design

State Space	Number of States	State Variables
S1	7	time, outdoor air temperature, solar radiation, and HVAC energy consumption, ZAT violation, fan speed, maximum/minimum zone terminal damper position
S2	6	time, outdoor air temperature, solar radiation, HVAC energy consumption, ZAT violation, fan speed
S3	5	time, outdoor air temperature, solar radiation, HVAC energy consumption, and ZAT violation

For the implementation, a flexible containerized framework [48] is leveraged where the building model is interfaced with the state-of-the-art DRL library Tianshou [49] through the functional mockup unit (FMU). Tianshou is a highly modularized DRL library in Python based on pure PyTorch [50] and has supported more than 20 classic algorithms. Tianshou's performances are reported to be comparable or better than the best reported results for most algorithms in the open literature [49]. In this study, the Proximal Policy Optimization (PPO) [24] is selected as the DRL algorithm because it suits the continuous action space in our case. In addition, PPO is demonstrated to perform the same or better than state-of-the-art approaches and is simpler for users to implement and tune algorithms. Still, several critical hyperparameters in PPO need to be tuned [51]. For example, Step Per Collect (also called Time Horizon), i.e., how many steps to collect before adding it to the experience buffer; Batch size (also called Minibatch), i.e., how many experiences are used for each gradient descent update; and Updated time, i.e., how many times the data collected are reused, etc. are hyperparameters that could have significant impacts on the DRLC performance.

To fine-tune the proposed DRLC, various factors are considered, including the penalty coefficient, the state design, the deep neural network architecture, and critical hyperparameters. The penalty coefficient α was first swept to determine the appropriate value based on the resulting reward value. Then different common values are grid-searched in other aspects to find the best hyperparameters. Table 3-4 lists the sweeping parameters for tuning the DRLC. The DRL policy is trained and tested for 800 epochs in each scenario (i.e., different combinations of parameters). One epoch length is one week. The computation time for one epoch training takes around 10 minutes on a Windows 10 machine with Intel® Core™ i5-9500 @3.00 GHz CPU and 16 GB RAM. That being said, the training time for 800 epochs would be around 5.5 days. Due to the large

computation cost for the hyperparameter tuning of the DRLC, different scenarios are assigned to different cores in the high-performance computing cluster.

Table 3-4 Sweeping parameters for DRLC tuning considering various factors

Aspects	State design	Entropy coefficient	Step per collect	Batch size	Repeat per collect	State normalization	Advantage normalization	Value Clip	DNN architecture
Value	S1, S2, S3	0, 0.01	384, 512	64, 128	5, 10	True, False	True, False	True, False	$[128]^3$,$[128]^4$, $[128]^5$
Number	3	2	2	2	2	2	2	2	3

3.6 Results and Discussion

In this section, the simulation experimental results for the OBC and DRLC after fine-tuning are reported, respectively in Section 3.5.1 and Section 3.5.2. Section 3.5.3 presents a comparison of two intelligent controllers with GDL36 SOO.

3.6.1 OBC

3.6.1.1 Tuning of Penalty Coefficient α

As mentioned earlier in Section 3.4.1, different α values decide on the balance of the HVAC energy consumption and thermal comfort. Figure 3-5 depicts one example of the effect of α in the cooling season week. It can be seen that a small α corresponds to a smaller HVAC energy consumption but a larger temperature violation and vice versa. With an α larger than 25, the OBC could achieve the same level of thermal comfort but also a modest energy saving. Therefore, for the cooling season, we use the value of 25 for α. Similar investigation was conducted for the shoulder season, and the value of 25 was also selected.

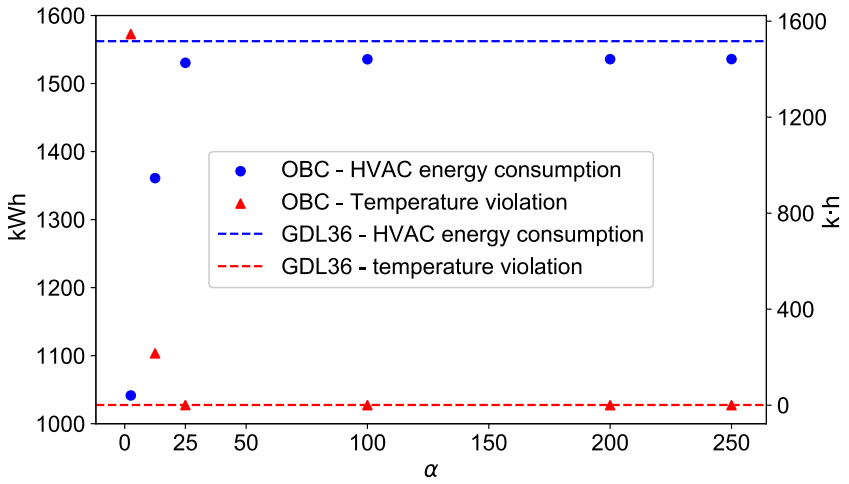

Figure 3-5 The HVAC energy consumption and ZAT violation under different α values

3.6.1.2 Cooling Season Results

The OBC performance in the cooling season week (07/24-07/31) under different control intervals are reported and discussed in this section. Table 3-5 summarizes the results for all the OBCs and the GDL36 controller. For aesthetic reasons (avoid line overlapping), Figure 3-6 to Figure 3-9 only depict two representative OBCs with 30 minutes (denoted as OBC-30min) and 2 hours (denoted as OBC-2h) as the control interval.

Table 3-5 summarizes the results for all the OBCs and the GDL36 controller, including the HVAC energy consumption, ZAT violation, and the integrated objective function. For the cooling season week, the OBC with the smallest control interval (i.e., 15min) has the lowest energy consumption and ZAT violation. However, such savings are very marginal to the OBC-30min and OBC-1h. For the control interval larger than 2h, the ZAT violation could not be maintained at the comparable level of GDL36 SOO.

Table 3-5 Summary results for all the OBCs and the GDL36 controller in the cooling week

Controller	HVAC Energy Consumption, kWh	HVAC Energy Saving Ratio, %	ZAT Violation, K·h	ZAT Violation Improvement, %	Objective Function, -	Objective Function Saving Ratio, %
GDL36	1562.3	-	1.02	-	2.29	0.00%
OBC-15min	1528.0	2.20%	0.37	63.73%	2.21	3.49%
OBC-30min	1530.4	2.04%	0.54	47.06%	2.22	3.06%
OBC-1h	1533.6	1.84%	0.75	26.47%	2.24	2.18%
OBC-2h	1522.7	2.53%	1.53	-50.00%	2.25	1.75%
OBC-4h	1477.8	5.41%	43.06	-4121.57%	3.68	-60.70%

Figure 3-6 depicts the detailed time series of optimal setpoints and HVAC energy consumption under GDL36, OBC-30min, and OBC-2h during 07/24-07/31. From Figure 3-6(a) and (b), the three lines of setpoints generally follow a similar trend except at the early hour each day. Especially, for the OBC-30min, the static DP setpoint is at the highest level at the early hour. This is because the optimizer tries to minimize the ZAT violation by providing more air flows. The oscillation of static DP setpoints is observed for the GDL36 SOO due to the T&R control while that of OBCs barely appears. Figure 3-6(c) indicates that the HVAC power consumption for the three controllers is in a similar range in the cooling season week.

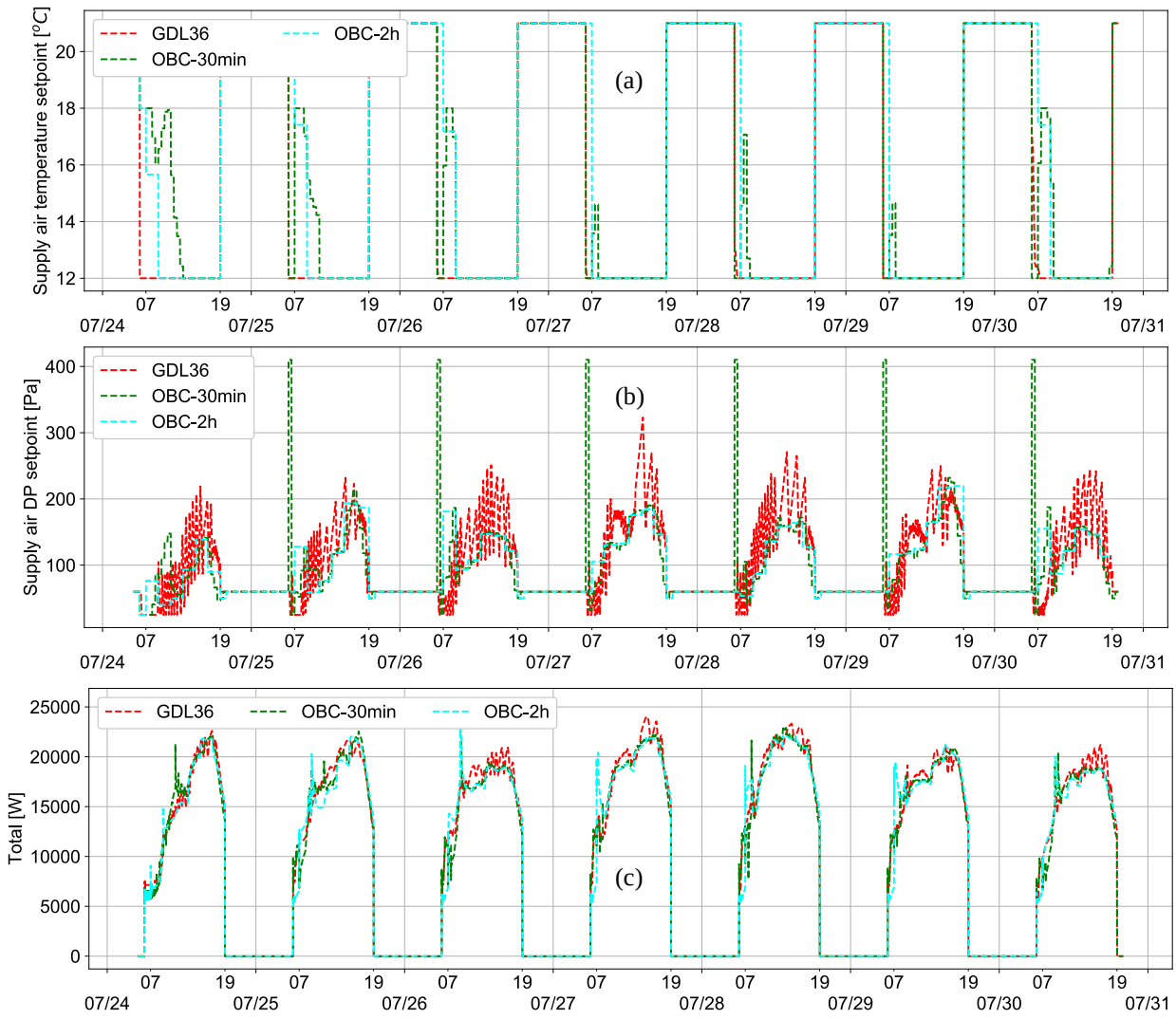

Figure 3-6 Time series of (a) SAT setpoint (b) static DP setpoint (c) Total HVAC power consumption during cooling season week for OBCs

Figure 3-7 shows the detailed energy results for the whole HVAC system and subsystems. It can be seen that the controllers share a similar power consumption profile with the OBC controllers expending slightly less power consumption.

Figure 3-8 is the time series plot for the five-zone air temperatures in the cooling season week. There are more oscillations for ZAT in GDL36 SOO due to the coordination between the T&R control and zone-level control. It is also noted that the ZAT under OBCs has more time wandering near the upper and lower bounds compared to the GDL36 SOO. In addition, the ZAT

in OBC-2h has a larger violation than that in OBC-30min in some zones (e.g., west, north, and core zones), especially in early and late hours each day. This is because a 2-hour control interval is not short enough to control the zone air temperature within the comfort bound at a certain period.

Figure 3-9(a) depicts the box plot of the ZAT distributions. The OBCs have a dense distribution near the upper bound compared to the GDL36. Figure 3-9(b) illustrates the accumulated ZAT violation through the week and we can also verify that the OBC with a control interval of 2h has a larger violation than the GDL36.

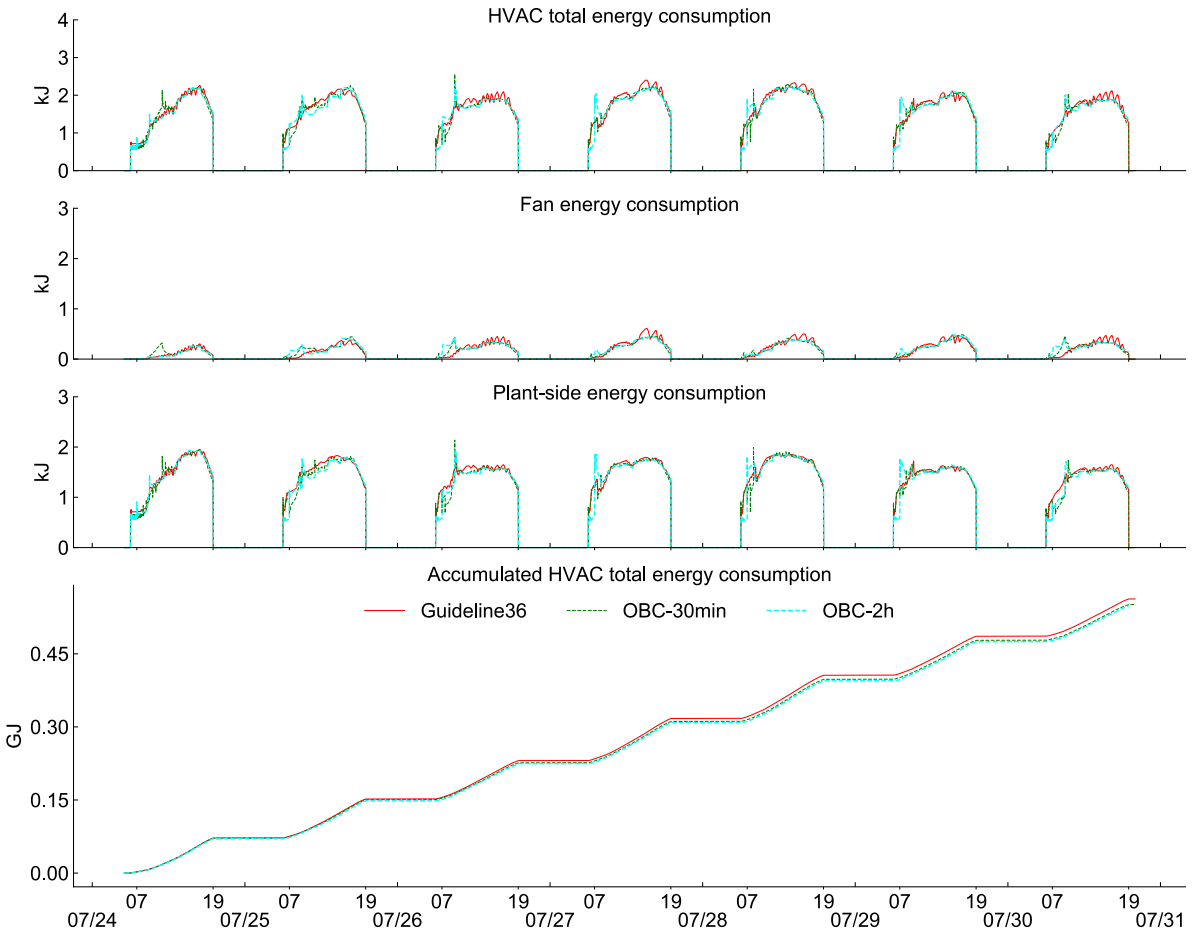

Figure 3-7 Detailed energy results for the whole HVAC system and subsystems in the cooling season week for OBCs

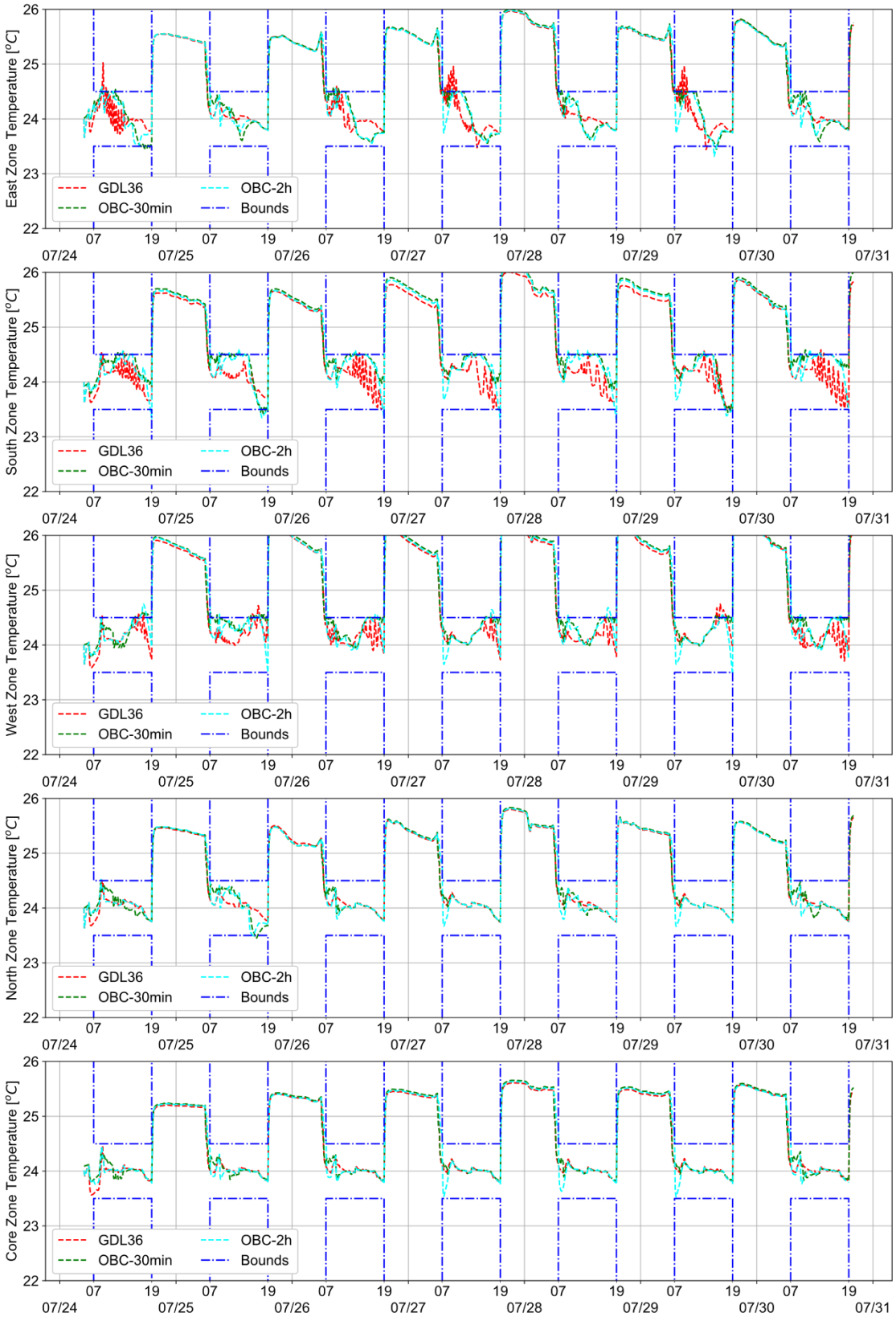

Figure 3-8 Time series of ZAT in cooling season week for OBCs

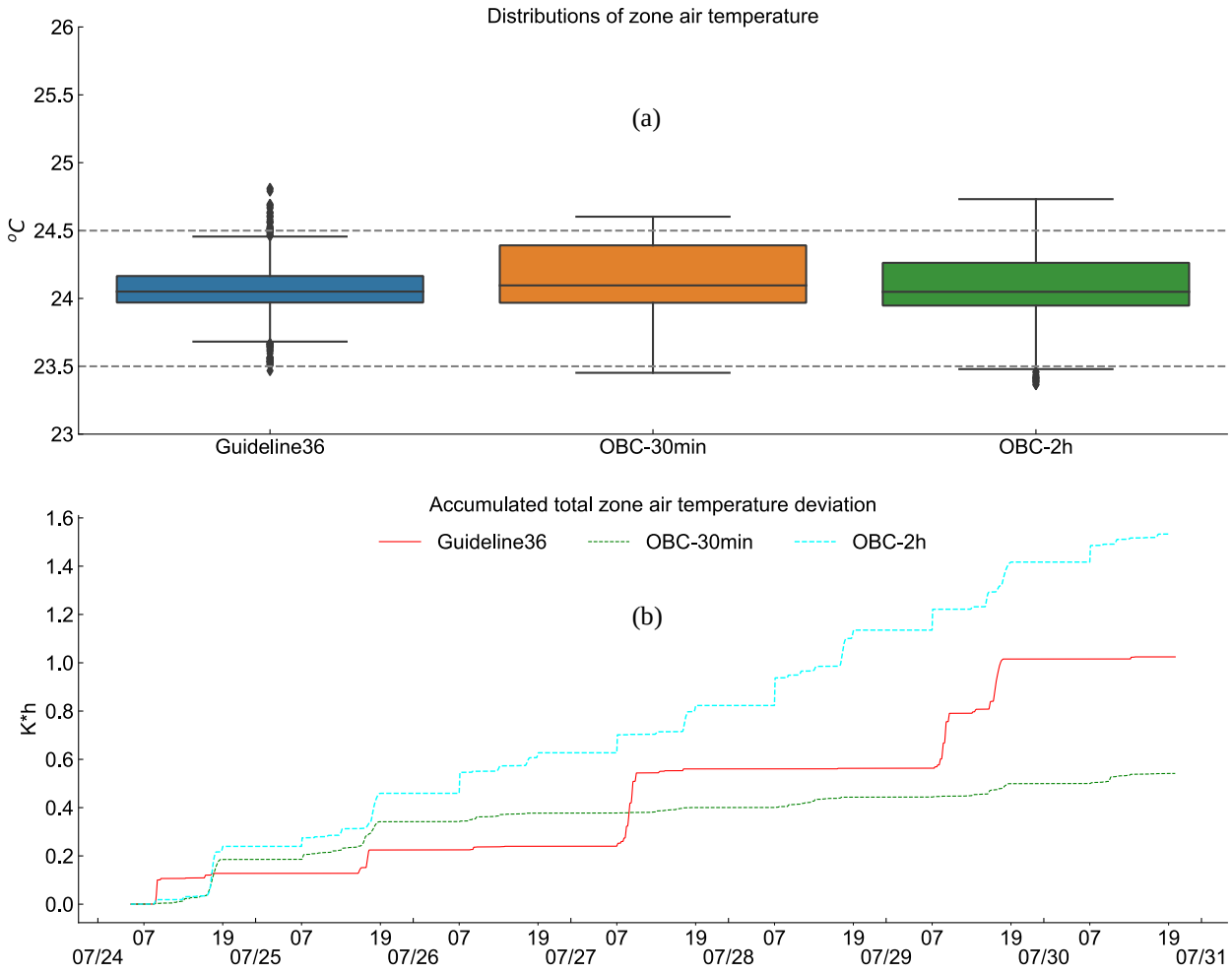

Figure 3-9 (a) Box plot of ZAT distribution (b) accumulated ZAT violation in cooling season week for OBCs

3.6.1.3 Shoulder Season Results

The OBC performance in the shoulder season week (06/09-06/16) under different control intervals are reported and discussed in this section.

Table 3-6 summarizes the results for all the OBCs and the GDL36 controller in the shoulder season week, including the HVAC energy consumption, ZAT violation, and the integrated objective function. Unlike the results in cooling season week, OBC with the smallest control interval (i.e., 15min) does not have the lowest energy consumption and ZAT violation probably due to the continuous ramping of the control setpoints. Instead, the OBC-30 min has the least

integrated cost with an energy saving ratio of 7%. Similar to the cooling season week, with the control interval larger than 2h, the ZAT violation could not be maintained at the comparable level of GDL36 SOO.

Table 3-6 Summary results for all the OBCs and the GDL36 controller in the shoulder week

Controller	HVAC Energy Consumption, kWh	HVAC Energy Saving Ratio, %	ZAT Violation, K·h	ZAT Violation Improvement, %	Objective Function, -	Objective Function Saving Ratio, %
GDL36	1197.7	0.00%	1.39	0.00%	1.77	0.00%
OBC-15min	1125.6	6.02%	0.48	65.47%	1.64	7.34%
OBC-30min	1114.0	7.00%	0.51	63.31%	1.62	8.47%
OBC-1h	1117.6	6.69%	0.64	53.96%	1.63	7.91%
OBC-2h	1118.1	6.65%	1.83	-31.65%	1.68	5.08%
OBC-4h	1102.0	8.00%	31.22	-2146.04%	2.71	-53.11%

The following analysis explains why a larger HVAC energy saving ratio was achieved in the shoulder season week. Figure 3-10 depicts the detailed time series of optimal setpoints and HVAC energy consumption under GDL36, OBC-30min, and OBC-2h in the shoulder season week. Figure 3-10 (a) and (b) show the optimal SAT setpoint and static DP setpoint. Different from the cooling season results, the optimal setpoints for the OBCs have more upwards and downwards ramping in the shoulder season to balance the cooling and fan energy consumption. It is apparent that on the Day of 06/10, the OBCs save more HVAC energy consumption than the other day. Detailed results are shown in Figure 3-11. The economizer was enabled during the whole day. According to the GDL36 SOO, the SAT setpoint was reset to the maximum value in order to fully utilize the outdoor air. However, cooling loads in some zones cannot be covered and

thus the static DP was increased based on the zone requests. In contrast, the SAT setpoints determined by the OBC were generally equal to or slightly lower than the outdoor air temperature. In this way, the cooling energy from the plant system did not increase a lot. The zone cooling loads were met, and the fan energy was saved. For the energy efficiency performance of the other days, the OBCs perform at parity with or slightly better than GDL36.

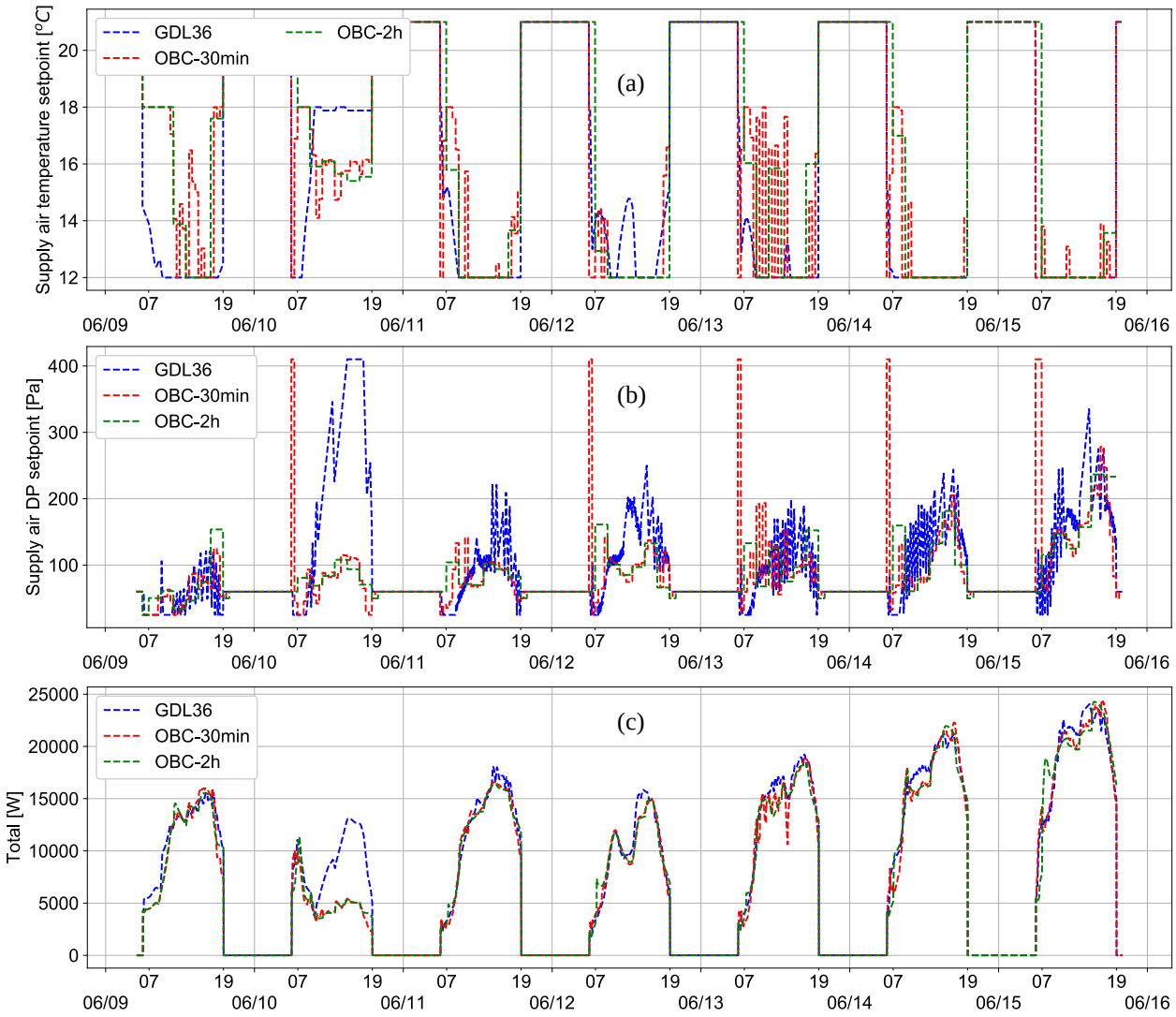

Figure 3-10 Time series of (a) SAT setpoint (b) static DP setpoint (c) Total HVAC power consumption during shoulder season week for OBCs

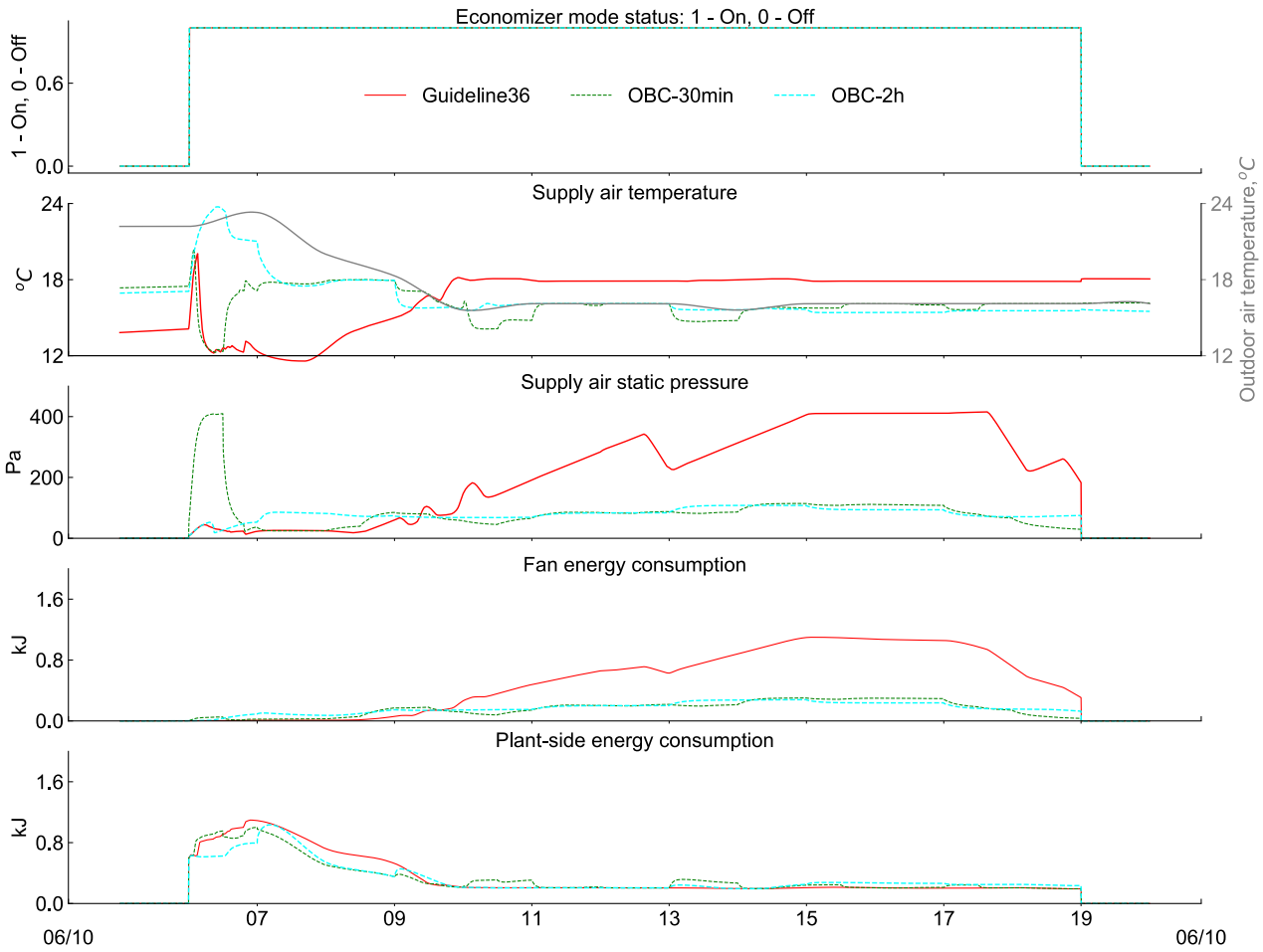

Figure 3-11 Time series of different spots on Day 06/10

Figure 3-12 is the time series plot for the five-zone air temperatures in the shoulder season week. Similar observations can be found: (1) more oscillations for ZAT were found in GDL36 SOO due to the T&R controls; (2) ZAT under OBCs are generally closer to the upper and lower bounds but has less violation in critical zones (e.g., south zone and west zone) compared to the GDL36 SOO; (3) The OBC with the control interval of 2h has a larger violation than the GDL36. These observations could also be verified by the ZAT distribution and accumulated ZAT violation plots, as shown in Figure 3-13.

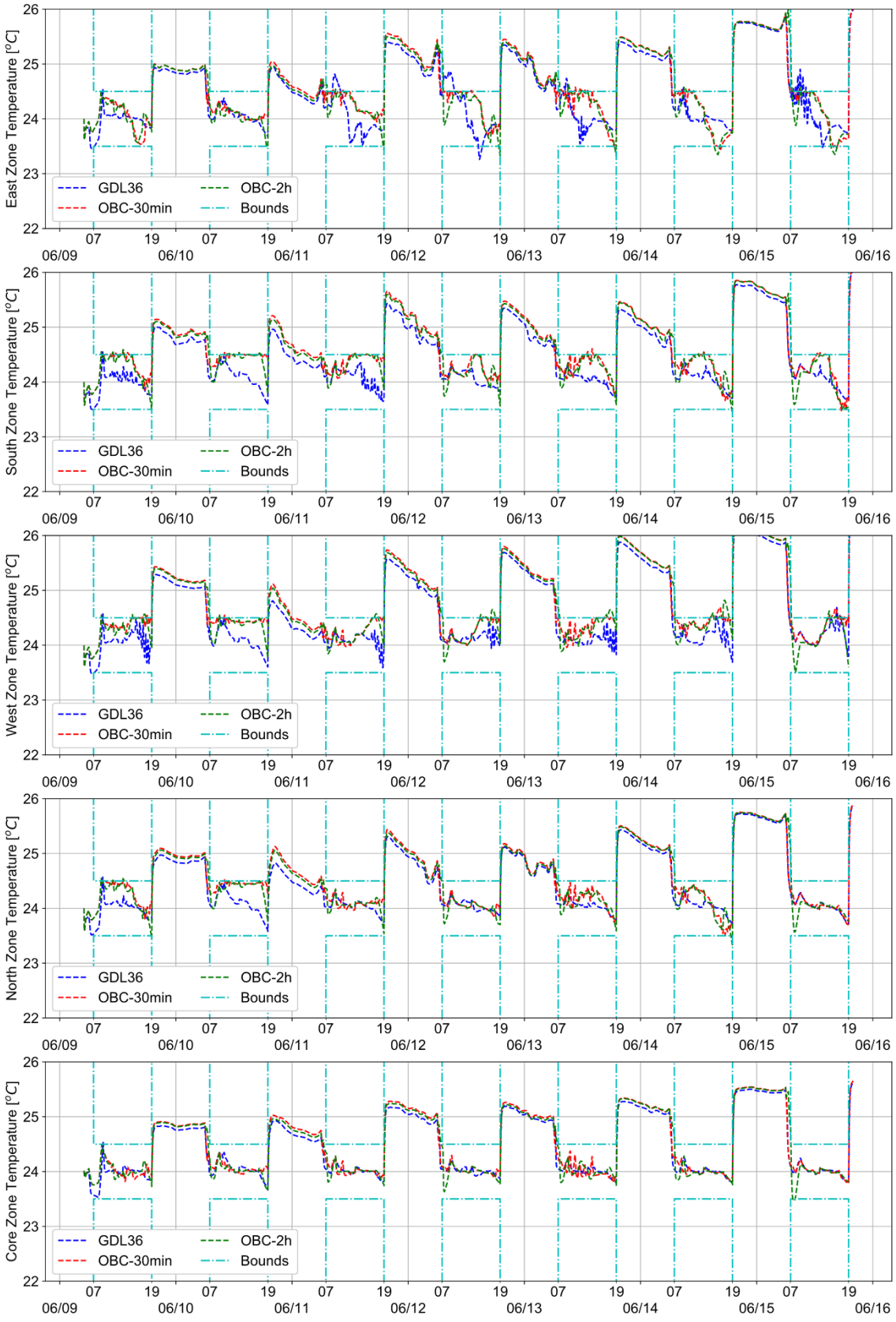

Figure 3-12 Time series of ZAT in shoulder season week for OBCs

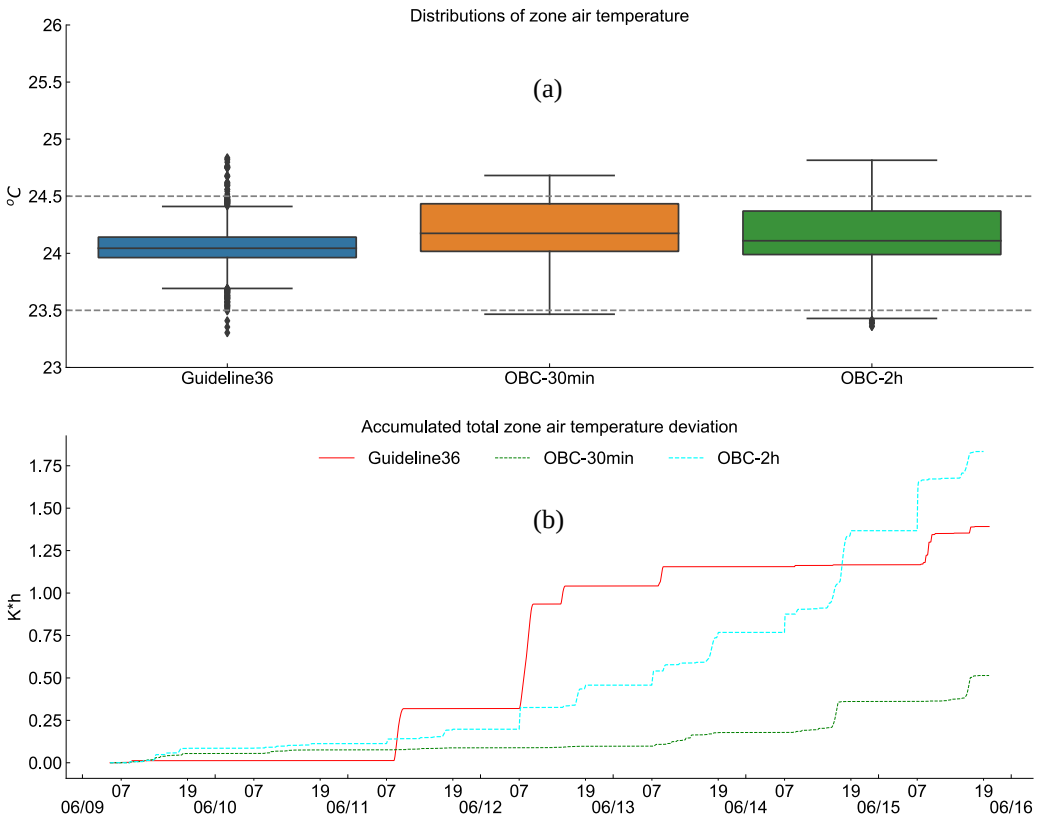

Figure 3-13 (a) Box plot of ZAT distribution (b) accumulated ZAT violation in the shoulder season for OBCs

3.6.2 DRLC

In this section, the experimental results for DRLC after the hyperparameter tuning are reported analyzed. Recall that for each scenario (i.e., the combination of the hyperparameters), the DRL policy has been trained and tested for 800 epochs (each epoch denotes one week).

3.6.2.1 Cooling Season Results

Figure 3-14 illustrates the rewards under different scenarios using the parallel coordinate plot. Each line denotes one epoch under different combinations of the hyperparameters. The color of the line represents the reward value. The redder represents the higher reward value, while the bluer represents the lower reward value. The reward value of the GDL36 SOO is annotated in the color bar on the right side. It can be seen that the DRLC under the cooling season needs to be

trained for at least 300 epochs. The larger number of Step Per Collect and Repeat Per Collect is generally beneficial to the final rewards but increases the DRLC training time.

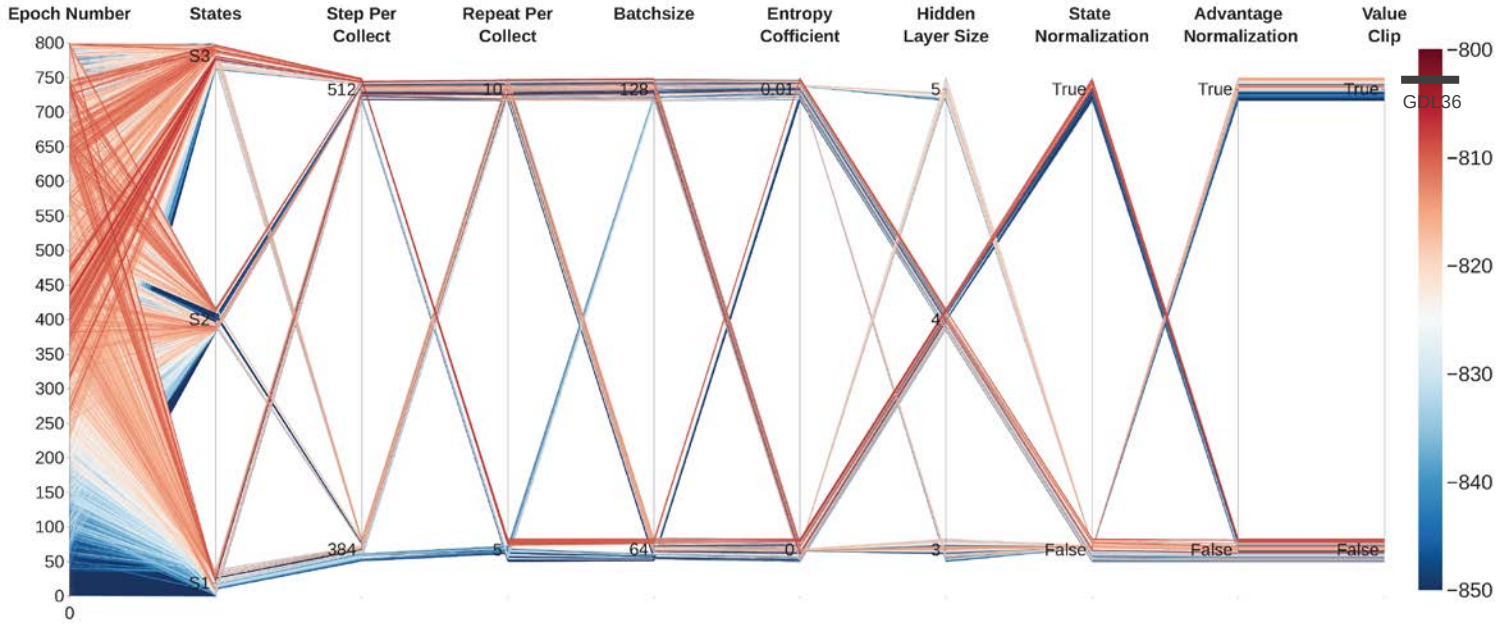

Figure 3-14 Parallel coordinate plot of rewards under different scenarios in the cooling season

Figure 3-15 shows the reward evolution throughout the epochs for the best scenario in the cooling season week. The hyperparameter setting for the best scenario is also provided. The blue line represents the entire reward for the GDL36 SOO. It can be seen that after 800 epochs of training, the DRLC performance in the cooling season week could nearly chase up with the GDL36 SOO in terms of the reward. The HVAC energy consumption for the best scenario of DRLC increases 2.2% compared to the GDL36 SOO while decreasing 0.83 K·h temperature violation in the cooling season week. This indicates the energy efficiency performance of GDL36 SOO is comparable to DRLC in the cooling week for this specific study. In addition, the DRLC is still subject to the curse of the high training time to achieve comparable performance. Figure 3-16 and Figure 3-17 show the detailed energy and thermal comfort results for the DRLC in the cooling season week.

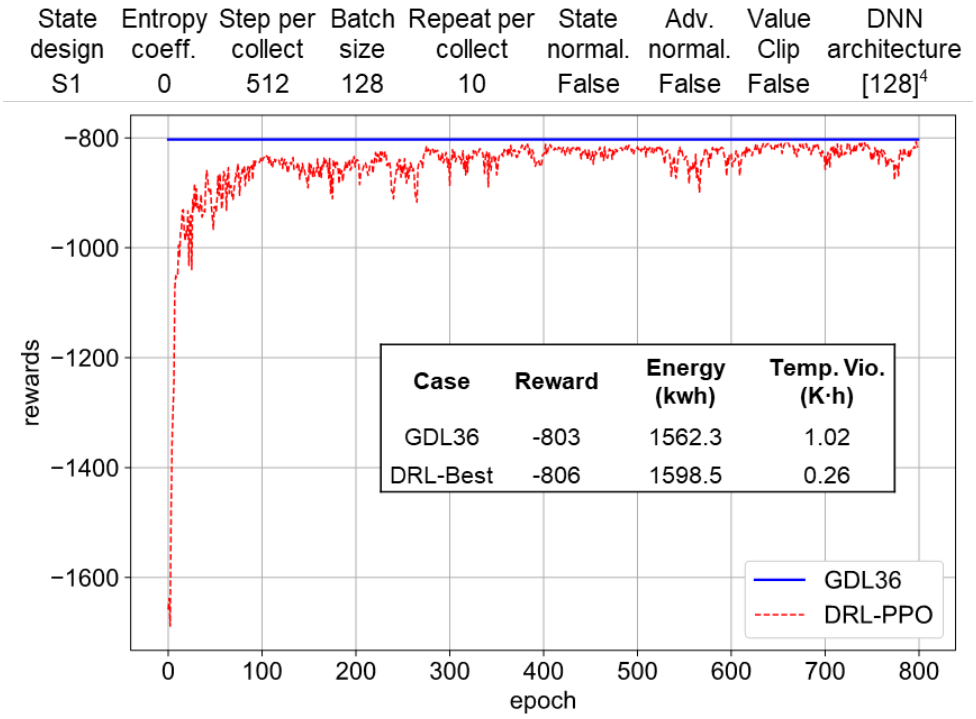

Figure 3-15 Reward per epoch for the best scenario in the cooling season

Compared to the SAT setpoints in GDL36 staying at the lowest value (i.e., 12 ℃), the SAT setpoints have a frequent variation between 12-14 ℃ in the case of DRLC. For the static DP setpoints, the DRLC generally has a higher value throughout the operation hours. Figure 3-16(c) shows that the DRLC lines of HVAC power consumption overlap for most of the days with the GDL36 SOO, while DRLC expending slightly less power consumption at some periods.

For simplicity, instead of visualizing ZAT for five zones, Figure 3-17 depicts the time series of ZAT in critical zones (i.e., east and south zones). Although the DRLC consumes more HVAC energy, it has fewer oscillations of ZAT and less frequent violation out of the bounds.

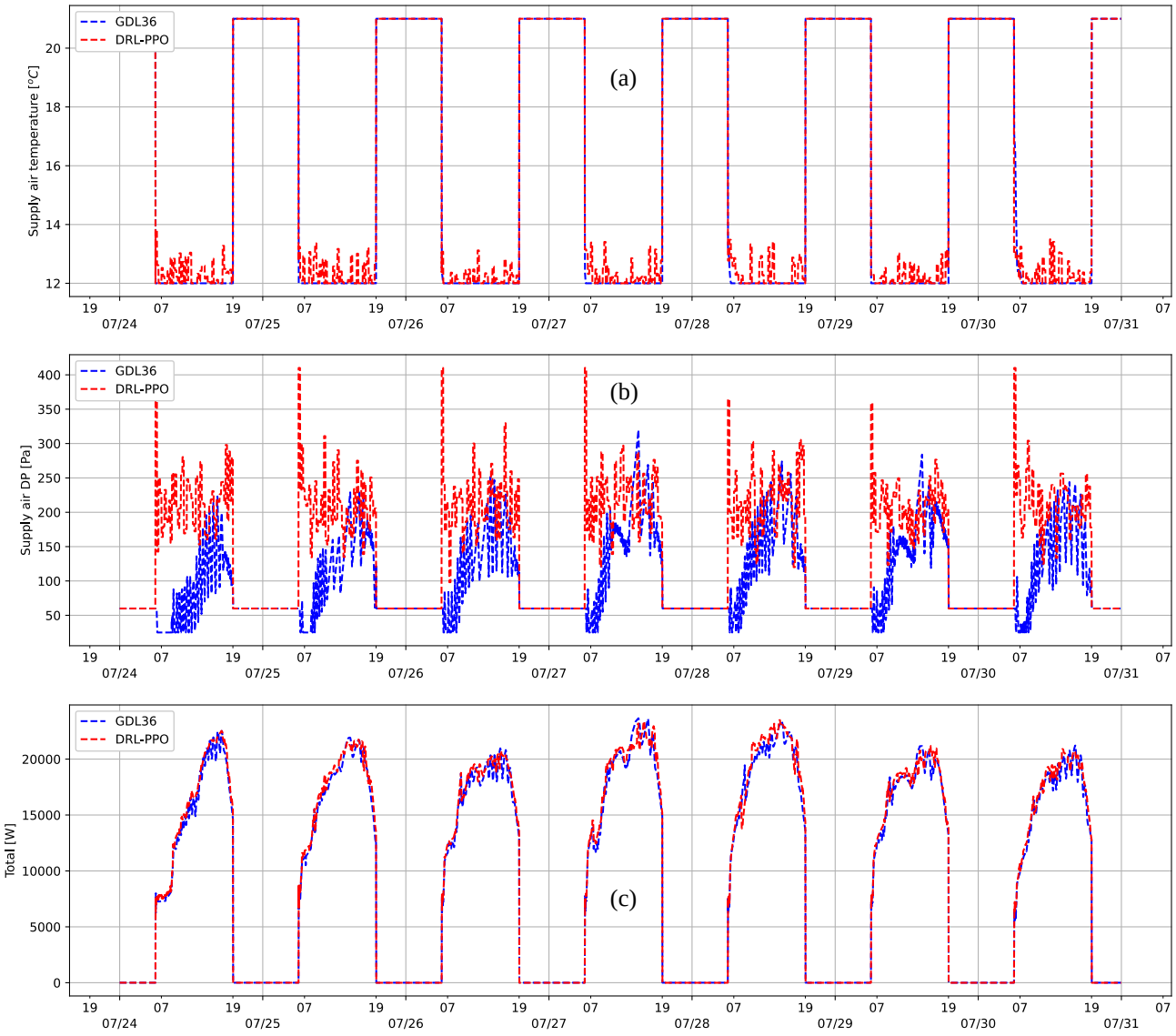

Figure 3-16 Time series of (a) SAT setpoint (b) static DP setpoint (c) Total HVAC power consumption during the cooling season for DRLC

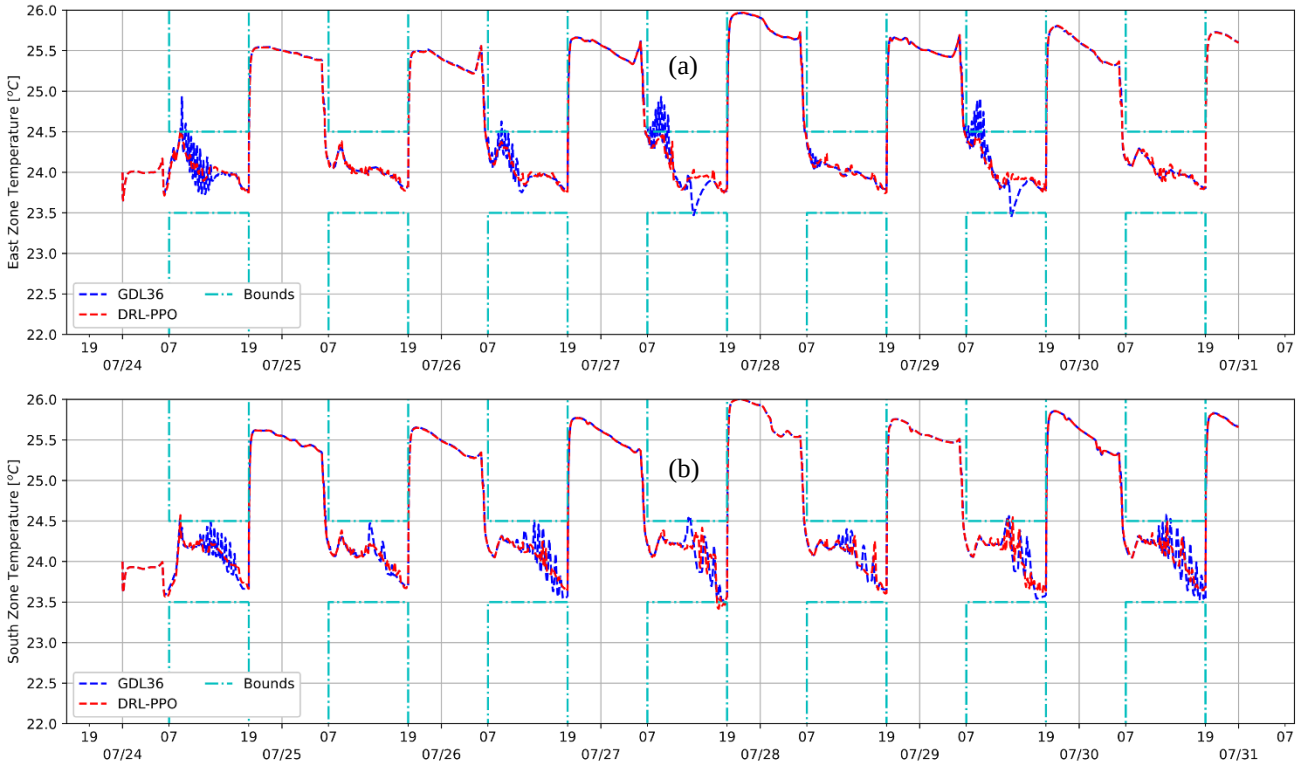

Figure 3-17 Time series of ZAT for (a) east zone and (b) south zone in the cooling season for DRLC

3.6.2.2 Shoulder Season Results

Similarly, the rewards under different scenarios are illustrated in Figure 3-18. The reward value of the GDL36 SOO is annotated in the color bar on the right side. Roughly after 150 epochs' training, DRLC under the shoulder season week could achieve an equivalent level performance with GDL36 SOO. Figure 3-19 depicts the details regarding the best scenario in the shoulder season week. The best reward for the shoulder season week is -596, which is 4.64% higher than the baseline GDL36. The following Figure 3-20 and Figure 3-21 will present the energy efficiency and thermal comfort performance in detail.

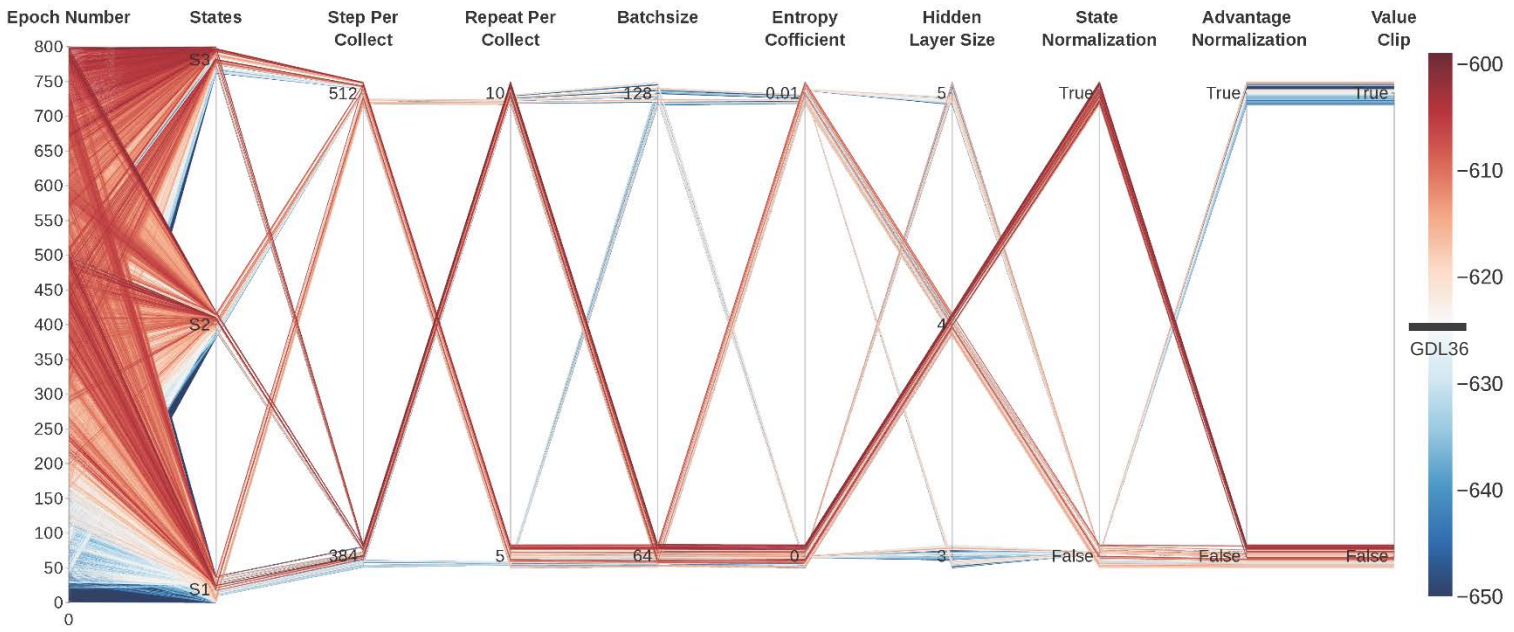

Figure 3-18 Parallel coordinate plot of rewards under different scenarios in the shoulder season

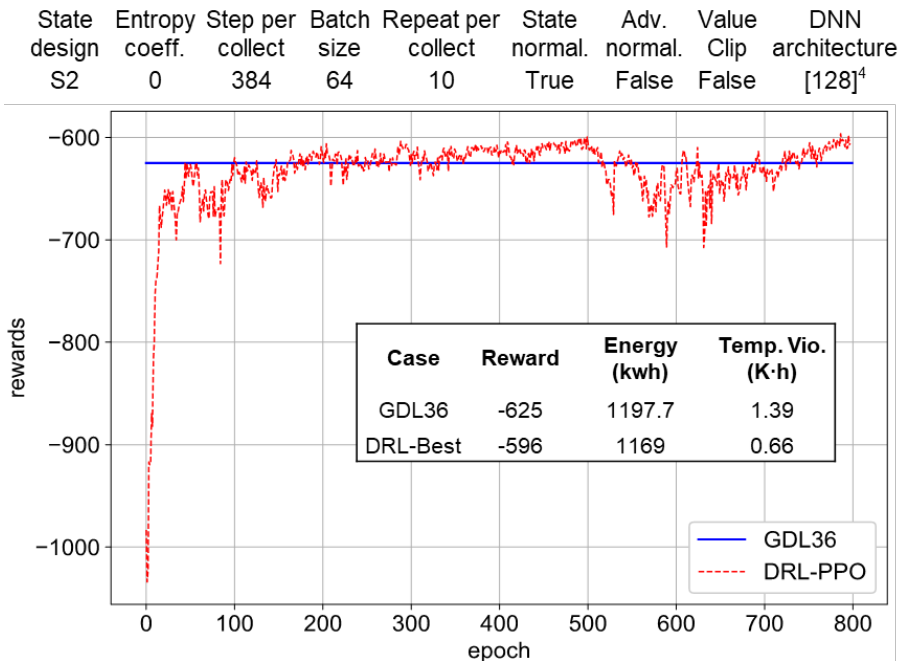

Figure 3-19 Reward per epoch for the best scenario in the shoulder season

Figure 3-20(a) and (b) shows the optimal setpoints for DRLC in the shoulder season week.

From Figure 3-20(c), it is apparent that DRLC could save more energy on day 06/10 than the other

days, which is similar to OBC. However, unlike the OBC energy efficiency performance as shown in Figure 3-10, the DRLC does not save more energy on the other days.

Figure 3-21 shows the ZAT variations in two critical zones: east and south zones. The DRLC has less ZAT violation in the east zone but also observes some oscillations in the south zone.

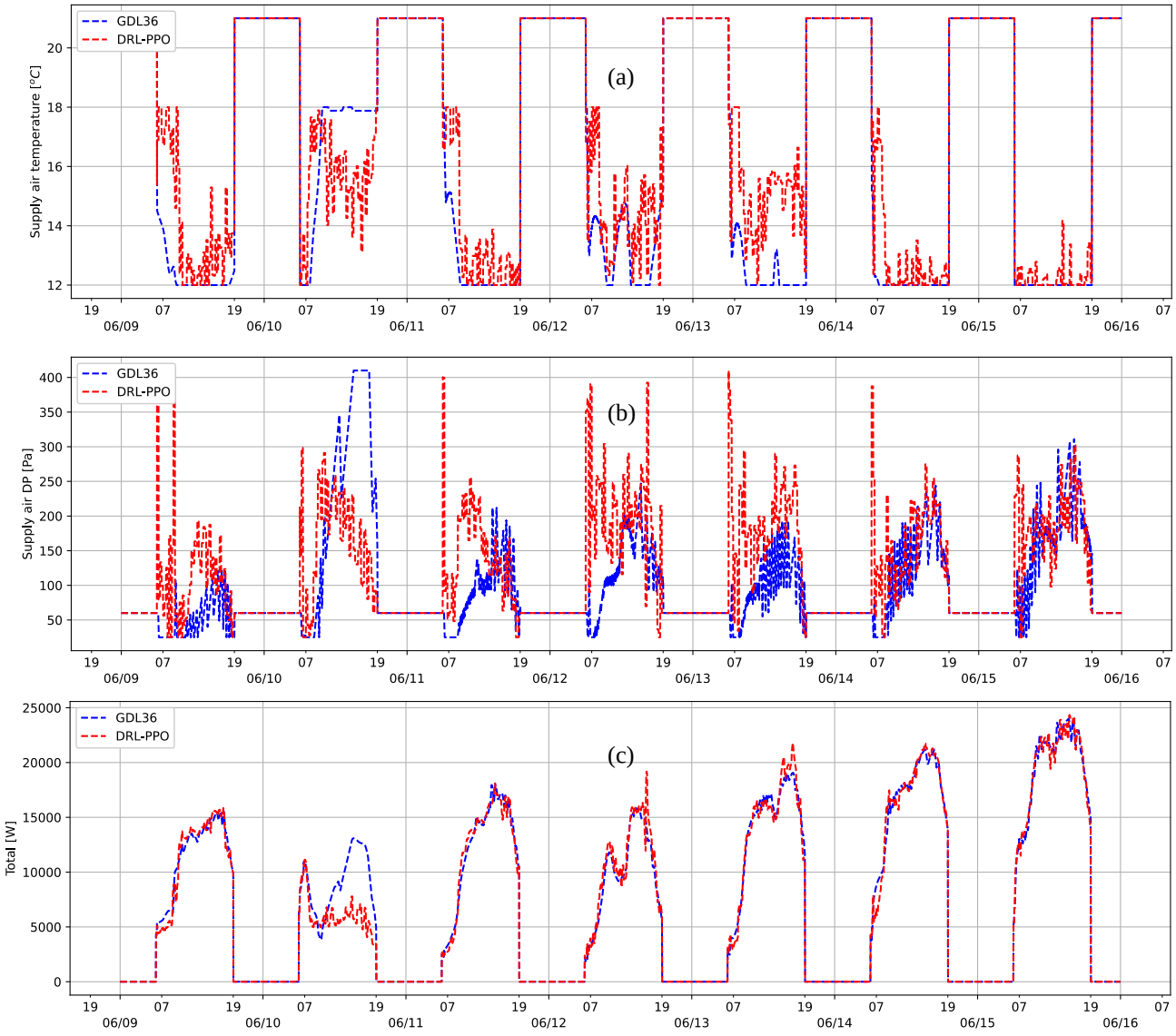

Figure 3-20 Time series of (a) SAT setpoint (b) static DP setpoint (c) Total HVAC power consumption during the shoulder season for DRLC

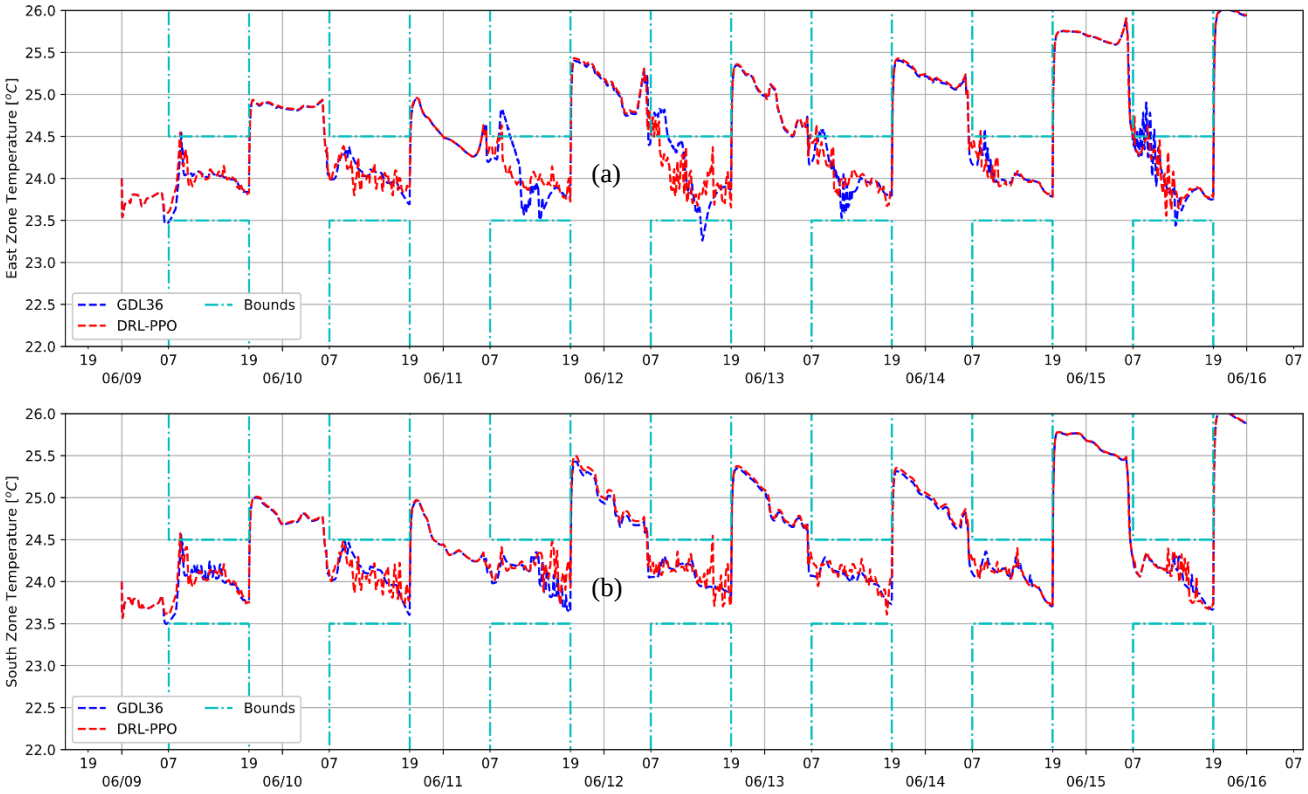

Figure 3-21 Time series of ZAT for (a) east zone and (b) south zone in the shoulder season for DRLC

3.6.3 Summary

Based on the detailed results and analysis in Section 3.5.1 and Section 3.5.2, the comparison of three types of controllers is presented in Table 3-7 for both cooling and shoulder season weeks. For the thermal comfort metric, three controllers can all maintain the ZAT within the predefined comfort bounds with minor temperature violation. The intelligent controllers have slightly less temperature violation than the GDL36 SOO. For the HVAC energy consumption in the cooling season week, the OBC saves 2.2% but the DRL consumes 2.3% more compared to GDL36 SOO. In the shoulder season week, the OBC and the DRL save 2.4% and 7.0%, respectively. The savings are mainly from the day 06/10 as discussed earlier. That day is one example that showcases the benefits of intelligent controllers over the reactive controllers such as the GDL36 SOO. Figure 3-22 depicts the integrated performance of energy consumption and

thermal comfort for the two typical weeks. It can be seen that the GDL36 is comparable to DRLC in two typical weeks but slightly inferior to the OBC for this case study.

Table 3-7 Summary results for types of controllers in terms of HVAC energy and consumption temperature violation

	Cooling (07/24-07/31)			Shoulder (06/09-06/16)		
	GDL36	**DRL-Best**	**OBC-Best**	**GDL36**	**DRL-Best**	**OBC-Best**
HVAC energy consumption (kWh)	1562.3	1598.5	1528	1197.7	1169	1114
Temperature Violation (K·h)	1.02	0.26	0.37	1.39	0.66	0.51

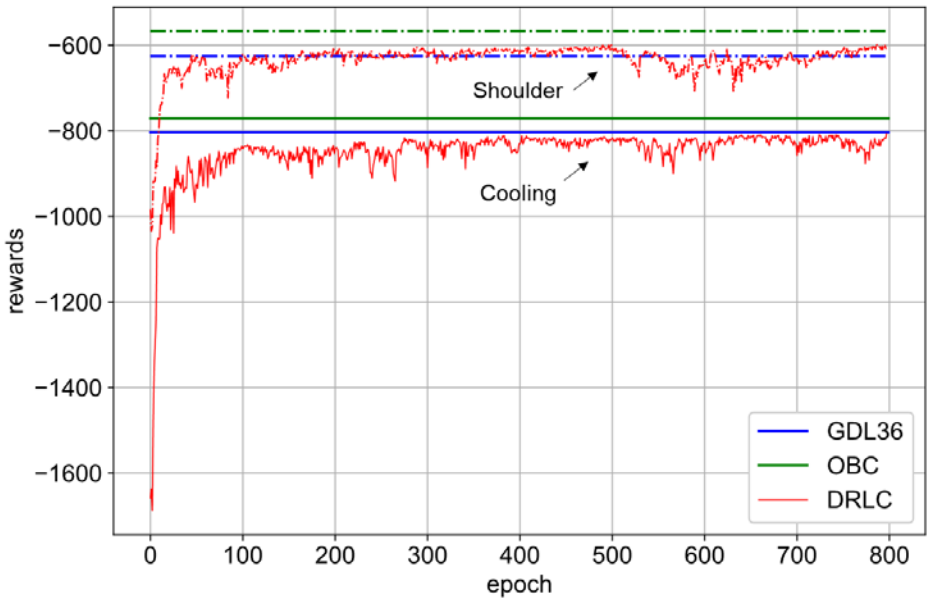

Figure 3-22 Comparison of integrated performance (i.e., reward) for three controllers

3.7 Conclusions, Limitations, and Future Work

ASHRAE GDL36 has demonstrated the energy efficiency benefits over the conventional rule-based controls. In this study, the energy and thermal comfort performance of GDL36 are compared with two intelligent controllers: OBC and DRLC. This study is conducted with a five-zone VAV cooling system virtual testbed in Chicago, IL. The baseline control system is

implemented with the high-performance airside and waterside GDL36 SOO. The OBC and DRLC replace the airside supervisory level control loops. In other words, the optimal SAT and static DP are determined by the optimization problems in OBCs and trained control policy by DRLC.

The OBC and DRLC were formulated to minimize the HVAC energy consumption and zone air temperature violations. The OBCs with different control intervals and DRLCs with different hyperparameters in the PPO algorithm were studied and fine-tuned. The results showed that the GDL36 SOO has a comparable energy performance (within a 3% deviation) with DRLC in both high and mild cooling loads. It also has a comparable energy performance (within a 3% deviation) with OBC in a high cooling load, but it expends 7% more energy in the tested shoulder week. The energy saving of the OBC mainly comes from one special day when the outdoor air temperature is low, but the zone load is still high. The GDL36 resets its SAT to the maximum. However, the zone load cannot be met and therefore large fan energy is compensated. This case demonstrates the weakness of GDL36 due to its reactive nature. For the thermal comfort metric, the GDL36 has slightly more ZAT violation in both typical weeks compared to two intelligent controllers.

For this case study, the GDL36 has demonstrated its comparable performance in terms of energy efficiency and thermal comfort with the two intelligent controllers. The GDL36 is good enough considering the complexity and tuning efforts of the intelligent controllers. However, there are several limitations of this study to be noted. First, the intelligent controllers are formulated ideally only for theoretical comparison studies. They are not deployable for real applications. For OBCs, the predictive model is assumed to be the same as the virtual testbed while in real applications the system model identification needs to be conducted. For the DRLC, the control policies are trained and tested for the same week, which is also not realistic in practice. Second,

the performance of OBCs and the DRLCs might be further improved by considering more complex aspects. For example, the OBCs only consider the scenarios under the prediction horizon as one control timestep. For DRLCs, only the PPO algorithm is explored and other DRL algorithms are not studied. Third, the simulation-based study is only experimented in a five-zone medium office building, one single climate zone, and only cooling season. The effect of the climate, building type, internal loads, and operation time on the final results are not investigated. Therefore, the future work includes the expansion of the evaluation studies to other building types with different HVAC systems and climate zones; and the comparison studies for more complicated intelligent controllers.

3.8 References

[1] Pritoni M, Prakash A, Blum D, Zhang K, Tang R, Granderson J, et al. Advanced control sequences and FDD technology. Just shiny objects, or ready for scale? 2020.

[2] Wang Z, Hong T. Reinforcement learning for building controls: The opportunities and challenges. Applied Energy. 2020;269:115036.

[3] Wetter M, Hu J, Grahovac M, Eubanks B, Haves P. OpenBuildingControl: Modeling feedback control as a step towards formal design, specification, deployment, and verification of building control sequences. Building Performance Modeling Conference and SimBuild2018.

[4] Lee ZE, Zhang KMJAE. Generalized reinforcement learning for building control using Behavioral Cloning. 2021;304:117602.

[5] Putta V, Zhu G, Kim D, Hu J, Braun J. Comparative evaluation of model predictive control strategies for a building HVAC system. 2013 American Control Conference: IEEE; 2013. p. 3455-60.

[6] Ma Y, Borrelli F, Hencey B, Coffey B, Bengea S, Haves PJITocst. Model predictive control for the operation of building cooling systems. 2011;20:796-803.

[7] Huang GJCep. Model predictive control of VAV zone thermal systems concerning bi-linearity and gain nonlinearity. 2011;19:700-10.

[8] Huang S, Zuo W, Sohn MDJAE. Amelioration of the cooling load based chiller sequencing control. 2016;168:204-15.

[9] Ma Z, Wang S, Xu X, Xiao FJEC, Management. A supervisory control strategy for building cooling water systems for practical and real-time applications. 2008;49:2324-36.

[10] Braun JEJAt. Reducing energy costs and peak electrical demand through optimal control of building thermal storage. 1990;96:876-88.

[11] Nassif N, Kajl S, Sabourin RJH, Research R. Optimization of HVAC control system strategy using two-objective genetic algorithm. 2005;11:459-86.

[12] Hou J, Luo X, Huang G, Zhang L, Yu Z, Eftekhari MJJoBPS. Development of event-driven optimal control for central air-conditioning systems. 2020;13:378-90.

[13] Drgoňa J, Arroyo J, Figueroa IC, Blum D, Arendt K, Kim D, et al. All you need to know about model predictive control for buildings. 2020;50:190-232.

[14] Privara S, Široký J, Ferkl L, Cigler JJE, Buildings. Model predictive control of a building heating system: The first experience. 2011;43:564-72.

[15] Kim D, Braun JEJE, Buildings. Development, implementation and performance of a model predictive controller for packaged air conditioners in small and medium-sized commercial building applications. 2018;178:49-60.

[16] Kim D, Braun JEJAE. Model predictive control for supervising multiple rooftop unit economizers to fully leverage free cooling energy resource. 2020;275:115324.

[17] Huang S, Lin Y, Chinde V, Ma X, Lian JJAE. Simulation-based performance evaluation of model predictive control for building energy systems. 2021;281:116027.

[18] Drgoňa J, Arroyo J, Figueroa IC, Blum D, Arendt K, Kim D, et al. All you need to know about model predictive control for buildings. Annual Reviews in Control. 2020.

[19] Koehler S, Borrelli F. Building temperature distributed control via explicit MPC and "Trim and Respond" methods. 2013 European Control Conference (ECC): IEEE; 2013. p. 4334-9.

[20] Liang W, Quinte R, Jia X, Sun J-QJB, Environment. MPC control for improving energy efficiency of a building air handler for multi-zone VAVs. 2015;92:256-68.

[21] Raman NS, Chaturvedi RU, Guo Z, Barooah PJAJoEfSB, Cities. Model Predictive Control-Based Hierarchical Control of a Multi-Zone Commercial HVAC System. 2021;2.

[22] Chen X, Qu G, Tang Y, Low S, Li NJapa. Reinforcement learning for decision-making and control in power systems: Tutorial, review, and vision. 2021.

[23] Konda V, Tsitsiklis JJAinips. Actor-critic algorithms. 1999;12.

[24] Schulman J, Wolski F, Dhariwal P, Radford A, Klimov OJapa. Proximal policy optimization algorithms. 2017.

[25] Leurs T, Claessens BJ, Ruelens F, Weckx S, Deconinck G. Beyond theory: Experimental results of a self-learning air conditioning unit. 2016 IEEE International Energy Conference (ENERGYCON): IEEE; 2016. p. 1-6.

[26] Costanzo GT, Iacovella S, Ruelens F, Leurs T, Claessens BJJSE, Grids, Networks. Experimental analysis of data-driven control for a building heating system. 2016;6:81-90.

[27] Wang Y, Velswamy K, Huang BJP. A long-short term memory recurrent neural network based reinforcement learning controller for office heating ventilation and air conditioning systems. 2017;5:46.

[28] Jia R, Jin M, Sun K, Hong T, Spanos CJEP. Advanced building control via deep reinforcement learning. 2019;158:6158-63.

[29] Yuan X, Pan Y, Yang J, Wang W, Huang Z. Study on the application of reinforcement learning in the operation optimization of HVAC system. Building Simulation: Springer; 2021. p. 75-87.

[30] Yu L, Sun Y, Xu Z, Shen C, Yue D, Jiang T, et al. Multi-agent deep reinforcement learning for HVAC control in commercial buildings. 2020;12:407-19.

[31] Azuatalam D, Lee W-L, de Nijs F, Liebman AJE, AI. Reinforcement learning for whole-building HVAC control and demand response. 2020;2:100020.

[32] Zhang Z, Chong A, Pan Y, Zhang C, Lam KPJE, Buildings. Whole building energy model for HVAC optimal control: A practical framework based on deep reinforcement learning. 2019;199:472-90.

[33] Chen B, Cai Z, Bergés M. Gnu-rl: A precocial reinforcement learning solution for building HVAC control using a differentiable mpc policy. Proceedings of the 6th ACM international conference on systems for energy-efficient buildings, cities, and transportation2019. p. 316-25.

[34] Chen Y, Norford LK, Samuelson HW, Malkawi AJE, Buildings. Optimal control of HVAC and window systems for natural ventilation through reinforcement learning. 2018;169:195-205.

[35] Ahn KU, Park CSJS, Environment TftB. Application of deep Q-networks for model-free optimal control balancing between different HVAC systems. 2020;26:61-74.

[36] Yang L, Nagy Z, Goffin P, Schlueter AJAE. Reinforcement learning for optimal control of low exergy buildings. 2015;156:577-86.

[37] Liu S, Henze GP. Evaluation of reinforcement learning for optimal control of building active and passive thermal storage inventory. 2007.

[38] Liu S, Henze GPJE, buildings. Experimental analysis of simulated reinforcement learning control for active and passive building thermal storage inventory: Part 2: Results and analysis. 2006;38:148-61.

[39] Wei T, Wang Y, Zhu Q. Deep reinforcement learning for building HVAC control. Proceedings of the 54th annual design automation conference 20172017. p. 1-6.

[40] Hanumaiah V, Genc SJapa. Distributed Multi-Agent Deep Reinforcement Learning Framework for Whole-building HVAC Control. 2021.

[41] Wang S, Ma ZJH, Research R. Supervisory and optimal control of building HVAC systems: A review. 2008;14:3-32.

[42] Lu X, Fu Y, O'Neill Z, Wen JJE, Buildings. A holistic fault impact analysis of the high-performance sequences of operation for HVAC systems: Modelica-based case study in a medium-office building. 2021;252:111448.

[43] Wetter M, Zuo W, Nouidui TS, Pang X. Modelica buildings library. Journal of Building Performance Simulation. 2014;7:253-70.

[44] The U.S. Department of Energy (DOE). DOE Commercial Prototype Building Models. Building Energy Codes Program2020.

[45] Lu X, Adetola V, O'Neill ZJE, Buildings. What are the Impacts on the HVAC System when it Provides Frequency Regulation?–A Comprehensive Case Study with a Medium Office Building. 2021:110995.

[46] Hinkelman K, Wang J, Fan C, Zuo W, Gautier A, Wetter M, et al. A Case Study on Condenser Water Supply Temperature Optimization with a District Cooling Plant. Modelica Conferences2021. p. 587-95.

[47] Hinkelman K, Wang J, Zuo W, Gautier A, Wetter M, Fan C, et al. Modelica-Based Modeling and Simulation of District Cooling Systems: A Case Study. 2021.

[48] Fu Y, Xu S, Zhu Q, O'Neill Z. Containerized framework for building control performance comparisons: model predictive control vs deep reinforcement learning control. Proceedings of the 8th ACM International Conference on Systems for Energy-Efficient Buildings, Cities, and Transportation2021. p. 276-80.

[49] Weng J, Chen H, Yan D, You K, Duburcq A, Zhang M, et al. Tianshou: a Highly Modularized Deep Reinforcement Learning Library. 2021.

[50] Paszke A, Gross S, Massa F, Lerer A, Bradbury J, Chanan G, et al. Pytorch: An imperative style, high-performance deep learning library. 2019;32.

[51] Raval S. Best Practices when training with PPO. 2021.

CHAPTER IV COMPREHENSIVE FAULT IMPACT ANALYSIS AND FAULT ROBUSTNESS ASSESSMENT OF GDL36 SOO*

4.1 Introduction

In real building operations, HVAC systems are inevitably subject to various aging and operation faults [1], which will offset the energy savings from the adoption of the high-performance control sequences. To mitigate the fault impact and facilitate building energy managers to more effectively operate buildings, the GDL36 includes rule-based automatic fault detection and diagnostics. The sets of the possible diagnostics are provided when certain fault conditions are met or violated. These rules, based on the NIST air handling unit (AHU) Fault Detection and Diagnosis (FDD) research [2, 3] and the engineering experience [4], are general to any AHU-based systems but may not be specific to the systems under the GDL36. In other words, the fault symptoms are still not presented clearly and systematically in the GDL36 since the faults at the component level may propagate through the whole system and cause cascading fault impacts. Furthermore, the SOO in the GDL36 are sophisticated enough to hardly predict impacts from a single fault impacts on the whole system. Haleem et al. [18] investigated the performance of the Guideline36 in handling uncertainty from sensors and actuators in energy use and indoor environmental quality. They concluded that using low-grade sensors and actuators instead of the standard tier would significantly degrade the system performance for the GDL36 SOO. Through a sensitivity analysis, they also stated that the inaccuracy in temperature sensors such as supply air

*Reprinted with permission from "A holistic fault impact analysis of the high-performance sequences of operation for HVAC systems: Modelica-based case study in a medium-office building" by Xing Lu, Yangyang Fu, Zheng O'Neill, and Jin Wen, 2021. Energy and Buildings, 252, 111448, Copyright [2021] by Elsevier.

temperature and zone air temperature sensors produced the most degradation compared to the AHU economizer dampers, terminal unit heating valves, and the fan loop components. Apart from the aforementioned uncertainties in the real building operations, the HVAC systems are susceptible to large amounts of faults coming from both individual components (e.g., HVAC equipment, sensors, etc.) and whole system (e.g., controls, design, and operation) [19]. As far as the authors' best knowledge, there are no existing studies that pertain to the comprehensive fault impact analysis of the high-performance SOO for HVAC systems, and how GDL36 handles and adapts to the various types of faults is still largely unknown. Given that, this chapter presents a comprehensive fault impact analysis, with the aim of providing more comprehensive and well-defined fault symptoms and identifying the faults with the most negative repercussions towards the high-performance SOO for HVAC systems.

4.2 Literature Review

4.2.1 Fault Impact Analysis

There exist some studies on fault simulation and fault impact assessment of HVAC systems in buildings. Kim et al. [5] evaluated and prioritized common faults in HVAC systems using proprietary impact estimation methods for the energy and financial perspectives. Instead of conducting a rough estimate, many researchers performed the fault simulation on top of the building energy simulation programs with the development of necessary fault models [6]. Zhang et al. [7] developed new fault objects in EnergyPlus to model operational faults of HVAC systems including the sensor bias, fouling coils, and the dirty air filters. Li et al. [8] presented a large-scale EnergyPlus-based fault impact analysis framework in which parametric sensitivity analysis was adopted to determine and rank the fault criticality. A total of 129 fault modes were simulated for a medium-sized office building model. The considered faults include the physical faults from

HVAC mechanical equipment and sensors and the scheduling faults. Using a similar approach, Lu et al. [9] investigated a comprehensive sensor error impact analysis and ranked the sensor importance in a demand-controlled ventilation HVAC system. Kim et al. [10] developed and validated 25 fault models that represent in a small commercial building using EnergyPlus/OpenStudio. They generated the curated fault model simulation data set for FDD purposes [11] based on the developed fault models.

4.2.2 Limitations

Most existing fault simulation on HVAC systems have several common limitations in terms of modeling fidelity and fault simulation coverage [6]. Most studies integrate the fault models into EnergyPlus, which is hard to directly model the pressure-related faults. To simulate the duct fouling in EnegyPlus, one needs to reflect the fault impact by adjusting the parameters in the fan model, e.g., pressure rise and maximum airflow rate. Furthermore, few studies consider the control-related faults and capture all the control sequence elements. The control-related and dynamic physical faults are difficult to simulate in EnergyPlus since EnergyPlus assumes a perfect control regarding the local controllers and its smallest simulation interval is only 1 minute. Given the significance of the control sequences on the HVAC quality of service, it is crucial to account for the control-related faults. In addition, the physical faults could have different fault symptoms depending on the control loop. For instance, different fault symptoms are found when the outdoor air damper under the GDL36 SOO compared to the conventional SOO [12]. Therefore, oversimplification of the control sequences will influence the fault modeling fidelity. Chen et al. [13] captured the dynamic and steady-state effects of several physical faults of a large commercial building using a virtual testbed in Modelica. Their simulation results showed that the physical fault impacts were correlated to the control sequences and the load conditions. However, they only

considered a limited number of the physical faults, and the control sequences of the large office building are based on the ASHRAE 90.1-1989 and 90.1-1999.

4.3 Contributions and Chapter Organization

Based on the above literature review, the contributions of this chapter are summarized as follows:

- Different from the idealization of the control sequences in most existing fault modeling studies, this study captures the fast-dynamic effects of the faults on the performance of the control sequences over the airside, waterside, and zone systems.
- Only a part of the physical faults is considered in the open literature. This study performs a comprehensive fault impact analysis including the faults from sensors, duct & pipes, dampers & valves, HVAC mechanical equipment, control-related elements, building envelope, system scheduling, and design aspects. There are a total of 359 scenarios simulated in this study.
- This study generates massive faulty data and reveals the associated fault impacts of the high-performance SOO for HVAC systems, under different fault intensities and three seasonal operating conditions. The faults with the most adverse impacts are identified and ranked. The robustness of the high-performance SOO with various faults is evaluated for multiple Key Performance Indexes (KPIs).

This chapter is organized as follows. Section 4.4 describes what common faults are studied, how faults are injected into the building system model, and how the batch fault simulation is performed. Section 4.5 discusses the KPI used for this study. Section 4.6 presents the fault impact analysis and fault robustness analysis of the high-performance SOO for three seasonal operating conditions. Section 4.7 summarizes our findings, limitations, and future work.

4.4 Fault Injection and Simulation

The simulated building was a single-floor five-zone VAV system as described in CHAPTER II under both airside and waterside control sequences of GDL36 [14]. The original model was developed from the GDL36 model in Modelica Buildings Library 7.0.0 [15].

To cover a wide range of common faults, a thorough literature review was conducted over the multiple resources, including the existing building fault simulation [6-8, 10, 11, 13, 16], fault experiment datasets [17, 18], commissioning tools [19-21], FDD routines [22-24], and conversation with the building experts. The considered faults are categorized into different fault types, as tabulated in Table 4-1.

Table 4-1 Considered faults and their fault category

Fault Category	Fault Description
Sensor	• Airside system-level sensor bias (Outdoor airflow; Supply air temperature; Return air temperature; Mix air temperature; Supply fan static discharge pressure) • Waterside system-level sensor bias (Chiller/boiler leaving water temperature; Cooling tower leaving condenser water temperature; Pressure differential in the plant loop) • Zone-level sensor bias (Thermostat; Zone terminal airflow rate; Zone discharging air temperature)
Duct & Pipe	• Supply air main duct leakage • Air duct fouling • Chilled/hot water pipe fouling • Chilled/hot water pipe poor insulation
Valve& Damper	• Valve leakage (Cooling tower shutoff valve; chiller Condenser waterside isolation valve; Chiller chilled waterside isolation valve; Boiler isolation valve; AHU cooling/heating coil) • Stuck valve of AHU cooling/heating coil • Damper leakage of outdoor air (OA) damper • Stuck damper of the outdoor air damper

HVAC Equipment	• Cooling/heating Coil Fouling • Chiller mechanical problem (Fouling chiller condensers, Presence of no condensable in refrigerant, Nonstandard refrigerant charging, Chiller excess oil) • Pump mechanical problem (impellor fault, blade cavitation, motor degradation) • AHU Fan mechanical problem (motor degradation) • Fouling cooling tower • Fouling boiler
Control	• Inappropriate settings of Proportional–Integral- Derivative (PID) controls • Arbitrary control setpoints • Large hysteresis of control signals or components
Schedule	• HVAC setback error: delayed onset; early termination; no overnight setback
Design	• Equipment oversized design • Poor building airtightness

How various fault models are developed and injected into the building virtual testbed are discussed in the following. First, the component fault models are built upon the basic component models in Modelica Buildings Library [15]. A fault mode component is created as a record type in Modelica so we can define and group all the fault mode properties together. The fault mode properties include Boolean parameter ‘active’ to activate the fault, the fault start time and end time, etc. The fault mode component is embedded in the component fault model to define the fault simulation properties. The component fault models can be categorized into three different fault injection types: variable, parameter, connector. The ‘variable’ type denotes the output variable of the original model is overwritten if the fault mode is activated during the fault injection period. One example of the ‘variable’ type fault is the sensor fault where the sensed variable is overwritten by the faulty value. The second type ‘parameter’ means the parameters in the fault model would be overwritten. The third ‘connector’ type means the fault models are injected through the

connector. One typical example of the ‘connector’ type is the leakage fault where a leakage fault model is added to the leakage point through the connector.

Second, the system-level fault model is built using the newly built component fault models. All the required component fault models are added or replacing the original counterpart model in the baseline virtual testbed per fault scenarios. For example, when the fault scenario of the temperature sensor bias is injected, the original temperature sensor model is replaced by the newly built sensor bias fault model. Fault models for various components, including sensor, duct, and pipe, damper and valve, HVAC equipment, control, schedules, are developed are detailed as follows.

4.4.1 Sensor

Sensors are inevitably prone to different types of errors which could be decomposed into three parts: multiplicative errors, bias, and noise [25], as shown in Eq. (4-1).

$$V_{EP} = (1 + m) \cdot V_{EF} + \varepsilon_{bias} + \varepsilon_{noi} \,, \tag{4-1}$$

where V_{EP} and V_{EF} represent the error-presented value and the error-free value, respectively. m is the multiplicative offset of the scaling error. ε_{bias} and ε_{noi} denote the deviation caused by the bias errors and the noise. In this study, the fixed bias is assumed in different key system locations. Based on the sensors in the studied control sequences, we include the following sensors from the airside, waterside systems and zone terminals: chilled/condenser/hot water supply temperature sensor, chilled/hot differential pressure sensor, outdoor airflow rate sensor, supply air temperature sensor, mixed air temperature sensor, return air temperature sensor, air loop differential pressure sensor, zone air temperature sensor, zone discharging air temperature sensor, zone air flow rate sensor. Since the airside system of the studied building is a multi-zone VAV system, we do not consider all the zone sensor faults to avoid repetition. But without loss of the generality, we assume

the south zone sensor faults for the cooling and shoulder season, but the east zone sensor faults for the heating season.

Both positive and negative sensor biases are considered, and different fault intensities are used to represent different severities of the sensor faults. In this study, two tiers of sensor faults are considered to represent the moderate and the severe sensor faults. These fault intensity values are referred from the open literature [9, 26] and FDD routines [3, 23, 24]. For example, according to the default error thresholds for the supply water temperature [10], we set 1 and 2 K, respectively, representing the moderate and severe sensor bias for the chilled supply water temperature while 2 and 4 K, respectively, representing the moderate and severe sensor bias for the hot supply water temperature. The sensor fault is implemented as a 'variable' type. The output (sensed variable) of the original sensor model in Modelica Buildings Library is overwritten by the faulty value when the fault mode is activated.

4.4.2 Duct & Pipe

Ducts and pipes are the passages to deliver or remove the fluid in the HVAC system. The common faults include duct leakage, duct fouling, pipe clogging, and pipe poor insulation. Roth et al. identified duct leakage as the most critical fault that leads to the second largest energy waste [27] and Wray et al. pointed out that duct leakage had a complicated impact on the energy performance in VAV systems due to the system variable response [28]. Duct fouling increased the pressure drop of the air loop and increased the fan energy consumption at a certain level. Zhai et al. reported a change of -5.1 to 10.8% energy when the filters and ducts in the air loop were fouled [29]. Likewise, the pipe clogging due to the water pipe corrosion could increase the pump head and the pump energy consumption. Poor insulation in the piping system could result in undesirable heat gain or losses. ASHRAE Standard 90.1 increased the minimum pipe insulation thicknesses

requirement from the 2010 version but pipe insulation with a thickness less than designed values is still common [30].

The duct leakage is implemented as the 'connector' type. The mathematical expression is shown in Eq. (4-2).

$$\dot{m}_{EF} + \dot{m}_L = k\sqrt{\Delta p}, \tag{4-2}$$

where $\dot{m}_{EF}$ is the normal operation mass flow rate and $\dot{m}_L$ is the leakage mass flow rate. k is the friction factor and $\triangle$p is the pressure drop. Two fault scenarios with leakage mass flow rate equal to 10% and 20% of the main duct are considered.

The duct fouling and pipe clogging are implemented as the 'parameter' type. The nominal resistance of the duct/pipe is increased with 10% and 20% magnitude. The pipe poor insulation is implemented as the 'parameter'. We assume a perfectly insulated pipe for the baseline case. In the two fault scenarios, the insulation of a 20m pipe is damaged and its insulation thickness for the two scenarios is 20mm and 5mm respectively.

4.4.3 Damper & Valve

Damper/valve regulates the air/water flow and fulfils a wide range of functions and locations in the HVAC system. As one of the most prevalent faults in this category, the damper/valve stuck fault could be due to (1) the corrosion and degradation that cause the actuator to seize, which leaves the damper/valve in the fixed position; (2) the broken linkage; (3) the control system that fail to send or determine the position signal [27]. In addition, the damper/value leakage is also a common fault due to the aging and the oversizing. The leaky valves were reported to have an energy waste of 5 % of the building operational cost [27].

The damper/valve stuck fault is implemented as the 'variable' type since the output of the damper/valve is overwritten to a fixed value when the fault is injected. Different stuck positions

(0%, 15%, 65%, 100%) are considered in this study according to the ASHRAE RP-1312 [17]. The damper/valve leakage fault is implemented as the 'parameter' type. The leakage ratio in the damper/valve model is perturbed with the value of 0.001 and 0.01 to represent the moderate and severe fault levels. The leakage ratio, defined as the following Eq. (4-3), is the ratio of the flow coefficient at the full closed position and the flow coefficient at the full open position.

$$\mathrm{l} = \frac{kv(y=0)}{kv(y=1)}, \tag{4-3}$$

where *l* is the leakage ratio. *kv* is the flow coefficient, and *y* is the damper/valve opening position. The dampers/values considered in this study include the economizer outdoor air damper, the cooling tower shutoff valve, the chiller condenser waterside isolation valve, the AHU cooling/heating coil control valve, and the boiler isolation valve.

4.4.4 HVAC Equipment

How the HVAC equipment faults propagate to the whole system under GDL36 control sequences are investigated in this study. To be specific, the chiller mechanical faults, boiler fouling, AHU cooling/heating coil fouling, cooling tower fouling, pump mechanical faults, and fan reduced motor efficiency are considered.

The chiller mechanical faults include the fouling chiller condensers, presence of non-condensable in refrigerant, nonstandard refrigerant charging (overcharge), and chiller excess oil. The empirical chiller fault models [31] as expressed in Eq. (4-4)) are incorporated in the chiller model in Modelica Buildings Library. The original calculated chiller power is overwritten by the multiplier of the fault ratio as defined in Eq. (4-4). Two fault intensity ratios are selected for each fault to represent the moderate and severe fault levels.

$$\frac{\dot{W}_F}{\dot{W}_{EF}} = a_1 + a_2 T_{evap,out} + a_3 T_{cond,in} + a_4 \dot{Q}_{evap} + a_5 T_{evap,out} \dot{Q}_{evap} + a_6 T_{cond,in} \dot{Q}_{evap} + a_7 \dot{Q}_{evap}^{\ 2}, \quad (4\text{-}4)$$

where $\dot{w}_{EF}$ and $\dot{w}_F$ are the chiller power consumption under the fault-free and faulty conditions. a_1 - a_7 are the regression coefficients for the empirical models. It is noted that each chiller mechanical fault has its own sets of regression coefficients. $T_{evap,out}$ and $T_{cond,in}$ are the evaporator outlet water temperature and condenser inlet water temperature. $\dot{Q}_{evap}$ is the heat transfer rate in the chiller evaporator.

Deposits on the fireside and the water-side of the boiler tubes could impair the heat transfer and reduce the boiler efficiency [32]. The boiler efficiency could be reduced from 9.5% up to 69% depending on the deposit build-up thickness [33, 34]. The boiler fouling in this study is implemented as the 'parameter' type. The boiler efficiency curve is adjusted down by 10% and 20% for the two fault scenarios.

For the fouling of the AHU cooling/heating coil and the cooling tower, these faults are implemented as the 'parameter' type, reflected by the nominal overall heat transfer coefficient UA. Several field tests found the UA of the AHU cooling coil could decrease by 45-50% due to the fouling effects [35, 36]. Therefore, in this study, the UA values are perturbed to three tiers, 10%, 30%, and 50% lower than the baseline in the three fault scenarios.

Pumps and fans are the devices to move the fluid to the desired location. The common faults of pumps include the impellor fault, blade cavitation, bearing worn out, seal defect, motor degradation, etc. Sakthivel et al. [37] conducted the fault experiment and identified how different pump faults affected the pump pressure head, the pump overall efficiency, and the pump power. To model the mechanical problems in this study, the faulty pump curves under different fault types would overwrite the fault-free pump curve, as shown in Figure 4-1. In this study, the faulty pump

curves for the cavitation fault and impellor fault are used. The pump motor degradation is also implemented as the 'parameter' type. The pump motor efficiency is assumed to be reduced by 15% and 30 %, respectively for two fault scenarios. Due to the unavailability of the faulty fan curve data, we only consider the fan motor efficiency degradation fault. Likewise, the fan motor efficiency is assumed to be reduced by 15% and 30 %, respectively.

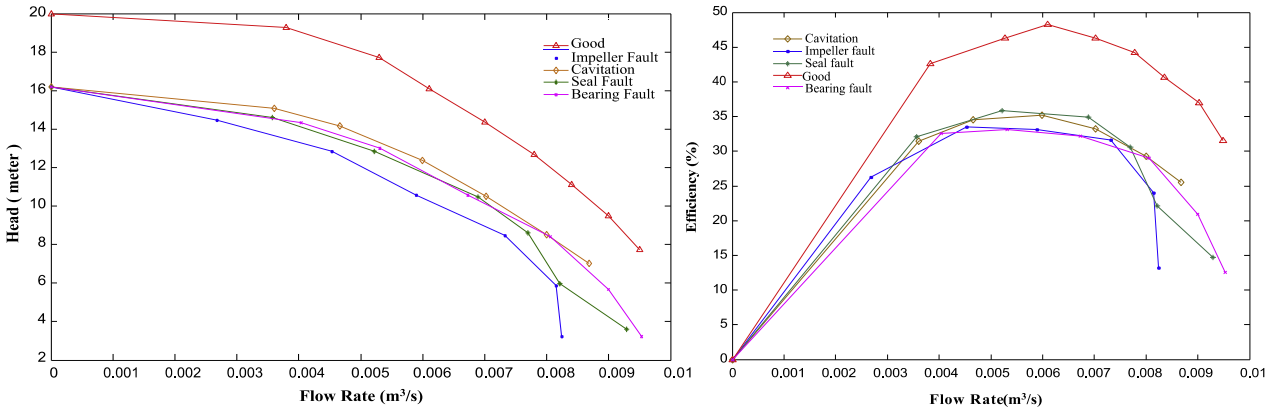

Figure 4-1 Pump curves under good and faulty conditions: Left: head-flowrate; Right: efficiency-flowrate

4.4.5 Control

The appropriate settings and configurations of the control system are essential for maintaining the overall HVAC system quality of service. The following categories of the control related faults are investigated: (1) inappropriate PID controller parameter settings; (2) arbitrary control loop setpoints or disabled reset routines; (3) hysteresis of control signals or components.

For the first fault type, we consider the fault scenarios in the following local control PID loops: Supply air temperature; Fan speed; Economizer outdoor airflow rate; Boiler hot water supply temperature; Chilled/Hot water pump speed; Cooling tower fan speed; Zone air temperature; Zone discharging air flow rate. The proportional gains P of the PID controller are perturbed to different order of magnitudes compared to the baseline setting. For instance, the normal P value for the cooling supply air temperature loop is 0.5. Accordingly, two fault scenarios

with P value equal to 5 and 0.05 respectively are designed to represent the aggressive tuning and the slow response case. For the second fault type, two fault scenarios are designed for each season: differential pressure setpoint is set to the maximum; Chilled/Hot supply water temperature is set to the maximum/minimum. The third fault type is implemented as the 'connector' type. Three fault scenarios are studied: Cooling/Heating coil valve input signal delay; Fan speed input signal delay; Chilled/Hot water pump speed input signal delay. The delay time is assumed to be 1 s for certain communication protocols [38, 39] while the baseline case assumes a perfect delay-free communication.

4.4.6 Scheduling

Approximately 90% of buildings do not operate around the clock and 70% of the buildings reduce the heating and cooling energy consumption during the unoccupied hours [40]. However, some building operators do not set back their HVAC system while unoccupied or unintentionally leave part of HVAC mechanical equipment on. The following scheduling fault scenarios are studied for each season: delayed onset and early termination by one or two hours, and no overnight setback. The occupancy schedule parameters are adjusted to inject these faults.

4.4.7 Design

In this study, two types of design faults are considered: HVAC mechanical equipment oversizing and poor building airtightness. The HVAC mechanical equipment is sometimes oversized by the designers to ensure sufficient cooling/heating by applying a certain safety factor. For example, the oversized water pumps would result in a large flow rate of the water system and the low delta-T syndrome. In this study, we consider the oversizing faults of the AHU including the supply fan, the cooling coil, the heating coil, chiller, boiler, and chilled/hot water pump. These faults are implemented as the 'parameter' type by changing the nominal values such as the nominal

flow rate, nominal differential pressure, or the nominal performance curves. Building airtightness is defined as the resistance to inward or outward air leakage in the building envelope. The poor airtightness design would lead to undesired infiltration and exfiltration. The building commissioning requirements of Standard 189.1 include a whole building test demonstrating the building meets a tightness limit requirement [41]. The infiltration fault belongs to the 'parameter' type. The nominal differential pressure between the zone and the outside in the air leakage model is overwritten to a smaller value under the same nominal mass flow rate, which indicates a decrease of the infiltration resistance. In this study, we consider two scenarios of the infiltration resistance reduced to 70% and 50% of the baseline value.

All the 359 fault scenarios are simulated under the ASHRAE climate zone 5A Chicago, IL. In total, 359 fault scenarios are injected to the system fault model for three seasonal operating conditions. The number of fault scenarios in the cooling, shoulder, and heating season week is 127, 127, 105, respectively. Table 4-2 shows an example of the fault scenarios in the cooling season. Appendix B.1 lists all the fault scenarios for the three seasonal operating conditions.

All the fault scenarios are simulated for one week and the injected fault is assumed to happen continuously for one week. A Python package BuildingsPy [42] is used to run all the fault scenarios while activating the fault as needed per the fault scenario to be simulated.

Table 4-2 Example of the studied fault scenarios in the cooling seasons

Index	Scenario Name	Fault Category	Description
1	TCHWSup_p1	Sensor	Chilled water supply temperature sensor positive bias - 1 K
2	TCHWSup_m1		Chilled water supply temperature sensor negative bias - 1 K
…	…		…
45	SupDucLea_10	Duct & Pipe	Air loop supply duct leakage – Fault Intensity (FI)=10%
46	SupDucLea_20		Air loop supply duct leakage - FI=20%
…	…		…
51	CHWPipIso_l02L25		Chilled water pipe isolation - 20mm
52	CHWPipIso_l005L25		Chilled water pipe isolation - 5mm
53	CooTowValLea_001	Valve& Damper	Cooling tower valve leakage - leakage ratio l=0.001
54	CooTowValLea_01		Cooling tower valve leakage - leakage ratio l=0.01
…	…		…
71	OADamStuck_65		Outdoor air damper stuck - Position =65%
72	OADamStuck_100		Outdoor air damper stuck - Position =100%
73	CooCoiFou_10	HVAC Mechanical Equipment	Cooling coil fouling - FI=10%
74	CooCoiFou_30		Cooling coil fouling -FI=30%
…	…		…
95	cooTowFou_30		Cooling tower fouling - FI=30%
96	cooTowFou_50		Cooling tower fouling - FI=50%
97	conkTSup_5	Control	Supply air temperature PID loop fault - P=5
98	conkTSup_05		Supply air temperature PID loop fault - P=0.05
…	…		…
114	supFanSpeDel_1		Supply fan speed control signal delay - 1s
115	yPumDel_1		Chilled water pump speed control signal delay - 1s
116	schedule_early_1	Schedule	Schedule fault - Early termination of setback for 1 hour
…	…		…
120	schedule_nosetback		Schedule fault - No temperature setback
121	AHUFan_oversized	Design	Oversized AHU supply fan

…	…		…
127	infiltration_50		More infiltration – FI=50%

4.5 Key Performance Indexes for Fault Impact Analysis

Key performance indexes used in this study are described, including the aspects from the energy consumption, energy cost, control quality factor, thermal comfort, ventilation, and the power system.

4.5.1 Energy and Cost

Operational cost, source energy, and site energy are used, as shown in Eq. (4-5)-(4-7) respectively.

$$C_{tot}(t_0, t_N) = C_{Ele}(t_0, t_N) + C_{Gas}(t_0, t_N) = \sum_{t_0}^{t_N} p_{ele}(t_i) \cdot E_{ele}(t_i) + p_{dem} \cdot \max\left(P_{ele}(t_i)\right) - Rev\left(t_0, t_f\right) + \sum_{t_0}^{t_N} p_{gas}(t_i) \cdot E_{gas}(t_i), \quad (4\text{-}5)$$

$$E_{Sit,tot} = \sum_{t_0}^{t_N} E_{ele}(t_i) + \sum_{t_0}^{t_N} E_{gas}(t_i), \quad (4\text{-}6)$$

$$E_{Sou,tot} = f_{ele} \cdot \sum_{t_0}^{t_N} E_{ele}(t_i) + f_{gas} \cdot \sum_{t_0}^{t_N} E_{gas}(t_i), \quad (4\text{-}7)$$

where N is the sampling number for each operation time step point t. C_{tot}, C_{Ele}, C_{Gas} represents the total cost, electricity cost, and the natural gas cost. E_{ele} and E_{gas} are the site energy for the electricity and natural gas. p_{ele}, p_{dem}, and p_{gas} are the electricity energy price, the electricity demand charge, and the natural gas energy price. We assumed a fixed energy price for both electricity (0.12 $/kWh) [43] and natural gas (1.7 $/therm) [44]. The demand charge is not considered in this study. $E_{Sit,tot}$ and $E_{Sou,tot}$ are the total site energy and source energy. f_{ele} and f_{gas} are the site-to-source ratio [45] with 2.80 and 1.05 applied for electricity and natural gas.

4.5.2 Control Loop Quality Factor

GDL36 contains multiple local control loops, most of which are a proportional–integral (PI) type. Poor control loop quality could increase the energy consumption and threaten equipment life. Therefore, two verified control quality factors (CQF) are used [46, 47]: Harris Index (denote as H) and Exponentially Weighted Moving Average (EWMA) Index (denote as G). The mathematical forms are expressed in Eq. (4-8)-(4-9). Two CQFs are then time-averaged and mapped to 0-5 (5 means the best, 0 means the worst) to represent the weighted CQF scores over a given period.

$$H(t_i) = 1 - \frac{{\sigma^2}_{mv}(t_i)}{{\sigma^2}_{y}(t_i)}, \tag{4-8}$$

$$G(t_i) = K(1 - e^{-\frac{\bar{y}(t_i) - r(t_i)}{r(t_i)}}), \tag{4-9}$$

where ${\sigma^2}_{mv}$ is the expected minimum variance and ${\sigma^2}_{y}$ is the variance of the control outputs. K is the scale factor. $\bar{y}$ is the EWMA filtered value of the control outputs and r is the reference value. Please refer to [46, 47] for further details. In the GDL36, the cooling and hearing coil valve position, return air damper position, and outdoor air damper position are all sequenced together to maintain the supply air temperature. In addition, the output of the supply air temperature control loop is also one of the key inputs in the plant on/off control. Therefore, the supply air temperature control loop is evaluated due to its significance in the GDL36.

4.5.3 Thermal Comfort

The maximum zone air temperature deviation, total zone air temperature deviation, the unmet ratio, and the predicted percent of dissatisfied (PPD) are used, as expressed in Eq. (4-10)-(4-13). The maximum zone air temperature deviation dt_{max} calculates the sum of the largest deviation of the zone air temperature in the five zones over the operation time period (t_0,t_N). The total zone air temperature deviation dt_{tot} adds up the zone air temperature deviation in the five

zones over the operation time period (t_0,t_N). The zone air temperature unmet ratio Unm_{dt} is the ratio of the operation hours when the zone air temperature is out of the boundary and the total operation hours. The PPD index is a function of the Predicted Mean Vote (PMV) [48], which is corelated to the dry bulb air temperature, mean radiant temperature, air velocity, metabolic rate, and clothing level. It provides an estimate of the proportion of the occupants in a space who would feel dissatisfied by the thermal conditions.

$$dt_{max}(t_0, t_N) = \sum_{z \in Z} \max_{t_0 < t_i < t_N} (|s_z(t_i)|), \tag{4-10}$$

$$dt_{tot}(t_0, t_N) = \sum_{z \in Z} \sum_{t_0}^{t_N} |s_z(t_i)|, \tag{4-11}$$

$$Unm_{dt}(t_0, t_N) = \frac{\sum_{z \in Z} \sum_{t_0}^{t_N} c_z(t_i)}{t_N - t_0}, \tag{4-12}$$

$$PPD = 100 - 95e^{-0.03353PMV^4 - 0.2179PMV^2}, \tag{4-13}$$

z is the zone index for the set of zones, and s_z is the deviation from the lower and upper setpoint temperatures. The zone air cooling and heating temperatures setpoint are 24 ℃ and 20 ℃ in this study, respectively. The deviation range in this study is ± 1 ℃ from the setpoint. c_z is the boolean function that determine if the zone air temperature is out of the deviation range. The mean radiant temperature is assumed to be 0.4 ℃ higher than the dry bulb zone air temperature using the conclusion from [49]. The air velocity is assumed as 0.1 m/s and the metabolic rate is set as 1 met. The clothing level for the cooling and heating season are 0.7 and 1.2 respectively.

4.5.4 Ventilation

The outdoor air ratio (OAR) [50] is defined as the ratio of the actual outdoor air flow rate and the required outdoor air flow rate calculated based on ASHRAE 62.1-2019 [51]. Two OAR-based metrics are used: mean OAR OAR_{ave} and OAR met ratio Met_{OAR}, as shown in Eq. (4-15)-(4-16). OAR_{ave} represents the mean OAR value over the operation time period (t_0,t_N), which is

the larger, the better. OAR met ratio Met_{OAR} is the ratio of the operation hours when the OAR is larger than 0.9 and the total operation hours. The rationale of the selection of 0.9 as a cut-off point [52] is because outdoor air flow meters will general exhibit at least 10% measurement error in practice.

$$OAR(t_i) = \frac{V_{OA,act}(t_i)}{V_{OA,req}(t_i)} \tag{4-14}$$

$$OAR_{ave}(t_0, t_N) = \frac{\sum_{t_0}^{t_N} OAR(t_i)}{t_N - t_0}, \tag{4-15}$$

$$Met_{OAR}(t_0, t_N) = \frac{\sum_{t_0}^{t_N} c_{OAR}(t_i)}{t_N - t_0}, \tag{4-16}$$

where $V_{OA,act}$ and $V_{OA,req}$ are actual outdoor air flow rate and required outdoor air flow rate based on ASHRAE 62.1-2019 [51]. c_{OAR} is the Boolean function that determine if the OAR is larger than 0.9.

4.5.5 Power System

Peak power pea and power diversity factor div are used as KPIs from the power system perspective, as shown in Eq. (4-17)-(4-18). Peak power pea is simply the highest electrical power demand of all the HVAC equipment over the operation time period (t_0,t_N). The power diversity factor div is defined as the ratio of the sum of the maximum electrical power demands of all the HVAC equipment to the coincident maximum demand of the HVAC system. The power diversity factor normally has a value larger than 1 and is equal to 1 if all the individual equipment electrical power demands occur simultaneously.

$$pea(t_i) = \max_{t_0 < t_i < t_N} \sum_{equ \in E} P_{equ}(t_i)\,, \tag{4-17}$$

$$div(t_0, t_N) = \frac{\sum_{equ \in E} \max_{t_0 < t_i < t_N} P_{equ}(t_i)}{\max_{t_0 < t_i < t_N} (\sum_{equ \in E} P_{equ}(t_i))}\,, \tag{4-18}$$

where P_{equ} denotes the power demand of equipment equ which belongs to the HVAC equipment set E.

4.5.6 Fault Impact

Fault impact ratio (FIR) in Eq. (4-19) represents how negative the performance has changed due to the fault in respect to the performance that is normally expected [53]. The FIR is larger than zero for the negative impact while is smaller than zero for the positive impact. KPIs in Eqs. (4-5)-(4-13), (4-15)-(4-18) can be directly represented by this fault impact ratio. The sign function *sgn* depend on the KPIs as shown in Eq. (4-20).

$$FIR = sgn(\text{KPI}) \cdot \frac{\text{KPI}_{faulted} - \text{KPI}_{unfaulted}}{\text{KPI}_{unfaulted}}, \tag{4-19}$$

$$sgn = \begin{cases} 1, & \text{KPI for Eqs. (4-5)} - \text{(4-7)}, \text{(4-10)} - \text{(4-13)}, \text{(4-17)} \\ -1, & \text{KPI for Eqs. (4-8)} - \text{(4-9)}, \text{(4-15)} - \text{(4-16)}, \text{(4-18)}. \end{cases} \tag{4-20}$$

4.6 Results and Discussion

4.6.1 Fault Impact Analysis for Each Fault Category

In this section, representative results of the fault impact analysis are presented to keep the chapter reasonably concise, as shown in Table 4-3. The results that have not been presented included in Appendix B.2.

KPIs are calculated for different fault scenarios and visualized using color maps shown in Figure 4-2 - Figure 4-9. The row represents different fault scenarios, and the column represents different KPIs. For each KPI column, the cell color represents the normalized FIR, which is the FIR value divided by the maximum FIR in each column. The color bar scale is from the most positive fault impact of -1 to the most negative fault impact of 1.

Table 4-3 Fault impact analysis results presented in this section

Fault Category	Seasonal Load Conditions	Presented in this Section
Sensor	Cooling Season	√
	Shoulder Season	×*
	Heating Season	×
Duct & Pipe	Cooling Season	√
	Shoulder Season	√
	Heating Season	√
Valve& Damper	Cooling Season	√
	Shoulder Season	√
	Heating Season	√
HVAC Equipment	Cooling Season	√
	Shoulder Season	×
	Heating Season	×
Control	Cooling Season	√
	Shoulder Season	√
	Heating Season	×
Schedule	Cooling Season	√
	Shoulder Season	√
	Heating Season	√
Design	Cooling Season	√
	Shoulder Season	√
	Heating Season	√

* ×: the results are represented in the Appendix B.2.

4.6.1.1 Sensor

Figure 4-2 shows the fault impacts over the KPIs of sensor faults in the cooling season week. Since the cooling season consumes little gas consumption for the heating and the fixed electricity rate is adopted in this study, the fault impacts of the operational cost, the site energy, and the source energy share a similar trend for each fault scenario.

In terms of the operational cost/site energy/source energy, cooling water temperature sensor, outdoor air flow rate sensor, AHU supply air temperature sensor, zone air temperature sensor, and zone air flow rate sensor are comparatively most fault-influential for the high-performance SOO. We can also see that different sensor bias directions (e.g., positive, negative)

and faulty sensor intensities (e.g., 1K, 2K) will influence the results differently. Taking the cooling water temperature sensor positive bias as an example, the positive sensor bias will increase the setpoints used in the cooling tower speed control and lead to more cooling effects on the chiller condenser side than required in the normal case, which results in the cooling tower fan energy increase and the chiller energy decrease. The negative sensor bias will have an opposite effect. However, it is noted that even the worst case (cooling water supply temperature sensor positive bias of 2K) only has a fault impact ratio of 6.5%. From here we can conclude that the high-performance SOO have a robust energy and cost performance for the common sensor bias faults in the cooling season.

Regarding the control loop performance of the supply air temperature, only the sensor bias from the AHU supply air temperature could worsen the control performance since this sensor directly acts on the supply air temperature control loop.

For the zone air temperature variations, the results show that only the zone air temperature sensor will have a direct negative impact compared to the sensor faults in other locations. As a direct thermal comfort metric, the PPD does not have a significant increase over all the cooling fault scenarios.

For the ventilation performance, the return air temperature sensor is the most critical in all the sensor fault scenarios. This is because the economizer high-end limit is using a differential dry-bulb temperature in the studied sequences. When the return air temperature sensor has a severe positive bias, the economizer operation will be falsely disabled with the misjudgment that the return air temperature is warmer than the outside air temperature. The outdoor airflow rate sensor is also critical due to its direct effect on the ventilation control.

For the HVAC system peak power, severe positive bias of the AHU supply air temperature sensor and severe negative bias of the zone discharging air temperature sensor will both lead to a non-negligible power spike. This is because these two faults will cause the overcooling of the zones and thus the spasmodic operation of the zone terminal electric reheat coils. Furthermore, the considered sensor faults will not downgrade the power diversity in the cooling season.

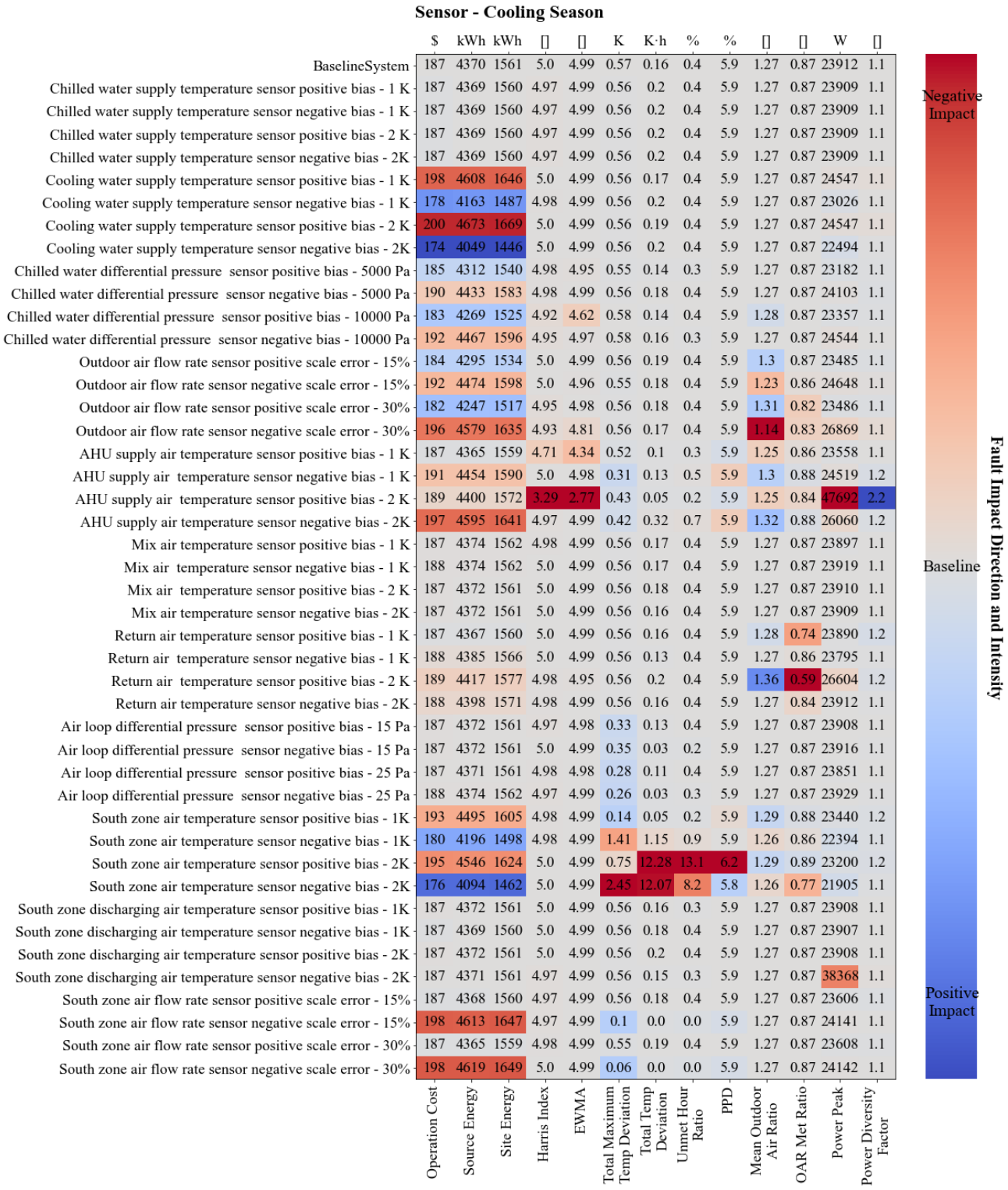

Figure 4-2 Fault impact over key KPIs of sensor faults in the cooling season

4.6.1.2 Duct & Pipe

Figure 4-3 shows the fault impact over key KPIs of duct & pipe faults in three seasons. From the energy and cost perspective, the supply duct leakage faults have a dominant impact compared to the other faults. The severe duct leakage will not only increase the fan energy consumption but also the energy consumption from the waterside HVAC equipment. We can also see that the poor pipe insulation in the heating season has more effects than that in the other seasons. For the supply air temperature control loop quality, the severe air duct leakage in the cooling and heating season has a more negative effect than that in the shoulder season. For the zone air temperature variations, thermal comfort, ventilation, and power diversity, the faults from pipe and duct have no discernible impact. It is also noted that the severe duct leakage could lead to a power spike in all three seasons.

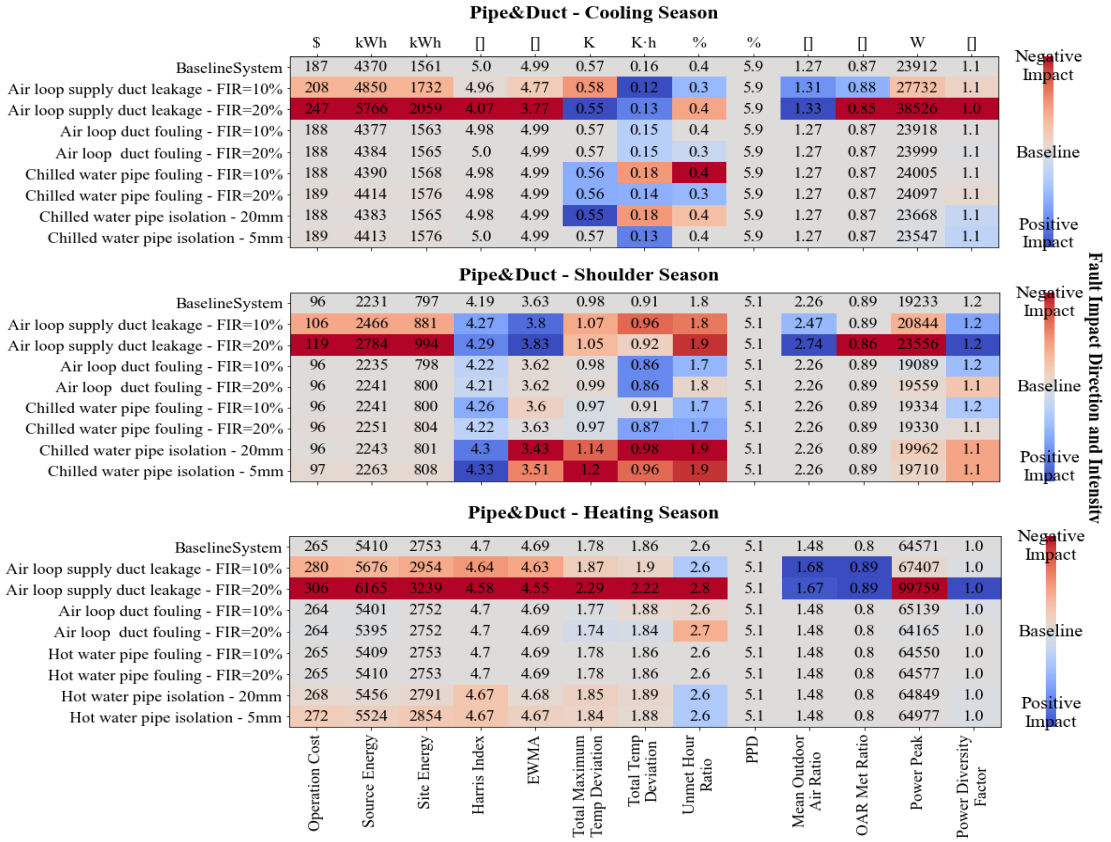

Figure 4-3 Fault impact over key KPIs of duct & pipe faults in three seasons

4.6.1.3 Damper & Valve

Figure 4-4 shows the fault impact over key KPIs of damper & valve faults in three seasons. It can be seen that the valve/damper leakage has a negligible impact on all the KPIs in all three seasons. This is because the valve/damper leakage only has some effects when the valve/damper is near full closed. However, this occasion is very limited for both modulating/isolation valve/damper in the study.

The cooling/heating coil stuck has different fault impacts for different stuck positions. When the valve is stuck at a smaller position than normal, the supply air temperature could not be maintained. Therefore, the AHU fan would be driven to a higher speed and consume more energy consumption. When stuck at certain very small valve positions, the bypass valve will be opened to maintain the plant equipment minimum flow rate and the plant equipment will operate under a small thermal load condition. On the other hand, when the valve is stuck at a fully open position, the waterside equipment will consume more energy consumption while the fan consumption will be reduced. If the zone is overcooled or heating is not sufficient, the electric reheat will be triggered to maintain the zone air temperature requirement. These are the main reasons why we have different fault impact results in terms of the energy and cost for different stuck positions and seasons. In the cooling season, the cooling coil valve stuck at the 65% open position has the most negative impact on the energy and cost. In the shoulder season, the cooling coil valve stuck at small open positions has the worst effect on the energy and cost. In the heating season, the heating coil valve stuck at the full closed position consumes the most source energy and cost. For the supply air temperature, the control quality for the three seasons is undermined because the valve is the actuator in this control loop. For the zone air temperature variations, the valve stuck at smaller positions in all seasons have an obvious impact. For thermal comfort, the valve stuck at

smaller positions in the cooling and shoulder season will cause comfort degradation while in the heating season the thermal comfort is unaffected because the zone terminal reheat will be activated if the heating is insufficient from the system-level. It is also noted that the peak power is largely increased for the fully open stuck valve in the cooling and shoulder season. This is because the zone is overcooled due to the provided low supply air temperature, thus triggering the instantaneous electric reheat in the VAV terminals.

The results show that the OA damper stuck fault will not only influence the energy and ventilation performance but also the thermal comfort in the cooling and shoulder season for the high-performance SOO sequences. The economizer dampers are not interlocked, and they are sequenced together with the cooling/heating coil valves per Section 5.16.2.3 in GDL36 [23]. Contrary to the conventional economizer SOO, the OA damper stuck near full closed in the cooling and shoulder season will influence the determination of the return air damper position, thereby causing the instability behavior of the whole system. From the energy and cost perspective, the OA damper stuck at a large opening position has the most negative impact due to the excessive outdoor air. For the supply air temperature control loop quality, the OA damper stuck near full closed in the cooling and shoulder season will have a propagating effect on this control loop. Furthermore, the zone air temperature variations, thermal comfort, ventilation, peak power, and power diversity are all impacted by the fault. It is also noted that the OA damper stuck at a higher opening position in the heating season will harm the energy, cost, zone air temperature variations, and power peak. The power spike is mainly from the increased fan power and instantaneous zone terminal electric reheat caused by the excessive outdoor air.

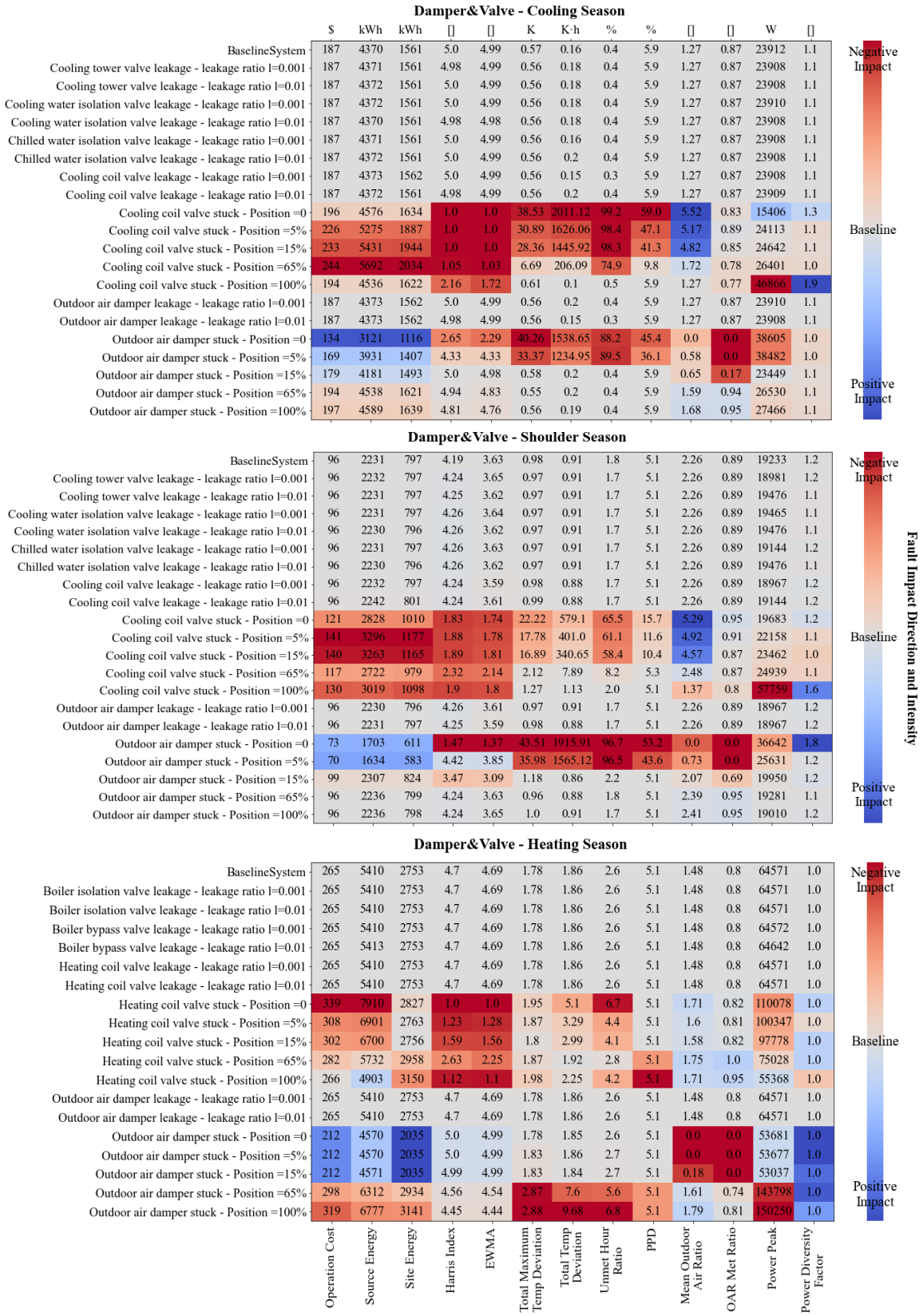

Figure 4-4 Fault impact over key KPIs of damper & valve faults in three seasons

4.6.1.4 HVAC Equipment

Figure 4-5 shows the fault impacts over key KPIs of HVAC equipment faults in the cooling season week. From the energy and cost perspective, the severe cooling coil fouling has the largest fault impact. The severe chiller non-condensable gas fault needs also to be noted. For the supply air temperature control loop, the quality declines sharply when the cooling coil has severe fouling. The thermal comfort, zone air temperature variations, peak power, and power diversity are all affected by this fault. The HVAC mechanical equipment faults seem to have little impact on the ventilation performance in the cooling season.

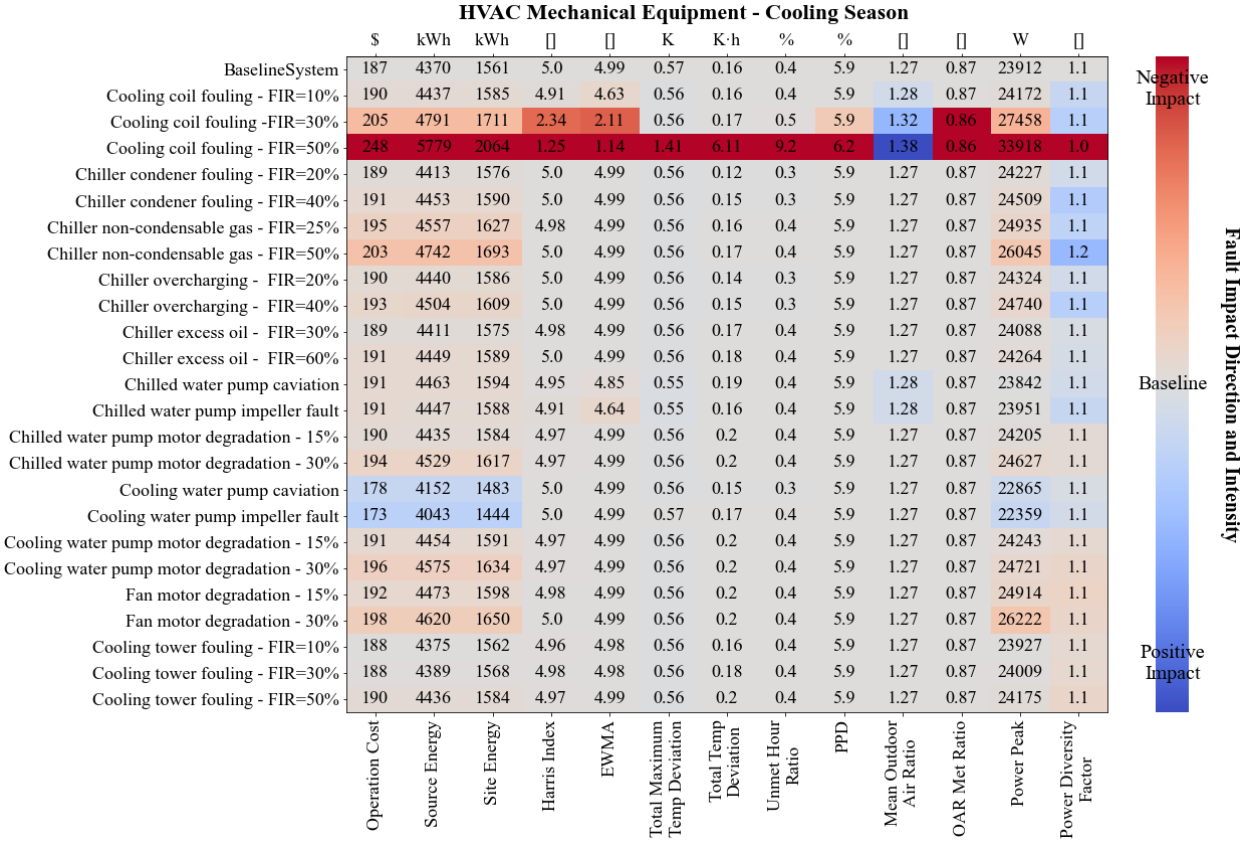

Figure 4-5 Fault impact over key KPIs of HVAC equipment faults in the cooling season

4.6.1.5 Control

Figure 4-6 shows the fault impacts over key KPIs of control faults in the cooling season week. In terms of energy and cost, the results show the inappropriate PID settings over the critical local controls in GDL36 do not have a substantial effect. The worst fault comes from the small P value scenario of the economizer PID loop, which increases the energy consumption by 4.8% due to the slow response of the outdoor damper position. When the chilled water temperature setpoint is fixed and set to the maximum value (10 ℃), the energy penalty is 19.6% of the baseline because the cooling provided from the plant is insufficient which drives the AHU supply fan to work much harder. This fault will also jeopardize the supply air temperature control quality and peak power. For the zone temperature variations and the thermal comfort, only the slow response tuning from the zone air cooling control loop matters. The aggressive tuning of the economizer PID loop would harm the ventilation performance.

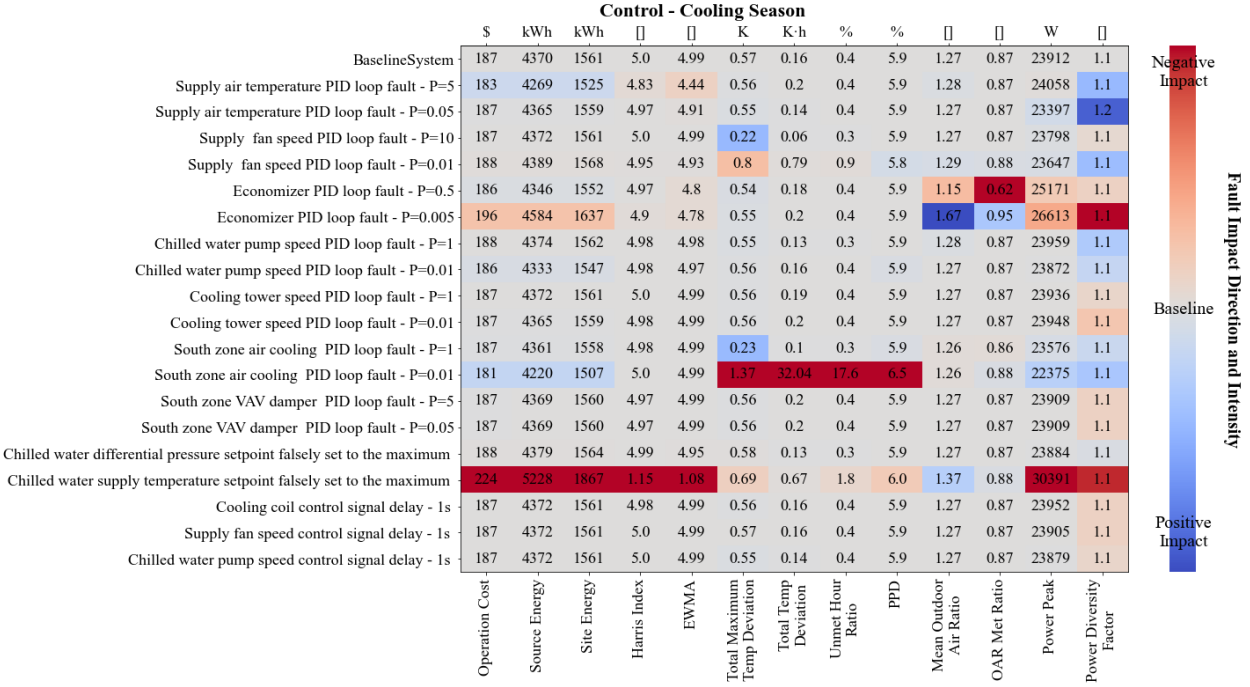

Figure 4-6 Fault impact over key KPIs of control faults in the cooling season

Figure 4-7 shows the fault impacts over key KPIs of control faults in the shoulder season week. Different from the cooling season, the supply air temperature air PID loop settings are more fault- influential in terms of multiple KPIs. If the P value is set too small in the shoulder season, the chiller would be called on late and more fan energy consumption is consumed at this time due to the sluggish response of the supply air temperature and the cooling coil valve position. The supply air temperature air control quality, thermal comfort, ventilation, and peak power will all then be jeopardized. When the chilled water temperature setpoint is set to its maximum value (10 ℃), the supply air temperature could not well track its setpoint and the energy and cost will be increased by 6%.

4.6.1.6 Scheduling

Figure 4-8 shows the fault impacts over key KPIs of scheduling faults in three season weeks. The results show that all the faults exert a negative impact on the energy and cost in all the seasons. It is noted that no temperature setback of the zone thermostats has the worst FIR on the operational cost of 19.8%, 12.5%, and 50.6%, respectively for the cooling, shoulder, and heating week. Although this fault has little influence on the zone air temperature variations and thermal comfort during the occupied period, the ventilation performance indexes decline due to the reduced supply air flow rate and the resulting reduced outdoor airflow rate.

4.6.1.7 Design

Figure 4-9 shows the fault impacts over key KPIs of design faults in three season weeks. The oversized cooling water pump has a worse impact on the energy cost than other oversized equipment in the cooling and shoulder season because the cooling water pump is only operated at the constant speed in the studied system. The oversized equipment faults have little impact on the other KPIs besides the energy and cost in three seasons. For the poor building airtightness, the

simulation shows it has a noticeable impact on the energy and cost in the heating season compared to the other two seasons. This fault would also have minimal effects on the other KPIs besides the energy and cost in the three seasons.

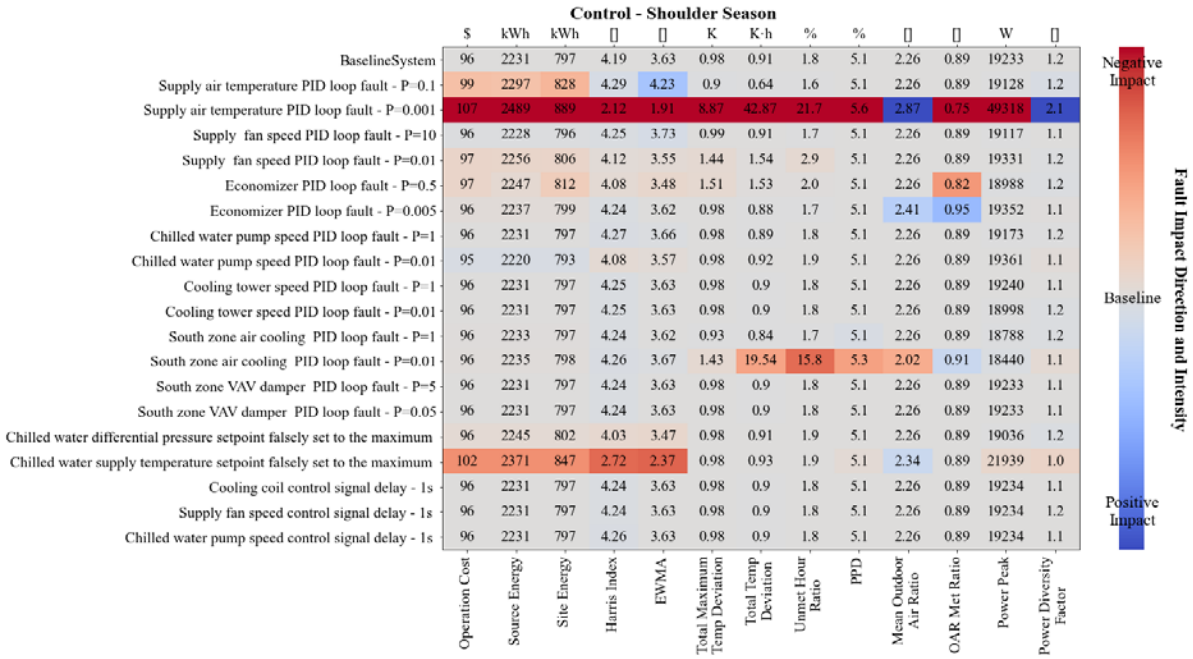

Figure 4-7 Fault impact over key KPIs of control faults in the shoulder season

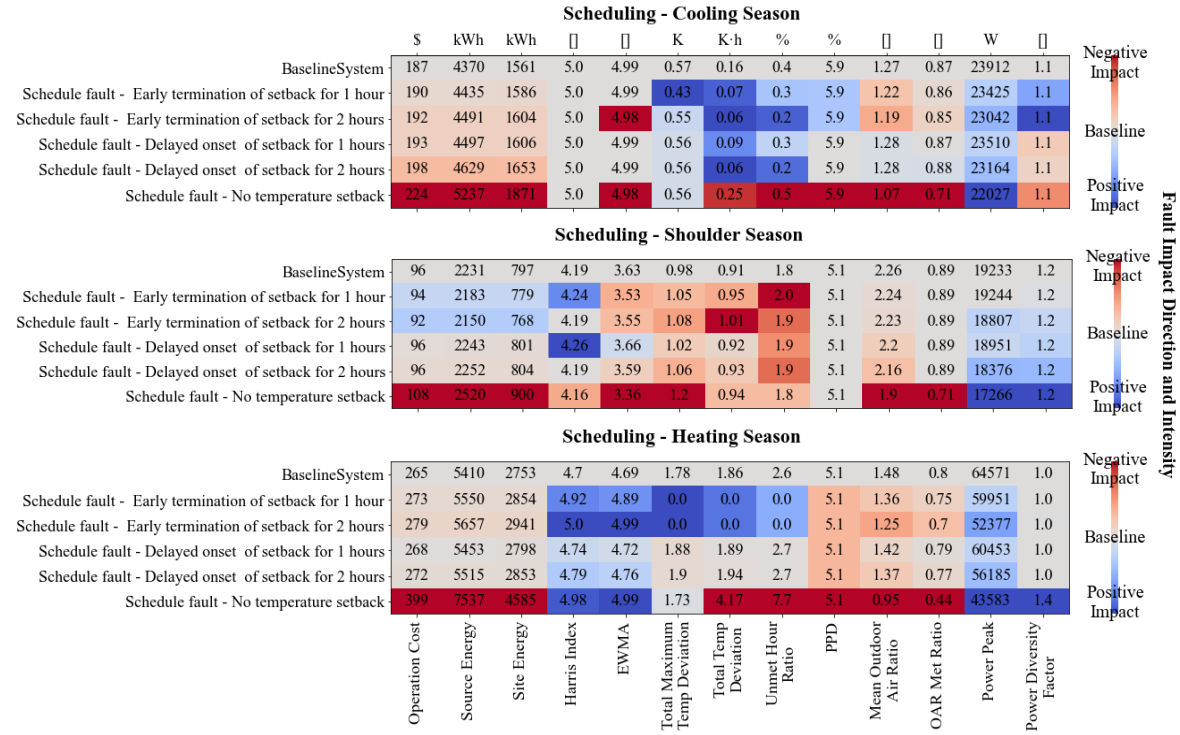

Figure 4-8 Fault impact over key KPIs of scheduling faults in three seasons

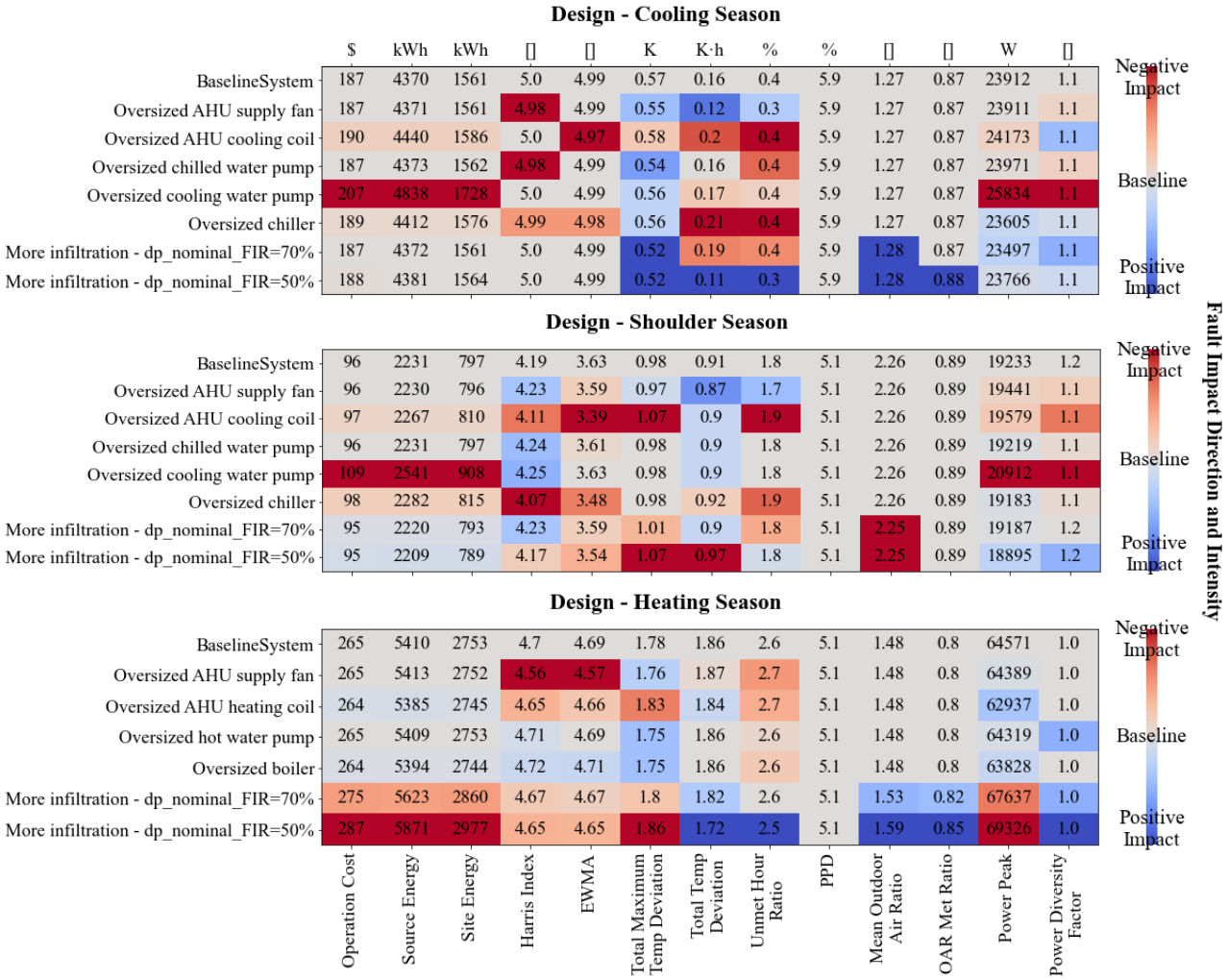

Figure 4-9 Fault impact over key KPIs of design faults in three seasons

4.6.2 Fault Ranking for Each Seasonal Operating Condition

Section 4.6.1 indicates the fault impact is correlated to the seasonal operation conditions. Having discussed the detailed results for each fault category, in this section, we will identify the most negative impact faults for each seasonal operating condition. The similarity and difference of the fault ranking among different seasonal operating conditions are also pointed out.

Legend	Fault Scenario: FIR	Font color in each cell represents the fault category as shown below					
	Sensors	Duct&Pipe	Valve&Damper	HVAC Equipment	Control	Schedule	Design

Rank	Operation Cost	Source Energy	Site Energy	Harris Index	EWMA	Total Maximum Temp Deviation	Total Temp Deviation	Unmet Hour Ratio	PPD	Mean Outdoor Air Ratio	OAR Met Ratio	Power Peak	Power Diversity Factor
1	CooCoiFou_50: 32.2	CooCoiFou_50: 32.2	CooCoiFou_50: 32.2	CooCoiValStuck_0: 80	CooCoiValStuck_0: 80	OADamStuck_0: 6963	CooCoiValStuck_0: 1256850	CooCoiValStuck_0: 28240	CooCoiValStuck_0: 904	OADamStuck_0: 100	OADamStuck_0: 100	TSup_p2: 99.4	SupDucLea_20: 9.6
2	SupDucLea_20: 31.9	SupDucLea_20: 31.9	SupDucLea_20: 31.9	CooCoiValStuck_5: 80	CooCoiValStuck_5: 80	CooCoiValStuck_0: 6660	CooCoiValStuck_5: 1016188	CooCoiValStuck_5: 28014	CooCoiValStuck_5: 700	OADamStuck_5: 54.3	OADamStuck_5: 100	CooCoiValStuck_100: 96	OADamStuck_0: 7.9
3	CooCoiValStuck_65: 30.3	CooCoiValStuck_65: 30.2	CooCoiValStuck_65: 30.3	CooCoiValStuck_15: 80	CooCoiValStuck_15: 80	OADamStuck_5: 5754	OADamStuck_0: 961556	CooCoiValStuck_15: 27983	OADamStuck_0: 672	OADamStuck_15: 48.8	OADamStuck_15: 80.5	OADamStuck_0: 61.4	OADamStuck_5: 7.4
4	CooCoiValStuck_15: 24.3	CooCoiValStuck_15: 24.3	CooCoiValStuck_15: 24.5	CooCoiValStuck_65: 79	CooCoiValStuck_65: 79.4	CooCoiValStuck_5: 5319	CooCoiValStuck_15: 903600	OADamStuck_5: 25469	CooCoiValStuck_15: 603	schedule_nosetback: 15.7	TRet_p2: 32.2	SupDucLea_20: 61.1	CooCoiFou_50: 6.7
5	CooCoiValStuck_5: 20.8	CooCoiValStuck_5: 20.7	CooCoiValStuck_5: 20.9	maxCHWTSupSP: 77	maxCHWTSupSP: 78.4	CooCoiValStuck_15: 4875	OADamStuck_5: 771744	OADamStuck_0: 25114	OADamStuck_5: 515	Vout_m30: 10.2	conkMinOut_5: 28.7	OADamStuck_5: 60.9	CooCoiValStuck_65: 6.4
6	schedule_nosetback: 19.8	schedule_nosetback: 19.8	schedule_nosetback: 19.9	CooCoiFou_50: 75	CooCoiFou_50: 77.2	CooCoiValStuck_65: 1074	CooCoiValStuck_65: 128706	CooCoiValStuck_65: 21291	CooCoiValStuck_65: 66.3	conkMinOut_5: 9.4	schedule_nosetback: 18.4	TSupSou_m2: 60.5	OADamStuck_100: 5.7
7	maxCHWTSupSP: 19.6	maxCHWTSupSP: 19.6	maxCHWTSupSP: 19.6	CooCoiValStuck_100: 56.8	CooCoiValStuck_100: 65.5	TAirSou_m2: 330	conVAVSoukCoo_01: 19925	conVAVSoukCoo_01: 4943	conVAVSoukCoo_01: 10.5	schedule_early_2: 6.3	TRet_p1: 14.9	CooCoiFou_50: 41.8	CooCoiValStuck_5: 5.4
8	SupDucLea_10: 11	SupDucLea_10: 11	SupDucLea_10: 11	CooCoiFou_30: 53.2	CooCoiFou_30: 57.7	TAirSou_m1: 147	TAirSou_p2: 7575	TAirSou_p2: 3637	TAirSou_p2: 5.8	schedule_early_1: 3.9	TAirSou_m2: 11.5	maxCHWTSupSP: 27.1	Vout_m30: 4.6
9	CWPump_oversized: 10.7	CWPump_oversized: 10.7	CWPump_oversized: 10.7	OADamStuck_0: 47	OADamStuck_0: 54.1	CooCoiFou_50: 147	TAirSou_m2: 7444	CooCoiFou_50: 2517	CooCoiFou_50: 5.1	Vout_m15: 3.1	CooCoiValStuck_100: 11.5	SupDucLea_10: 16	CooCoiValStuck_15: 4.6
10	CooCoiFou_30: 9.6	CooCoiFou_30: 9.6	CooCoiFou_30: 9.6	TSup_p2: 34.2	TSup_p2: 44.5	conVAVSoukCoo_01: 140	CooCoiFou_50: 3719	TAirSou_m2: 2243	maxCHWTSupSP: 2	TSup_p1: 1.6	CooCoiValStuck_65: 10.3	OADamStuck_100: 14.9	OADamStuck_65: 4.4

Figure 4-10 Fault ranking of top ten faults in terms of fault impact ratio in cooling season

Legend	Fault Scenario: FIR	Font color in each cell represents the fault category as shown below					
	Sensors	Duct&Pipe	Valve&Damper	HVAC Equipment	Control	Schedule	Design

Rank	Operation Cost	Source Energy	Site Energy	Harris Index	EWMA	Total Maximum Temp Deviation	Total Temp Deviation	Unmet Hour Ratio	PPD	Mean Outdoor Air Ratio	OAR Met Ratio	Power Peak	Power Diversity Factor
1	CooCoiValStuck_5: 47.8	CooCoiValStuck_5: 47.8	CooCoiValStuck_5: 47.8	OADamStuck_0: 64.9	OADamStuck_0: 62.3	OADamStuck_0: 4340	OADamStuck_0: 210440	OADamStuck_0: 5365	OADamStuck_0: 939	OADamStuck_0: 100	OADamStuck_0: 100	CooCoiValStuck_100: 200	maxCHWTSupSP: 9.3
2	CooCoiValStuck_15: 46.2	CooCoiValStuck_15: 46.3	CooCoiValStuck_15: 46.3	CooCoiValStuck_0: 56.3	CooCoiValStuck_0: 52.1	OADamStuck_5: 3571	OADamStuck_5: 171891	OADamStuck_5: 5351	OADamStuck_5: 751	OADamStuck_5: 67.7	OADamStuck_5: 100	TSup_p2: 158	CooCoiValStuck_15: 9
3	CooCoiValStuck_100:	CooCoiValStuck_100:	CooCoiValStuck_100:	CooCoiValStuck_5: 55.1	CooCoiValStuck_5: 51	CooCoiValStuck_0: 2167	CooCoiValStuck_0: 63537	CooCoiValStuck_0: 3599	CooCoiValStuck_0: 207	CooCoiValStuck_100: 39.4	OADamStuck_15: 22.5	conkTSup_01: 156	CooCoiFou_50: 8.2
4	CooCoiValStuck_0: 26.8	CooCoiValStuck_0: 26.8	CooCoiValStuck_0: 26.8	CooCoiValStuck_15: 54.9	CooCoiValStuck_100: 50.4	CooCoiValStuck_5: 1714	CooCoiValStuck_5: 43966	CooCoiValStuck_5: 3352	CooCoiValStuck_5: 127	Vout_m30: 26.1	schedule_nosetback: 20.2	TSup_p1: 149	CooCoiValStuck_65: 7.4
5	SupDucLea_20: 24.8	SupDucLea_20: 24.8	SupDucLea_20: 24.8	CooCoiValStuck_100: 54.7	CooCoiValStuck_15: 50.1	CooCoiValStuck_15: 1624	CooCoiValStuck_15: 37334	CooCoiValStuck_15: 3202	CooCoiValStuck_15: 104	TRet_m2: 15.9	conkTSup_01: 15.7	OADamStuck_0: 90.5	CooCoiValStuck_5: 6.4
6	CooCoiValStuck_65: 22.3	CooCoiValStuck_65: 22	CooCoiValStuck_65: 22.9	conkTSup_01: 49.4	conkTSup_01: 47.4	conkTSup_01: 805	conkTSup_01: 4611	conkTSup_01: 1128	conkTSup_01: 9.4	schedule_nosetback: 15.9	TRet_m2: 13.5	TSupSou_m2: 68.9	CooCoiFou_30: 5.2
7	CooCoiFou_50: 14.5	CooCoiFou_50: 14.5	CooCoiFou_50: 14.5	CooCoiValStuck_65: 44.6	CooCoiValStuck_65: 41	TAirSou_m2: 205	TAirSou_m2: 3290	TAirSou_m2: 805	TAirSou_m2: 4.7	Vout_m15: 12.8	CooCoiValStuck_100: 10.1	TSupSou_m1: 44.8	TAirSou_p2: 5
8	CWPump_oversized: 13.9	CWPump_oversized: 13.9	CWPump_oversized: 13.9	maxCHWTSupSP: 35.1	maxCHWTSupSP: 34.7	TAirSou_p2: 143	conVAVSoukCoo_01: 2047	conVAVSoukCoo_01: 792	conVAVSoukCoo_01: 4.3	conVAVSoukCoo_01: 10.6	conkMinOut_5: 7.9	OADamStuck_5: 33.3	pumChiImpeller: 4.3
9	schedule_nosetback: 13	schedule_nosetback: 13	schedule_nosetback: 13	CooCoiFou_50: 28.9	CooCoiFou_50: 30.9	TSup_m2: 139	CooCoiValStuck_65: 767	TAirSou_p2: 462	CooCoiValStuck_65: 6.7	TSup_p2: 10.2	TRet_p2: 6.7	CooCoiValStuck_65: 29.7	conVAVSoukCoo_01: 3.9
10	TCWSup_p2: 11.8	TCWSup_p2: 11.8	TCWSup_p2: 11.8	OADamStuck_15: 17.2	OADamStuck_15: 14.9	CooCoiValStuck_65: 116	TAirSou_p2: 560	CooCoiValStuck_65: 366	TAirSou_p2: 1.6	TRet_m1: 8.8	TRet_m1: 5.6	CooCoiFou_50: 24.9	RelPreCHW_m10000: 3.1

Figure 4-11 Fault ranking of top ten faults in terms of fault impact ratio in shoulder season

Legend Fault Scenario: FIR

Font color in each cell represents the fault category as shown below

Sensors | Duct&Pipe | Valve&Damper | HVAC Equipment | Control | Schedule | Design

Rank	Operation Cost	Source Energy	Site Energy	Control Harris Index	Control EWMA Index	Thermal Comfort Maximum Delta-T	Thermal Comfort Total Delta-T	Thermal Comfort Unmet Hour Ratio	PPD	Ventilation Mean Outdoor Air Ratio	Ventilation Outdoor Air Unmet Ratio	Peak Power	Power Diversity Factor
1	schedule_nosetback: 50.6	HeaCoiValStuck_0: 46.2	schedule_nosetback: 66.6	HeaCoiValStuck_0: 78.7	HeaCoiValStuck_0: 78.7	conkFanSpe_01: 219	TAirEas_p2: 3566	TAirEas_p2: 895	TAirEas_p2: 10.3	OADamStuck_0: 100	OADamStuck_0: 100	OADamStuck_100: 133	conkMinOut_1: 0.5
2	HeaCoiValStuck_0: 28.1	schedule_nosetback: 39.3	TAirEas_m2: 25	HeaCoiValStuck_100: 76.2	HeaCoiValStuck_100: 76.5	TAirEas_p2: 72.5	OADamStuck_100: 420	TAirEas_p1: 268	TAirEas_p1: 2	OADamStuck_5: 100	OADamStuck_5: 100	OADamStuck_65: 123	TSup_m2: 0.3
3	TAirEas_m2: 25.5	HeaCoiValStuck_5: 27.6	boiFou_20: 19.1	HeaCoiValStuck_5: 73.8	HeaCoiValStuck_5: 72.7	OADamStuck_100: 61.8	conkFanSpe_01: 361	TAirEas_m2: 195	TAirEas_m2: 1.5	OADamStuck_15: 87.8	OADamStuck_15: 100	HeaCoiValStuck_0: 70.5	HeaCoiValStuck_100 :
4	OADamStuck_100: 20.6	TAirEas_m2: 25.9	SupDucLea_20: 17.7	HeaCoiValStuck_15: 66.2	HeaCoiValStuck_15: 66.7	OADamStuck_65: 61.2	OADamStuck_65: 309	schedule_nosetback: 195	schedule_nosetback: 1.5	schedule_nosetback: 35.8	conkMinOut_1: 51.2	HeaCoiValStuck_5: 55.4	HeaCoiFou_50: 0.3
5	HeaCoiValStuck_5: 16.2	OADamStuck_100: 25.3	HeaCoiValStuck_10 0:	HeaCoiValStuck_65: 44	HeaCoiValStuck_65: 52	TAirEas_m2: 41	TAirEas_p1: 238	OADamStuck_100: 158	HeaCoiValStuck_100: 1	Vout_m30: 29.7	schedule_nosetback: 45	SupDucLea_20: 54.5	TAirEas_p1: 0.2
6	SupDucLea_20: 15.5	HeaCoiValStuck_15: 23.8	OADamStuck_100: 14.1	conkTSup_1: 38.1	HeaCoiFou_50: 30.9	SupDucLea_20: 28.7	TAirEas_m2: 206	HeaCoiValStuck_0: 154	TAirEas_m1: 0.5	conkMinOut_1: 27.7	Vout_m30: 42.5	HeaCoiValStuck_15: 51.4	THWSup_m2: 0.1
7	boiFou_20: 14.2	OADamStuck_65: 16.7	boiFou_10: 11.6	HeaCoiFou_50: 25.7	minHWTSupSP: 22	TAirEas_p1: 11.8	HeaCoiValStuck_0: 174	OADamStuck_65: 113	TSupEas_p1: 0.5	schedule_early_2: 15.5	Vout_m15: 16.2	conkFanSpe_01: 26.4	RelPreHW_m5000: 0.1
8	HeaCoiValStuck_15: 14	SupDucLea_20: 14	TAirEas_m1: 10.3	minHWTSupSP: 17.2	conkTSup_1: 20.3	HeaCoiValStuck_100: 11.2	schedule_nosetback: 124	conkFanSpe_01: 87.8	TSupEas_p2: 0.5	Vout_m15: 14.9	schedule_early_2: 12.5	HeaCoiFou_50: 25.8	RelPreHW_m10000: 0.1
9	OADamStuck_65: 12.5	boiFou_20: 10.8	infiltration_50: 8.2	HeaCoiFou_30: 5.5	conkTSup_01: 10	RelPreAir_p15: 9.6	HeaCoiValStuck_5: 76.9	HeaCoiValStuck_5: 69.1	HeaCoiValStuck_65: 0.5	schedule_early_1: 8.1	OADamStuck_65: 7.5	HeaCoiValStuck_65: 16.2	VSupEas_flow_m15: 0.1
10	TAirEas_m1: 10.2	TAirEas_m1: 10.2	HeaCoiValStuck_65: 7.5	OADamStuck_100: 5.3	HeaCoiFou_30: 7.9	HeaCoiValStuck_0: 9.6	HeaCoiValStuck_15: 60.8	HeaCoiValStuck_100: 61.1	OADamStuck_65: 0.5	TMix_m2: 7.4	schedule_early_1: 6.3	minHWTSupSP: 14	HeaCoiValStuck_5: 0.1

Figure 4-12 Fault ranking of top ten faults in terms of fault impact ratio in heating season

4.6.2.1 Fault Ranking for the Cooling Season

Figure 4-10 illustrates the fault ranking list of the top ten faults in terms of fault impact ratio in the cooling season. For the energy and cost, the top five negative impact faults come from the severe cooling coil fouling, severe supply air duct leakage, and cooling coil valve stuck fault at the positions smaller than the normal case; For the supply air temperature control loop quality, the most influential faults are the cooling coil valve stuck at the positions smaller than the normal case and inappropriate CHW supply temperature setpoint; For the zone air temperature variations and thermal comfort, top five negative impact faults come from the cooling coil valve stuck fault at small positions and OA damper stuck at the very small position. It is noted that their impact is even higher than the zone terminal control and sensor faults. For the ventilation performance, the top five negative impact faults come from OA damper stuck at small positions and return air temperature sensor positive bias. The severe supply air temperature positive bias and cooling coil valve stuck at fully open almost double the peak power, which needs attention from the power grid perspective; The maximum FIR for power diversity factor is less than 10%, which indicates the insignificance of the fault impact on this KPI; Looking at all the KPI columns, we can see that the severe cooling coil fouling and cooling coil valve stuck at the positions smaller than the normal case appear in the majority of the columns, which indicates they are most fault-influential in the cooling season considering multiple KPIs.

4.6.2.2 Shoulder Season

Figure 4-11 illustrates the fault ranking list of the top ten faults in terms of fault impact ratio in shoulder season. For the energy and cost, the top five negative impact faults come from cooling coil valve stuck fault at the positions smaller than the normal case and the severe supply air duct leakage; For the supply air temperature control loop quality, the most influential faults are

the OA damper stuck at full closed and the cooling coil valve stuck fault; For the zone air temperature variations and thermal comfort, similar findings could be obtained that the top five negative impact faults come from the cooling coil valve stuck fault at small positions and OA damper stuck at very small position, whose impact is higher than the zone terminal control and sensor faults; For the ventilation performance, top five negative impact faults come from OA damper stuck at small positions, no temperature setback scheduling fault, and the slow response setting of the supply air temperature control; In terms of the peak power, cooling valve stuck at 100%, supply air temperature sensor severe positive bias, and supply air temperature control fault are top three negative impact faults on the power grid; Looking at all the KPI columns in the shoulder season, we can see that the cooling coil valve stuck at the positions smaller than the normal case appear in majority of the columns. Overall, although some ranking sequences are different for certain KPI, the faults that appear in the ranking list look similar to the cooling season.

4.6.2.3 Heating Season

Figure 4-12 illustrates the fault ranking list of the top ten faults in terms of fault impact ratio in the heating season. For the energy and cost, the top negative impact faults come from no temperature setback scheduling fault, and the coil valve stuck at full closed. The zone air temperature severe sensor negative bias will impact heavily on the overall energy and cost due to the major increase from the terminal electric resistance coil power consumption; For the supply air temperature control loop quality, the most influential faults are the heating coil valve stuck faults; For the zone air temperature variations and thermal comfort, top negative impact faults come from the zone air temperature sensor faults, which is different from results in the cooling and shoulder season. The sluggish tuning of the supply fan speed control also negatively impacts the thermal comfort; For the ventilation performance, the top five negative impact faults come

from OA damper stuck at small positions, no setback schedule fault, and economizer control fault; In terms of the peak power, the OA damper stuck at a large position and heating valve stuck faults matter the most. Overall, the faults in the ranking list are more diversified in terms of the fault category and the fault list appears to be dissimilar compared to the cooling and shoulder season.

4.6.3 Fault Impact Ratio Distribution for Each KPI

In this section, the fault impact ratio distributions in each seasonal operating condition for different KPIs are illustrated in the form of the boxplot as shown in Figure 4-13 - Figure 4-17. To provide the insight of the FIR high limit for the majority of the fault scenarios, the interquartile range (IQR) rules with the multiplier of 1.5 are used to exclude the “outliers” that represent the fault scenarios with the outstanding FIRs. In the boxplots, the raw data are also depicted as the stripplot to show the observations along with some representation of the underlying distribution. The median value and the maximum value after excluding the “outliers” are also annotated in the figures.

4.6.3.1 Energy and Cost

Figure 4-13 depicts the fault impact ratio distribution in terms of operational cost, source energy, and site energy overall fault scenarios in three seasons. It can be seen that the FIR distributions for the operational cost and source energy show a subtle distinction while the FIR distributions for the site energy in the cooling and shoulder season have a wider spread than that in the heating season. The FIR upper fences for these KPIs are less than 6% which indicates that the overwhelming majority of the faults (~90%) have minor effects on the energy and cost for the GDL36 sequences.

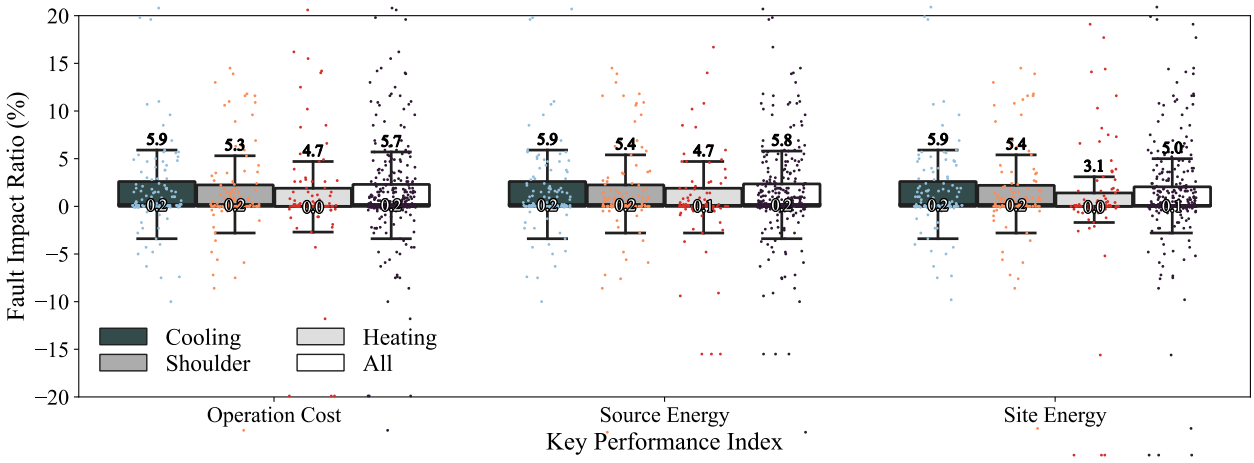

Figure 4-13 Fault impact ratio distribution in terms of energy and cost

4.6.3.2 Supply Air Temperature Control Loop Quality

Figure 4-14 depicts the fault impact ratio distribution in terms of the supply air temperature control loop quality overall fault scenarios in three seasons. For the two indexes, the FIR distribution in the shoulder season is more distinctive than that in the cooling and heating season. The FIR upper fence for this control loop is less than 5% over the three seasons which indicates that the vast majority of the faults (~90%) have slight impacts on the supply air temperature control loop for the GDL36 sequences.

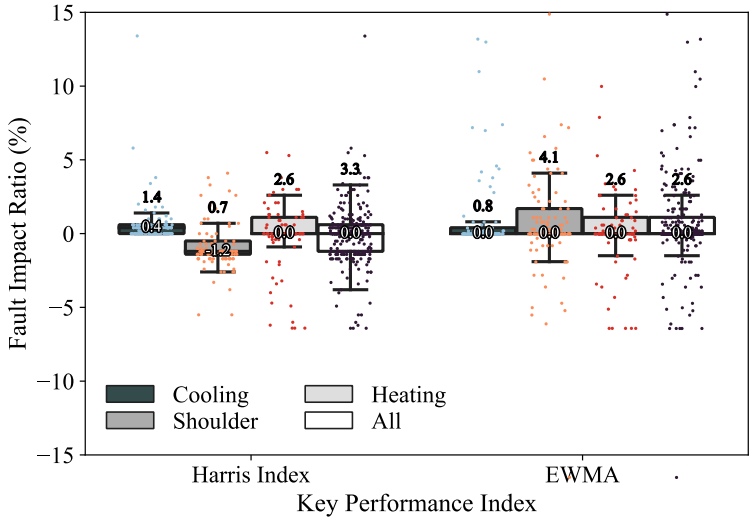

Figure 4-14 Fault impact ratio distribution in terms of control loop quality

4.6.3.3 Thermal Comfort

Figure 4-15 depicts the fault impact ratio distribution for the thermal comfort metrics overall fault scenarios in three seasons. For the maximum value of the zone air temperature deviation, the FIR distribution in the shoulder season has a wider range compared to the cooling and heating season. For the total zone air temperature deviation and the unmet hour ratio, the FIR distribution in the cooling has a broader spectrum compared to the other two seasons. Although the FIR of these two KPIs has a wider range in the cooling season, the PPD in the cooling season is barely affected. This is because the total zone air temperature deviation and the unmet hour ratio for the baseline case are very small, which are 0.16 K·h and 0.4%, respectively. Even with an FIR of 100%, these two KPIs become 0.32K·h and 0.8%, which are considered as small temperature deviation and unmet hour ratio. As for the PPD in all three seasons, the maximum and median values are both rounded to 0, which implies all the fault scenarios would have no bearing on the thermal comfort.

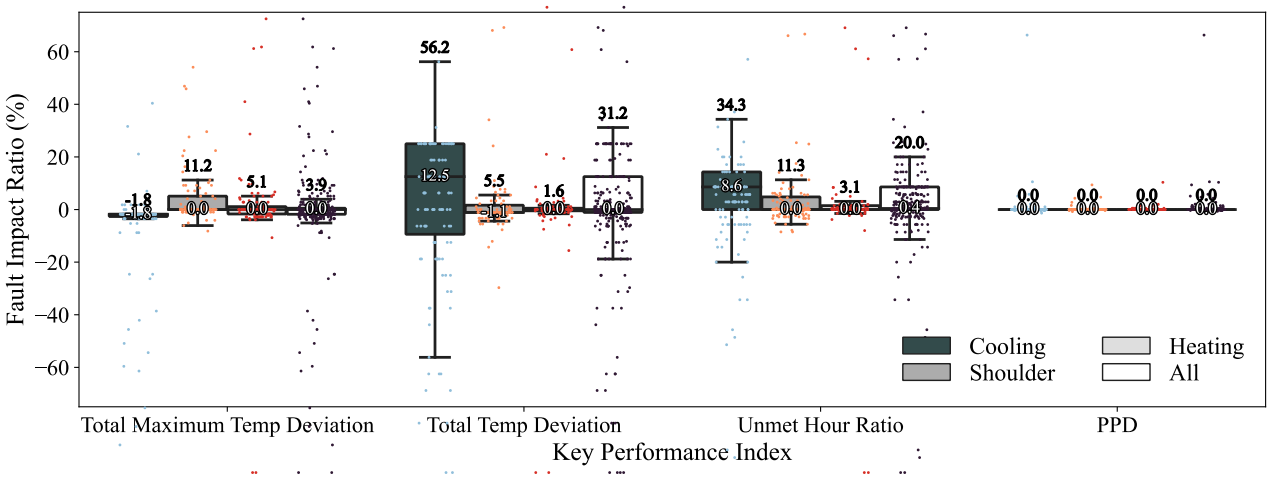

Figure 4-15 Fault impact ratio distribution in terms of thermal comfort

4.6.3.4 Ventilation

Figure 4-16 depicts the fault impact ratio distribution for the ventilation performance overall fault scenarios in three seasons. notwithstanding the fact that some fault scenarios reduce

the ventilation performance in a great ratio, the majority of the fault scenarios are insignificant as the maximum FIR values for all the seasons are 0.

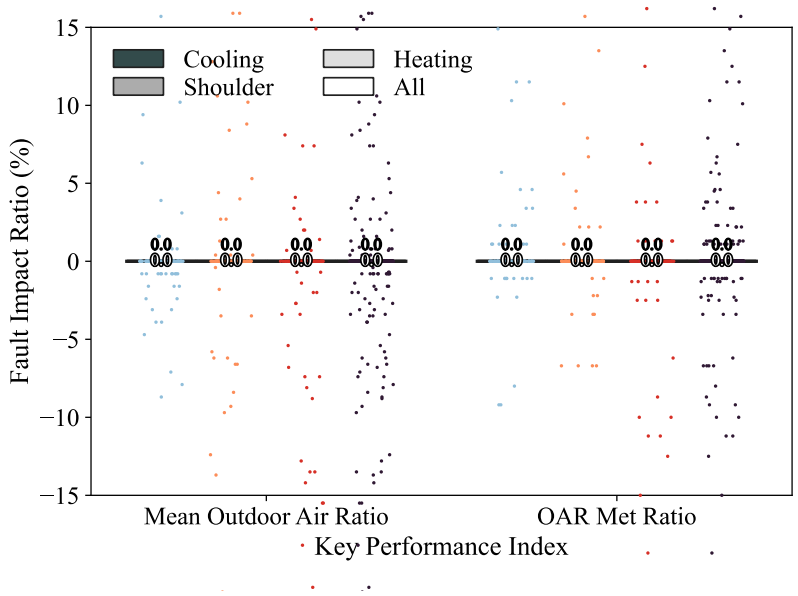

Figure 4-16 Fault impact ratio distribution in terms of ventilation

4.6.3.5 Power System

Figure 4-17 depicts the fault impact ratio distribution from the power system perspective overall fault scenarios in three seasons. For the peak power, the FIR distributions in three seasons make a slight difference and the maximum FIR value is less than 7% over the three seasons. For the power diversity factor, the ranges of distribution are narrow, which suggests all the fault scenarios would influence the power diversity with minimal effects.

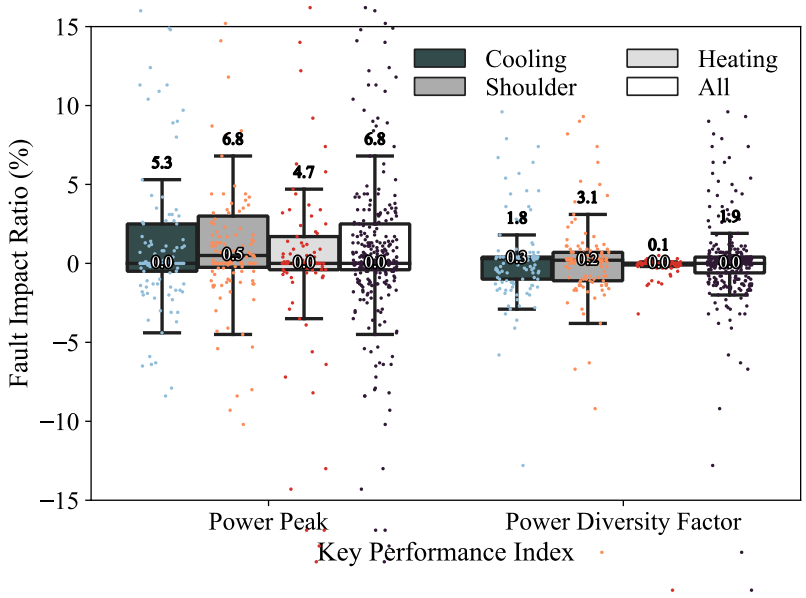

Figure 4-17 Fault impact ratio distribution in terms of power grid

4.7 Conclusions, Limitations, and Future Work

Robustness to various types of faults should also be one of the aspects to claim the high-performance sequences of operation. In this chapter, comprehensive fault impact analysis and robustness assessment of the GDL36 were conducted in the Modelica-based five-zone VAV system virtual testbed. A total of 359 fault scenarios in three different seasonal operating conditions are injected into the baseline model. The evaluated KPIs include the operational cost, source energy, site energy, control loop quality, thermal comfort, ventilation, and power system metrics.

The results show that the fault impact is related to the seasonal load conditions. For the same fault scenario, its FIR has a certain variance over the three load conditions. For the cooling season, severe cooling coil fouling and cooling coil valve stuck at positions smaller than the normal case are identified to be the most influential faults for the majority of the KPIs. For the shoulder season, cooling coil valve stuck at positions smaller than the normal case is still the top influential fault, but the severe cooling coil fouling has fewer effects over multiple KPIs. For the heating

season, the top influential faults become more diversified. The no temperature setback fault, the heating coil stuck fault, and the zone air temperature bias are top-ranked among multiple KPIs.

The vast majority (~90%) of all the fault scenarios have an FIR of less than 6% on the energy consumption and energy cost with a fixed-rate structure, which suggests GDL36 sequences are well adapted for the faults from the energy and cost perspective in this study. Likewise, for the other KPIs, the FIR distributions indicate that most of the fault scenarios would influence the supply air temperature control quality, the thermal comfort, the ventilation performance, and the power system, with a limited impact.

The comprehensive fault simulation was conducted in Chicago, 5A. Only scenarios with a single fault are studied, and all the faults are assumed to happen at all times in each seasonal week. In addition, the fault impact and robustness analysis are applied to the five-zone VAV system virtual testbed following GDL36. The future work includes the consideration of the detailed fault occurrence, the degradation faults, and the annual fault impact analysis on the other commercial building types and weather profiles.

4.8 References

[1] Kim W, Katipamula S. A review of fault detection and diagnostics methods for building systems. Science Technology for the Built Environment. 2018;24:3-21.

[2] House JM, Vaezi-Nejad H, Whitcomb JM. An expert rule set for fault detection in air-handling units/Discussion. ASHRAE Transactions. 2001;107:858.

[3] Schein J, Schein J. Results from field testing of embedded air handling unit and variable air volume box fault detection tools: US Department of Commerce, National Institute of Standards and Technology; 2006.

[4] Kiriu R, Taylor ST. Automatic Fault Detection and Diagnostics and Hierarchical Fault Suppression in ASHRAE RP-1455. ASHRAE Transactions. 2017;123.

[5] Kim J, Cai J, Braun JE, Frank SM. Common Faults and Their Prioritization in Small Commercial Buildings. 2018.

[6] Li Y, O'Neill Z. A critical review of fault modeling of HVAC systems in buildings. Building Simulation. 2018;11:953-75.

[7] Zhang R, Hong T. Modeling of HVAC operational faults in building performance simulation. Applied Energy. 2017;202:178-88.

[8] Li Y, O'Neill Z. An innovative fault impact analysis framework for enhancing building operations. Energy and Buildings. 2019;199:311-31.

[9] Lu X, O'Neill Z, Li Y, Niu F. A novel simulation-based framework for sensor error impact analysis in smart building systems: A case study for a demand-controlled ventilation system. Applied Energy. 2020;263:114638.

[10] Kim J, Frank S, Braun JE, Goldwasser D. Representing small commercial building faults in energyplus, Part I: Model development. Buildings. 2019;9:233.

[11] Leach M, Kim J. Curated Modeled Fault Data Set. 2019.

[12] ASHRAE. Sequences of Operation for Common HVAC Systems: American Society of Heating Refrigerating and Air-Conditioning Engineers; 2005.

[13] Chen Y, Huang S, Vrabie D. A simulation-based approach to impact assessment of physical faults: large commercial building HVAC case study. 2018 Building performance modeling conference and SimBuild co-organized by ASHRAE and IBPSA-USA Chicago, IL, USA2018.

[14] Lu X, Fu Y, O'Neill Z, Wen JJE, Buildings. A holistic fault impact analysis of the high-performance sequences of operation for HVAC systems: Modelica-based case study in a medium-office building. 2021;252:111448.

[15] Wetter M, Zuo W, Nouidui TS, Pang X. Modelica buildings library. Journal of Building Performance Simulation. 2014;7:253-70.

[16] Shia J. Continuous Commissioning of Buildings: HVAC Fault Detection and Diagnosis: UC Berkeley; 2018.

[17] Wen J, Li S. RP-1312 Tools for Evaluating Fault Detection and Diagnostic Methods for Air-Handling Units. The American Society of Heating, Refrigerating and Air-Conditioning Engineers (ASHRAE); 2012.

[18] Granderson J, Lin G, Harding A, Im P, Chen YJSd. Building fault detection data to aid diagnostic algorithm creation and performance testing. 2020;7:1-14.

[19] Ferretti NM, Galler MA, Bushby ST. Performance Monitoring of Chilled-Water Distribution Systems Using HVAC-Cx. ASHRAE Transactions. 2017;123:53.

[20] Ferretti NM, Milesi-Ferretti N, Galler MA, Bushby ST, Sorra J. Commissioning ASHRAE High-performance Sequences of Operation for Multiple-zone Variable Air Volume Air Handling Units: US Department of Commerce, National Institute of Standards and Technology; 2019.

[21] Milesi-Ferretti NS, Galler MA, Bushby ST, Leader R, Whitcomb J, Rush DW. Retro-Commissioning a Performing Arts Center using HVAC-Cx. 2019.

[22] Schein J, Bushby ST. Fault detection & diagnostics for AHUs and VAV boxes. ASHRAE journal. 2005;47:58.

[23] ASHRAE Guideline 36. High Performance Sequences of Operation for HVAC Systems. American Society of Heating, Refrigerating, and Air-conditioning Engineers (ASHRAE); 2018.

[24] Taylor Engineering. RP-1711 Advanced Sequences of Operation for HVAC Systems – Phase II Central Plants and Hydronic Systems. The American Society of Heating, Refrigerating and Air-Conditioning Engineers (ASHRAE); 2017.

[25] Li Z, Huang G. Preventive approach to determine sensor importance and maintenance requirements. Automation in construction. 2013;31:307-12.

[26] Haleem SMA, Pavlak GS, Bahnfleth WP. Performance of advanced control sequences in handling uncertainty in energy use and indoor environmental quality using uncertainty and sensitivity analysis for control components. Energy and Buildings. 2020;225:110308.

[27] Roth KW, Westphalen D, Feng MY, Llana P, Quartararo L. Energy impact of commercial building controls and performance diagnostics: market characterization, energy impact of building faults and energy saving potential. Prepared by TAIX LLC for the US Department of Energy. 2005.

[28] Wray CP, Matson NE. Duct leakage impacts on VAV system performance in California large commercial buildings. Lawrence Berkeley National Lab. (LBNL), Berkeley, CA (United States); 2003.

[29] Zhai ZJ, Johnson SN. Full-scale laboratory test on energy dependence on pressure drops in HVAC systems. Procedia Engineering. 2017;205:2133-40.

[30] Taylor S. ASHRAE Guideline 36 - High Performance Sequences of Operation for HVAC Systems (Part 2). 2020.

[31] Cheung H, Braun JE. Empirical modeling of the impacts of faults on water-cooled chiller power consumption for use in building simulation programs. Applied thermal engineering. 2016;99:756-64.

[32] Bonaros V, Gelegenis J, Harris D, Giannakidis G, Zervas K. Analysis of the energy and cost savings caused by using condensing boilers for heating dwellings in Greece. The 5th International Conference on Applied Energy ICAE2013, Pretoria, Paper2013. p. 1-4.

[33] Dockrill P, Friedrich FD. Boilers and Heaters: Improving Energy Efficiency: Natural Resources Canada, Office of Energy Efficiency; 2001.

[34] Kermeli A, Worrell E. Energy Efficiency and Cost Saving Opportunities for Breakfast Cereal Production: An ENERGY STAR® Guide for Energy and Plant Managers. 2018.

[35] Liang J, Du R. Model-based fault detection and diagnosis of HVAC systems using support vector machine method. International Journal of refrigeration. 2007;30:1104-14.

[36] Bendapudi S, Braun JE. Development and validation of a mechanistic, dynamic model for a vapor compression centrifugal liquid chiller. Report of ASHRAE. 2002.

[37] Sakthivel N, Sugumaran V, Babudevasenapati. Vibration-based fault diagnosis of monoblock centrifugal pump using decision tree. Expert Systems with Applications. 2010;37:4040-9.

[38] Song WS, Hong SH, Park TJ. The effects of service delays on a BACnet-based HVAC control system. Control Engineering Practice. 2007;15:209-17.

[39] Song WS, Hong SH, Bushby ST. A performance analysis of bacnet® local area networks. HVAC&R Research. 2008;14:289-305.

[40] EIA. 2012 Commercial Buildings Energy Consumption Survey (CBECS). 2015.

[41] Emmerich SJ, Persily AK. Analysis of US commercial building envelope air leakage database to support sustainable building design. International Journal of Ventilation. 2014;12:331-44.

[42] Wetter M. BuildingsPy. Lawrence Berkeley National Lab.(LBNL), Berkeley, CA (United States); 2019.

[43] EIA. Average Price of Electricity to Ultimate Customers by End-Use Sector. 2021.

[44] Constellation. What Is the Average Cost Per Therm of Natural Gas? 2020.

[45] EnergyStar. Source Energy - Use Portfolio Manager. Technical Reference2020.

[46] Li Y, O'Neill ZD, Zhou X. Development of control quality factor for HVAC control loop performance assessment I—Methodology (ASHRAE RP-1587). Science Technology for the Built Environment. 2019;25:656-73.

[47] Liu R, Li Y, O'Neill ZD, Zhou XJS, Environment TftB. Development of control quality factor for HVAC control loop performance assessment—II: Field testing and results (ASHRAE RP-1587). Science Technology for the Built Environment. 2019;25:873-88.

[48] Fanger P. Thermal environment—Human requirements. Environmentalist. 1986;6:275-8.

[49] Dawe M, Raftery P, Woolley J, Schiavon S, Bauman F. Comparison of mean radiant and air temperatures in mechanically-conditioned commercial buildings from over 200,000 field and laboratory measurements. Energy and Buildings. 2020;206:109582.

[50] Lu X, Yang T, O'Neill Z, Zhou X, Pang Z. Energy and ventilation performance analysis for CO2-based demand-controlled ventilation in multiple-zone VAV systems with fan-powered terminal units (ASHRAE RP-1819). Science Technology for the Built Environment. 2020;27:139-57.

[51] ASHRAE. ANSI/ASHRAE Standard 62.1-2019 Ventilation for Acceptable Indoor Air Quality 2019.

[52] O'Neill ZD, Li Y, Cheng HC, Zhou X, Taylor STJS, Environment TftB. Energy savings and ventilation performance from CO2-based demand controlled ventilation: Simulation results from ASHRAE RP-1747 (ASHRAE RP-1747). 2020;26:257-81.

[53] Frank SM, Lin G, Jin X, Singla R, Farthing A, Zhang L, et al. Metrics and methods to assess building fault detection and diagnosis tools. National Renewable Energy Lab.(NREL), Golden, CO (United States); 2019.

CHAPTER V DEVELOPMENT AND EVALUATION OF CO_2-BASED DCV SOO IN MULTIPLE ZONE VAV SYSTEMS WITH FAN-POWERED TERMINAL UNITS*

5.1 Introduction

CO_2-based DCV has been popular in the heating, ventilation, and air-conditioning (HVAC) industry for the last forty years. We have seen the penetration and acceptance of this technology in the market and its mandatory stipulation in many building codes regarding energy efficiency and occupant health. ASHRAE Standard 90.1 Energy Standard for Buildings Except Low-Rise Residential Buildings [1] mandates the DCV system for densely occupied spaces since the 1999 version and also requires the DCV system be in compliance with ASHRAE Standard 62.1 [2], which stipulates that the minimum outdoor air intake be based on the sum of ventilation rates required to dilute pollutants generated by occupants (e.g., bioeffluents) as well as the sum of the floor area. DCV was also required in the California Building Energy Efficiency Standards [3] for high-density applications during low occupancy periods. ASHRAE Standard 62.1 User's Manual [2] has provided a detailed procedure on how to apply the CO_2-based DCV since 2004. To be specific, the ASHRAE Standard 62.1 User's Manual includes an appendix showing the underlying theory and a control scheme for using CO2 concentration for DCV in accordance with the Ventilation Rate Procedure (VRP) of ASHRAE Standard 62.1. The DCV is also suggested in a building certification process, WELL Building Standard™ (WELL) [4] keep carbon dioxide levels

* Reprinted with permission from "Energy and ventilation performance analysis for CO2-based demand-controlled ventilation in multiple-zone VAV systems with fan-powered terminal units (ASHRAE RP-1819)" by Xing Lu, Tao Yang, Zheng O'Neill, Xiaohui Zhou, and Zhihong Pang, 2020. Science and Technology for the Built Environment, 0, 1-19, Copyright [2020] by ASHRAE.

in the space below 800 ppm for spaces with an actual or expected occupant density greater than 25 people per 93 m².

ASHRAE project 1747 developed control sequences that are practical and implementable in typical multi-zone single-duct VAV systems with DDC systems [5]. The current GDL36 includes the specifications for determining the zone-level minimum airflow setpoints and minimum outdoor airflow setpoints. However, the CO_2-based SOO have yet to be merged into the current GDL36. In addition, the CO_2-based DCV SOO for the multi-zone VAV systems with recirculating paths have not been developed.

5.2 Literature Review

5.2.1 CO_2-based DCV SOO in the Literature

Demand-controlled ventilation (DCV) is defined as a system that achieves 'automatic reduction of outdoor air intake below design rates when the actual occupancy of spaces served by the system is less than design occupancy [1]. Measuring the zone carbon dioxide (CO_2) concentration could be an indirect approach to monitor the level of bioeffluents generated by occupants since, in general, the CO_2 generation rate is proved to be proportional to odorous bioeffluent generation rates [6, 7].

DCV technologies in different HVAC system configurations have been explored with varying strategies of control, such as the single-zone VAV system, multiple-zone single-path VAV systems, multiple-zone VAV systems with multiple recirculation paths, and split air-conditioning system [8]. Table 5-1 summarizes the existing studies in the last decade for different system configurations and control strategies.

Using CO_2-based DCV in simple single-zone HVAC systems is relatively well understood in the early year. With a single-zone system, the breathing zone CO_2 concentration can be used to

directly control the outdoor air (OA) damper. Three control methods were used. The setpoint control method opens or closes the outdoor air intake damper depending on the indoor CO_2 concentration. The proportional control method adjusts intake damper or outdoor air fan flow proportionally to the CO_2 concentration level. The PI (proportional-integral) control method [9] also considers the rate of change in the CO_2 concentration level [10]. Apart from these control methods, model-based controls are also proposed in the literature. Lu et al. [11] proposed a simple model-based DCV control for sports training arenas and similar kinds of buildings, which used an exponential relationship between the CO_2 concentration level and the ventilation rate. The results show that the estimated indoor CO_2 concentrations are much closer to the CO_2 set point than those with the proportional control approach, and +34% of energy usage related to ventilation air can be saved. Similarly, Wang et al. also [12] presented a model-based control of CO_2 concentration for multiple-zone systems aiming at achieving a high indoor air quality level. The Lyapunov function approach was introduced to prove the stability of the system. In addition, an internal model control (IMC) system was designed with an internal loop, which continually checks the momentary CO_2 concentration, and makes the necessary adjustments to the airflow for a gallery building [13]. The results showed a significant reduction in the CO_2 level when using an IMC controller, in comparison with a feedback controller. Lachhab et al. [14] proposed a CO_2-based DCV strategy using a state feedback technique for a single-story commercial building using an EnergyPlus simulation. The simulation results indicated that the CO_2-based state feedback control led to a better comfort with improved energy efficiency as compared to the traditional On/Off and PI controls. In their latest study, the internet of sensors and data fusion techniques were incorporated with the DCV state feedback control [15]. Closed-loop model-based predictive control (MPC)

controller and open-loop MPC controller were designed and compared to control the CO_2 concentrations below a certain limit and minimize the energy consumption [16].

With a multiple-zone single-duct VAV system, each zone in the system requires a different fraction of OA, while the primary air delivers the same fraction of OA to all zones. To ensure the proper ventilation that satisfies the ventilation requirement, the critical zone should be adequately ventilated while all others are over-ventilated, and the unused OA from the noncritical zones is accounted for during recirculation. As a result, the system OA intake should be modulated to ensure the critical zone is maintained at no less than the current required minimum. There exists a few CO_2-based DCV control strategies for multiple zone HVAC systems in literature and practice including 1) Supply air CO_2-based DCV control strategies [17, 18], 2) DCV control strategy from California Title 24 [3]. Lin et al. proposed the theoretical equations required to use CO_2 concentration as an indicator of real-time occupant-related ventilation requirements [19] and developed the control logic (refer to RP-1547 Logic) that provides potential energy savings while ensuring compliance with Standard 62.1 [20]. However, RP-1547 control sequences are complex, and iterations used in control logic algorithms cannot be implemented into real Direct Digital Control (DDC) systems in modern buildings. To address this limitation, O'Neill et al. developed control sequences that are practical and implementable in typical multiple-zone single-duct VAV systems with DDC systems [5]. Their logic was referred to as the ASHRAE Project 1747 (RP-1747) Logic. They tested the proposed logic in realistic simulations that account for varying occupancy and concurrent cooling loads [21]. In addition, they also assessed the proposed sequences in a well-instrumented testing facility - the Iowa Energy Center's Energy Resource Station.

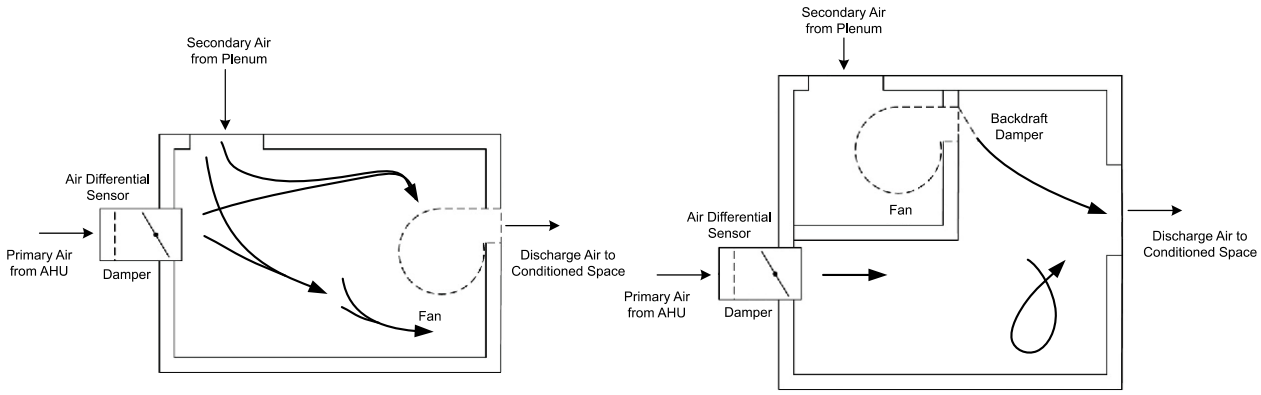

Figure 5-1 Simplified schematics of (a) Series (b) Parallel fan-powered terminal unit

5.2.2 Limitations

Although these studies demonstrated considerable energy savings and good ventilation compliance implementing DCV in multiple zone systems, they were limited to single-duct VAV systems. There still a gap remained for researchers and practitioners to implement DCV following ASHRAE standard 62.1 for multiple zone VAV systems with multiple recirculation paths. As a part of which, fan-powered terminal units (FPTUs), are zonal terminal equipment to maintain zone setpoint temperature [22, 23]. Two air streams, namely the primary air processed by AHUs and the secondary air drawn from the plenum area of the conditioned space, are mixed and delivered to the conditioned space. There are two configurations for FPTUs: series and parallel, as depicted in Figure 5-1 [24]. The fans in series FPTUs (SFPTUs) are in line with the supply airstream and operating continuously while fans in parallel FPTUs (PFPTUs) are outside the primary airflow and run only in the heating mode. The DCV control sequences for FPTUs have not been developed yet in part due to the mathematical complexity of CO_2 mass balance equations for these systems. In addition, there is a lack of building simulation or field testbeds to evaluate the performance of the proposed control sequences due to the system intricacy.

Table 5-1 Summary of CO_2-based DCV in different systems and control strategies

Year	Authors	System Type	DCV Control Strategies	Simulation/Field Test	Room/Building Type	CO_2 Sensor Location
2011	Lu et al.	Single zone VAV	Simple model-based (Open-loop)	Simulation	Sports training arena	AHU return duct
2013	Lü et al.	Single zone VAV	Zone CO_2 setpoint feedback control	Simulation	Sports training center	In the zone
2013	Wang et al.	Multiple zone Single Path VAV	Model-based (Open-loop)	Field Test	Not mention	Each zone; fixed on stands with a height of 1.5m
2014	Gruber et al.	Single zone VAV	Zone CO_2 setpoint PI control; Closed-loop model predictive controller; Open-loop predictive controller	Simulation	A seminar room	Exhaust duct
2014	Škrjanc et al.	Single zone VAV	Internal model control	Simulation	A gallery room	In the zone
2014	Nassif	Multiple zone Single Path VAV	CO_2 Supply air setpoint feedback	Simulation	Classroom building	Supply air duct
2014	Lin et al.	Multiple zone Single Path VAV	AHU and zone CO_2-based dynamic reset	Simulation	Office building	Zone, AHU primary air, return air
2014	Fan et al.	Package air conditioner with energy recovery ventilator	Zone CO_2 setpoint PI control	Field Test	Office building	In the zone center
2014	Liu et al.	Single zone VAV	Multivariate model predictive control	Simulation	A server room	In the zone
2018	Schibuola et al.	Multiple zone Single Path VAV	CO_2 return air setpoint feedback	Field Test	Library	AHU return duct
2018	Lachhab et al.	Single zone VAV	State-feedback control	Field Test	A security staff office	In the zone
2019	Shriram et al.	Ductless split air conditioners	CO_2 setpoint ON/OFF	Both	Single workspace	In the zone

2019	O’Neill et al.	Multiple zone Single Path VAV	AHU and zone CO_2-based dynamic reset	Both	Office building	Zone, AHU primary air
2020	Zhao et al.	Multiple zone Single Path VAV	Discrete outdoor airflow rate determination	Field Test	A postgraduate office	AHU return duct

5.3 Contributions and Chapter Organization

In this context, the contributions of this chapter are listed as follows:

- To develop the theoretical equations required to use CO_2 concentration as an indicator of occupant related pollutant concentration for multiple zone VAV systems with FPTUs.
- To develop practical sequences for DCV in the VAV system with FPTUs.
- To simulate the sequences in realistic models to evaluate energy and ventilation performance.

The chapter is organized as follows. First, the studied VAV systems with FPTUs are briefly illustrated, and corresponding control sequences are summarized. In particular, the theoretical equations required to use CO_2 concentration as an indicator of occupant related pollutant concentration are deducted using the CO_2 mass balance. Next, the development of a simulation-based testbed and case description of an office building is presented using four typical climate zones (i.e., 1A (Miami, FL), 3A (Atlanta, GA), 3C (Oakland, FL), and 5A (Chicago, IL)). In the next section, we discuss the energy and ventilation performance of the DCV control sequences, followed by conclusions. We will first present the detailed simulation results in one climate zone using the VAV system with SFPTU as an example, and then discuss the energy and ventilation performance in four climate zones for the VAV system with SFPTU and the VAV system with PFPTU.

5.4 Description of the Studied Systems

The studied systems include multiple zone VAV systems with the series fan-powered terminal unit and the parallel fan-powered terminal unit, as shown in Figure 5-2 and Figure 5-3. Local controls for zone terminals and air handling units (AHUs) comply with ASHRAE Guideline

36-2018 [25]. GDL36 offers multiple variations and sequences of control for common terminal types. Currently, only the following terminal control sequences are considered in this study: a parallel fan-powered terminal unit with a constant volume fan, a series fan-powered terminal unit with a constant volume fan.

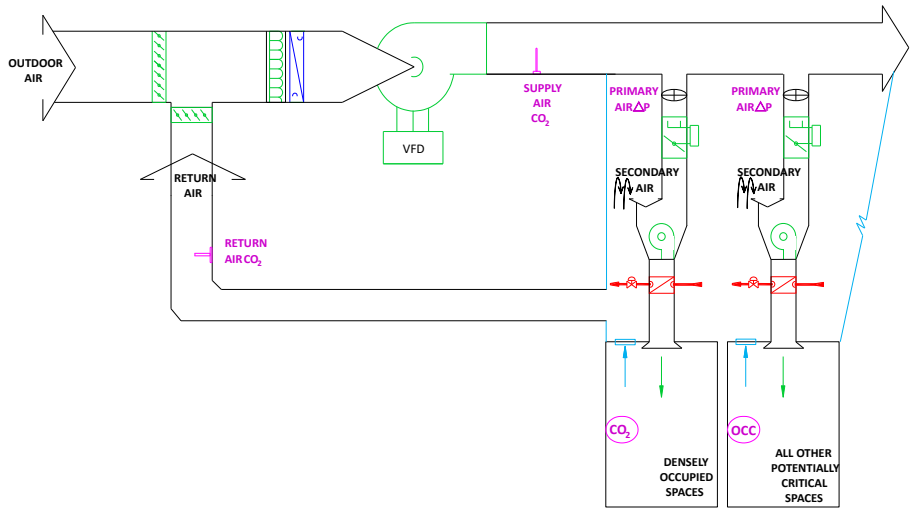

Figure 5-2 Control schematic of VAV system with series fan-powered terminal units

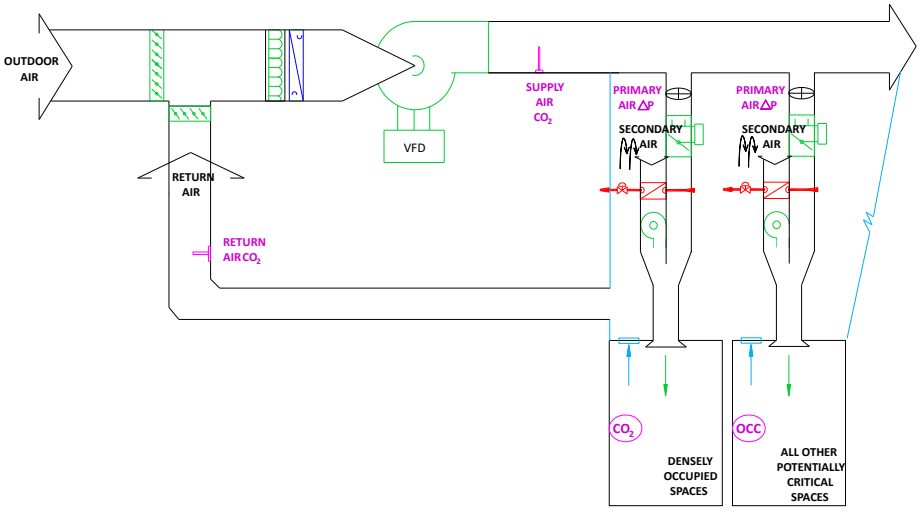

Figure 5-3 Control schematic of VAV system with parallel fan-powered terminal units

The key sensors for the proposed control logic are:

- System-level CO_2 sensor:

- Supply air CO_2 sensor at the AHU level
- Return air CO_2 sensor at the AHU level

- Inlet airflow sensor within the primary airstream of FPTU
- Discharging airflow sensor at some distance downstream the terminal unit
- Densely occupied zones with CO_2 sensors
- Other zones with occupancy sensors
- Sparsely occupied zones with no additional controls

5.4.1 Summary of the DCV Control Sequences

The sequences developed for multiple zone VAV systems with FPTUs is similar to sequences developed in the ASHRAE RP-1747 [5, 21], in which the logic is broken into zone-level and system-level calculations to reduce the network traffic.

At the zone-level, actual zone ventilation needs are dynamically determined using CO_2 (or occupancy) and airflow sensors for occupant component, adjusted for zone air distribution effectiveness. For the zones with CO_2 sensors, the required breathing zone outdoor airflow (V_{bz}) is calculated using the readings from CO_2 and airflow sensors in different locations for different systems. The subsection will present the detailed calculation procedure based on the CO_2 mass balance.

5.5 Deduction of Required Breathing Zone Outdoor Airflow Using CO_2 Mass Balance

The theoretical equations required to use CO_2 concentration as an indicator of occupant related pollutant concentration are developed based on the CO_2 mass balance for the two systems. In the following we use SFPTU as an example to illustrate the derivation process. Using a similar approach, the theoretical equations can also be deducted for the PFPTU.

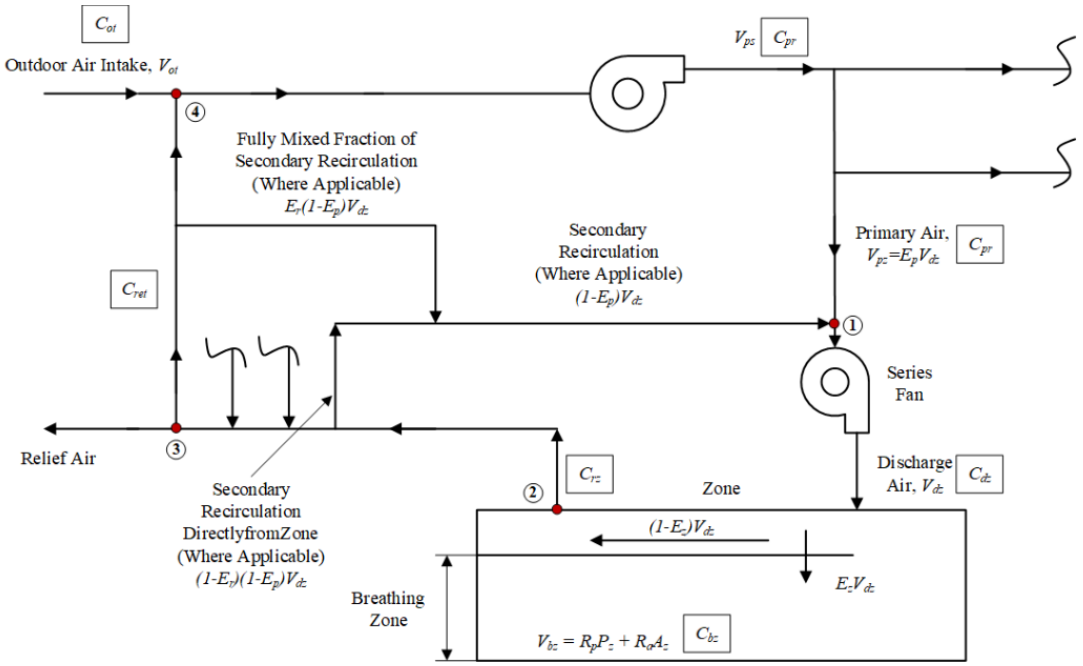

Figure 5-4 CO_2-based demand control ventilation system schematic for series fan-powered terminal units

1) Breathing zone

Using a control volume around the breathing zone, we have a mass balance Eq. (5-1) for CO_2 for the SFPTU as shown in Figure 5-4.

$$\dot{N} + E_z V_{dz} C_{dz} - E_z V_{dz} C_{bz} = V \frac{\partial C_{bz}}{\partial t} \tag{5-1}$$

2) Supply air side (Point 1)

We have a mass balance Eq. (5-2) for the supply air point:

$$C_{dz} = C_{rz}(1 - E_r)(1 - E_p) + C_{pr}E_p + C_{ret}E_r(1 - E_p) \tag{5-2}$$

3) Return air side (Point 2)

We have a mass balance Eq. (5-3) for the return air point at a zone-level:

$$C_{rz} = C_{dz}(1 - E_z) + C_{bz}E_z \tag{5-3}$$

4) Combining Eq.(5-2) and Eq. (5-3):

$$C_{dz} = \frac{C_{bz}E_z(1-E_r)(1-E_p) + C_{pr}E_p + C_{ret}E_r(1-E_p)}{1-(1-E_z)(1-E_r)(1-E_p)} \quad (5\text{-}4)$$

5) Assuming it is steady-state, Eq.(5-1) can be simplified in to:

$$\dot{N} = E_z V_{dz} C_{bz} - E_z V_{dz} C_{dz} \quad (5\text{-}5)$$

6) If people are the only sources of CO_2 in the zone, then the source strength of CO_2 is:

$$\dot{N} = kmP \cdot 10^6 \quad (5\text{-}6)$$

7) Combining equations (5-2)-(5-5), we have:

$$P = \frac{E_z V_{dz}[C_{bz}(1-(1-E_r)(1-E_p)) - C_{pr}E_p - C_{ret}E_r(1-E_p)}{k \cdot m \cdot F_c \cdot 10^6} \quad (5\text{-}7)$$

8) For the zones with CO_2 sensors in the SFPTU, we have

$$V_{bz} = MIN(\, V_{bz-P} + V_{bz-A}\,,$$

$$\frac{\max\left[0,\ C_{b_z}\left(1-(1-E_r)\left(1-E_p\right)\right) - C_{pr}E_p - C_{ret}E_r\left(1-E_p\right)\right] \cdot E_z \cdot V_{dz} \cdot R_t}{k \cdot m \cdot F_c \cdot 10^6} \quad (5\text{-}8)$$

$$+ V_{bz-A}\,),$$

where

C_{pr}: the concentration of CO_2 in the primary air, ppm.

C_{ret}: the concentration of CO_2 in the return air at the air handler, ppm.

E_p: the primary air fraction. The fraction of the primary air in the discharge air to the ventilation zone.

E_r: the secondary recirculation fraction. In systems with the secondary recirculation of the return air, the fraction of the secondary recirculated air to the zone that is representative of the average system return air rather than the air directly recirculated from the zone.

E_z: the zone air distribution effectiveness: a measure of the effectiveness of supply air distribution to the breathing zone.

F_c: the outdoor air fraction. The fraction of outdoor air to the ventilation zone that includes sources of air from outside the zone. $F_c=1-(1-E_z) * (1-E_r) * (1-E_p)$ (This is the same definition in ASHRAE 62.1 Appendix A).

P: the estimated number of people in the zone serving by an FPTU system.

V_{bz-P}: the population component of the breathing zone outdoor airflow.

V_{bz-A}: the area component of the breathing zone outdoor airflow.

V_{bz}: the breathing zone outdoor airflow, cfm.

V_{dz}: the zone discharge airflow, cfm. It is normally measured using a discharge airflow sensor at some distance downstream of the terminal unit.

Using a similar approach, the V_{bz} for the zones with CO_2 sensors in the PFPTU can be derived. It is noted that the series and parallel fan-powered terminal unit systems share the same theoretical equations (5-7) and (5-8).

The zone primary airflow minimums are then reset using T&R logic. If the primary air is rich with outdoor air due to an economizer operation, zone minimums are reduced. Otherwise, the zone minimums are increased for critical zones only to ensure the required outdoor airflow rate at AHU is never above the design rate. At the system-level, the required AHU outdoor air intake (V_{ot}) is dynamically determined using the ASHRAE Standard 62.1 Ventilation Rate Procedure. This value is then the input to the economizer control to maintain the supply air temperature by adjusting the outdoor air and return air damper positions. On top of that, the outdoor air ratio (OAR, the ratio of actual outdoor airflow to the required AHU outdoor air intake) is calculated to determine whether the outdoor air is rich and sufficient. The OAR rich binary value is broadcasted to the zone controllers to adjust minimum setpoints in the T&R logic. The rationale behind the logic is that when primary air is mostly outdoor air due to economizer operation, zone airflow minimums

can be very low, all the way down to the zone minimum ventilation rate when supply air is 100% outdoor air. When the economizer is disabled, the zone minimums in the critical zones go the other way: they are increased to induce more primary airflow in the critical zones. It is possible for the minimum airflow in the critical zone to increase to its maximum airflow.

The kernel of the developed RP-1819 sequence is similar to the one developed in the ASHRAE RP-1747 [5, 21]. The major differences lie in (1) Calculation of required breathing zone outdoor airflow V_{bz} using CO_2 mass balance for the zone with CO_2 sensors, as detailed in the last subsection; (2) Definition of the critical zones; and (3) Calculation of the system ventilation efficiency E_v (e.g., Equations (5-9)-(5-12) for FPTUs) using the ASHRAE Standard 62.1 Ventilation Rate Procedure. Apart from these details, the general ideas behind the logics are very similar between the RP-1747 and RP-1819.

$$E_v = \min\left(E_{vz}\right) \tag{5-9}$$

$$E_{vz} = 1 + X_s - Z_{pz} \times F_c \tag{5-10}$$

$$X_s = \frac{V_{ou}}{V_{ps}} \tag{5-11}$$

$$F_c = 1 - (1 - E_z) \times (1 - E_r) \times (1 - E_P), \tag{5-12}$$

where X_s is the average OA fraction, and F_c is the fraction of outdoor air to the ventilation zone that includes sources of air from outside the zone. E_z is the zone air distribution effectiveness. E_r is the secondary recirculation fraction and equal to 0 for the FPTUs. E_p is the primary air fraction, that is, the fraction of the primary air in the discharge air to the ventilation zone.

5.6 Simulation Testbed

5.6.1 Co-simulation

A co-simulation [26] of EnergyPlus and CONTAM [27] through Functional Mock-up Unit (FMU) is conducted, which is similar to the ASHRAE RP-1747 approach [5]. EnergyPlus is used

for the energy simulation, while CONTAM is used for the airflow simulation. The detailed airflow simulation using CONTAM could lead to a more accurate infiltration calculation, which will have a large impact on the CO_2 concentration results. The outputs from CONTAM program provide the zone infiltration flow rates and zone mixing air flow rates to EnergyPlus. These variables overwrite the counterparts in the zone contaminant calculation in EnergyPlus. On the other hand, EnergyPlus takes care of the zone contaminant calculation, demand control ventilation, and building energy simulation. The DCV related control sequences are coded in the EnergyPlus Energy Management System (EMS) module. How these DCV control sequences are implemented is described in Section *EnergyPlus Models*. EnergyPlus thus sends back CONTAM boundary conditions such as zone air temperatures, outdoor environmental parameters, system-level air flow rates, and the outdoor air fractions. The results from EnergyPlus are also used to evaluate the energy saving potential from the proposed practical DCV control strategies and verify whether ASHRAE Standard 62.1 required ventilation rates can be satisfied in each space.

5.6.2 Case Description

The candidate building for simulation is the former Iowa Energy Center Energy Resource Station (ERS). This building was also the testbed for ASHRAE RP-1747. Simulation inputs including building geometry, internal heat gains, and dynamic occupancy schedules are exactly the same as those in the EnergyPlus model of RP-1747 [21]. HVAC equipment and system in the original RP-1747 model are replaced with the system of interests for this work. There are eight test rooms, four offices, two classrooms, and a media center. The proposed DCV control strategies are applied to eight test rooms (office West A, office West B, office South A, office South B, office Interior A, conference East A, conference South B, and conference Interior A). Three conference test rooms have CO_2 sensors. Four office rooms install occupancy sensors and one open office

West A does not have either CO_2 sensor or occupancy sensors. Table 5-2 lists the design ventilation parameters for the eight test zones.

Table 5-2 Design ventilation parameters for eight test zones

Room	Occ Type	Area (A_z)	OA Flow/ Area (R_a)	Zone Popula-tion (P_z)	OA Flow/ Person (R_p)	Metabolic Rate (m)	CO_2 sensor ?	Occ Sensor?	Occ Standby Allowed ?
Units	--	ft^2	cfm/ft^2	#	cfm/p	met	--	--	--
West B	Private office	266	0.06	2	5	1	N	Y	Y
South A	Private office	266	0.06	2	5	1	N	Y	Y
East B	Private office	266	0.06	1	5	1	N	Y	Y
Interior B	Conference	320	0.06	8	5	1	Y	Y	Y
Interior A	Private office	266	0.06	2	5	1	N	Y	Y
West A	Open office	600	0.06	4	5	1	N	N	N
South B	Conference	600	0.06	20	5	1	Y	Y	Y
East A	Conference	280	0.06	14	5	1	Y	Y	Y

5.6.3 EnergyPlus Models

EnergyPlus has been used for modeling FPTUs [23, 28-31]. Through ASHRAE research projects and an AHRI project, three major issues with FPTU models in EnergyPlus were identified: 1) variable airflow FPTUs, 2) leakage from parallel FPTUs, and 3) specification of input parameters. Since this study is focusing on the FPTU with a constant volume fan, the first limitation will not be applied to this study. Furthermore, the objective of the proposed simulation is to evaluate the energy and ventilation performance, assumptions of no leakage for both the

baseline and the proposed cases are valid. To resolve the third issue, suggestions from Faris et al. [32] are carefully followed using the default values found in EnergyPlus and necessary domain knowledge of an expected range of supply air temperature, pressure drop, and fan/motor efficiencies.

EnergyPlus models are developed using the ERS building in four different climate zones. We use the version 9.0.1. The internal load schedules and occupancy schedules for each zone are taken from ASHRAE RP-1747 [21]. Figure 5-5 shows the air loop configurations of the SFPTU in EnergyPlus as an example. The VAV terminal local controls are constant volume series fan-powered VAV zone control and constant volume parallel fan-powered VAV zone control [25]. The economizer control is using a fixed dry-bulb temperature following ASHRAE 90.1. The high-limit shut off temperature is 66 ˚F, 66 ˚F, 75 ˚F, and 70 ˚F for Miami, Atlanta, Oakland, and Chicago, respectively.

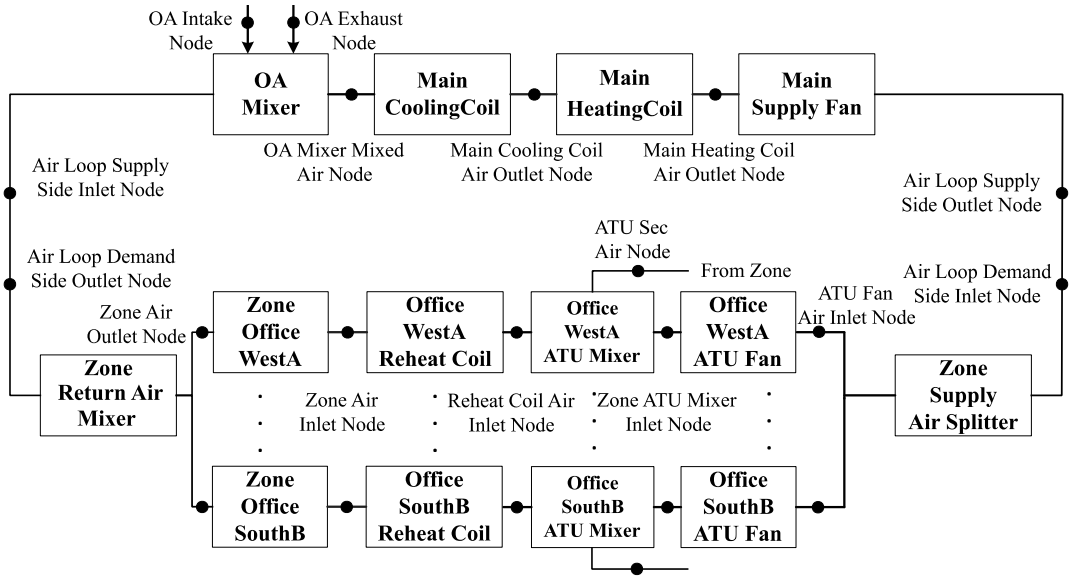

Figure 5-5 Air loop configuration of the SFPTU in EnergyPlus

To implement the proposed control sequences including the DCV control and local terminal unit controls, EMS module is adopted. EMS sensor module will get the CO_2 concentrations from individual zones, and then pass the information to the EMS subroutines with

the control logics. The DCV control requires a dynamic reset of zone and system-level airflow minimum setpoints (minimum primary airflow for the FPTUs). Eq. (5-8) is used to calculate the zone-level minimum air flow setpoints and Eqs. (5-9)-(5-12) are unitized to calculate the system-level airflow minimum setpoints. The dynamic reset is achieved by using actuators in EMS that override actuator's variable inside EnergyPlus whenever there is a need for the reset. However, the standard EnergyPlus package does not have available actuators for zone-level airflow minimum setpoints. Therefore, a customized EnergyPlus needs to be compiled to have the actuator of 'Minimum Primary Air Flow Fraction' in *AirTerminal:SingleDuct :SeriesPIU:Reheat* Module and *AirTerminal:Single Duct:ParallelPIU:Reheat* Module. The system-level AHU minimum outdoor airflow is dynamically reset by manipulating 'Minimum Outdoor Air Schedule' in *Controller:OutdoorAir* Module, which is already existing in the actuator list from a standard EnergyPlus. On top of that, actual control logics such as T&R logic to reset the zone minimum setpoints with "requests" are modeled using EMS subroutines, and such logic only involves simple and straightforward mathematical equations. In the field testing, the ASHRAE RP-1747 control sequence uses a T&R ratio of 5% with an updating frequency of 1 minute. Due to the limitation of the EnergyPlus building envelope conduction heat transfer algorithm, it is not feasible to have a time step of 1 minute in EnergyPlus. Simulation time steps in both EnergyPlus and CONTAM were set as 5 minutes. After a sensitivity study, the T&R ratio is set as 12.5% for all simulation studies presented.

5.6.4 CONTAM Model

CONTAM model was built for exchanging airflow information with EnergyPlus. It was created through the pseudo-geometry concept, without drawing the actual building floor plans to scale. It is required to have inputs, including the actual thermal zone areas, window sizes, and door

sizes, etc. The AHU system is also required for supply air terminals and return air terminals at each thermal zone. Details of the CONTAM model can be found from ASHRAE RP-1747 [5, 21].

5.6.5 Baseline

Two baselines are considered. The first baseline is following a simplified compliance approach from an addendum in ASHRAE 62.1, while the second baseline is following California Title 24. The simplified ASHRAE 62.1 approach is used to replace the current Table 6.2.5.2 in ASHRAE 62.1. The new approach would provide a new method to determine the system ventilation efficiency (E_v) and also determine the zone minimum primary airflow as 1.5 times of zone required outdoor air (V_{oz}). The primary goal with this approach, and why it is used as a baseline here, is that it provides a simple, deterministic approach to establish the system-level required outdoor air (V_{ot}). The zone airflow minimums (V_{z_min}) for eight test rooms are listed in Table 5-3 with zone air distribution effectiveness (E_z) values of 0.8. The system-level outside air minimums are 583 CFM and 880 CFM for the baselines of the simplified ASHRAE 62.1 and California Title 24, respectively.

Table 5-3 Zone air flow minimums for two baselines

Room	Simulated Area A_z	Zone Population P_z	Diversified Population	Design Breathing Zone Ventilation	Simplified 62.1 Zone Minimum	Title 24 Zone Minimum
Units	ft^2	Number	Number	CFM	CFM	CFM
West B	266	2	1	26	48.7	39.9
South A	266	2	1	26	48.7	39.9
East B	266	1	1	21	39.3	39.9
Interior B	320	8	4	59.2	111	120
Interior A	266	2	1	26	48.7	39.9
West A	600	4	4	56	105	90
South B	600	20	13	136	255	300
East A	280	14	10	86.8	162.8	210

Table 5-4 Zone and system-level HVAC design air flow rate in Atlanta, GA

Room	West A	Interior A	South A	East A	Interior B	East B	South B	West B
$V_{coolmax}$: m^3/s	0.2906	0.1015	0.1918	0.3006	0.1549	0.2429	0.2585	0.2780
$V_{coolmax}$: CFM	616	215	406	637	328	515	548	589
AHU Maximum Air Flow: CFM	3856							
AHU Maximum Air Flow: m^3/s	1.820							

Zone-level design maximum airflow rates in the cooling mode and AHU maximum airflow rate in Atlanta are provided in Table 5-4. Based on the above calculations, zone-level terminal parameter settings for the two baselines are tabulated in Table 5-5 for the SFPTU and PFPTU, respectively, including maximum airflow rates, minimum airflow rates, constant fan sizing value, and the fan on flow fraction. For EnergyPlus input parameter of the “fan on flow fraction”, we set this value to be 0, which indicates when the terminal fan schedule is on, the constant speed fan will only operate if there is a heating load, or if a reheat is required, or if an availability manager

cycles zone fans on only. The parallel fan which sits in the secondary air flow works in the heating mode to meet the heating load requirement. Considering the design heating airflow rate is less than the design cooling airflow rate, the maximum secondary air flow rate is assumed to be 60% of the cooling design airflow [1, 33, 34].

Table 5-5 Zone-level terminal parameter settings for the two baselines

System	Item		West A	Interior A	South A	East A	Interior B	East B	South B	West B
PFPTU	Maximum Primary Air Flow Rate		0.291	0.102	0.192	0.301	0.155	0.243	0.258	0.278
	Maximum Secondary Air Flow Rate/ Constant Fan Sizing		0.174	0.061	0.115	0.180	0.093	0.146	0.155	0.167
	Minimum Primary Air Flow Fraction	62.1	0.171	0.226	0.120	0.256	0.338	0.076	0.466	0.083
		T24	0.146	0.186	0.098	0.330	0.366	0.078	0.548	0.068
	Fan On Flow Fraction		0	0	0	0	0	0	0	0
SFPTU	Maximum Primary Air Flow Rate		0.291	0.102	0.192	0.301	0.155	0.243	0.258	0.278
	Minimum Primary Air Flow Fraction	62.1	0.171	0.226	0.120	0.256	0.338	0.076	0.466	0.083
		T24	0.146	0.186	0.098	0.330	0.366	0.078	0.548	0.068

5.7 Detailed Energy and Ventilation Performance Results for Series Fan-powered Terminal Units in Atlanta

Simulations are conducted in the following ASHRAE Climate Zones to assess the performance of the DCV control sequences: 1A (Miami, FL), 3A (Atlanta, GA), 3C (Oakland, CA), and 5A (Chicago, IL). In the following, SFPTU in 3A (Atlanta) will be used as an example to illustrate detailed results and avoid repetition. Then, we will show the result comparisons across four different climate zones for both SFPTU and PFPTU.

EnergyPlus-CONTAM co-simulation (Dols et al. 2016) was conducted using Atlanta weather for the VAV system with FPTUs. Source energy saving potential from the proposed control logic and associated ventilation performance are compared with baselines. Only eight test rooms and associated HVAC equipment are included in the analysis (the ERS facility and the simulation model also include other spaces that are separated from the test rooms). The ventilation performance is evaluated using under-ventilation and over-ventilation hours compared with the proposed ASHRAE 62.1 simplified approach. We will discuss the energy and ventilation performance for the two systems in the following sections, respectively.

5.7.1 Energy Performance

Figure 5-6 shows the annual HVAC source and site energy saving percentages from the proposed DCV compared with two baselines for the SFPTU. The site to source energy conversion factors are 3.167 for electricity and 1.084 for natural gas, respectively. Baselines from Title 24 (green bar) consumed the most energy compared with others. The proposed DCV control strategy saves 9.5% and 15.0% in terms of source energy compared with the two baselines. It saves 11.3% and 18.6% in terms of site energy compared with the two baselines. Majority savings are due to the reduced required zone ventilation (i.e., zone minimums). This is because the zone minimums from the proposed DCV logic are dynamically reset based on occupancy conditions and less than those from the baselines.

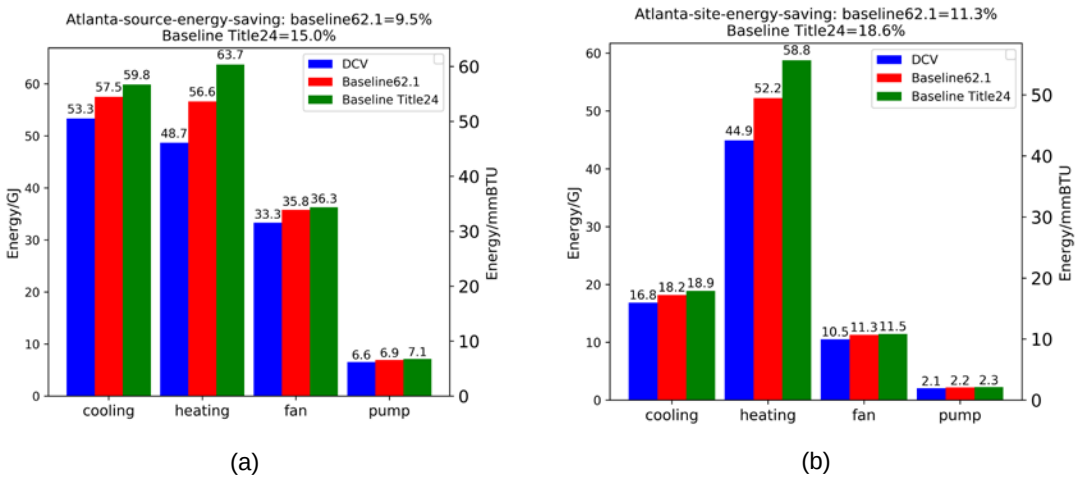

Figure 5-6 (a) HVAC source energy consumption and (b) HVAC site energy consumption by end use in Atlanta: SFTPU case

5.7.2 Ventilation Performance

The ratio of actual outside air flow rate (V_{oa}) to the system-level required outdoor airflow (V_{ot}) is calculated to evaluate the ventilation performance of the DCV control strategy of the VAV system with SFPTU. Figure 5-7(a) shows the scatter plot of OAR vs. outdoor air temperature (OAT) for the Atlanta case. Figure 5-7(b) depicts the OAR distribution in bins. The hourly average data when the system is on (2,340 hours in total) are used. There are no under-ventilated hours (OAR<0.9). The rationale of the selection of 0.9 as a cut-off point is because, in practice, outdoor airflow meters will generally exhibit at least 10% measurement error [35]. As expected, actual outdoor airflow is higher than the required ventilation airflow in the economizer mode.

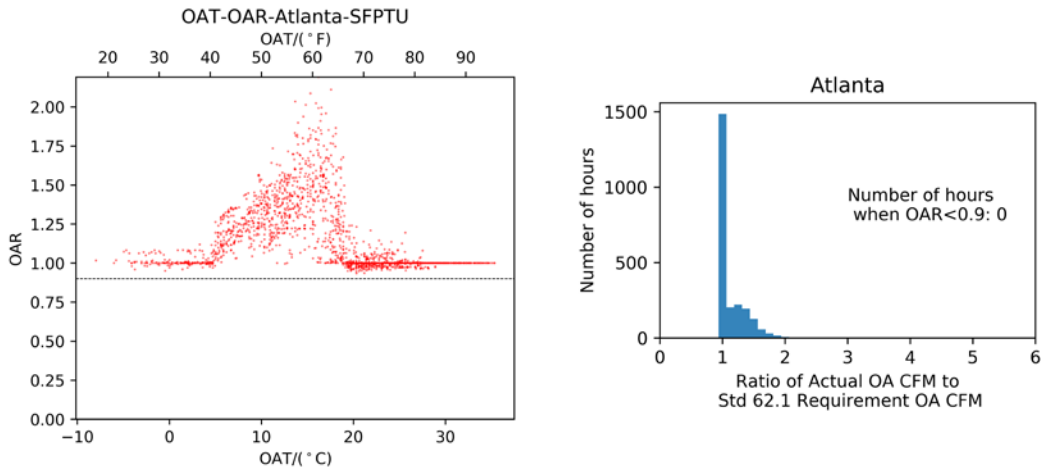

(a) (b)

Figure 5-7 (a) Scatter plot of OAR vs. OAT (b) Bin plot of OAR: SFTPU case

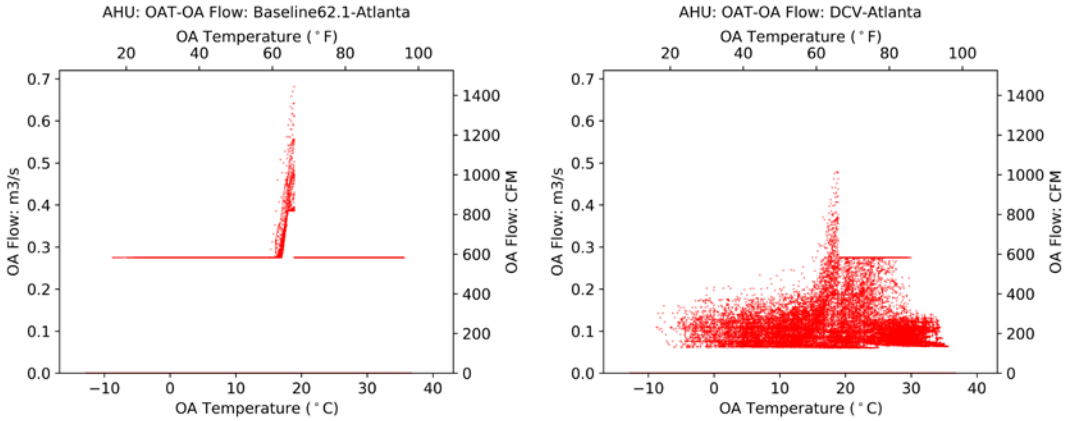

(a) (b)

Figure 5-8 (a) Scatter plot of OA flow vs. OAT for baseline 62.1 (b) Scatter plot of OA flow vs. OAT for DCV control strategy: SFTPU case

Figure 5-8(a) and (b) show the comparison of OA flow rates between the baseline ASHRAE 62.1 and RP-1819 DCV control strategy. The scattered points are five-minute time step EnergyPlus data. For the baseline case, when the economizer is enabled, the OA flow is way higher than the minimum airflow rate while OA flow maintains the constant minimum when the economizer is off. However, in the RP-1819 DCV control scenario, the minimum OA flow rate dynamically reset when the economizer is not enabled. It is noted that when the maximum OA

flow rate at low OA temperatures is less than that at high OA temperatures. The reason behind this is that E_v is normally smaller in the heating season than the E_v in the cooling season, and thus the required outdoor air is relatively less.

To further display the comparison of the system-level ventilation performance between the RP-1819 DCV control logic and two baselines, probability density function (PDF) curves of the OA flow and SA flow are plotted, as shown in Figure 5-9. PDF curve is a statistical expression that defines a probability distribution (the likelihood) for a discrete random variable (e.g., airflow rate) as opposed to a continuous random variable. The red lines represent the RP-1819 DCV control logic, the blue lines represent the proposed simplified ASHRAE 62.1 baseline, and the green lines represent the Title 24 baseline. From the OA flow PDF curves, compared with two baselines, the OA flow rates from the RP-1819 DCV logic are less than those from the baselines for the majority of the time. The same pattern can be observed for the total SA flow rate, which results in less fan energy, cooling, and heating energy consumption.

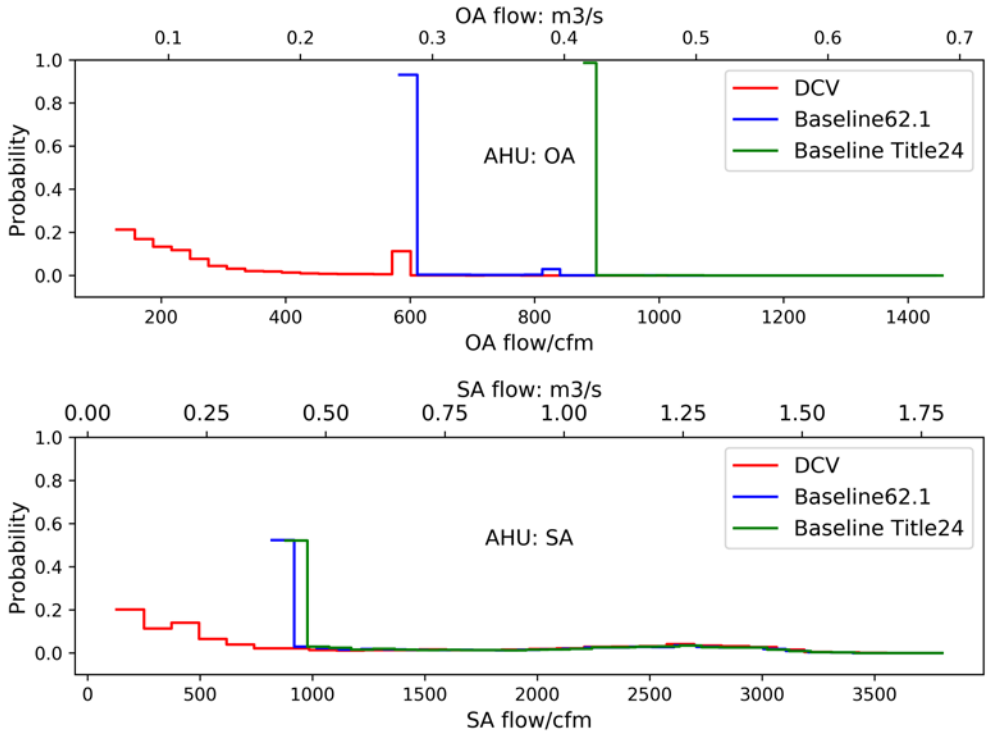

Figure 5-9 Probability density function (PDF) curves of AHU outdoor air (OA) and supply air (SA) flow rate: SFTPU case

In addition, several key variables in the proposed DCV control logic will be analyzed using boxplots from the annual simulation data. Boxplots depict median and 25/75th percentile values with whiskers representing the minimum and maximum values of the dataset. All the boxplots are based on the data with a sampling frequency of five minutes when the system is on.

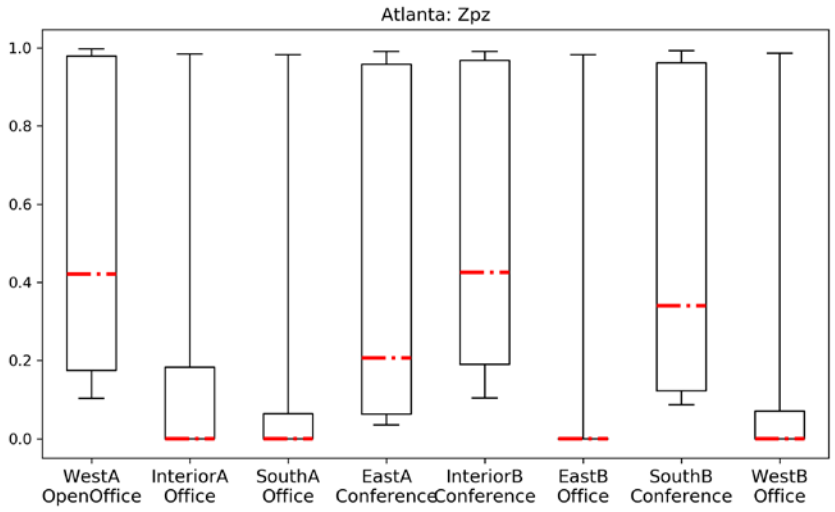

(a)

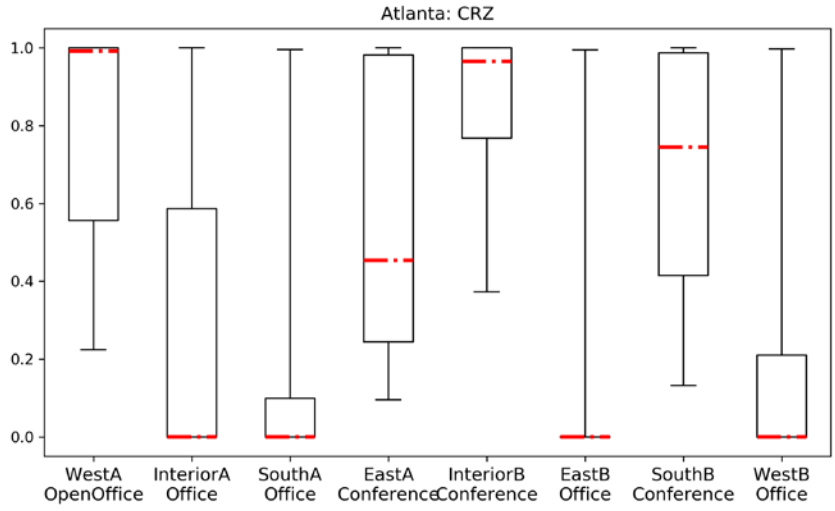

(b)

Figure 5-10 Boxplots of (a) zone primary outdoor air fraction (Z_{pz}) (b) zone criticalness (C_{rz}); SFTPU case

Figure 5-10 shows the boxplots of the zone primary outdoor air fraction (Z_{pz}) and the zone criticalness (C_{rz}). Z_{pz} is defined as the ratio of V_{oz} and $V_{pz,}$ and it is a critical variable to calculate the zone criticalness, which is defined as the ratio of Z_{pz} and the maximum Z_{pz} among the eight zones. It can be seen that three conference zones and one open office have a large median of the zone criticalness, which corresponds to the fact that these zones have either constant large

occupancy or peak occupancy density. The median values for the other private offices are close to zero because these zones are frequently unoccupied and have a lower occupancy.

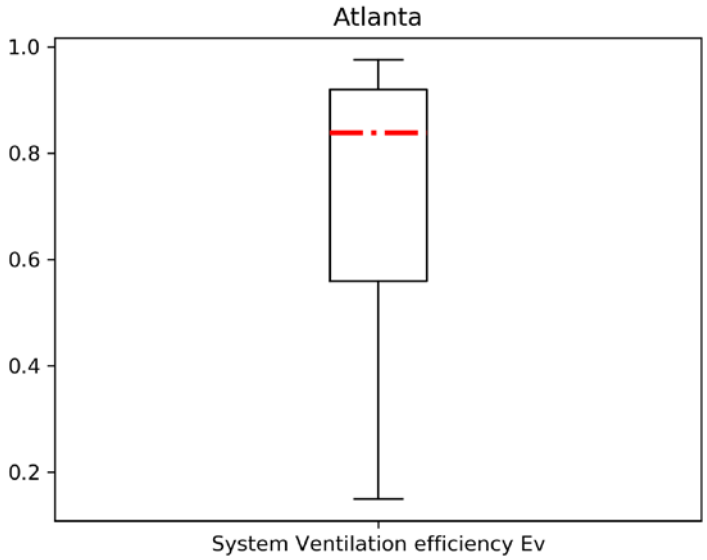

Figure 5-11 System ventilation efficiency (E_v) for the SFPTU

System ventilation efficiency is defined as the minimum zone ventilation efficiency for the SFPTU, as shown in Equations (5-9)-(5-12). The median value is 0.8385, with a minimum of 0.15, as shown in Figure 5-11.

Figure 5-12 depicts box plots of zone CO_2 concentration for the SFPTU. The maximum CO_2 levels in three conference rooms (East A, Interior B, and South B) and the open office West A are consistently higher than in other private offices.

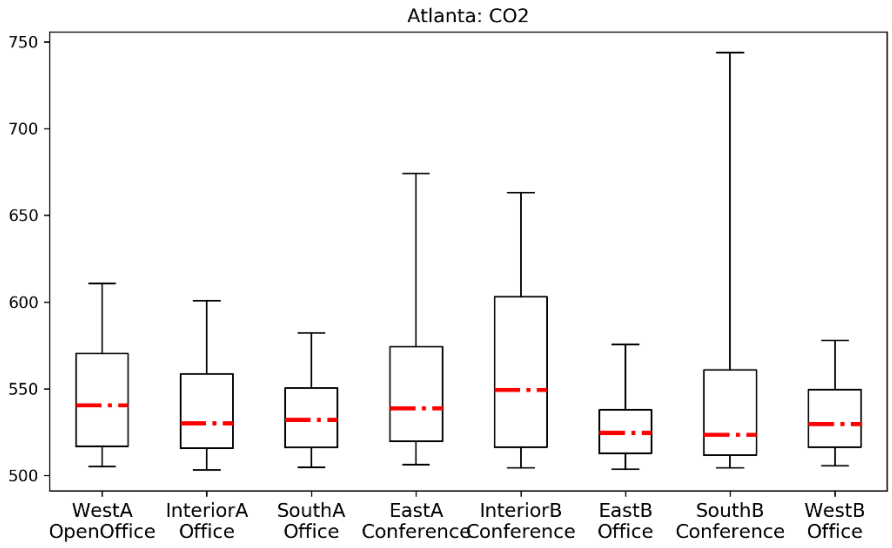

Figure 5-12 Box plots of zone CO_2 concentration for the SFPTU

5.7.3 Summary of the Energy and Ventilation Performance Results for FPTUs in a Climate Zone

In the previous section, the energy and ventilation performance of the VAV system with SFPTU is detailed. In this section, we summarize the energy-saving ratios of the SFPTU and PFPTU in Table 5-6 for two baselines in terms of the source energy and site energy consumption. It can be seen that the energy-saving performance of PFPTU is better than the SFPTU. The reason lies in that the PFPTU operates intermittently, and the sizing of constant speed fan in PFPTU system is smaller than the one for SFPTU.

Table 5-6 Energy Performance of FPTU compared with two baselines (saving potential percentages) in Atlanta, GA

System	Source Energy 62.1	Source Energy T24	Site Energy 62.1	Site Energy T24
SFPTU	9.5%	15.0%	11.3%	18.6%
PFPTU	11.3%	17.0%	14.0%	21.3%

Table 5-7 presents the detailed ventilation performance of the two systems. From the time-averaged (2,340 hours of system operation) OAR and OAR incompliance ratio, we can see that both systems could meet the ventilation requirement from ASHRAE Standard 62.1.

Table 5-7 Ventilation performance of VAV system with FPTUs

System	OAR<0.9 Hour Ratio (1hr Time Step)	OAR<0.9 Hour Ratio (5 min Time Step)	Median E_v
SFPTU	0%	2.07%	0.8385
PFPTU	0%	1.70%	0.8357

5.8 Energy and Ventilation Performance Results in Four Climate Zones

In this section, we will present the summary of the energy and ventilation results for both systems in four climate zones.

5.8.1 Summary of Energy Performance Results in Four Climate Zones

Figure 5-13(a) presents the source energy end-use saving potentials from the proposed DCV control strategy (blue bar) compared with two baselines for the SFPTU. Baselines from Title 24 (green bar) consumed more energy compared with those from the proposed ASHRAE simplified 62.1 approach (red bar). This is because the zone minimums from DCV logic are dynamic and less than those baselines. Most of the savings are from the heating end use except Miami. Oakland saves the most source energy in terms of the ratio compared to the other three climate zones. This is because Oakland has the most of the time when the cooling/heating load is small, and the ventilation rate could be set down. However, in terms of the energy-saving amount, Chicago saves the most source energy since it has a significant thermal load. Figure 5-13(b) presents the source energy end-use savings potential from the proposed DCV control strategy (blue

bar) compared with two baselines for PFPTU. Baselines from Title 24 (green bar) consumed more energy compared with those from the proposed ASHRAE simplified 62.1 approach (red bar). Oakland saves the most source energy compared to the other three climate zones. Most energy savings are from the cooling in Miami, while in the other three climate zones, most energy savings are from the heating. The PFPTUs have a larger energy-saving ratio due to the smaller upper limit of the maximum zone primary airflow for the zone minimum dynamic reset compared to the SFPTU.

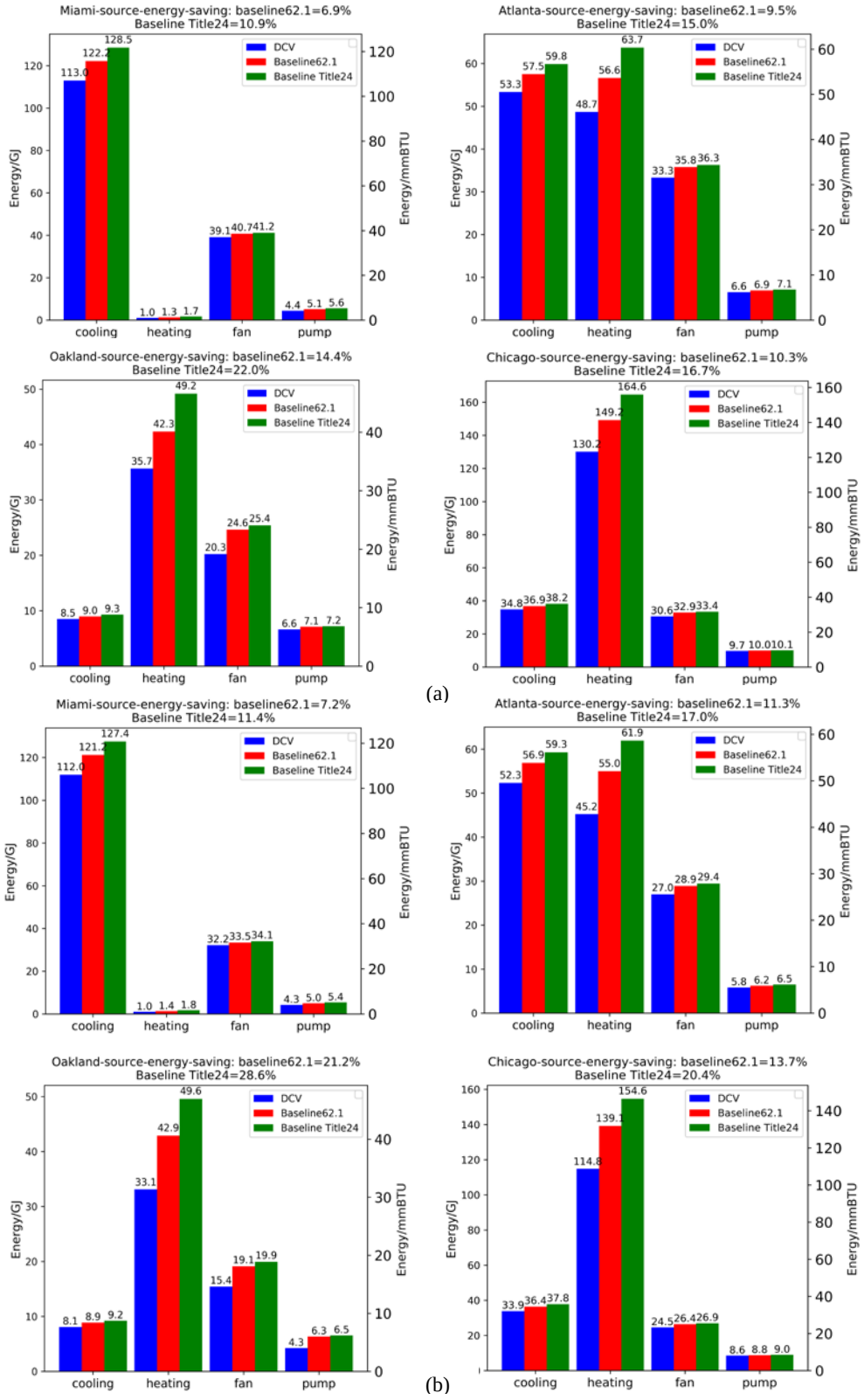

Figure 5-13 HVAC source energy consumption by end use and climate zone for the (a) SFPTU (b) PFPTU

The comparison of energy performance in four different climate zones is shown in Table 5-8, in terms of the source energy saving ratio, and source energy saving absolute value. The simulation results show that the DCV control logic could lead to 7-14% and 7-21% HVAC source energy savings for the SFPTU and PFPTU compared with the baseline of the simplified ASHRAE 62.1 approach, respectively. In terms of the source energy saving ratio, the DCV control sequences in Oakland outperform than all other DCV cases in different climate zones. Regarding the source energy saving amount, the DCV control sequences in Chicago has the edge over the one in other climate zones.

Table 5-8 Comparison of energy performance in four climate zones

HVAC Related Source Energy Saving (Relative Ratio)					
System	Baselines	Miami	Atlanta	Oakland	Chicago
SFPTU	Simplified 62.1	7%	10%	14%	10%
	Title 24	11%	15%	22%	17%
PFPTU	Simplified 62.1	7%	11%	21%	14%
	Title 24	11%	17%	29%	20%
HVAC Related Source Energy Saving (Absolute Value, mmBTU)					
System	Baselines	Miami	Atlanta	Oakland	Chicago
SFPTU	Simplified 62.1	11.1	14.1	11.4	22.4
	Title 24	18.3	23.7	19.0	38.9
PFPTU	Simplified 62.1	10.9	15.7	15.5	27.4
	Title 24	18.2	25.3	23.1	44.1

5.8.2 Summary of Ventilation Performance Results in Four Climate Zones

Figure 5-14(a) shows the scatter plots of OAR vs. OAT by climate zone for the SFPTU. The hourly average data from EnergyPlus outputs with a sampling frequency of 5 minutes are used for these plots. For the majority of hours (i.e., 99% of the time when AHUs are on), OARs are larger than 0.9 for these four climate zones. These figures also show that much more outdoor airflow is provided in the economizer mode than what is required for the ventilation. Figure 5-14(b)

shows the scatter plots of OAR vs. OAT by climate zone for the PFPTU system. The hourly average data from EnergyPlus outputs with a sampling frequency of 5 minutes are used for these plots. OARs are larger than 0.9 in all the hours for these four climate zones. The comparison of ventilation performance in four different climate zones is shown in Table 5-9, in terms of compliance rate with 1-hour time step and 5-min time step (total 2340 operation hours). We can see that the DCV control sequences in the FPTUs could achieve good compliance with ventilation requirements in ASHRAE Standard 62.1-2019. The SFPTU and PFPTU have a similar ventilation performance.

Table 5-9 Comparison of OAR compliance rate between 1 hour and 5 minute time step data in four climate zones

OAR Compliance Rate when $V_{oa} \geq 90\%\ V_{ot}$								
	1 hr Time Step				5 min Time Step			
System	Miami	Atlanta	Oakland	Chicago	Miami	Atlanta	Oakland	Chicago
SFPTU	100%	100%	100%	99.9%	98.5%	97.9%	97.8%	97.8%
PFPTU	100%	100%	100%	100%	98.6%	98.3%	98.3%	98.2%

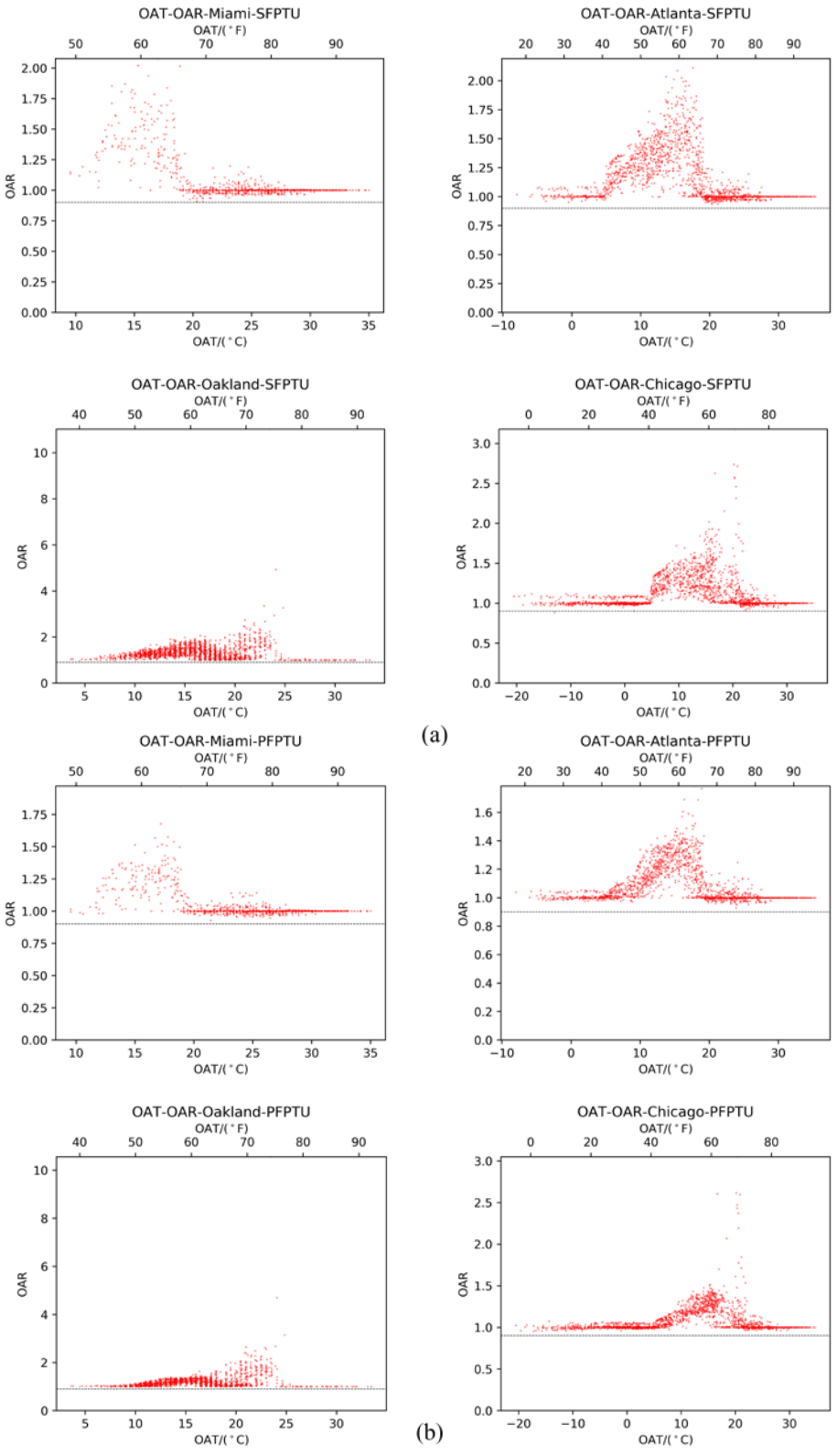

Figure 5-14 Scatter plot of OAR vs. OAT in four climate zones for the (a) SFPTU (b) PFPTU

5.9 Conclusions, Limitations, and Future Work

This chapter investigates the energy and ventilation performance of CO_2- based DCV sequences for the multiple zone VAV systems with fan-powered terminal units. Two FPTUs are studied: a parallel fan-powered terminal unit with a constant volume fan and a series fan-powered terminal unit with a constant volume fan. For each system, two baselines for ventilation requirements (ASHRAE 62.1 simplified approach, California Title 24) are considered. An office building is used as a case study to demonstrate the benefits from CO_2-based DCV strategies for the multiple zone VAV systems with fan-powered terminal units in four different climate zones. Following conclusions, limitations, and future work are summarized and listed:

1) The DCV control logic resulted in 7~14% and 7~21% HVAC energy savings on a source energy basis compared with the baseline of a simplified ASHRAE 62.1 approach for the SFPTU and PFPTU, respectively.
2) The DCV control logic resulted in 11~22% and 11~29% HVAC energy savings on a source energy basis compared with the baseline of Title 24 for the SFPTU and PFPTU, respectively.
3) The provided outdoor airflow met or exceeded the ASHRAE Standard 62.1 ventilation requirement in the four climate zones for at least 98% of the time for the FPTUs.
4) In general, the proposed DCV logic performed well in the EnergyPlus-CONTAM co-simulation virtual testbed. The DCV control logic generally results in a modest HVAC energy-saving ratio and good compliance of the ventilation requirement for the FPTUs.
5) The simulation results may have the uncertainties from the co-simulation scheme and its data exchange timestep. The data exchange timestep is mainly constrained by the EnergyPlus simulation engine. In this study, we use a timestep of five minutes. It is

acknowledged that the CO_2 level may vary slightly within five minutes. Based on the experimental data and field practice, such variations are not big concerns for CO_2-based DCV in commercial buildings [5, 36]. Also, the simulation artifacts may also exist due to the data exchange between the instantaneous output values of CONTAM (as low as one second) and the integrated outputs of EnergyPlus (minimum of one minute), which would impact the final simulation results.

6) The future work includes the testing of the DCV control sequences in a real facility and the validation of the simulation results. Also, model predictive controls will be studied and applied to the DCV of the FPTUs.

5.10 References

[1] ASHRAE. ANSI/ASHRAE Standard 90.1-2019, Energy standard for buildings except low rise residential buildings. Atlanta, GA, USA: ASHRAE, Inc; 2019.

[2] ASHRAE. ANSI/ASHRAE Standard 62.1-2019, Ventilation for Acceptable Indoor Air Quality. Atlanta, GA, USA.: ASHRAE, Inc.; 2019.

[3] California Energy Commission. Building Energy Efficiency Standards for Residential and Nonresidential Buildings.: California Code of Regulations, Title 24.; 2019.

[4] The International WELL Building Institute. The WELL Building Standard v1. 2019.

[5] O'Neill ZD, Li Y, Cheng HC, Zhou X, Taylor ST. ASHRAE 1747-RP. Implementation of RP-1547 CO2-based Demand Controlled Ventilation for Multiple Zone HVAC Systems in Direct Digital Control Systems. 2017.

[6] Lin X, Lau J. Demand controlled ventilation for multiple zone HVAC systems: CO2-based dynamic reset (RP 1547). Hvac & R Research. 2014;20:875-88.

[7] Lin X, Lau J, Yuill GK. Evaluation on the Validity of the Assumptions Underlying CO 2-Based Demand-Controlled Ventilation by a Literature Review. ASHRAE Transactions. 2014;120.

[8] Shriram S, Ramamurthy K. Assessment of CO2-based demand controlled ventilation requirement for a flexible work environment with ductless split air conditioners. Science Technology for the Built Environment. 2019;25:805-18.

[9] Iliev V, Badunski D, Seso I, Andovski SI. Direct Digital Control of HVAC System and CO2-Based Demand Controlled Ventilation. International Journal of Innovative Technology Exploring Engineering. 2014.

[10] Lü X, Lu T, Viljanen M, Kibert CJ. A new method for controlling CO2 in buildings with unscheduled opening hours. Energy and Buildings. 2013;59:161-70.

[11] Lu T, Lü X, Viljanen M, buildings. A novel and dynamic demand-controlled ventilation strategy for CO2 control and energy saving in buildings. Energy and Buildings. 2011;43:2499-508.

[12] Wang H, Xie L, Liu S, Xu J. A model-based control of CO2 concentration in multi-zone ACB air-conditioning systems. 2016 12th IEEE International Conference on Control and Automation (ICCA): IEEE; 2016. p. 467-72.

[13] Škrjanc I, Šubic B. Control of indoor CO2 concentration based on a process model. Automation in Construction. 2014;42:122-6.

[14] Lachhab F, Essaaidi M, Bakhouya M, Ouladsine R. A state-feedback approach for controlling ventilation systems in energy efficient buildings. 2015 3rd International Renewable and Sustainable Energy Conference (IRSEC): IEEE; 2015. p. 1-6.

[15] Lachhab F, Bakhouya M, Ouladsine R, Essaaidi MJPotIoME, Part I. Context-driven monitoring and control of buildings ventilation systems using big data and Internet of Things–based technologies. Journal of Systems Control Engineering. 2019;233:276-88.

[16] Gruber M, Trüschel A, Dalenbäck J-O. CO2 sensors for occupancy estimations: Potential in building automation applications. Energy and Buildings. 2014;84:548-56.

[17] Warden D. Supply air CO2 control of minimum outdoor air for multiple space systems. ASHRAE journal. 2004;46:26.

[18] Nassif N. A robust CO2-based demand-controlled ventilation control strategy for multi-zone HVAC systems. Energy and Buildings. 2012;45:72-81.

[19] Lin X, Lau J, Yuill G. ASHRAE 1547-RP. CO2-Based Demand Controlled Ventilation for Multiple Zone HVAC Systems. 2013.

[20] Lin X, Lau J. Demand-controlled ventilation for multiple-zone HVAC systems—Part 2: CO2-based dynamic reset with zone primary airflow minimum set-point reset (RP-1547). Science and Technology for the Built Environment. 2015;21:1100-8.

[21] O'Neill ZD, Li Y, Cheng HC, Zhou X, Taylor ST. Energy Savings and Ventilation Performance from CO2-based Demand Controlled Ventilation: Simulation Results from ASHRAE RP-1747 (ASHRAE RP-1747). Science and Technology for the Built Environment. 2019:257-81.

[22] Furr JC, Davis MA, Cramlet A. Performance of VAV fan-powered terminal units: Experimental setup and methodology. ASHRAE Transactions. 2008;114:75.

[23] Sardoueinasab Z, Yin P, O'Neal D. Energy modeling and analysis of inherent air leakage from parallel fan-powered terminal units using EMS in EnergyPlus. Energy and Buildings. 2018;176:109-19.

[24] Davis MA, O'Neal DL, Bryant JA, Cramlet A. Modeling the Performance of Single-Duct VAV Systems that use Fan Powered Terminal Units. ASHRAE Transactions. 2009;115.

[25] ASHRAE. ASHRAE Guideline 36-2018. High Performance Sequences of Operation for HVAC Systems. 2018.

[26] Dols WS, Emmerich SJ, Polidoro BJ. Coupling the multizone airflow and contaminant transport software CONTAM with EnergyPlus using co-simulation. Building Simulation. 2016;9:469-79.

[27] Walton G, Dols WS. CONTAM 3.2 user guide and program documentation. 2016.

[28] O'Neal D, Reid C, Ingram D, Li D, Bryant J, Gupta S, et al. Developing fan power terminal unit performance data and models compatible with EnergyPlus. Report; 2016.

[29] Bryant JA, Kanaan B. Differential Pressure Rise Measurements and Impact in EnergyPlus Modeling for Series VAV Fan-Powered Terminal Units Using PSC Motors. ASHRAE Transactions. 2017;123.

[30] O'Neal DL, Ingram DD, Reid CL. Modeling Fan-Powered Terminal Unit Fan/Motor Combinations Controlled by Silicon Controlled Rectifiers. ASHRAE Transactions. 2015;121.

[31] Lu D. Annual Energy Performance Evaluation of Series and Parallel Fixed-Airflow Fan-Powered Terminal Units. ASHRAE Transactions. 2018;124:148-58.

[32] Faris G, Int-Hout D, O'Neal D. Fan-Powered VAV Terminal Units: Application and Modeling Implications From Past and Current Research. ASHRAE Journal. 2017;59.

[33] Sipes J. Tech Tips: Fan-Powered Terminal Units. 2010.

[34] Titus. Q&A: How Do You Size Parallel Fan Powered Terminal Units? 2012.

[35] Lu X, O'Neill Z, Li Y, Niu F. A novel simulation-based framework for sensor error impact analysis in smart building systems: A case study for a demand-controlled ventilation system. Applied Energy. 2020;263:114638.

[36] Apte MG. A review of demand control ventilation. LBNL-60170 Report, Lawrence Berkeley National Laboratory, Berkeley, CA, USA. 2006.

CHAPTER VI PERFORMANCE EVALUATION OF THE HVAC SYSTEM UNDER GDL36 SOO FOR FREQUENCY REGULATION SERVICE PROVISION*

6.1 Introduction

Modern building controls are becoming advanced and intricate with the potential integration of on-site distributed energy resources. In addition, buildings need to provide the grid service through load shifting enabled by the grid-interactive control, which increases another layer of complexity to building controls. The U.S. Department of Energy launched an initiative on Grid-interactive Efficient Buildings (GEB), which aims to develop innovative technologies for grid responsive buildings to achieve energy efficiency, demand flexibility, and resiliency. In this context, the future high-performance rule-based SOO should have the compatibility of integrating the grid-interactive controls to provide the grid service, such as the frequency regulation (FR).

This chapter evaluates the impacts of FR provision from the multi-zone VAV system when the AHU fan provides the FR service. An experimentally validated FR control scheme is integrated with the GDL36 SOO. The impacts on the HVAC system and potential conflicts are identified.

6.2 Literature Review

6.2.1 Frequency Regulation Service Provided by HVAC System

The growing electricity demand, combined with the clean energy commitments, drives a considerable increase of renewable energy integration in the U.S electrical grid. The share of renewables in the U.S. electricity generation mix now accounts for 19% and is anticipated to

* Reprinted with permission from "What are the impacts on the HVAC system when it provides frequency regulation? A comprehensive case study with a Multi-Zone variable air volume (VAV) system." by Xing Lu, Veronica Adetola, Zheng O'Neill, 2021. Energy and Buildings, 2021, 243, 110995, Copyright [2021] by Elsevier.

double in 2050 [1]. This transition is imposing significant challenges on the stability and reliability of grid operation. The intermittent nature of the large renewable penetration will cause a power supply-demand imbalance and frequency fluctuations. Any significant deviation from the prescribed frequency, which is 60Hz in North America, could harm the power grid equipment, interfere with the system protection schemes, and even cascade to the system collapse [2]. On the other hand, conventional generators with large spinning masses are impacted by the rise of renewables that do not have similar generation characteristics in the way that the level of synchronous inertia is set to decline, which makes the system more sensitive to disturbances.

Thus, ancillary services are deployed to ensure the system balance in different timescales and maintain the grid reliability under unforeseen contingencies. In particular, the frequency regulation (FR), as a fast and highest-priced ancillary service on the order of the seconds [3], is procured to ensure an instantaneous power supply-demand balance. Traditionally, the frequency is regulated by the conventional generators due to the high inertia and automatic generation controls (AGCs) that call upon the generator reserves to ramp up or down. However, the modern bulk power system with the increasing penetration of renewables is making it difficult to maintain the FR [4]. Together with the recent rulings encouraging the demand side participation from the Federal Energy Regulatory Commission [5], the interest is on the rise in exploiting demand side resources. Various demand resources have been proved to provide FR capability, including the plug-in electric vehicles [6, 7], data center loads [8], residential loads [9], and commercial buildings [10, 11].

Among the available demand side FR resources, heating, ventilation, and air-conditioning (HVAC) systems in commercial buildings have several advantages for providing secondary frequency regulation. 1) First, commercial buildings consume a large electric load. Roughly 36%

of the U.S. total electricity use goes toward powering commercial buildings [12], which emerges as a considerable resource when aggregated for a regulation [13]; 2) Second, the adoption of the variable frequency drives (VFDs) in major HVAC equipment components allows for a continuous modulation of power output, which provides a better flexibility in controls [14]; 3) Third, the large thermal masses of the building envelope enable buildings to be grid-responsive in the FR service period without sacrificing much quality of service (e.g., indoor thermal comfort) as indicated in many relevant studies [15-17]; and 4) Fourth, various experimental studies have demonstrated that commercial buildings have a high performance when providing the FR. Figure 6-1 shows a comparison of the average FR performance score (see Eq. (6-1)-(6-4) in Section 3.2 [18] for the definition) provided by the commercial building HVAC system components [13-17, 19-28] and from the power grid [29] in the literature, respectively. The red dashed line denotes the minimum test score requirement (0.75) [18] for bidding in the Pennsylvania, Jersey, Maryland Regional Transmission Organization (PJM) regulation market. The orange and blue dots represent the PJM regulation signals RegA (traditional regulation AGC signal) and RegD signal (dynamic regulation AGC signal), respectively.

Table 6-1 summarizes the FR performance and the associated HVAC component and control methods reported in the literature. From Figure 1 and Table 1, it can be seen that the FR performance provided by the commercial building HVAC systems is generally not inferior to that from the grid side resources except for the indirect FR control of the chiller [25] and the modulation of the thermostat setpoint [26]. The indirect FR control of the chiller and the FR control by modulating the thermostat cannot track the FR signals, even for the comparatively slow RegA signals. In particular, the Air Handling Unit (AHU) fans [14, 19-22], chilled water pumps [17],

heat pumps [23, 27, 28, 30], and rooftop units [16] with continuous modulation capability manifest the potential to provide the FR with high quality for both RegA and RegD signals.

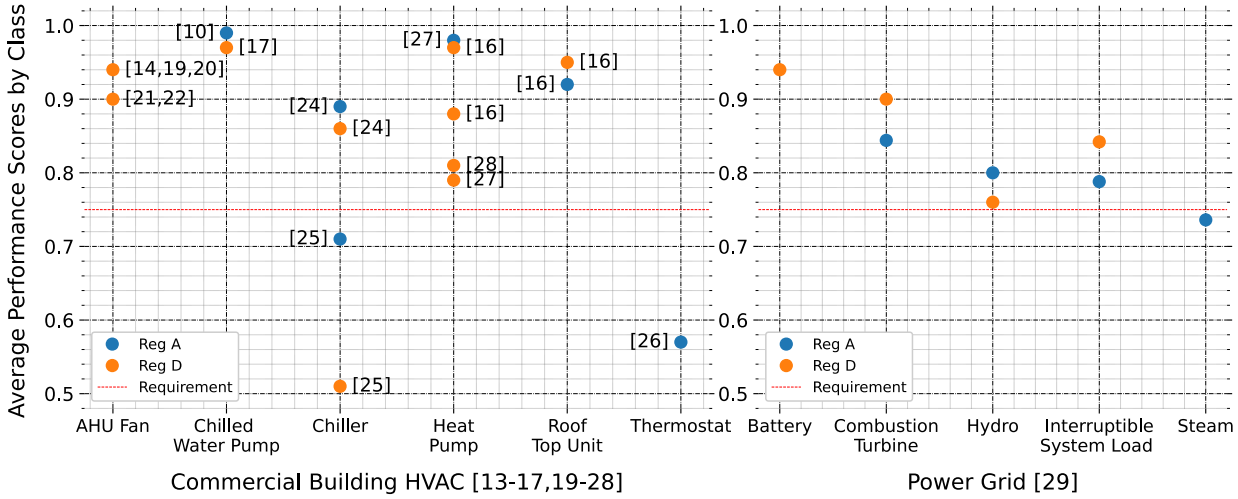

Figure 6-1 Average FR performance score by class from commercial building HVAC components and grid in existing literature (Note: numbers in the figure are the reference number for each paper)

Table 6-1 FR performance and its associated FR control sequence for different HVAC components

Ref	Year	HVAC Component	Composite Performance Score*	Regulation Capacity	FR Control Variable	Control Method
[14]	2015	AHU Fan	0.77, 0.81, 0.89 for fast, slow Area Control Error (ACE), and Reg D	40% of the nominal power	Supply airflow	Direct
[19, 20]	2016	AHU Fan	0.94 0.98 for RegD	40% of the nominal power	Supply airflow	Direct
[21]	2014	AHU Fan	0.9 for RegD	Not known	Supply duct static pressure	Indirect
[22]	2018	AHU Fan	0.89, 0.92 for Reg D signal	18.9 % rated power	Supply duct static pressure	Indirect
[23]	2016	Air-source Heat Pump	0.77-0.81 Reg D for different ambient temperatures	37% of rated power	Supply water temperature	Indirect
[16, 27]	2019	Air-source Heat Pump	Heat Pump: 0.98 for Reg A; 0.97 for Reg D;	6.5% of the rated power	Discharge air temperature (and fan speed)	Indirect
[28]	2020	Ground-source Heat Pump with a water storage	Above 0.8 for RegD	28% of the rated power	Rotational compressor speed	Direct
[16]	2019	Rooftop Unit	0.92 for Reg A; 0.95 for Reg D	7.9% of the rated power	Discharge air temperature	Indirect
[24, 25]	2015	Chiller	Reg A 0.89 and Reg D 0.86 for Fraunhofer chiller; Reg A 0.61, 0.63, 0.74, 0.77,0.81 and Reg D 0.45, 0.56 for MIT chiller	25% of the rated power	Chilled water supply (with AHU supply air temperature)	Indirect
[17]	2020	Chilled Water Pump	0.989 for Reg A 0.968 for Reg D	30 % of the rated power	Pump frequency	Direct
[13]	2019	Thermostats	Not known	Not known	Zone air temperature	Indirect
[26]	2016	Thermostats	0.57 Reg A	Not known	Zone air temperature	Indirect
[31]	2016	Electric heaters	Not known	43 % of the installed capacity	Heater power	Direct

*Note: Composite performance score is an average score that considers the accuracy, precision, and delay performances. The detailed mathematical representation is shown in Eq. (6-1)-(6-4).

6.2.2 Existing Studies on the Impacts of FR Provision on HVAC System

With the proven potential for commercial buildings providing the FR service, many studies started to look into the impacts and side effects of the FR service on the building HVAC system, especially in terms of thermal comfort and energy efficiency. For the thermal comfort, most experimental studies reached a consensus that the FR had negligible impacts on the occupants' thermal comfort [15-17]. Vrettos et al. [20] conducted a controlled testing of two rooms with or without FR and pointed out that the FR signal with limited energy content had little impact on the room air temperature. Wang et al. [17] reported a fluctuation of 0.45 ℃ to 0.80 ℃ for zone air temperatures during the chilled water pump FR testing. For the humidity conditions, Cai et al. [16] revealed a condensate re-evaporation phenomenon and a higher zone relative humidity when the heat pump offered the FR.

However, for energy efficiency, there have been controversies on whether the FR increases the HVAC system energy consumption compared with the baseline. Table 6-2 summarizes the different energy efficiency claims and the concluded impact regarding this issue in the literature. From the table, we can see that the AHU fan is the leading building HVAC equipment used for the FR in terms of Research & Development (R&D) and field demonstrations. Most field/experimental tests show that the FR consumes more energy regardless of different HVAC equipment providing the FR [20, 26, 32]. In other words, the round-trip efficiency (RTE) of different HVAC equipment, which is defined as the fraction of energy charged into the storage that can be retrieved when they are deemed as a virtual battery, is less than 1. However, for the studies where the FR is provided by the AHU fan [20, 32-34], the energy efficiency claims show a discrepancy. A field test showed a slight decrease in HVAC energy usage for a single zone Variable Air Volume (VAV) system [20] while a large efficiency degradation was found in a

multi-zone VAV system [32]. Lin et al. [33] reached the conclusion that buildings consumed more energy than the baseline during up-down events while buildings consumed less energy compared with the baseline during down-up events. The study partially explained the inefficiencies using a quasi-steady-state physics-based building and HVAC models; however, the model neglects the dynamics of building HVAC systems. Raman et al. [34] proposed a detailed numerical model to investigate the energy efficiency versus the FR provision with a rigorous mathematical formulation and reasoning. The authors concluded that no inefficiency would occur (the RTE would be equal to 1) as long as the HVAC system was repeatedly used as a virtual battery. However, the asymptotic RTE could be lower than 1 if the zone air temperature constraint was relaxed [35].

Table 6-2 Summary of mainstream claims on the energy efficiency while providing the FR

Ref	Study Type	Building/ System Type	HVAC Component	Energy Efficiency Claim	Energy Efficiency Impact *
[20]	Experiment	Small Office; Single zone	AHU fan	Reported a slight decrease in energy usage compared to the baseline;	-
[32]	Experiment	Large Office; Multi-zone (80 terminals)	AHU fan	Led to a considerable reduction in the efficiency of energy usage;	--
[33]	Simulation	Simplified model; Single-zone	AHU fan	The sequence of the square wave signal impacted the efficiency. During up-down events, buildings consume more energy than the baseline. During down-up events, buildings consume less than the baseline.	+ or -
[34, 35]	Simulation	Simplified model; Single-zone	AHU fan	When the HVAC system is repeatedly used as a virtual battery, the asymptotic RTE is 1; Recent experimental and simulation work are an artifact of the experimental/ simulation setup.	=
[16]	Experiment	Single Zone	Heat pump	Frequency regulation does not cause energy efficiency degradation.	=
[26]	Experiment	Three large campus buildings (Multi-zone)	Zone thermostats	Round-trip efficiency ranged from 34% to 81 %;	--

*Note: --: Large decrease; -: Slight decrease; = No impact; +: Slight increase; ++: Large increase

6.2.3 Limitations

As acknowledged by all the existing literature, many factors drive the inefficiency of building responses, and they are still largely unknown. Generally, the inefficiency could be categorized as the “reserve availability inefficiency” and “reserve utilization inefficiency” [36].

The former term means the inefficiency due to the suboptimal or inappropriate reserve scheduling under different load conditions. The latter term is the energy inefficiency that occurs during the frequency regulation signal tracking. The existing experimental studies do reflect the ground truth. Still, they might be an artifact of the experimental setup because it is difficult to control the variables related to energy efficiency in real buildings [34]. The inefficiency in the existing building tests could be due to a variety of causes and effects. On the other hand, the existing simulation work generally uses simplified models (quasi-steady-state HVAC models) which cannot capture the key physical and control-related phenomena in the FR event and real buildings. It is highly likely that the results could be different by neglecting these dynamic effects. It is also noted that a majority of the existing studies focus on a single zone building with simplified HVAC control.

In this context, this chapter aims to study how FR impacts the HVAC system operation, using a controlled and dynamic multi-zone building simulation testbed. The FR service is provided by the building AHU fan. However, the impact assessment considers all the components of a multi-zone VAV-based HVAC system, the building response, and the interactions between the FR control and the existing building control loops. The virtual testbed adopts the state-of-the-art HVAC control sequences as specified in the GDL36, High-Performance Sequences of Operation for HVAC Systems [37], which captures best-in-class standardized HVAC control sequences, while the FR control is a proven method that has been validated and demonstrated in a multi-zone medium-sized real building [22].

6.3 Contributions and Chapter Organization

The main contributions of this chapter are:

- A comprehensive investigation of FR impacts on the given commercial building HVAC system (i.e., a multi-zone VAV system as it is the most common HVAC system configuration for the commercial buildings in the U.S., including office, school, hotel, etc. [38]), accounting for the during and post-response effects, under different FR capacities (i.e., 5%, 10%, 15%, and 20% of the rated fan power), FR signals (three standardized test signals - RegA1, RegA2, and RegD1 [39]) and building load conditions (16 U.S. climate zones).
- A holistic assessment based on multiple performance indices, including the FR quality quantification (FR capacity and standardized performance scores), energy efficiency, occupants' thermal comfort, and building control related metrics.
- A deep exploration of the performance of best-in-class HVAC airside control sequence (e.g., GDL36) when the AHU fan is providing the FR sequence using dynamic HVAC models instead of quasi-steady-state models used in the literature.

The rest of the chapter is organized as follows. Section 6.4 discusses the development of the simulation testbed and the associated control methods. Section 6.5 describes the case study setups and the key performance indexes of interest. Section 6.6 presents the impact of FR control on the HVAC system operation. Conclusions and future work can be found in Section 6.7.

6.4 Simulation Testbed

The simulation testbed for this study was developed based on a five-zone VAV system model in Modelica Buildings Library 6.0.0. Modelica is an equation-based, object-oriented, and multi-domain modeling language for modeling of complex engineered systems [40]. The Buildings Library [41] contains both steady-state and dynamic models for the building energy and control systems and supports for the rapid prototyping. The simulation testbed includes a building

thermal model of five interconnected rooms, a VAV HVAC system, a frequency regulation controller (FRC) as depicted in Figure 6-2.

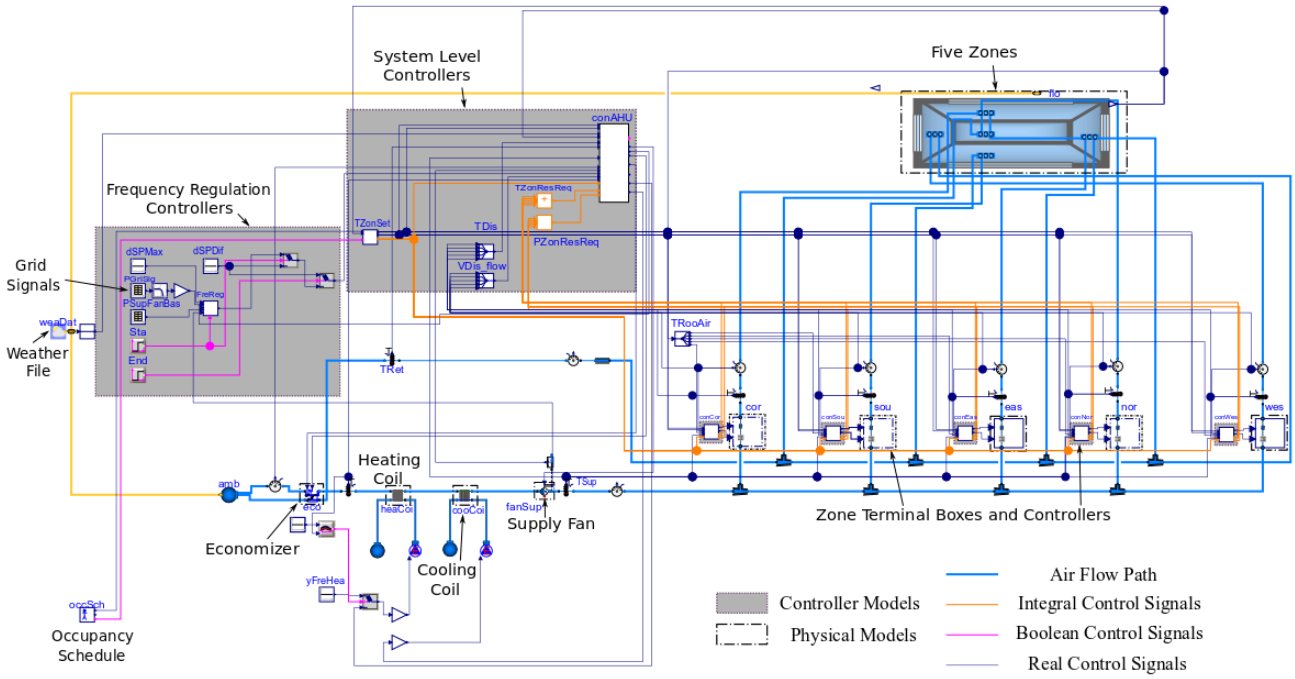

Figure 6-2 Schematics of Modelica implementation of the simulation testbed

6.4.1 Building thermal and HVAC Model

The five-zone thermal model consists of four perimeter zones and one core zone, which is representative of one mid-floor of the new construction medium office building, as described in the set of DOE Commercial Prototype Building Models [30]. Each single zone model calculates the transient heat exchange between different surfaces and constructions through conduction, convection, and infrared and solar radiation. The air exchange within the multi-zone model is determined by the wind pressure and HVAC static pressure among the five thermal zones. It is noted that the zone model was validated by comparing to other simulators and ASHRAE standard method of tests in [42-44]. The air flow rates for the multi-zone air flow model have also been validated using the results from CONTAM program [45].

The setting of envelope thermal properties are derived from the DOE Commercial Prototype Building Models [30] in EnergyPlus and meets the ASHRAE Standard 90.1-2016 [46]. Table 6-3 lists the technical specifications of the five thermal zones in the Modelica model and its comparison between the prototype building model in Chicago, IL. It can be seen that the Modelica model calculates a similar range in terms of the zone peak cooling load compared to the DOE Commercial Prototype Building Models. Mathematical equations and modeling details for the building thermal model were documented in studies [47, 48].

Table 6-3 Building thermal model technical specifications in Chicago, IL

Zone	Area [m^2]	Peak cooling load – Modelica [W]	Peak cooling load - Prototype [W]	Cooling maximum airflow - Modelica [m^3/s]	Cooling maximum airflow - Prototype [m^3/s]
East zone	131.4	9,157	8,356	0.68	0.63
South zone	207.6	11,077	10,080	0.83	0.75
West zone	131.4	9,930	9,939	0.74	0.74
North zone	207.6	7,230	7,043	0.54	0.52
Core zone	983.5	27,982	28,497	2.10	2.10

The HVAC system, as illustrated in Figure 6-3, is a VAV system with an airside economizer [49], a water-to-air heating coil and a water-to-air cooling coil in the AHU. Each zone VAV terminal box includes a reheat coil and a supply air damper. Note that in this study, we have a simplified waterside and only calculate the required energy used at the cooling/heating coil. The conversion factors [50, 51] are used to calculate the site electricity use from the coil required energy. This simplification is valid, assuming the waterside equipment of the targeted building has a large rise time [11]. A water-to-air cooling coil model that considers the humidity condensation is implemented using a finite volume model in which each pipe is discretized along its flow path while the water-to-air heating coil is modeled using the effectiveness-NTU (Number of Transfer Units) method [52]. The fan model takes the speed control signal and uses performance curves that

compute pressure rise, electrical power draw and efficiency as a function of the volume flow rate and the speed. All air flows are dynamically calculated using the fan performance curves and the duct static pressure distribution. Different from other building energy performance simulators like EnergyPlus in which air pressure is not considered, the airflow calculation in Modelica is computed in an iterative manner and determined considering the fan performance curves under different fan speed and the duct static pressure distribution.

The HVAC system control sequences follow the state-of-the-art control sequences in GDL36 [37], including the economizer control, minimum outdoor air control, supply air temperature control, and fan speed control for the AHU; as well as the air damper and reheat valve controls for the zone terminals. The GDL36 control strategies intend to maximize the free cooling and avoid excess energy consumption to run fans and provide mechanical heating and cooling [53]. Figure 6-4 shows he detailed schematic of the AHU (system-level) controller [51]. In the economizer control, the economizer dampers are modulated based on the supply air temperature control loop output, which is also used to control heating and cooling coil valves in the AHU. In the outdoor air ventilation control, a minimum outdoor air flow rate, which is dynamically reset based on the system ventilation efficiency, is maintained to provide an ASHRAE 62.1 code-compliant ventilation. The outdoor air damper and the return air damper are sequenced together to maintain this minimum outdoor air flow rate based on the outdoor air flow measurement. In the supply air temperature reset control, the supply air temperature setpoints are reset considering the outdoor air temperature, the zone terminal reset requests, and the zone operation states. In the supply fan control that adopts a trim-respond logic, the supply fan speed is adjusted to track the duct static pressure setpoint that is dynamically reset, to be illustrated with details in the next paragraph. For the zone terminal controls, the VAV damper and reheat coil implement a dual

maximum control that determines the zone air flow rate setpoint to improve energy efficiency and occupant comfort [54].

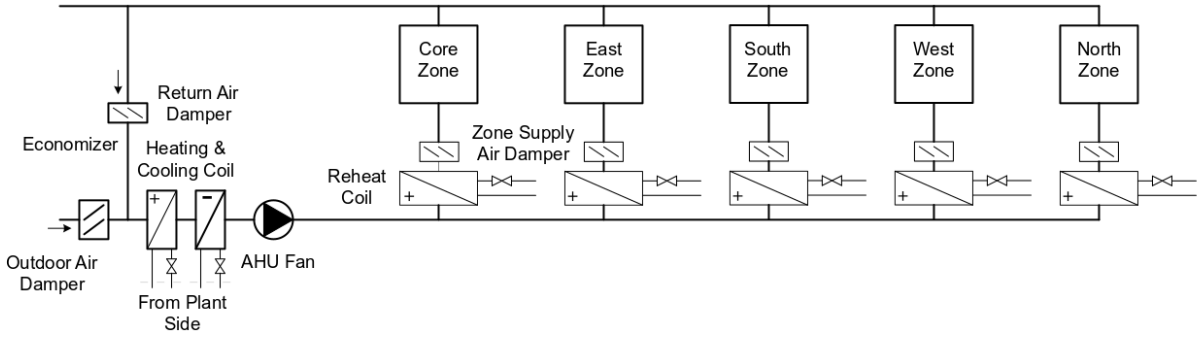

Figure 6-3 Simplified schematics of the studied HVAC system [41]

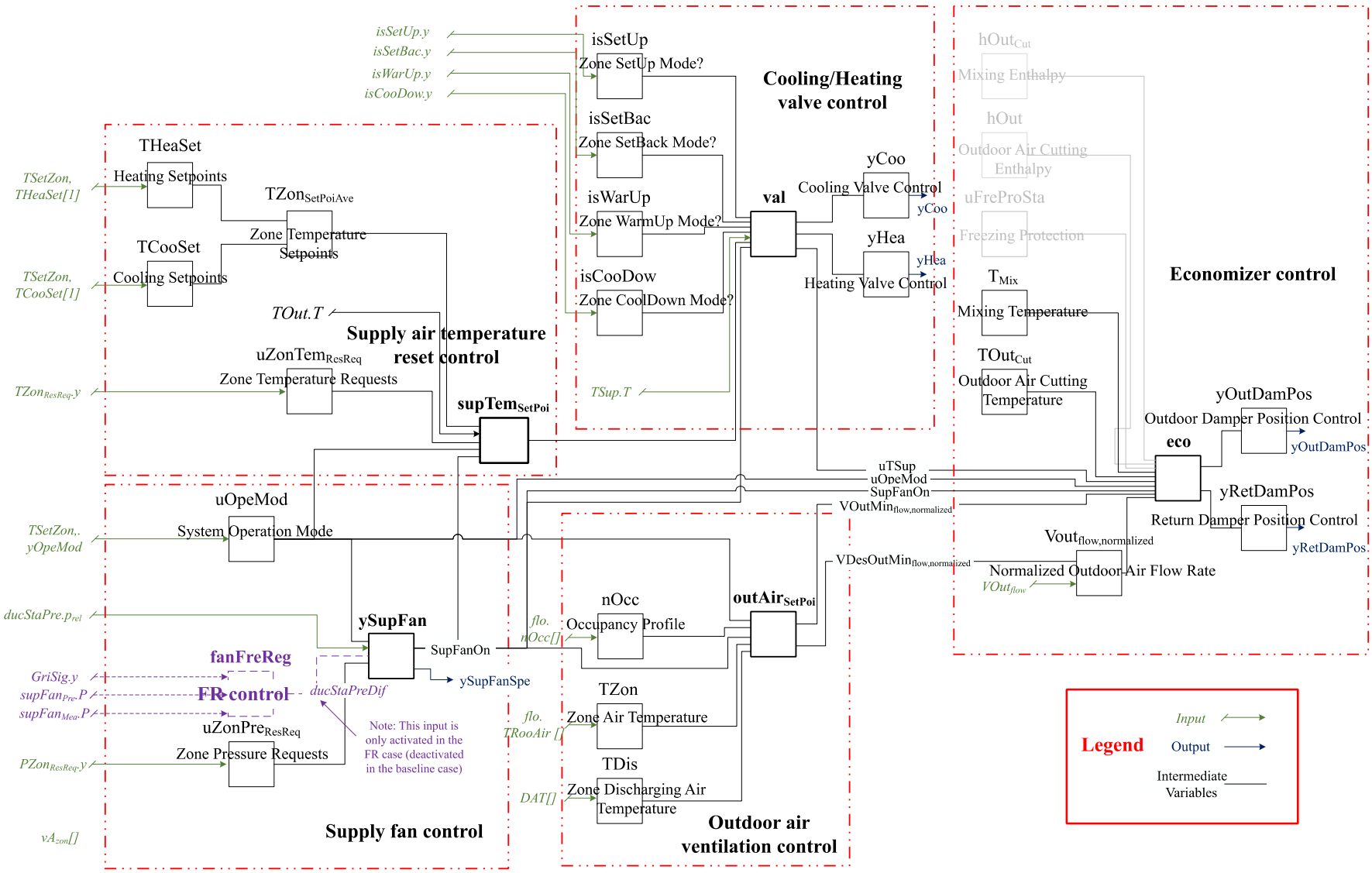

Figure 6-4 Control schematic of the system-level controller model for both the baseline (without FR control) and the FR case

Since the AHU fan serves as the FR in our study, it is important to assess if the FR control interferes with the HVAC controls. The assessment includes the performance comparison of the baseline case and the FR case. For the baseline case, the fan speed is controlled with a proportional–integral (PI) feedback controller to maintain supply duct static pressure (DSP) at the setpoint. The DSP setpoint (SPT) is dynamically reset using the T&R logic based on the total number of the zone pressure reset requests [37]. When the T&R logic is activated, at every sampling time step, the DSP setpoint is first trimmed by a certain amount. If any of the zones is starved for airflow, it will request a system-level zone pressure reset. If the total zone requests are larger than the number of ignored requests (e.g., 2 in this study), the DSP setpoint shall be increased by the responding amount larger than the trimmed amount. The trimmed amount, the responding amount, the sampling time step, and other parameters in the DSP T&R logic are tuned for the virtual testbed, as listed in Table 6-4. Figure 6-5 shows the workflow of the fan speed control in the baseline case. For the FR cases, the frequency regulation controller is incorporated with the supply fan speed control. We will present the details in the next section.

Table 6-4 Parameter settings in DSP T&R logic

Variable	Definition	Value
Device	Associated device	AHU Supply Fan
SP_0	Initial duct static pressure setpoint, Pa	60
SP_{min}	Minimum duct static pressure setpoint, Pa	25
SP_{max}	Maximum duct static pressure setpoint, Pa	300
tim_{sam}	Sampling time step, s	120
R_{ign}	Number of ignored requests	2
SP_{trim}	Duct static pressure trim amount, Pa	12
SP_{res}	Duct static pressure respond amount, Pa	15
$SP_{res,max}$	Maximum response per time interval, Pa	32

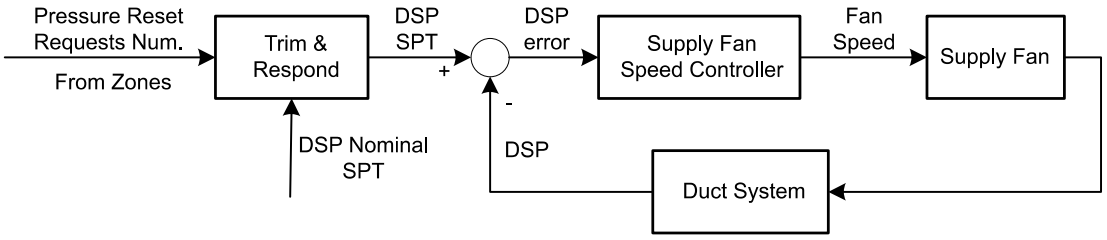

Figure 6-5 Schematics of the fan speed control in the baseline case

6.4.2 Frequency Regulation Controller (FRC) and Fan Speed Control in the FR Case

The architecture for the FR controller in this study is shown in Figure 6-6 based on the control logic in [22]. The performance of the FRC has been demonstrated and validated in a real building [22]. The FRC varies the fan power consumption by indirectly changing the DSP setpoint to track the grid tracking signal. The output of the FRC (ΔDSP setpoint) is added to the nominal DSP setpoint ($DSP_{wo/FR}$). The upper and lower limits of the FRC output are set so that the new DSP ($DSP_{w/FR}$) setpoint is between its confined range. The FRC includes two modules: 1) a reference tracking controller, which is a classic feedback controller that tracks the power deviation from the ACE grid signal; and 2) a nominal fan power estimator that predicts the nominal fan power consumption without the FR.

The differences of FRC implementation between this study and [22] are summarized as follows: (1) the dynamic DSP nominal setpoint is determined from the T&R control in this study while in [22] the DSP nominal setpoint is fixed; (2) the control parameters for the reference tracking controller are tuned using the virtual building in this study compared to the real building in [22]; and (3) the nominal power estimator in this study is a perfect predictor (uses pre-recorded baseline power consumption data) while in [22] it is estimated using a DSP-to-power data-driven model identified as a second order transfer function based on the tested frequency response data.

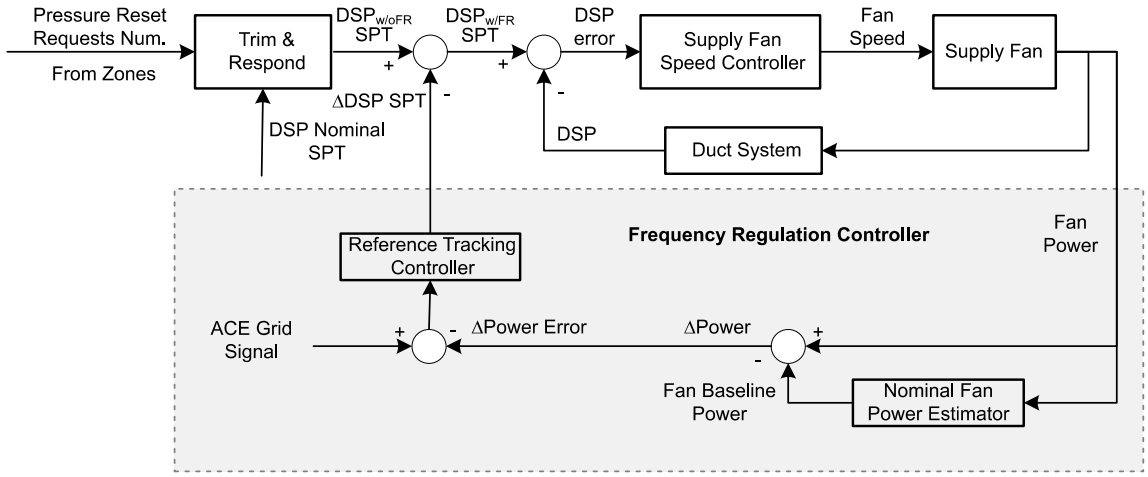

Figure 6-6 Schematics of the fan speed control in the FR case

6.5 Case Studies Description

6.5.1 Overview

To have a controlled testing to evaluate how the FR service impacts the HVAC system, we designed our case study as follows. Our grid signals are segmented as energy neutral, meaning that the FR resources that strictly follow these signals would consume the same amount of energy without providing the FR. Doing so is to rule out the uncertainty that arises from the energy content of the grid signal on the building environment. Our FR testing time is 2,700s (45 minutes), and the post FR event evaluation is 3,300s (55 minutes), making a total testing time of 6,000s (100 minutes) per test scenario. The post FR event duration is sufficient to capture all the possible impacts from providing the FR service.

Figure 6-7 shows the timeline of a single FR test. To investigate the impact of different signals on the HVAC system, three test signals, RegA1, RegA2, and RegD1 are segmented from PJM regulation self-test signals [39], as shown in Figure 6-7. These three signals are segmented and processed as energy neutral. RegA1 (traditional regulation AGC signal) and RegD1 (dynamic

regulation AGC signal) are of different frequencies but in the same regulation signal sequence (both are up-down signals that ramp up first). RegA1 and RegA2 are of the same signal content, but RegA2 in an opposite regulation signal sequence (down-up signal that ramps down first). To investigate the impact of different FR capacities on the HVAC system performance, we considered 5%, 10%, 15%, and 20% (four FR capacity magnitudes) of the rated fan power as the sweeping parameter of the regulation capacity. These regulation capacity values were then multiplied by the FR signal, which is typically between -1 and 1.

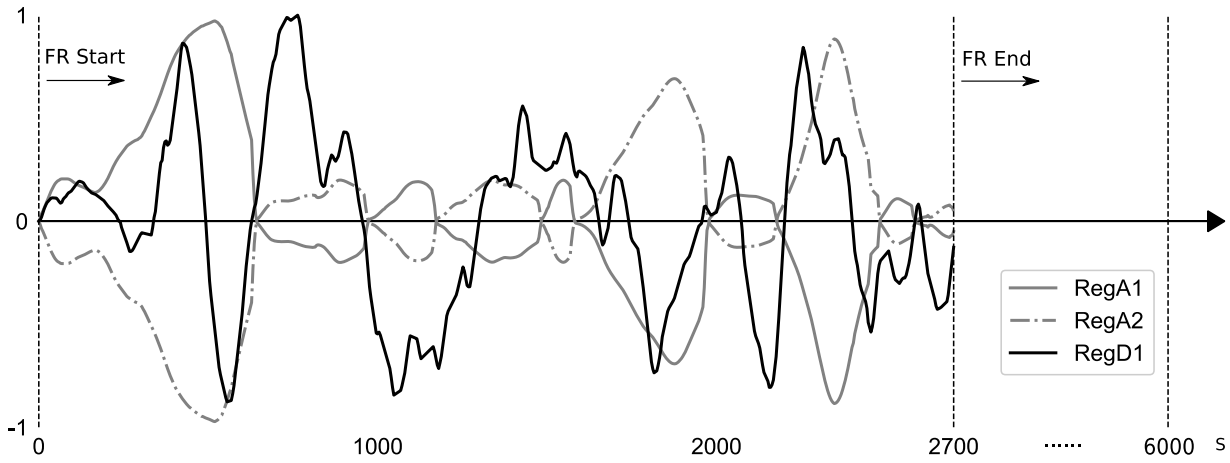

Figure 6-7 Timeline of a frequency regulation test

To analyze the impact of the different signals and FR capacities under various building thermal load profiles, we performed the testing in different periods and different climate zones. We consider different typical climate conditions, as shown in Table 6-5. For each climate condition, the testing periods start from 12:00 p.m. to 12:45 p.m. in four typical days, which include a hot summer day, a cold winter day, a mild summer day, and a mild winter day. For each climate zone, the hot summer day is defined as the day with the largest cooling load over the summer (June-September) while the cold winter day is the day with the largest heating load over the winter (November-February). The mild summer/winter day is the day with a median

cooling/heating load over the summer (June-September)/the winter (November-February). The building envelope parameters meet the minimum requirement in the ASHRAE Standard 90.1-2016 [46], and the HVAC system is resized accordingly. Batch simulation testing was thus performed to study how the HVAC system responds to the FR service under different load conditions. For each condition, the assessment will be performed on the baseline case and the FR case. The fan speed control as shown in Figure 6-5 is adopted in the baseline case while the FR case implements the control architecture as shown in Figure 6-6. Therefore, a total of 832 case studies (including 64 baseline cases) were conducted in this study. The summary of the case study description is presented in Table 6-6.

Table 6-5 Climate zones considered

City	Climate Zones	Type
Miami	1A	Very hot and humid
Houston	2A	Hot and humid
Phoenix	2B	Hot and dry
Atlanta	3A	Warm and humid
Los Angeles	3B	Warm and marine
Las Vegas	3B	Warm and dry
San Francisco	3C	Warm and marine
Baltimore	4A	Mild and humid
Albuquerque	4B	Mild and dry
Seattle	4C	Mild and marine
Chicago	5A	Cold and humid
Boulder	5B	Cold and dry
Minneapolis	6A	Cold and Humid
Helena	6B	Cold and dry
Duluth	7	Very Cold
Fairbanks	8	Sub-Arctic

Table 6-6 Summary of the case study description

	Periods	Climate Zones	FR Magnitudes	FR Signals	Total
Scenarios	12:00 p.m. to 12:45 p.m. on a hot summer day, a cold winter day, a mild summer day, and a mild winter day	ASHRAE typical climate zones	5%, 10%, 15%, and 20% of the rated fan power	RegA1, RegA2, RegD1	-
FR Cases	4	16	4	3	768
Baseline Cases	4	16	-		64

6.5.2 Key Performance Indexes

The key performance indexes (KPI) used in this study include the FR quality quantification metrics (the FR performance scores and the symmetric FR capacity), the energy efficiency metrics (the fan electricity consumption, the coil required energy, and site electricity use), the thermal comfort metric (zone air temperature deviation), and key control variable metrics (e.g., supply air temperature deviation). The specific definitions of the KPIs of interest are provided in Eq.(6-1)-Eq.(6-11).

$$\text{Precision Score: } S_p = 1 - \frac{1}{N} err(P_g, P_r) \tag{6-1}$$

$$\text{Correlation Score: } S_c = r(P_g, P_r(\tau^*, \tau^* + 5mins)), \tag{6-2}$$

$$\text{Delay Score: } S_d = \left|\frac{\tau^* - 5\ mins}{5\ mins}\right| \tag{6-3}$$

$$\text{Composite Score: } S_c = \frac{1}{3}(S_p + S_c + S_d) \tag{6-4}$$

where S_p, S_c, S_d, S_c represents the precision performance score, correlation score, delay score, and composite score, respectively. *N* is the sampling number. P_g and P_r are the power trajectory of the grid and the response signals. The operators $err(\cdot,\cdot)$ and $r(\cdot,\cdot)$ represent the absolute error and statistical correlation between the power response and the grid signal. The correlation score S_c and

delay score S_d are determined together. τ represents the time shift between P_g and P_r. τ^* is the time shift when the maximum correlation occurs, and the highest correlation coefficient value is defined as the correlation score S_c. The calculation procedures for the performance scores are detailed in [16, 18]. It is noted that we do not consider the controller communication delay in this study.

$$\text{Symmetric Regulation Capacity (SRC): } C_{sym} = \min(C_{up}, C_{down}), \tag{6-5}$$

where C_{sym} is the regulation capacity for the symmetric FR, which equals to the minimum of the regulation-up capacity C_{up} and regulation-down capacity C_{down}.

$$\text{Fan Electricity Consumption: } E_{fan} = \sum_{t=1}^{N} P_{fan}(t) \tag{6-6}$$

$$\text{Coil Required Energy: } E_{coil} = \sum_{t=1}^{N} Q_c(t), \tag{6-7}$$

$$\text{Site Electricity Use: } E_{ele} = \sum_{t=1}^{N} P_{HVAC}(t) = \sum_{t=1}^{N} Q_c(t)\,\eta(t) + \sum_{t=1}^{N} P_{fan}(t), \tag{6-8}$$

where P_{fan} is the instantaneous power use of the fan at the time *t*. Q_c is the instantaneous energy exchanged at the AHU cooling and heating coils. P_{HVAC} is the instantaneous site electricity consumed by the HVAC system equipment. To calculate the site electricity use from the cooling and heating coil required energy, we use the conversion factor η (1/4.4 for cooling, 1/2.8 for heating) from [50, 51].

$$\text{Sum of the zone air temperature deviation in the testing period: } D_z = \sum_{z \in Z} \sum_{t=1}^{N} |s_z(t)| \tag{6-9}$$

$$\text{Average supply air temperature deviation ratio:} \tag{6-10}$$

$$\overline{\delta T_{sup}} = \frac{\sum_{t=1}^{N} \left| \frac{T_{sup}(t) - T_{sup,set}(t)}{T_{sup,set}(t)} \right|}{N}$$

Maximum supply air temperature deviation ratio:

$$\delta T_{sup,max} = \max_t \left| \frac{T_{sup}(t) - T_{sup,set}(t)}{T_{sup,set}(t)} \right|, \quad (6\text{-}11)$$

where N is the sampling number for each time step point t, z is the zone index for the set of zones, and $s_z(t)$ is the deviation from the lower and upper setpoint temperatures. The zone air cooling and heating temperatures setpoint are 24 ℃ and 20 ℃ in this study, respectively. The deviation range in this study is ± 0.5 ℃ from the setpoint. In other words, we assume the occupant thermal comfort bound is 23.5-24.5 ℃ for the cooling period and 19.5- 20.5 ℃ for the heating period. T_{sup} and $T_{sup,set}$ are the supply air temperature and its setpoint.

6.6 Results and Discussions

Batch simulation tests of 832 cases were performed, and the results were analyzed and discussed in this section. Section 6.6.1 and 6.6.2 discuss the impacts on the HVAC system during the FR event and after the FR event, respectively.

6.6.1 Impacts on the HVAC System during FR Events

As described in Section 6.5.1, the FR event lasts 45 minutes, and the grid regulation signal is energy neutral. Results of different FR capacities (5%, 10%, 15%, and 20% of the rated fan power) and regulation signals (RegA1, RegA2, and RegD1) are presented in Section 6.6.1.1 and 6.6.1.2, respectively. Moreover, the results for the different FR capacities and regulation signals under various building load conditions are provided in section 4.1.3.

6.6.1.1 Different FR Capacities

We performed the test of different regulation capacity magnitudes using the RegD1 signal on a hot summer day in Chicago, IL (climate zone 5A). Figure 6-8 depicts the FR tracking

performance of 5%, 10%, 15%, and 20% of the rated fan power. The blue line is the grid FR signal in a 4-second time step, and the red curve is the frequency regulation response. It can be seen that the two lines almost overlap which indicates the FR controller tracks the grid regulation signal well for all the FR capacity magnitudes. Table 6-7 summarizes the simulation results; the FRC performance is consistent across the test scenarios, and the composite score is 0.98 for all the FR capacities.

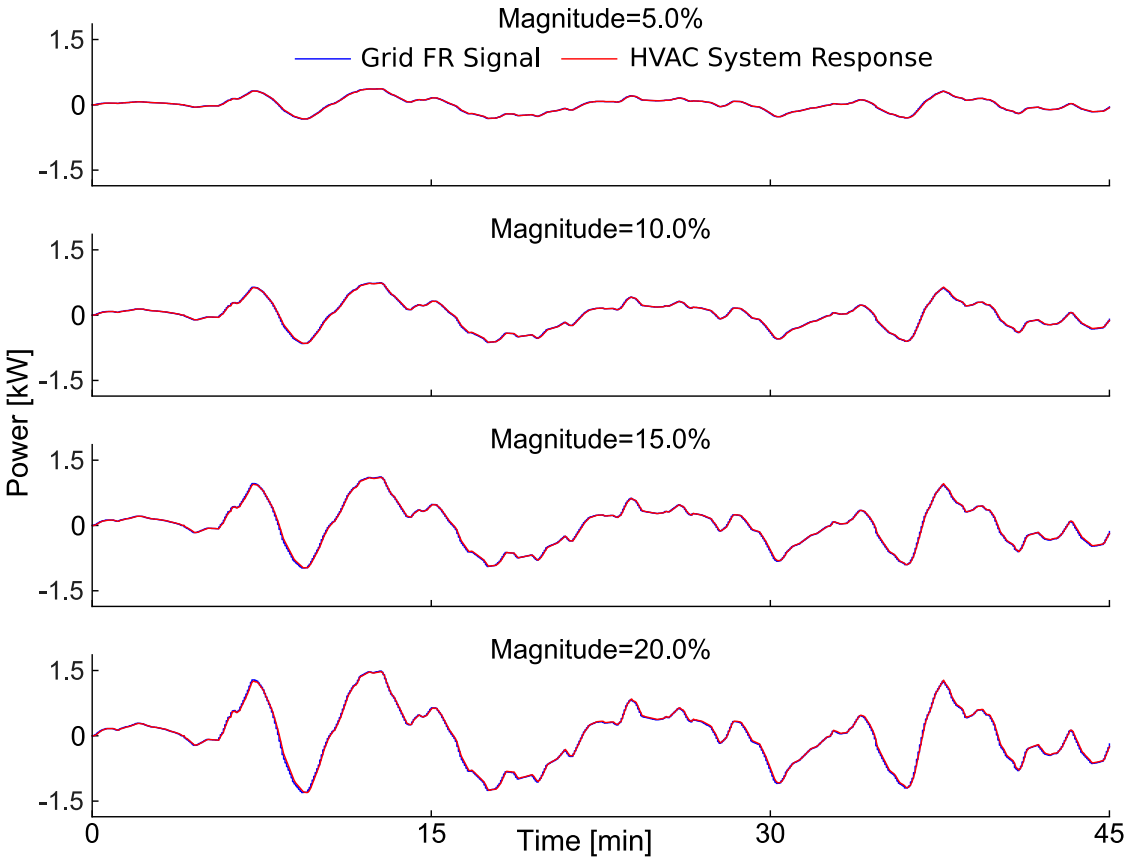

Figure 6-8 FR tracking performance for different regulation capacity magnitudes

Table 6-7 Summary of FR performance for different regulation capacity magnitudes

Regulation Capacity Magnitude	Symmetric Regulation Capacity [%]	Composite Score	Precision Score	Correlation Score	Delay Score
5.00%	4.36	0.98	0.96	0.99	0.99
10.00%	8.71	0.98	0.96	0.99	0.99
15.00%	13.07	0.98	0.96	0.99	0.99
20.00%	17.53	0.98	0.96	0.99	0.99

Figure 6-9 shows the AHU supply air temperature for the different regulation capacity magnitudes. The blue and red solid lines represent the actual AHU supply air temperature and its setpoint while providing FR. The green dashed line represents the nominal AHU supply air temperature. For all four different cases, the actual AHU supply air temperature cannot maintain its setpoint, and the fluctuation increases with the size of the FR capacity. This suggests significant interactions between the baseline supply air temperature control and the FRC. The PI feedback control that modulates the cooling coil valve is unable to reject the disturbance introduced by the FRC loop. The AHU supply air temperature deviations for the 5% and 10% cases are less than 0.5 ℃. The maximum AHU supply air temperature deviation is 1.5 ℃ for the 20% case.

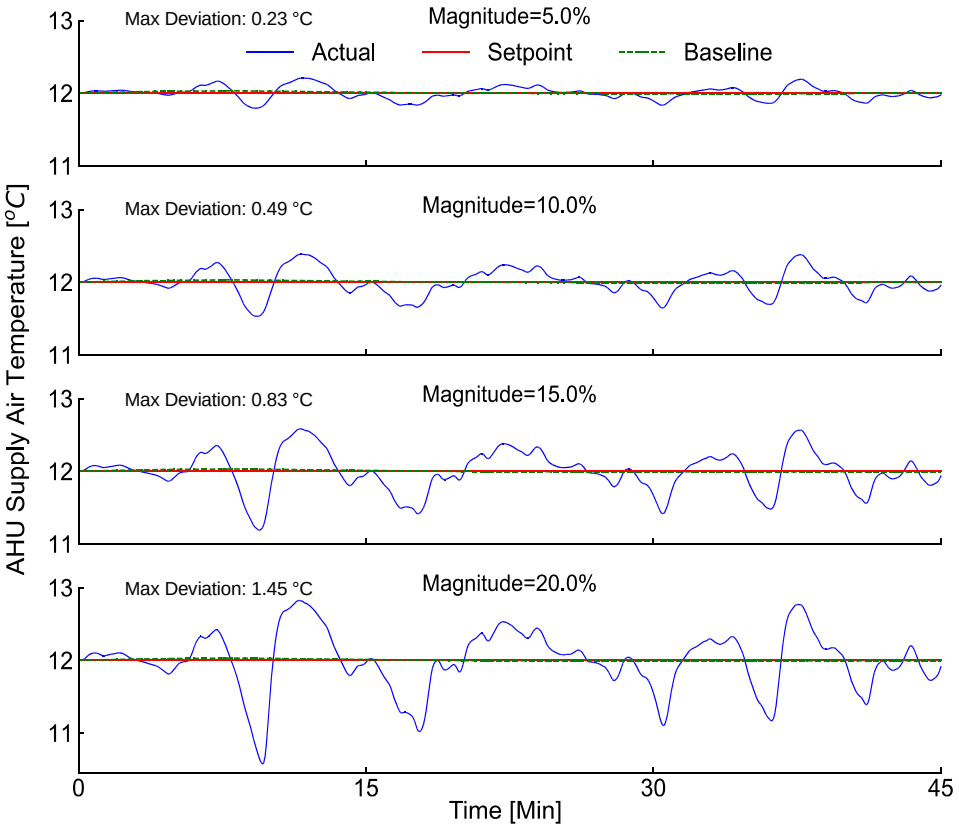

Figure 6-9 AHU supply air temperature behaviors in cases with different regulation capacity magnitudes

Figure 6-10 shows the AHU supply airflow rate for different regulation capacity magnitudes. The airflow rate fluctuates more when the fan power follows a FR signal with a larger magnitude. The air flow deviations for the four cases are 8.4 %, 18.0%, 30.8%, and 52.9%, respectively.

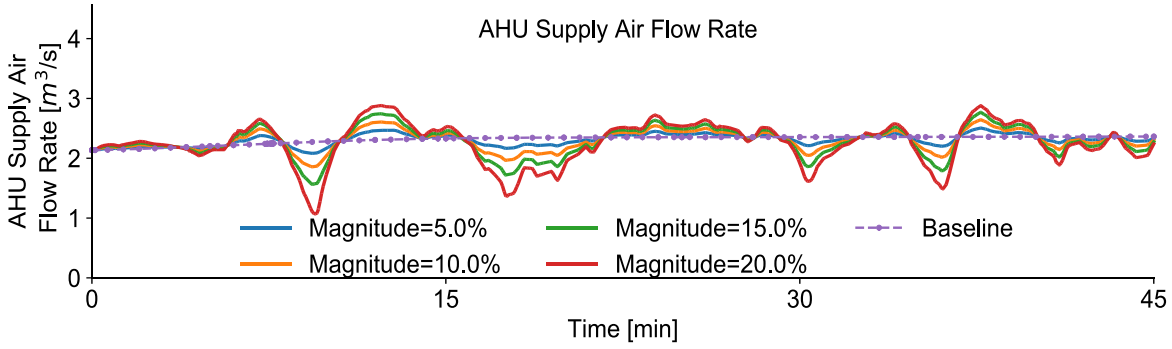

Figure 6-10 AHU supply airflow rate in cases with different regulation capacity magnitudes

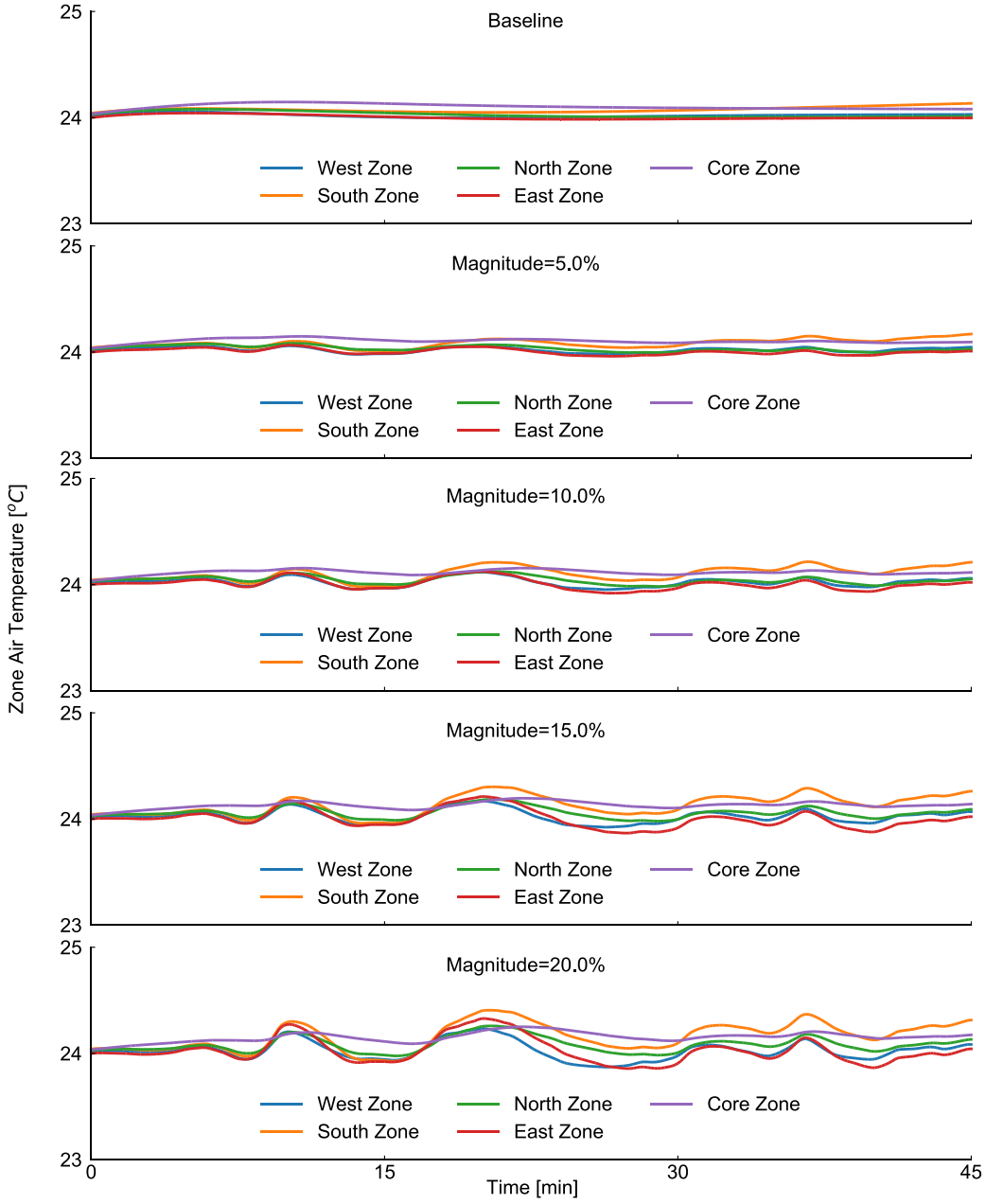

Figure 6-11 Zone air temperatures in cases with different regulation capacity magnitudes

Figure 6-11 depicts the zone air temperature profile for the different regulation capacity magnitudes. The five zones have similar air temperature profiles in the baseline case, while the evolution of the air temperature diverges with increased regulation capacity magnitudes. The air temperature fluctuation level in different zones becomes different since they are competing for the airflow when the fan power is regulated down [55]. The south zone has the largest temperature

variation due to its larger thermal load. Still, the deviations (even for the case with a 20% regulation capacity magnitude) do not exceed ± 0.5 ℃, which is well within the occupant thermal comfort bound.

Table 6-8 summarizes the zone air temperature deviation, the supply air temperature deviation, and the zone pressure request number for the different regulation capacity magnitudes. There are no cases that zone air temperature variations exceed the comfort threshold of ± 0.5 ℃. The maximum supply air temperature deviation ratio is 12%. With the increase of the regulation capacity magnitudes, the number of the time-averaged zone pressure request also surges because the zones become more starved for airflow.

Table 6-8 Summary of impact on the HVAC system for different regulation capacity magnitudes

Regulation Capacity Magnitude	Sum of Zone Air Temperature Deviation [K·s]	Average Supply Air Temperature Deviation Ratio [%]	Maximum Supply Air Temperature Deviation Ratio [%]	Time-averaged Zone Pressure Request*
Baseline	0	0	0	1.0
5.00%	0	0.8	2.1	1.0
10.00%	0	1.2	4.3	1.4
15.00%	0	2.3	7.4	1.9
20.00%	0	3.1	11.8	3.5

* The number of ignored requests for the supply fan T&R control is 2.

Table 6-9 summarizes the energy efficiency metrics for the four cases. It can be seen that FRC has no negative impact on energy efficiency. With the increase of the regulation capacity magnitudes, the fan electricity consumption has a very slight increase. The energy consumed by the coil has a slight decrease mainly due to the nonlinearity of the coil energy consumption under different loads. It is noted that the small decrease of the coil energy comes at the expense of the slightly reduced ventilation air and slightly more zone air temperature violation. The site electricity consumption is also estimated to have a slight decrease.

Table 6-9 Summary of HVAC system energy efficiency for different regulation capacity magnitudes

	Regulation Capacity Magnitude				
	Baseline	5.00%	10.00%	15.00%	20.00%
Fan Electricity Consumption [MJ]	4.12	4.12	4.12	4.12	4.14
Fan Electricity Baseline Deviation [%]	-	0	0.1	0.2	0.5
Cooling Coil Energy [MJ]	123.5	123.3	122.7	121.9	120.5
Coil Energy Baseline Deviation [%]	-	-0.2	-0.6	-1.3	-2.4
Site Electricity Consumption Baseline Deviation [%]	-	-0.2	-0.6	-1.2	-2.2

Note: '+' means the increase and '-' represents the decrease compared to the baseline

6.6.1.2 Different Regulation Signals

In this subsection, we tested different regulation signals to investigate their impact on the HVAC system. First, we compared the HVAC system performance when responding to regulation signal RegA1 and RegD1. These signals are both energy neutral and in the same sequence (up-down sequence signals that ramp up first) but have different frequency content. RegA is designed for slow-acting resources, while RegD is a fast regulation service signal. Next, we repeated the assessment for regulation signal RegA1 versus RegA2, which have similar signal content but are in an opposite sequence (up-down, down-up, respectively).

Table 6-10 and Table 6-11 compare the FR controller performance, energy efficiency, and the associated HVAC impact for different signal frequencies (RegA1 and RegD1). For the FR performance, different signal frequencies have little impact on the tracking score as well as the symmetric regulation capacity (i.e., the minimum of the up-down FR capacity and the down-up FR capacity). For energy efficiency, the fan electricity consumption is similar for both cases. The cooling coil energy consumption decreases with the increase of the regulation capacity magnitude for both cases due to the difference of the cooling coil heat transfer efficiency at different thermal

loads. The RegA1 case appears to decrease slightly more in terms of the coil energy compared to the RegD1 case. For the HVAC system impact, the RegA1 signal case has more influence on the zone air temperature than the RegD1 signal case. The zone controller requests more pressure resets when the regulation capacity regulation is high for the RegA1 case. These observations are justified because the slower nature of the RegA1 signal resulted in some interactions between the FRC and the zone-level controls. RegD1 signal is more dynamic and tends to have less impact on the zone thermal comfort, but the supply air temperature fluctuated more under the RegD1 signal.

Table 6-10 and Table 6-11 also compare the FR performance, energy efficiency, and the associated HVAC impact for different regulation signal sequences (up-down RegA1 vs. down-up RegA2). The tracking performance score for the first three frequency capacity magnitudes (5-15%) is the same. The tracking performance is slightly lowered for the RegA2 case compared with the RegA1 when the regulation capacity magnitude is 20%. The reduced tracking performance of the FRC when tracking the Reg A2 at 20% demand level is because the fan power decreases to its minimum and could not be further reduced due to the fan VFD limitation (a minimum speed of 30% of the VFD rated speed is recommended to prevent motor overheating due to an inadequate airflow [56]). In terms of energy efficiency, the fan electricity consumption is similar for the two signals. Due to the nonlinearity of the coil heat exchange performance under different airflow rates, the energy consumed by the coil for the RegA2 is slightly higher than that for the RegA1. Regarding the zone air temperature and AHU supply air temperature, the down-up RegA2 signal also performs worse than the up-down Reg A1 signal.

Table 6-10 Comparison of the FR performance for different regulation signal frequencies and sequences

	Composite Score			Symmetric Regulation Capacity [%]			Fan Electricity Baseline Deviation [%]			Coil Energy Baseline Deviation [%]			Site Electricity Consumption Baseline Deviation [%]		
Signal	Reg A1	Reg D1	Reg A2	Reg A1	Reg D1	Reg A2	Reg A1	Reg D1	Reg A2	Reg A1	Reg D1	Reg A2	Reg A1	Reg D1	Reg A2
5%	0.98	0.97	0.98	4.4	4.4	4.5	0	0	0	-0.7	-0.2	0.3	-0.6	-0.2	0.3
10%	0.98	0.97	0.98	8.7	8.7	8.9	0.1	0.1	0.3	-1.5	-0.6	0.4	-1.4	-0.6	0.4
15%	0.97	0.97	0.97	13.1	13.1	13.3	0.3	0.2	0.5	-2.6	-1.3	0	-2.4	-1.2	0
20%	0.97	0.97	0.95	17.6	17.5	17.5	0.3	0.5	0.8	-4.1	-2.4	-0.6	-3.7	-2.2	-0.5

Table 6-11 Comparison of the HVAC impact for different regulation signal frequencies and sequences

	Sum of Temperature Deviation [K·s]			Average Supply Air Temperature Deviation Ratio [%]			Maximum Supply Air Temperature Deviation Ratio [%]			Time-averaged Zone Pressure Request*		
Signal	Reg A1	Reg D1	Reg A2	Reg A1	Reg D1	Reg A2	Reg A1	Reg D1	Reg A2	Reg A1	Reg D1	Reg A2
Baseline	0	0	0	0	0	0	0	0	0	1.0	1.0	1.0
5%	0	0	0	0.3	0.8	0.4	0.5	2.1	1.5	1.1	1.0	2.1
10%	0	0	0	0.7	1.2	0.8	1.8	4.3	3.7	1.6	1.4	3.1
15%	0	0	8	0.9	2.3	1.1	3.9	7.4	5.8	2	1.9	4.5
20%	3	0	121	1.2	3.1	1.9	7.2	11.8	9.3	2.5	3.5	6.4

* The number of ignored requests for the supply fan T&R control is 2.

6.6.1.3 Different Load Profiles

In this subsection, a large-scale simulation was conducted to investigate how the system responds during the FR event under different building thermal load profiles. We performed the

testing in various typical climate zones and periods. Cases of different FR capacities and different test signals were examined under different load profiles. In this subsection, we present the results for the RegD1 signal in a hot summer day under different load profiles. Each simulation experiment was conducted for 45 minutes, starting at noon.

Figure 6-12 depicts the FR performance score in different climate zones. For the FR tracking performance score, different climate zones have a similarly high score except for some mild and cold climate zones when the regulation capacity magnitude is 20%. With the relatively small cooling load in these mild and cold climate zones, the fan VFD typically operates at a low speed and has little room to adjust its power consumption downwards. Figure 6-13 shows the map of the frequency regulation symmetric capacity in a hot summer day for different climate zones. It can be observed that the frequency regulation capacity is lower in Climate Zone 7 of Duluth and Climate Zone 8 of Fairbanks than the other climate zones during the test period. These two climate zones also have the lowest tracking score on average.

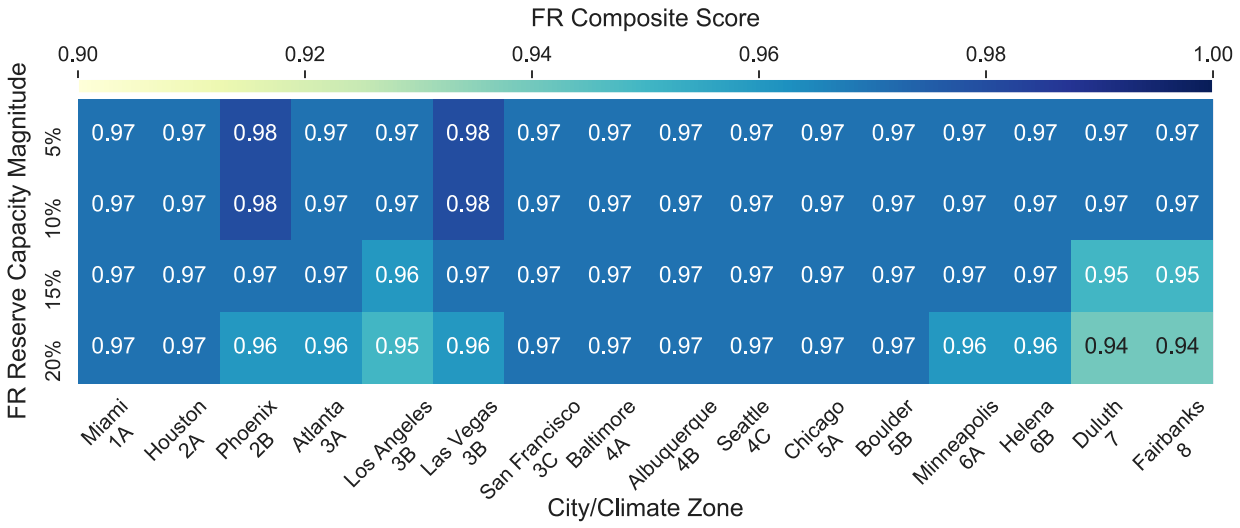

Figure 6-12 FR performance score for different climate zones with RegD1 signal

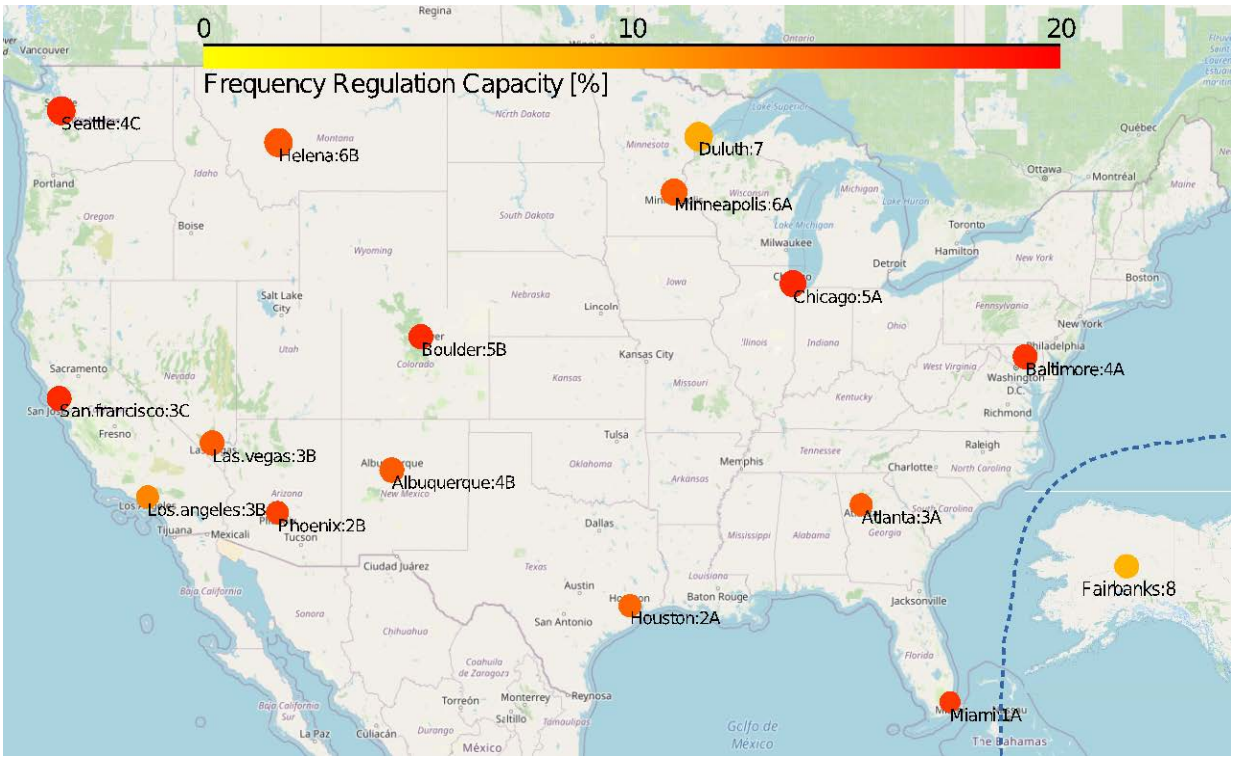

Figure 6-13 Symmetric regulation capacity for different climate zones with RegD1 signal in a hot summer day

The building thermal load conditions directly impacts the FR performance and symmetric regulation capacity due to the operating constraints on the fan VFD modulation. This result confirms the findings reported in [27] that the available regulation capacity is higher when the load condition is intermediate. To provide additional insight, we developed a correlation model between the symmetric regulation capacity and the average part load ratio based on the batch simulation data for all the RegD1 cases (i.e. 64 cases) under different thermal load conditions. The average part load ratio (PLR) is defined as the ratio of the actual average supply air mass flow rate and the nominal supply air mass flow rate. The highest average PLR is over 0.6, and the lowest is around 0.15 for all the simulated cases. Figure 6-14 shows the Gaussian model [57] fitted to the symmetric frequency regulation capacity and the average PLR data. The model has a high R-square value,

but the Root Mean Square Error (RMSE) is modest, especially for the cases with small PLR. FR capacity has a higher value when the part load ratio is at an intermediate level.

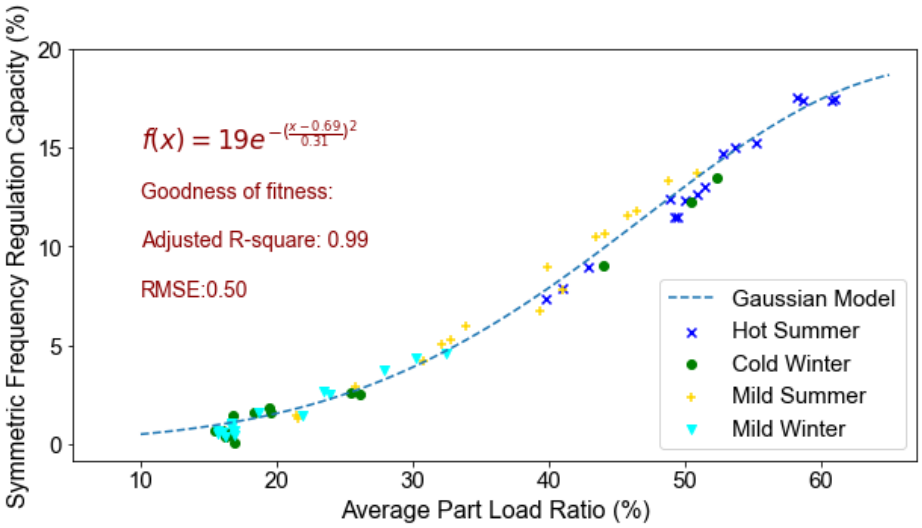

Figure 6-14 The correlation of FR symmetric capacity and the average part load ratio with RegD1 signal

Figure 6-15 depicts the heatmap of the HVAC energy efficiency in different climate zones. For the fan electricity consumption, different climate zones behave similarly with the small FR capacity magnitudes (i.e., 5%, and 10%). For the larger FR capacity magnitude, especially in the cold climate zones, the fan consumes more energy due to the fact that it could not track the lower end of the regulation signal, so the energy usage for the FR service is not neutral on average. For the energy consumed by the cooling coil, the different climate zones behave similarly. With the increase of the FR capacity magnitudes, the cooling coil consumed less energy due to the non-linearity of the cooling coil heat transfer performance at different loads. It is noted that the small decrease of the coil energy comes at the expense of slightly reduced ventilation air flow and more zone air temperature violations. For the site electricity use, it has a similar pattern with the energy consumed by the cooling coil since the latter contributes to most of the site electricity consumption.

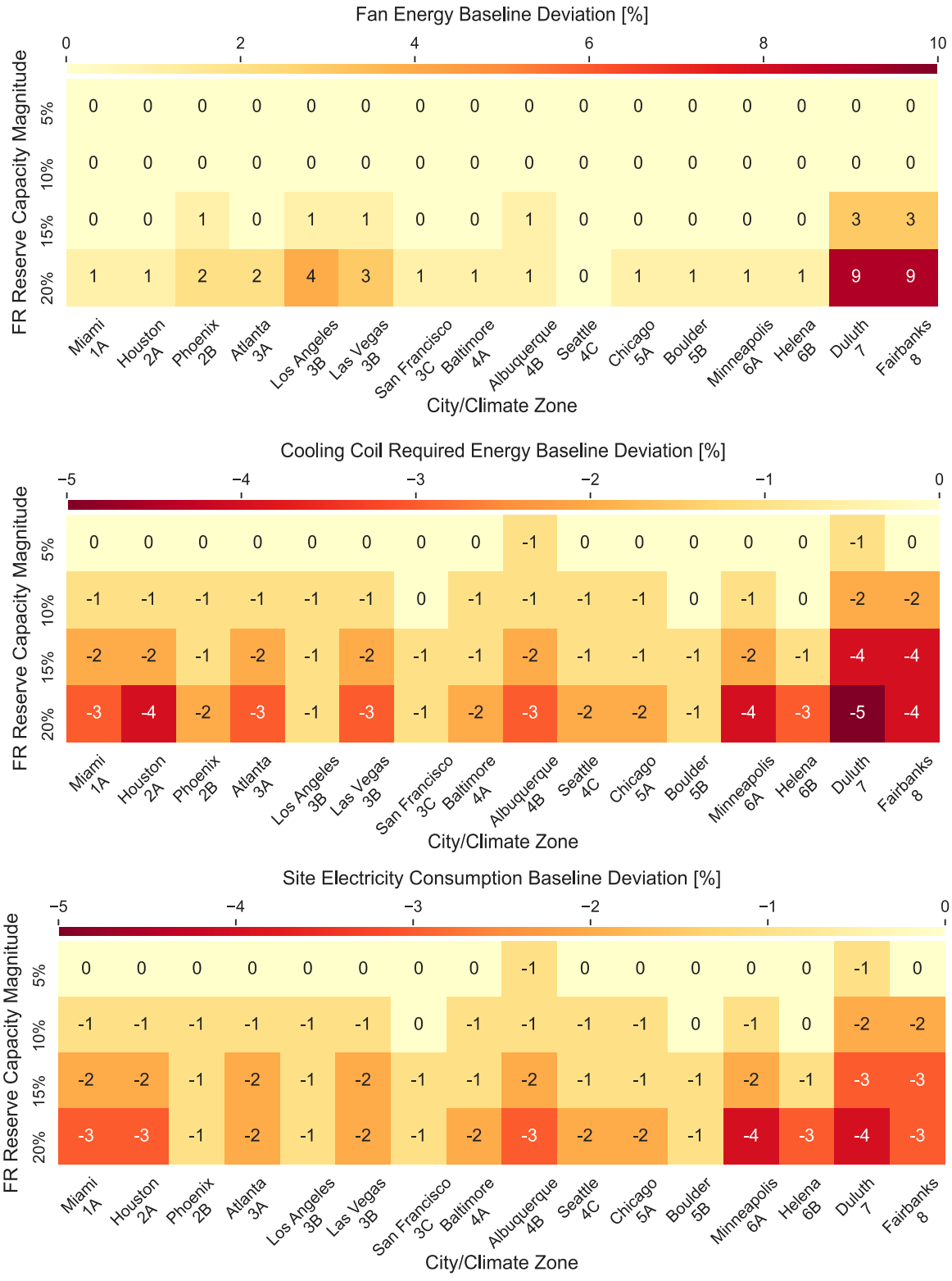

Figure 6-15 HVAC energy efficiency for different climate zones with RegD1 signal

Figure 6-16 shows the heatmap of zone air temperature and AHU supply air temperature profiles for different climate zones. With a FR capacity magnitude smaller than 10%, the zone air temperature is within the comfort limit of ± 0.5 ℃. When the FR capacity magnitude is 20%, half of the climate zones exceed the comfort threshold of ± 0.5 ℃ for a certain amount of time. The AHU supply air temperature fluctuates more with the FR capacity magnitude, and the fluctuation is similar in different climate zones for each FR capacity magnitude. The average AHU supply air temperature fluctuation ranges from 0.1 – 0.4 ℃ in different climate zones when the FR capacity magnitude is 20%.

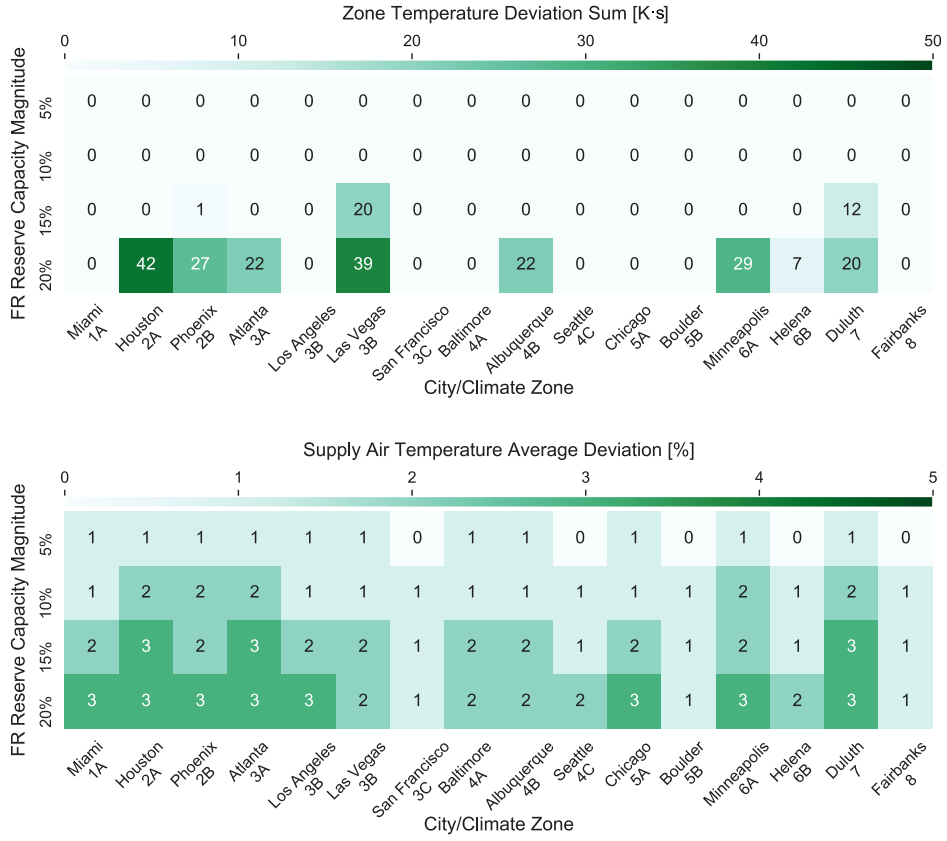

Figure 6-16 Zone air temperature and AHU supply air temperature for different climate zones with RegD1 signal

6.6.2 Impacts on HVAC system afterward the FR Event

In this subsection, the results of how the FR impacts the HVAC system after the FR event are presented. The FR service stopped after the 45-minute service period and it is expected that the HVAC system will rebound back to the baseline case without the FR. Two typical examples are summarized to demonstrate the typical phenomena.

6.6.2.1 Typical Example 1: Chicago Cold Winter

Figure 6-17 depicts the RegD1 FR service during a cold winter period in Chicago, IL. Although it is a cold winter period with a high heating load, the heating load is less than half of the design cooling load. The supply air flow rate is also way smaller than the design supply air flow rate. We consider this as the low load condition compared to the high cooling load. The energy consumed by the heating coil accounts for both the AHU heating coil and the zone terminal reheat coils. We can see that the system quickly resumes the normal operation after the FR event during this low load condition. The fan rebounds to the normal condition in less than 10 minutes and the heating coil rebounds back in about 20 minutes. Note that the time it takes for the system to return to normal increases with the FR capacity magnitude increase. Table 6-12 shows the energy efficiency metrics during the full evaluation period (during and post-event). The energy deviation for each scenario is calculated from the start of the FR till when the system recovers back to the baseline condition. The increase in the fan electricity consumption during the recovery period is relatively small. The larger deviation observed during the FR service is mainly due to the inability of the FRC to track the downside signal; thus, the average fan electricity consumption increases. Overall, there is a minimal change in the heat coil exchanged power consumption and site electricity use during the testing period.

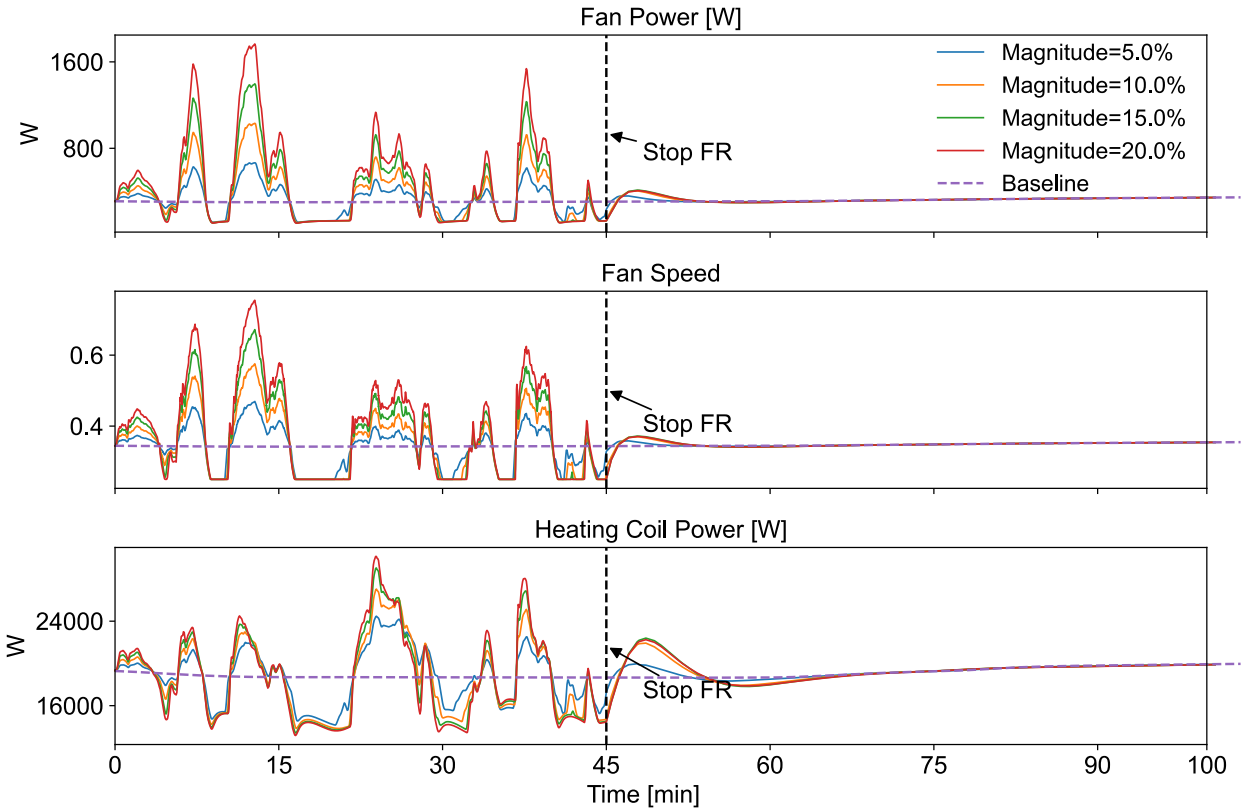

Figure 6-17 Time series plots of fan electrical power, heating coil exchanged heat, and fan speed during a Chicago cold winter period

Table 6-12 Energy efficiency summary during a Chicago cold winter period

KPI	Testing Period	Magnitude			
		5.00%	10.00%	15.00%	20.00%
Fan Power Consumption Deviation [%]	During FR	3.8	21.3	41.1	62.0
	After FR	1.1	1.9	2.1	2.1
	Whole Testing Period	2.5	11.8	22.1	32.9
Coil Energy Deviation [%]	During FR	-0.1	-0.6	-0.7	-0.7
	After FR	0.4	0.9	1.1	1.1
	Whole Testing Period	0.2	0.2	0.1	0.1
Site Electricity Deviation [%]	During FR	0.1	0.2	0.8	1.7
	After FR	0.4	0.9	1.1	1.2
	Whole Testing Period	0.3	0.7	1.0	1.5

6.6.2.2 Typical Example 2: Chicago Hot Summer

In the previous example, we do not observe any critical post-event impact of the FR on the HVAC system performance. The following case study shows that the HVAC energy efficiency can be significantly impacted after the FR event when the cooling load is high. Figure 6-18 depicts the RegD1 FR test results during a Chicago hot summer period. It is noted that the fan power surges to its rated power as soon as the FR event ends. This is because by the end of the event, the baseline control system had accumulated a lot of pressure reset requests that were not executed when the fan speed was mostly driven by the FRC. This control saturation represents a typical example of potential conflict between the FR control and the HVAC existing control (T&R control in this case study). With the increase of the higher FR magnitude, it takes a longer time for the HVAC equipment and system to recover back to the baseline status. Table 6-13 shows the energy efficiency metrics for the whole testing period. The energy deviation for each scenario is calculated from the start of the FR till when the system recovers back to the baseline condition. Although the fan does not consume more energy during the FR events, it has a sudden increase after the FR event. For the case with the regulation capacity magnitude of 20%, the fan electricity consumption increased by up to 55.2% compared to the baseline case. The site electricity use for the whole period is also increased by 7.3% although the site electricity use slightly decreases during the FR service period. This will not only offset the potential revenue a building can earn from offering the FR service, but the rebound power usage could have a negative effect on the grid. An anti-saturation control logic (with rate limiter effect) is thus needed to resolve the conflict and ensure a smooth transition to a post-FR operation. For the heat exchanged by coils, the energy consumption increase is minimal.

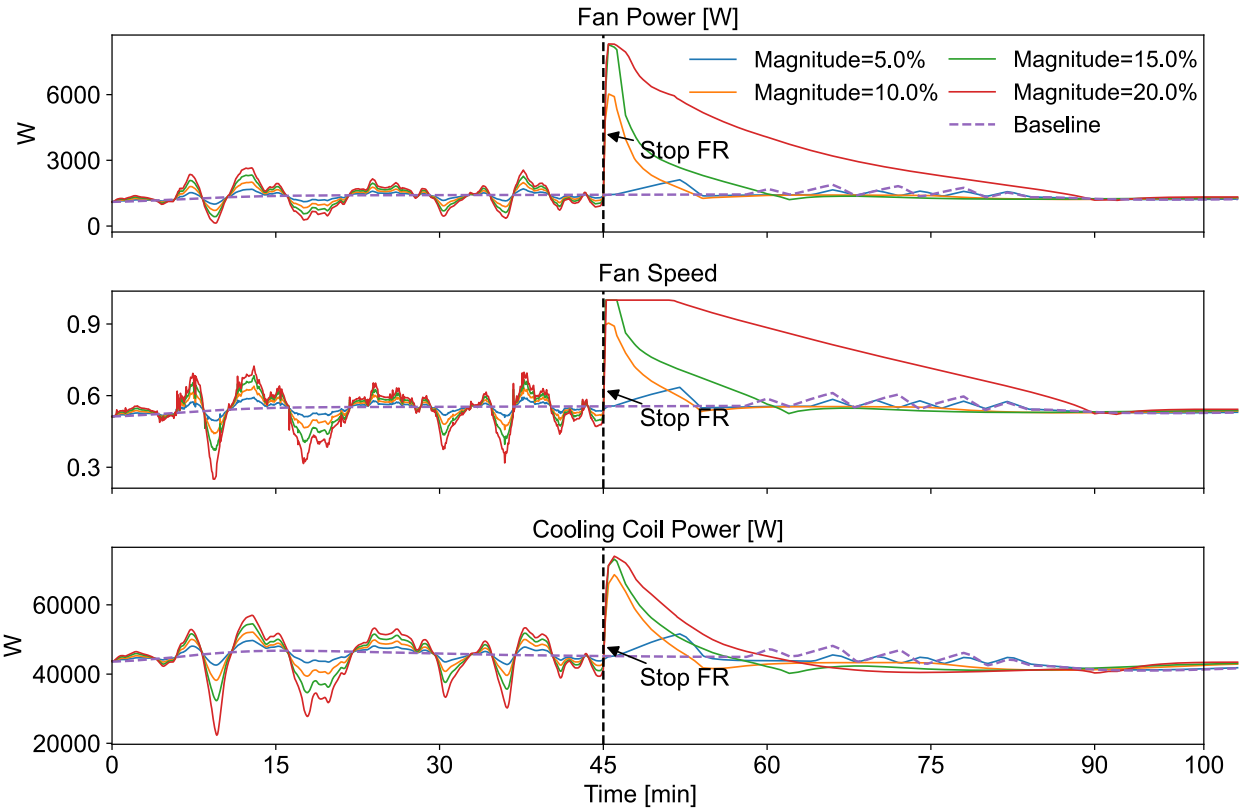

Figure 6-18 Time series plots of fan electrical power, cooling coil exchanged heat, and fan speed time series during a Chicago hot summer period

Table 6-13 Energy efficiency summary during a Chicago hot summer period

KPI	Testing Period	Magnitude			
		5.00%	10.00%	15.00%	20.00%
Fan Power Consumption Deviation [%]	During FR	0.0	0.1	0.2	0.5
	After FR	0.9	20.2	22.6	86.3
	Whole Testing Period	0.4	8.6	13.7	55.2
Coil Energy Deviation [%]	During FR	-0.2	-0.6	-1.3	-2.4
	After FR	-0.1	1.8	1.9	2.6
	Whole Testing Period	-0.1	0.3	0.6	0.7
Site Electricity Deviation [%]	During FR	-0.2	-0.6	-1.2	-2.2
	After FR	0.0	4.2	4.5	13.1
	Whole Testing Period	-0.1	1.3	2.1	7.3

6.7 Conclusions, Limitations, and Future work

This chapter investigates how the HVAC system is impacted during and after the FR service in a high-fidelity dynamic simulation testbed using different FR signals in 16 different climate zones in the U.S. The impact aspects include the FR performance, energy efficiency, thermal comfort, and HVAC controls. A dynamic Modelica-based five-zone VAV system with the AHU fan FR controller is developed, in which the state-of-the-art HVAC control sequences (e.g., T&R algorithms in the GDL36) [37] and an experimentally-validated FR control scheme [22] are adopted.

During the FR service period, the FR does not have a noticeable impact on the HVAC system when the regulation capacity is within a demand level that can be met by the building HVAC system. If the regulation capacity is overestimated, the FR performance will be degraded mainly due to the equipment's operating constraints (e.g., the lowest speed allowed by the VFD). The fan electricity consumption increases due to the inability to track the downside signal. The zone air temperature is shown not to be largely impacted during the FR service time. For the FR capacity within 15% of the rated fan power, the zone air temperature in a majority of the thermal zones stays in the comfort threshold of ±0.5 ℃. However, the AHU supply air temperature fluctuates and cannot maintain the setpoint with the increase of the FR capacity magnitude. The average fluctuation ranges from 0.1 – 0.4 ℃ in different climate zones when the FR capacity magnitude is 20%. RegA signal and RegD signal have a similar FR performance as well as a similar impact on the HVAC system performance when the AHU fan offers the FR service. Considering the fan operating constraints, the up-down regulation sequence performs better than the down-up regulation sequence in terms of the FR performance, zone air temperature deviation, and AHU supply air temperature fluctuation.

After the FR service time, the system takes a certain period to get back to normal. The settling time increases with the magnitude of the FR capacity. When the building thermal load is high, a control conflict is observed between the FR control and the existing HVAC control. For the regulation capacity magnitude of 20% in Chicago, IL, the fan electricity consumption increased noticeably by up to 55.2% compared to the baseline case and the site electricity consumption could increase by 7.3%. This will not only offset the potential revenue a building can earn from offering the FR service, but the rebound power usage could have a negative effect on the grid. An anti-saturation control logic (with rate limiter effect) is thus needed to resolve the conflict and ensure a smooth transition to a post-FR operation.

The simulation testbed used for this study only use the heating/cooling coil model and does not include a detailed modeling of the waterside (e.g., chiller and boiler plant). Therefore, we calculate how much energy is exchanged or required from the waterside and estimate the site electricity consumption using the conversion factors [50]. Although 1-4% site electricity consumption (the saved amount is less than the uncertainties from typical sensor measurements) could be saved at large FR capacity magnitudes in different climate zones, the ventilation air flow and zone air temperature are sacrificed (less OA and more zone air temperature deviations). In addition, the waterside HVAC equipment limitation (e.g., water pump, chiller, boiler) and detailed control sequences may impact the FR potential and associated energy efficiency performance. The communication delay of the building control system is not considered in this study as well.

Future work is to extend the dynamic Modelica model and impact analysis to include the waterside HVAC equipment and system. Another future direction is on the integration of the FR control with the HVAC existing state-of-the-art control. There is a need to modify the baseline controls to address potential conflicts between the existing building controls and the FR controls

and enable seamless and energy-efficient transitions between the two controls. More importantly, the time-varying FR capacity that a building can offer to the grid must be correctly estimated to assure the building quality of service and satisfactory grid service.

6.8 References

[1] The U.S. Energy Information Administration (EIA). Annual Energy Outlook 2021. 2021.

[2] Kirby BJ, Dyer J, Martinez C, Shoureshi RA, Guttromson R, Dagle J. Frequency control concerns in the North American electric power system: United States. Department of Energy; 2003.

[3] Lee ZE, Sun Q, Ma Z, Wang J, MacDonald JS, Max Zhang K. Providing Grid Services With Heat Pumps: A Review. ASME Journal of Engineering for Sustainable Buildings. 2020;1.

[4] Zhang S, Mishra Y, Shahidehpour M. Utilizing distributed energy resources to support frequency regulation services. Applied Energy. 2017;206:1484-94.

[5] MacDonald J, Cappers P, Callaway D, Kiliccote S. Demand response providing ancillary services: A comparison of opportunities and challenges in US wholesale markets. Grid-Interop. Irving, TX, USA2012.

[6] Han S, Han S, Sezaki K. Estimation of achievable power capacity from plug-in electric vehicles for V2G frequency regulation: Case studies for market participation. IEEE Transactions on Smart Grid. 2011;2:632-41.

[7] Peng C, Zou J, Lian L. Dispatching strategies of electric vehicles participating in frequency regulation on power grid: A review. Renewable Sustainable Energy Reviews. 2017;68:147-52.

[8] Li S, Brocanelli M, Zhang W, Wang X. Data center power control for frequency regulation. 2013 IEEE Power & Energy Society General Meeting: IEEE; 2013. p. 1-5.

[9] Hao H, Sanandaji BM, Poolla K, Vincent TL. Aggregate flexibility of thermostatically controlled loads. IEEE Transactions on Power Systems. 2014;30:189-98.

[10] Zhao P, Henze GP, Plamp S, Cushing V. Evaluation of commercial building HVAC systems as frequency regulation providers. Energy and Buildings. 2013;67:225-35.

[11] Wang H, Wang S, Tang R. Development of grid-responsive buildings: Opportunities, challenges, capabilities and applications of HVAC systems in non-residential buildings in providing ancillary services by fast demand responses to smart grids. Applied Energy. 2019;250:697-712.

[12] DOE. About the Commercial Buildings Integration Program. US Department of Energy, Office of Energy Efficiency Renewable Energy. 2019.

[13] Beil I, Hiskens I, Backhaus S. Frequency regulation from commercial building HVAC demand response. Proceedings of the IEEE. 2016;104:745-57.

[14] Lin Y, Barooah P, Meyn S, Middelkoop T. Experimental evaluation of frequency regulation from commercial building HVAC systems. IEEE Transactions on Smart Grid. 2015;6:776-83.

[15] Maasoumy M, Ortiz J, Culler D, Sangiovanni-Vincentelli A. Flexibility of commercial building HVAC fan as ancillary service for smart grid. arXiv preprint arXiv:13116094. 2013.

[16] Cai J, Braun J. Laboratory-based assessment of HVAC equipment for power grid frequency regulation: Methods, regulation performance, economics, indoor comfort and energy efficiency. Energy and Buildings. 2019;185:148-61.

[17] Wang H, Wang S, Shan K. Experimental study on the dynamics, quality and impacts of using variable-speed pumps in buildings for frequency regulation of smart power grids. Energy. 2020:117406.

[18] PJM. PJM Manual 12: Balancing Operations. Revision 40 2020.

[19] Vrettos E, Kara EC, MacDonald J, Andersson G, Callaway DS. Experimental demonstration of frequency regulation by commercial buildings—Part I: Modeling and hierarchical control design. IEEE Transactions on Smart Grid. 2016;9:3213-23.

[20] Vrettos E, Kara EC, MacDonald J, Andersson G, Callaway DS. Experimental demonstration of frequency regulation by commercial buildings—Part II: results and performance evaluation. IEEE Transactions on Smart Grid. 2016;9:3224-34.

[21] MacDonald J, Kiliccote S, Boch J, Chen J, Nawy R. Commercial building loads providing ancillary services in PJM. Lawrence Berkeley National Lab.(LBNL), Berkeley, CA (United States); 2014.

[22] Adetola V, Lin F, Yuan S, Reeve H. Building Flexibility Estimation and Control for Grid Ancillary Services. 5th International High Performance Buildings Conference. Purdue University2018.

[23] Kim Y-J, Fuentes E, Norford LK. Experimental study of grid frequency regulation ancillary service of a variable speed heat pump. IEEE Transactions on Power Systems. 2015;31:3090-9.

[24] Su L, Norford LK. Demonstration of HVAC chiller control for power grid frequency regulation—Part 1: Controller development and experimental results. Science Technology for the Built Environment. 2015;21:1134-42.

[25] Su L, Norford LK. Demonstration of HVAC chiller control for power grid frequency regulation—Part 2: Discussion of results and considerations for broader deployment. Science Technology for the Built Environment. 2015;21:1143-53.

[26] Keskar A, Anderson D, Johnson JX, Hiskens IA, Mathieu JL. Do commercial buildings become less efficient when they provide grid ancillary services? Energy Efficiency. 2019:1-15.

[27] Cai J, Braun J. A regulation capacity reset strategy for HVAC frequency regulation control. Energy and Buildings. 2019;185:272-86.

[28] Bünning F, Warrington J, Heer P, Smith RS, Lygeros J. Machine learning and robust MPC for frequency regulation with heat pumps. ArXiv preprint arXiv:06920. 2020.

[29] Benner S. Performance, mileage and the mileage ratio. PJM. 2015.

[30] DOE. Commercial Prototype Building Models. Building Energy Codes Program 2020.

[31] Fabietti L, Gorecki TT, Qureshi FA, Bitlislioğlu A, Lymperopoulos I, Jones CN. Experimental implementation of frequency regulation services using commercial buildings. IEEE Transactions on Smart Grid. 2016;9:1657-66.

[32] Beil I, Hiskens I, Backhaus S. Round-trip efficiency of fast demand response in a large commercial air conditioner. Energy and Buildings. 2015;97:47-55.

[33] Lin Y, Mathieu JL, Johnson JX, Hiskens IA, Backhaus S. Explaining inefficiencies in commercial buildings providing power system ancillary services. Energy and Buildings. 2017;152:216-26.

[34] Raman NS, Barooah P. On the round-trip efficiency of an HVAC-based virtual battery. EEE Transactions on Smart Grid. 2019;11:403-10.

[35] Raman NS, Barooah P. Analysis of round-trip efficiency of an HVAC-based virtual battery. 5th International High Performance Buildings Conference. Purdue University2018.

[36] Vrettos E, Andersson G. Scheduling and provision of secondary frequency reserves by aggregations of commercial buildings. IEEE Transactions on Sustainable Energy. 2015;7:850-64.

[37] ASHRAE. ASHRAE Guideline 36-2018 High Performance Sequences of Operation for HVAC Systems. 2018.

[38] Okochi GS, Yao YJR, Reviews SE. A review of recent developments and technological advancements of variable-air-volume (VAV) air-conditioning systems. 2016;59:784-817.

[39] PJM. Normalized Dynamic and Traditional Regulation Signals - May 2014 2014.

[40] Tiller M. Introduction to physical modeling with Modelica: Springer Science & Business Media; 2001.

[41] Wetter M, Zuo W, Nouidui TS, Pang X. Modelica buildings library. Journal of Building Performance Simulation. 2014;7:253-70.

[42] Nouidui TS, Wetter M, Zuo W. Validation of the window model of the Modelica Buildings library. Proceedings of SimBuild2012. p. 529-36.

[43] Nouidui TS, Phalak K, Zuo W, Wetter M. Validation and application of the room model of the Modelica buildings library. Proceedings of the 9th International MODELICA Conference; September 3-5; 2012; Munich; Germany: Linköping University Electronic Press; 2012. p. 727-36.

[44] Yuan S, O'Neill ZJPoS. Testing and validating an equation-based dynamic building program with ASHRAE standard method of test. 2008;3:45-52.

[45] Wetter M. Multizone airflow model in Modelica. Proc of the 5-th International Modelica Conference2006. p. 431-40.

[46] ASHRAE. ASHRAE/IES Standard 90.1-2013--Energy Standard for Buildings Except Low-Rise Residential Buildings. 2013.

[47] Wetter M. Modeling of heat transfer in rooms in the modelica buildings library. 2011.

[48] Wetter M, Zuo W, Nouidui TS. Recent Developments of the Modelica" Buildings" Library for Building Energy and Control Systems. Lawrence Berkeley National Lab.(LBNL), Berkeley, CA (United States); 2011.

[49] Yao Y, Wang LJE, Buildings. Energy analysis on VAV system with different air-side economizers in China. 2010;42:1220-30.

[50] Energy Star. Energy star portfolio manager. 2019.

[51] Haleem SMA, Pavlak GS, Bahnfleth WPJE, Buildings. Performance of advanced control sequences in handling uncertainty in energy use and indoor environmental quality using uncertainty and sensitivity analysis for control components. 2020;225:110308.

[52] Kays WM, London AL. Compact heat exchangers. 1984.

[53] Zhang K, Blum DH, Grahovac M, Hu J, Granderson J, Wetter M. Development and Verification of Control Sequences for Single-Zone Variable Air Volume System Based on ASHRAE Guideline 36. Proceedings of the American Modelica Conference 2020, Boulder, Colorado, USA, March 23-25, 20202020.

[54] Taylor S, Stein J, Paliaga G, Cheng H. Dual maximum VAV box control logic. ASHRAE Journal. 2012;54:16.

[55] Wang S, Tang R. Supply-based feedback control strategy of air-conditioning systems for direct load control of buildings responding to urgent requests of smart grids. Applied Energy. 2017;201:419-32.

[56] Treddinick. Variable Speed Pumping: How Low Can You Go. District Energy, Third Quarter. 2006.

[57] Tang H, Hui C. Gaussian Curve Fitting Solution Based on Matlab. Computer Digital Engineering. 2013;8.

CHAPTER VII CONCLUSIONS, LIMITATIONS, FUTURE WORK

7.1 Conclusions

The potential benefits from high-performance rule-based SOO (GDL36) are still unclear to the research community. This dissertation aims at enhancing the existing standardized high-performance control sequences by conducting a comprehensive simulation-based evaluation of GDL36 SOO in terms of energy efficiency, fault robustness, ventilation performance and grid ancillary service compatibility. The target HVAC systems are multi-zone VAV systems including both waterside and airside subsystems. A Modelica-based virtual testbed that follows both airside and waterside SOO was first developed and verified. Then the virtual testbed was used to answer following research questions, as outlined in Section 1.2:

1. Since the energy saving performance of GDL36 has the edge over conventional SOO, what is the performance regarding energy efficiency compared to the advanced intelligent controllers (i.e., OBC and DRLC)?

Conclusions: The comparison study was conducted with the five-zone VAV cooling system virtual testbed in Chicago, IL. The OBC and DRLC replaced the GDL36 airside supervisory level control loops. In other words, the optimal SAT and static DP setpoints were determined by the optimization problems in OBC and trained control policy by DRLC. The OBC and DRLC were formulated to minimize the HVAC energy consumption and zone air temperature violation. The OBCs with different control intervals and DRLCs with different hyperparameters in the PPO algorithm were exploited and fine-tuned. The simulation results show that the GDL36 has a comparable energy performance (within a 3% deviation) with DRLC in the cases with high or mild cooling loads. It also has a comparable energy performance (within a 3% deviation) with

OBC in the case with high cooling load. However, the case with GDL36 consumed 7% more energy in the shoulder week. For the thermal comfort metric, the GDL36 has slightly more ZAT violation in all testing scenarios compared to two intelligent controllers. From this case study, we can conclude that the GDL36 has demonstrated its comparable performance in terms of energy efficiency and thermal comfort with the two intelligent controllers. The GDL36 is good enough considering the complexity and tuning efforts of the intelligent controllers.

2. How robust GDL36 is towards various faults in HVAC systems? What are the most influential faults with negative impacts?

Conclusions: Common faults were injected into the five-zone VAV system virtual testbed in Chicago, IL. The results showed that GDL36 SOO are well adapted for the faults from the energy and cost perspective since the vast majority (~90%) of fault scenarios have a fault impact ratio smaller than 6% in terms of the energy consumption and energy cost. Likewise, for the other KPIs, the FIR distributions indicate that with GDL36 SOO, most of the fault scenarios only have limited influence on the supply air temperature control quality, thermal comfort, ventilation performance, and peak power.

3. CO_2-based demand control ventilation strategies that could potentially be merged into GDL36 have been developed to single-path multi-zone VAV systems. Can similar CO_2-based DCV be applied to the multi-zone VAV system with the multiple recirculating paths? What are energy saving performance and ventilation performance? CO_2-based demand control ventilation strategies that could potentially be merged into GDL36 have been developed to single-path multi-zone VAV systems.

Conclusions: A similar CO_2-based DCV SOO were expanded to the multi-zone VAV system with multiple recirculating paths (i.e., fan-powered terminal units). The developed SOO

could be directly merged into GDL36. To evaluate the energy and ventilation performance of the proposed DCV logic, an EnergyPlus-CONTAM co-simulation testbed was developed for a medium-office building. The proposed SOO were assessed in four typical ASHRAE climate zones. The simulation results show that the developed SOO generally achieved a modest HVAC energy-saving ratio and a good compliance with the ventilation requirement for the FPTUs. The DCV control logic resulted in 7~14% and 7~21% HVAC energy savings on a source energy basis compared with the baseline of a simplified ASHRAE 62.1 approach for the SFPTU and PFPTU, respectively.

4. The GDL36 SOO will probably add a new feature of grid service provision in its future version. One of the fundamental questions is: what are the impacts of the HVAC system when it provides the frequency regulation? Are there any conflicts between the frequency regulation scheme and GDL36 SOO?

Conclusions: The evaluation was conducted using the five-zone VAV system virtual testbed for 16 ASHRAE climate zones. The simulation results show that FR has little or no impact on the HVAC operation and occupant thermal comfort under GDL36 when the building is providing the service if an appropriate regulation capacity is pre-determined. However, if the regulation capacity is overestimated, the energy performance and FR service quality will be affected due to equipment operating constraints. In addition, the AHU supply air temperature will fluctuate, and the controller will not be able to maintain the desired setpoint as the FR magnitude is increased. After the FR service time, it takes a certain period for the system to return to normal operation. The rebound period usually prolongs with the increase in the FR magnitude. It is noted that there exists a conflict between the FR control and the existing GDL36 SOO during high load conditions, causing the fan speed to saturate. Such a conflict is found to increase the fan electricity

consumption and subsequently reduce the potential revenue a building can earn from offering the FR service.

7.2 Limitations and Future Work

This research aims at enhancing the existing standardized high-performance control sequences (GDL36) by conducting comprehensive Modelica-simulation based evaluations in terms of energy saving potential, fault robustness, ventilation compliance, and grid service compatibility. Limitations and future work are being detailed for each evaluation in CHAPTER III - CHAPTER VI, which is summarized as follows:

- First, it is noted that all the development and evaluation studies were conducted using a virtual testbed. Future field demonstrations are needed to test the high-performance SOO and verify the results in real buildings, which will help address concerns related to sensor and network communication latency, HVAC local controller performance, etc.
- Second, the conclusions of the research questions might only be applied to the case study itself. This limitation is valid to CHAPTER III - CHAPTER VI in this dissertation. For example, these studies are targeted at the five-zone VAV system in the medium office and the selection of building type could influence the final results. In addition, CHAPTER III and CHAPTER IV did not consider the effect of different climate zones. Therefore, the future work needs to assess if conclusions could be extrapolated to a broader level. The aspects to be considered include different building types, climate zones, zone internal loads, HVAC system operation hours, etc.
- Third, in CHAPTER III, the intelligent controllers are formulated ideally only for theoretical comparison studies. They are not deployable for real applications. For OBCs, the predictive model is assumed to be the same as the virtual testbed while a

computationally efficient system predictive model (e.g., a data-driven model through identifications) needs to be used for real-time online applications in buildings. For the DRLC, the control policies are trained and tested for the same week, which is also unrealistic and impractical. Furthermore, the performance of OBCs and the DRLCs might be further improved in the future by considering more complex aspects. For example, the OBCs only consider the scenarios under the prediction horizon as one control timestep. For DRLCs, only the PPO algorithm is explored and other DRL algorithms are not studied.

- Fourth, in CHAPTER IV, only scenarios with single fault are studied, and all the faults are assumed to happen at all times in each seasonal week. Future work includes the consideration of detailed fault occurrence, degradation faults, and annual fault impact analysis on the other commercial building types and weather profiles.
- Fifth, in CHAPTER V, the developed DCV SOO for multi-zone recirculating path systems need to be tested in the field, including the energy and ventilation performance, before they could be integrated into the future GDL36 SOO.
- Lastly, in CHAPTER VI, a control conflict was observed and identified between the FR control and the existing HVAC control. There is a need in the future work to modify the baseline controls to address potential conflicts between the existing building controls and the FR controls and enable seamless and energy-efficient transitions between the two controls.

APPENDIX A

A.1. Detailed High-Performance Operation Sequences in the Virtual Testbed

Airside (AHU and VAV terminals) and waterside (chilled water loop and hot water loop) are scheduled for automatic operation on a time-of-day basis for occupied mode and unoccupied mode. The occupied mode starts at 7am and ends at 7pm. It is noted that there are no specific holidays that are considered as unoccupied days in this study.

A.1.1. Air Loop Control

The airside control is following ASHRAE Guideline 36-2018. Detailed control sequences for different airside equipment are discussed as follows.

A.1.1.1. AHU

i). Fan status: The supply fan starts or continues to run during the occupied mode. During the unoccupied mode, the supply fan is off. The cooling coil valve closes and the OA damper close. System cycling ON and OFF to maintain the unoccupied heating and cooling setpoint.

ii). Fan speed control: The fan speed control is implemented according to PART 5.N.1. It outputs the Boolean signal to turn on or off the supply fan. In addition, based on the pressure reset request from the VAV zones controller, the sequence resets the duct pressure setpoint, and uses this setpoint to modulate the fan speed using a PI controller.

iii). Economizer damper control: The AHU shall enter economizer mode when the outdoor air temperature is lower than the return air temperature. The OA damper will modulate in sequence with return air damper to maintain the supply air temperature setpoint. The

cooling coil valve will be closed once the OA damper is 100% open. The cooling coil valve shall be enabled to maintain the supply air temperature setpoint.

iv). Minimum outdoor air control: According to current occupancy, supply operation status, zone temperatures and the discharge air temperature, the sequence computes the minimum outdoor airflow rate setpoint, which is used as input for the economizer control.

v). Supply air temperature control: Based on ASHRAE Guideline 36 PART 5.N.2, the sequence first sets the maximum supply air temperature based on reset requests collected from each zone. The outdoor temperature is used along with the maximum supply air temperature, for computing the supply air temperature setpoint.

A.1.1.2. Zone VAV Terminal

i). VAV box airflow and reheat coil control: Controller for the terminal box of VAV system with reheat according to ASHRAE Guideline 36, Part 5.E. The active maximum and minimum airflow are set according to Part 5.E.3-5. Damper position and reheat control for VAV reheat terminal unit refer to Part 5.E.6. The VAV reheat terminal units will submit the requests for the system-level controller, including the cooling supply air temperature reset requests, the static pressure reset requests.

ii). Zone air temperature control: The zone heating and cooling setpoint are 20 ℃ and 24 ℃ during the occupied time period. In the unoccupied mode, the zone air temperature heating setpoint is 15°F. The zone air temperature cooling setpoint is 28°F.

A.1.2. Chilled Water Loop

We followed ASHRAE RP-1711 for chilled plant-side control. Detailed control sequences for different chilled waterside equipment are discussed as follows.

A.1.2.1. Chiller Plant

i). Chilled water plant enable/disable control: Chiller plant is enabled in the lowest stage when the plant has been disabled for at least 15 minutes and: 1. The number of Chiller Plant Requests > I (I = Ignores shall default to 0, adjustable), and 2. OAT>CH-LOT, and 3. The chiller plant enable-schedule is active. Plant is disabled when it has been enabled for at least 15 minutes and: 1. The number of Chiller Plant Requests ≤ I for 3 minutes, or 2. OAT<CH-LOT – 1°F, or 3. The chiller plant enable-schedule is inactive. Chiller Plant Requests are generated by coil control valves per GDL36 sequences. Importance multipliers (IM) shall be added to Chiller Plant Requests in GDL36 to ensure that critical coils can independently cause the plant to start. For example, setting the importance multiplier of a large air handler's Chiller Plant Requests to 4 will cause four requests so that the air handler alone can start the plant even if I=4. Unimportant coils can be assigned an IM of zero so that they cannot cause the plant to start. Small coils can be assigned IM values less than one so that several are required to be active before the plant starts. CH-LOT represents the outdoor air lockout temperature below which the chiller plant is prevented from operating. The Lockout temperature is a safety to prevent plant operation when it should not be needed, e.g., due to Plant Request from a zone or AHU with an unusually cold setpoint. It is typically 60°F for plants serving systems with airside economizers. To keep the plant enabled under all conditions, make the setpoint below the coldest expected outdoor air temperature.

ii). Waterside cooling mode control: chilled water system will be determined by the weather condition to be operated in Free Cooling (FC) mode, Partially Mechanical Cooling (PMC) mode or Fully Mechanical Cooling (FMC) mode.

iii). Chiller staging control: The chiller is off when the cooling mode is Free Cooling. The chiller is on when the cooling mode is not Free Cooling.

iv). Chilled water supply temperature reset control: The plant chilled water supply temperature setpoint is reset based on the Chilled-Water Reset Requests using T&R logic. The chilled water supply temperature reset range is from minimum to 50 °F.

v). Minimum flow bypass valve control: The bypass valve is modulated to maintain minimum flow as measured by the chilled water flow meter at a setpoint that provides minimum flow through the chiller. A PID loop maintains minimum flow as measured by the chilled water flow meter at the setpoint. Reset valve position from 0% open at 0% loop output to 100% open at 100% loop output.

A.1.2.2. Cooling Tower

i). Cooling tower fan speed: When the system is in Fully Mechanical Cooling (FMC) mode, the cooling tower fan speed is controlled to maintain the condenser water supply temperature (CWST) at or around the setpoint. When the system is in Partially Mechanical Cooling (PMC) mode, the cooling tower fan speed is set as 100% to make condenser water as cold as possible and maximize the waterside economizer output. When the system is in Free Cooling (FC) mode, the cooling tower fan speed is controlled to maintain the chilled water supply temperature (CHWST) at or around its setpoint.

A.1.2.3. Chilled Water Pumps

i). Chilled water pump speed control: pump speed is controlled to maintain the differential pressure at or around the setpoint.

A.1.3. Hot Water Loop

We used ASHRAE 1711 for hot plant-side control. We followed ASHRAE 1711 for chilled plant-side control. Detailed control sequences for different hot waterside equipment are discussed as follows.

A.1.3.1. Boiler Plant

i). Hot water plant enable/disable control: hot water plant is enabled in the lowest stage when the plant has been disabled for at least 15 minutes and: 1. The number of Heating Hot-Water Plant Requests > I (I = Ignores shall default to 0, adjustable), and 2. OAT<HW-LOT, and 3. The Boiler plant enable schedule is active. Plant is disabled when it has been enabled for at least 15 minutes and: 1. The number of Heating Hot-Water Plant Requests ≤ I for 3 minutes, or 2. OAT>HW-LOT – 1°F, or 3. The Boiler plant enable schedule is inactive. HW-LOT represents the lockout temperature to prevent plant operation when it should not be needed, e.g., due to a Plant Request from a zone or AHU with an unusually high setpoint. It is typically 75°F for systems with zone-level reheat. It can be lower, e.g., 65°F, for dual fan dual duct systems and systems that use fan-powered terminal units to meet heating loads since they do not require reheat to prevent over-cooling zones with low, or no, cooling loads. To keep the plant enabled under all conditions, make the setpoint above the hottest expected outdoor air temperature.

ii). Boiler staging and heating power control: The boiler is staged on/off when the hot water plant is enabled/disabled. The heating power of the boiler is controlled by a feedback loop to maintain the temperature of the water leaving the boiler to be a predefined value.

iii). Hot water supply temperature reset control: The plant hot water supply temperature setpoint is reset based on the Hot-Water Reset Requests using T&R logic. The hot water supply temperature reset range is from 90 °F to the maximum.

iv). Minimum flow bypass valve control: The bypass valve is modulated to maintain minimum flow as measured by the hot water flow meter at a setpoint that provides minimum flow through the boiler. A PID loop maintains minimum flow as measured by the hot water flow meter at the setpoint. Reset valve position from 0% open at 0% loop output to 100% open at 100% loop output.

A.1.3.2. Hot water pump

i). Hot water pump staging and speed control: The hot water pump is staged on/off when the hot water plant is enabled/disabled. The hot water pumps share the same speed and the speed is controlled by a feedback loop to maintain the pressure difference in the hot water loop to be a predefined value.

A.2. HVAC Equipment Sizing

The sizing parameters for different HVAC equipment are listed in Table A-1.

Table A-1 HVAC equipment sizing parameters in the system model

Equipment	Qty.	Nominal Information in Each Equipment		Unit	Value
AHUs	1	Cooling Coil	Air Flowrate	m^3/s	5.595
			Cooling Capacity	kW	100.7
			Water Flowrate	kg/s	4
		Heating Coil	Capacity	kW	55.4
		Fan	Qty.	-	1
			Head	Pa	1381
			Power	kW	13.53
			Flowrate	m^3/s	4.8
Chiller	1	Nominal Capacity		kW	101
		Design COP		-	5.9
		Evaporator	Flowrate	m^3/s	0.004
			Design Outlet Temperature	℃	5.56
			Design Inlet Temperature	℃	11.56
		Condenser	Flowrate	m^3/s	0.0043
			Design Inlet Temperature	℃	Cooling tower entering wet bulb temperature +3
		Compressor	Number	-	1
			Speed Type	-	Variable Speed
			Power	kW	18.24
Chiller Water Pump	1	Head		kPa	255
		Power		kW	2.09
		Flowrate		m^3/s	0.0040
		Speed Type		-	Variable Speed
Condenser Water Pump	1	Head		kPa	215.7
		Power		kW	1.90
		Flowrate		m^3/s	0.0043
		Speed Type			Constant Speed
Cooling Tower	1	Design Approach Temperature		℃	3.89
		Cell Number		-	1
		Fan Number		-	1
		Fan Speed Type			Variable Speed
		Power		kW	4.30

Boiler	1	Nominal Capacity	kW	55
		Overall UA Value	W/K	92.3
		Efficiency	-	0.9
Hot Water Pump	1	Head	kPa	157
		Power	kW	0.43
		Flowrate	m^3/s	0.0013
		Speed Type	-	Variable Speed

APPENDIX B

B.1. Detailed Description of the Fault Scenarios

In total, 359 fault scenarios are injected to the system fault model for three seasonal operating conditions. The number of the fault scenarios in the cooling, shoulder, and heating season week is 127, 127, 105, respectively. Table B-1 shows the detailed description of the fault scenarios in the cooling and shoulder season. Table B-2 shows the detailed description of the fault scenarios in the heating season.

Table B-1 Fault scenarios for the cooling and shoulder season

Index	Scenario Name	Description
1	TCHWSup_p1	Chilled water supply temperature sensor positive bias - 1 K
2	TCHWSup_m1	Chilled water supply temperature sensor negative bias - 1 K
3	TCHWSup_p2	Chilled water supply temperature sensor positive bias - 2 K
4	TCHWSup_m2	Chilled water supply temperature sensor negative bias - 2K
5	TCWSup_p1	Cooling water supply temperature sensor positive bias - 1 K
6	TCWSup_m1	Cooling water supply temperature sensor negative bias - 1 K
7	TCWSup_p2	Cooling water supply temperature sensor positive bias - 2 K
8	TCWSup_m2	Cooling water supply temperature sensor negative bias - 2K
9	RelPreCHW_p5000	Chilled water differential pressure sensor positive bias - 5000 Pa
10	RelPreCHW_m5000	Chilled water differential pressure sensor negative bias - 5000 Pa
11	RelPreCHW_p10000	Chilled water differential pressure sensor positive bias - 10000 Pa
12	RelPreCHW_m10000	Chilled water differential pressure sensor negative bias - 10000 Pa
13	Vout_p15	Outdoor air flow rate sensor positive scale error - 15%
14	Vout_m15	Outdoor air flow rate sensor negative scale error - 15%
15	Vout_p30	Outdoor air flow rate sensor positive scale error - 30%
16	Vout_m30	Outdoor air flow rate sensor negative scale error - 30%
17	TSup_p1	AHU supply air temperature sensor positive bias - 1 K
18	TSup_m1	AHU supply air temperature sensor negative bias - 1 K
19	TSup_p2	AHU supply air temperature sensor positive bias - 2 K
20	TSup_m2	AHU supply air temperature sensor negative bias - 2K
21	TMix_p1	Mix air temperature sensor positive bias - 1 K
22	TMix_m1	Mix air temperature sensor negative bias - 1 K
23	TMix_p2	Mix air temperature sensor positive bias - 2 K

24	TMix_m2	Mix air temperature sensor negative bias - 2K
25	TRet_p1	Return air temperature sensor positive bias - 1 K
26	TRet_m1	Return air temperature sensor negative bias - 1 K
27	TRet_p2	Return air temperature sensor positive bias - 2 K
28	TRet_m2	Return air temperature sensor negative bias - 2K
29	RelPreAir_p15	Air loop differential pressure sensor positive bias - 15 Pa
30	RelPreAir_m15	Air loop differential pressure sensor negative bias - 15 Pa
31	RelPreAir_p25	Air loop differential pressure sensor positive bias - 25 Pa
32	RelPreAir_m25	Air loop differential pressure sensor negative bias - 25 Pa
33	TAirSou_p1	South zone air temperature sensor positive bias - 1K
34	TAirSou_m1	South zone air temperature sensor negative bias - 1K
35	TAirSou_p2	South zone air temperature sensor positive bias - 2K
36	TAirSou_m2	South zone air temperature sensor negative bias - 2K
37	TSupSou_p1	South zone discharging air temperature sensor positive bias - 1K
38	TSupSou_m1	South zone discharging air temperature sensor negative bias - 1K
39	TSupSou_p2	South zone discharging air temperature sensor positive bias - 2K
40	TSupSou_m2	South zone discharging air temperature sensor negative bias - 2K
41	VSupSou_flow_p15	South zone air flow rate sensor positive scale error - 15%
42	VSupSou_flow_m15	South zone air flow rate sensor negative scale error - 15%
43	VSupSou_flow_p30	South zone air flow rate sensor positive scale error - 30%
44	VSupSou_flow_m30	South zone air flow rate sensor negative scale error - 30%
45	SupDucLea_10	Air loop supply duct leakage – Fault Intensity (FI)=10%
46	SupDucLea_20	Air loop supply duct leakage - FI=20%
47	AirDucFou_10	Air loop duct fouling - FI=10%
48	AirDucFou_20	Air loop duct fouling - FI=20%
49	CHWPipFou_10	Chilled water pipe fouling - FI=10%
50	CHWPipFou_20	Chilled water pipe fouling - FI=20%
51	CHWPipIso_l02L25	Chilled water pipe isolation - 20mm
52	CHWPipIso_l005L25	Chilled water pipe isolation - 5mm
53	CooTowValLea_001	Cooling tower valve leakage - leakage ratio l=0.001
54	CooTowValLea_01	Cooling tower valve leakage - leakage ratio l=0.01
55	ChiConValLea_001	Cooling water isolation valve leakage - leakage ratio l=0.001
56	ChiConValLea_01	Cooling water isolation valve leakage - leakage ratio l=0.01
57	ChiEvaValLea_001	Chilled water isolation valve leakage - leakage ratio l=0.001
58	ChiEvaValLea_01	Chilled water isolation valve leakage - leakage ratio l=0.01
59	CooCoiValLea_001	Cooling coil valve leakage - leakage ratio l=0.001
60	CooCoiValLea_01	Cooling coil valve leakage - leakage ratio l=0.01
61	CooCoiValStuck_0	Cooling coil valve stuck - Position =0
62	CooCoiValStuck_5	Cooling coil valve stuck - Position =5%
63	CooCoiValStuck_15	Cooling coil valve stuck - Position =15%
64	CooCoiValStuck_65	Cooling coil valve stuck - Position =65%
65	CooCoiValStuck_100	Cooling coil valve stuck - Position =100%

66	OADamLea_001	Outdoor air damper leakage - leakage ratio l=0.001
67	OADamLea_01	Outdoor air damper leakage - leakage ratio l=0.01
68	OADamStuck_0	Outdoor air damper stuck - Position =0
69	OADamStuck_5	Outdoor air damper stuck - Position =5%
70	OADamStuck_15	Outdoor air damper stuck - Position =15%
71	OADamStuck_65	Outdoor air damper stuck - Position =65%
72	OADamStuck_100	Outdoor air damper stuck - Position =100%
73	CooCoiFou_10	Cooling coil fouling - FI=10%
74	CooCoiFou_30	Cooling coil fouling -FI=30%
75	CooCoiFou_50	Cooling coil fouling - FI=50%
76	ChiConFou_20	Chiller condenser fouling - FI=20%
77	ChiConFou_40	Chiller condenser fouling - FI=40%
78	ChiNonCon_25	Chiller non-condensable gas - FI=25%
79	ChiNonCon_50	Chiller non-condensable gas - FI=50%
80	ChiOveCha_20	Chiller overcharging - FI=20%
81	ChiOveCha_40	Chiller overcharging - FI=40%
82	ChiExcOil_30	Chiller excess oil - FI=30%
83	ChiExcOil_60	Chiller excess oil FI=60%
84	pumChiCavitation	Chilled water pump cavitation
85	pumChiImpeller	Chilled water pump impeller fault
86	pumChiMotDeg_15	Chilled water pump motor degradation - 15%
87	pumChiMotDeg_30	Chilled water pump motor degradation - 30%
88	pumCWCavitation	Cooling water pump cavitation
89	pumCWImpeller	Cooling water pump impeller fault
90	pumCWMotDeg_15	Cooling water pump motor degradation - 15%
91	pumCWMotDeg_30	Cooling water pump motor degradation - 30%
92	fanAHUMotDeg_15	Fan motor degradation - 15%
93	fanAHUMotDeg_30	Fan motor degradation - 30%
94	cooTowFou_10	Cooling tower fouling - FI=10%
95	cooTowFou_30	Cooling tower fouling - FI=30%
96	cooTowFou_50	Cooling tower fouling - FI=50%
97	conkTSup_5	Supply air temperature PID loop fault - P=5
98	conkTSup_05	Supply air temperature PID loop fault - P=0.05
99	conkFanSpe_10	Supply fan speed PID loop fault - P=10
100	conkFanSpe_01	Supply fan speed PID loop fault - P=0.01
101	conkMinOut_5	Economizer PID loop fault - P=0.5
102	conkMinOut_005	Economizer PID loop fault - P=0.005
103	conkPumSpe_1	Chilled water pump speed PID loop fault - P=1
104	conkPumSpe_01	Chilled water pump speed PID loop fault - P=0.01
105	conkCooTow_1	Cooling tower speed PID loop fault - P=1
106	conkCooTow_01	Cooling tower speed PID loop fault - P=0.01
107	conVAVSoukCoo_1	South zone air cooling PID loop fault - P=1
108	conVAVSoukCoo_01	South zone air cooling PID loop fault - P=0.01
109	conVAVSoukDam_5	South zone VAV damper PID loop fault - P=5
110	conVAVSoukDam_05	South zone VAV damper PID loop fault - P=0.05

111	maxCHWDifPreSP	Chilled water differential pressure setpoint falsely set to the maximum
112	maxCHWTSupSP	Chilled water supply temperature setpoint falsely set to the maximum
113	yCooDel_1	Cooling coil control signal delay - 1s
114	supFanSpeDel_1	Supply fan speed control signal delay - 1s
115	yPumDel_1	Chilled water pump speed control signal delay - 1s
116	schedule_early_1	Schedule fault - Early termination of setback for 1 hour
117	schedule_early_2	Schedule fault - Early termination of setback for 2 hours
118	schedule_delay_1	Schedule fault - Delayed onset of setback for 1 hours
119	schedule_delay_2	Schedule fault - Delayed onset of setback for 2 hours
120	schedule_nosetback	Schedule fault - No temperature setback
121	AHUFan_oversized	Oversized AHU supply fan
122	AHUCooCoil_oversized	Oversized AHU cooling coil
123	CHWPump_oversized	Oversized chilled water pump
124	CWPump_oversized	Oversized cooling water pump
125	Chiller_oversized	Oversized chiller
126	infiltration_70	Excessive infiltration – dp_nominal FI=70%
127	infiltration_50	Excessive infiltration - dp_nominal FI=50%

Table B-2 Fault scenarios for the heating season

Index	Scenario Name	Description
1	THWSup_p2	Hot water supply temperature sensor positive bias - 2 K
2	THWSup_m2	Hot water supply temperature sensor negative bias - 4 K
3	THWSup_p4	Hot water supply temperature sensor positive bias - 2 K
4	THWSup_m4	Hot water supply temperature sensor negative bias - 4K
5	RelPreHW_p5000	Hot water differential pressure sensor positive bias - 5000 Pa
6	RelPreHW_m5000	Hot water differential pressure sensor negative bias - 5000 Pa
7	RelPreHW_p10000	Hot water differential pressure sensor positive bias - 10000 Pa
8	RelPreHW_m10000	Hot water differential pressure sensor negative bias - 10000 Pa
9	Vout_p15	Outdoor air flow rate sensor positive scale error - 15%
10	Vout_m15	Outdoor air flow rate sensor negative scale error - 15%
11	Vout_p30	Outdoor air flow rate sensor positive scale error - 30%
12	Vout_m30	Outdoor air flow rate sensor negative scale error - 30%
13	TSup_p1	AHU supply air temperature sensor positive bias - 1 K
14	TSup_m1	AHU supply air temperature sensor negative bias - 1 K
15	TSup_p2	AHU supply air temperature sensor positive bias - 2 K
16	TSup_m2	AHU supply air temperature sensor negative bias - 2K
17	TMix_p1	Mix air temperature sensor positive bias - 1 K
18	TMix_m1	Mix air temperature sensor negative bias - 1 K
19	TMix_p2	Mix air temperature sensor positive bias - 2 K
20	TMix_m2	Mix air temperature sensor negative bias - 2K
21	TRet_p1	Return air temperature sensor positive bias - 1 K
22	TRet_m1	Return air temperature sensor negative bias - 1 K
23	TRet_p2	Return air temperature sensor positive bias - 2 K
24	TRet_m2	Return air temperature sensor negative bias - 2K
25	RelPreAir_p15	Air loop differential pressure sensor positive bias - 15 Pa
26	RelPreAir_m15	Air loop differential pressure sensor negative bias - 15 Pa
27	RelPreAir_p25	Air loop differential pressure sensor positive bias - 25 Pa
28	RelPreAir_m25	Air loop differential pressure sensor negative bias - 25 Pa
29	TAirEas_p1	East zone air temperature sensor positive bias - 1K
30	TAirEas_m1	East zone air temperature sensor negative bias - 1K
31	TAirEas_p2	East zone air temperature sensor positive bias - 2K
32	TAirEas_m2	East zone air temperature sensor negative bias - 2K
33	TSupEas_p1	East zone discharging air temperature sensor positive bias - 1K
34	TSupEas_m1	East zone discharging air temperature sensor negative bias - 1K
35	TSupEas_p2	East zone discharging air temperature sensor positive bias - 2K
36	TSupEas_m2	East zone discharging air temperature sensor negative bias - 2K

37	VSupEas_flow_p15	East zone air flow rate sensor positive scale error - 15%
38	VSupEas_flow_m15	East zone air flow rate sensor negative scale error - 15%
39	VSupEas_flow_p30	East zone air flow rate sensor positive scale error - 30%
40	VSupEas_flow_m30	East zone air flow rate sensor negative scale error - 30%
41	SupDucLea_10	Air loop supply duct leakage - FI=10%
42	SupDucLea_20	Air loop supply duct leakage - FI=20%
43	AirDucFou_10	Air loop duct fouling - FI=10%
44	AirDucFou_20	Air loop duct fouling - FI=20%
45	HWPipFou_10	Hot water pipe fouling - FI=10%
46	HWPipFou_20	Hot water pipe fouling - FI=20%
47	HWPipIso_l02L25	Hot water pipe isolation - 20mm
48	HWPipIso_l005L25	Hot water pipe isolation - 5mm
49	boiValLea_001	Boiler isolation valve leakage - leakage ratio l=0.001
50	boiValLea_01	Boiler isolation valve leakage - leakage ratio l=0.01
51	boiBypValLea_001	Boiler bypass valve leakage - leakage ratio l=0.001
52	boiBypValLea_01	Boiler bypass valve leakage - leakage ratio l=0.01
53	HeaCoiValLea_001	Heating coil valve leakage - leakage ratio l=0.001
54	HeaCoiValLea_01	Heating coil valve leakage - leakage ratio l=0.01
55	HeaCoiValStuck_0	Heating coil valve stuck - Position =0
56	HeaCoiValStuck_5	Heating coil valve stuck - Position =5%
57	HeaCoiValStuck_15	Heating coil valve stuck - Position =15%
58	HeaCoiValStuck_65	Heating coil valve stuck - Position =65%
59	HeaCoiValStuck_100	Heating coil valve stuck - Position =100%
60	OADamLea_001	Outdoor air damper leakage - leakage ratio l=0.001
61	OADamLea_01	Outdoor air damper leakage - leakage ratio l=0.01
62	OADamStuck_0	Outdoor air damper stuck - Position =0
63	OADamStuck_5	Outdoor air damper stuck - Position =5%
64	OADamStuck_15	Outdoor air damper stuck - Position =15%
65	OADamStuck_65	Outdoor air damper stuck - Position =65%
66	OADamStuck_100	Outdoor air damper stuck - Position =100%
67	HeaCoiFou_10	Heating coil fouling - FI=10%
68	HeaCoiFou_30	Heating coil fouling -FI=30%
69	HeaCoiFou_50	Heating coil fouling - FI=50%
70	boiFou_10	Boiler fouling - FI=20%
71	boiFou_20	Boiler fouling - FI=40%
72	pumHWCavitation	Hot water pump cavitation
73	pumHWImpeller	Hot water pump impeller fault
74	pumHWMotDeg_15	Hot water pump motor degradation - 15%
75	pumHWMotDeg_30	Hot water pump motor degradation - 30%
76	fanAHUMotDeg_15	Fan motor degradation - 15%
77	fanAHUMotDeg_30	Fan motor degradation - 30%
78	conkTSup_1	Supply air temperature PID loop fault - P=1
79	conkTSup_01	Supply air temperature PID loop fault - P=0.01
80	conkFanSpe_10	Supply fan speed PID loop fault - P=10
81	conkFanSpe_01	Supply fan speed PID loop fault - P=0.01
82	conkMinOut_1	Economizer PID loop fault - P=0.1

83	conkMinOut_001	Economizer PID loop fault - P=0.001
84	conkPumHWSpe_5	Hot water pump speed PID loop fault - P=5
85	conkPumHWSpe_05	Hot water pump speed PID loop fault - P=0.05
86	conVAVEaskCoo_1	East zone air cooling PID loop fault - P=1
87	conVAVEaskCoo_01	East zone air cooling PID loop fault - P=0.01
88	conVAVEaskDam_5	East zone VAV damper PID loop fault - P=5
89	conVAVEaskDam_05	East zone VAV damper PID loop fault - P=0.05
90	maxHWDifPreSP	Hot water differential pressure setpoint falsely set to the maximum
91	minHWTSupSP	Hot water supply temperature setpoint falsely set to the minimum
92	yHeaDel_1	Heating coil control signal delay - 1s
93	supFanSpeDel_1	Supply fan speed control signal delay - 1s
94	yPumHWDel_1	Hot water pump speed control signal delay - 1s
95	schedule_early_1	Schedule fault - Early termination of setback for 1 hour
96	schedule_early_2	Schedule fault - Early termination of setback for 2 hours
97	schedule_delay_1	Schedule fault - Delayed onset of setback for 1 hours
98	schedule_delay_2	Schedule fault - Delayed onset of setback for 2 hours
99	schedule_nosetback	Schedule fault - No temperature setback
100	AHUFan_oversized	Oversized AHU supply fan
101	AHUHeaCoil_oversized	Oversized AHU heating coil
102	HWPump_oversized	Oversized hot water pump
103	Boiler_oversized	Oversized boiler
104	infiltration_70	Excessive infiltration - dp_nominal FI=70%
105	infiltration_50	Excessive infiltration - dp_nominal FI=50%

B.2. Fault Impact Analysis Results Not Presented in the Main Body

The fault impact analysis results that have been presented in the manuscript are shown in this section. These results are listed in Table B-3.

Table B-3 Fault scenarios that have not been presented

Fault Category	Seasonal Load Conditions
Sensor	Cooling Season
	Shoulder Season
	Heating Season
HVAC Equipment	Shoulder Season
	Heating Season
Control	Heating Season

B.2.1. Sensor

Figure B-1 shows the fault impacts over key KPIs of sensor faults in the shoulder season week. In terms of the operational cost/site energy/source energy, cooling water temperature sensor, AHU supply air temperature sensor, zone air temperature sensor and zone air flow rate sensor are comparatively most fault-sensitive for the high-performance SOO. This is similar to the counterpart in the cooling season. The outdoor air flow rate sensor is not that fault-sensitive in the shoulder season mainly because the economizer is enabled for a long time in the shoulder season and thus the outdoor air damper will not suffer from the sensor bias. Similar findings in the cooling season can be shown: the zone air sensor bias is the only fault that affects the zone air temperature variations while the increase on the zone-averaged PPD over all the shoulder fault scenarios is negligible; The outdoor air flow rate sensor and return air temperature sensor are important for the ventilation; severe positive bias of the AHU supply air temperature sensor and severe negative bias of the zone discharging air temperature sensor will cause a power peak.

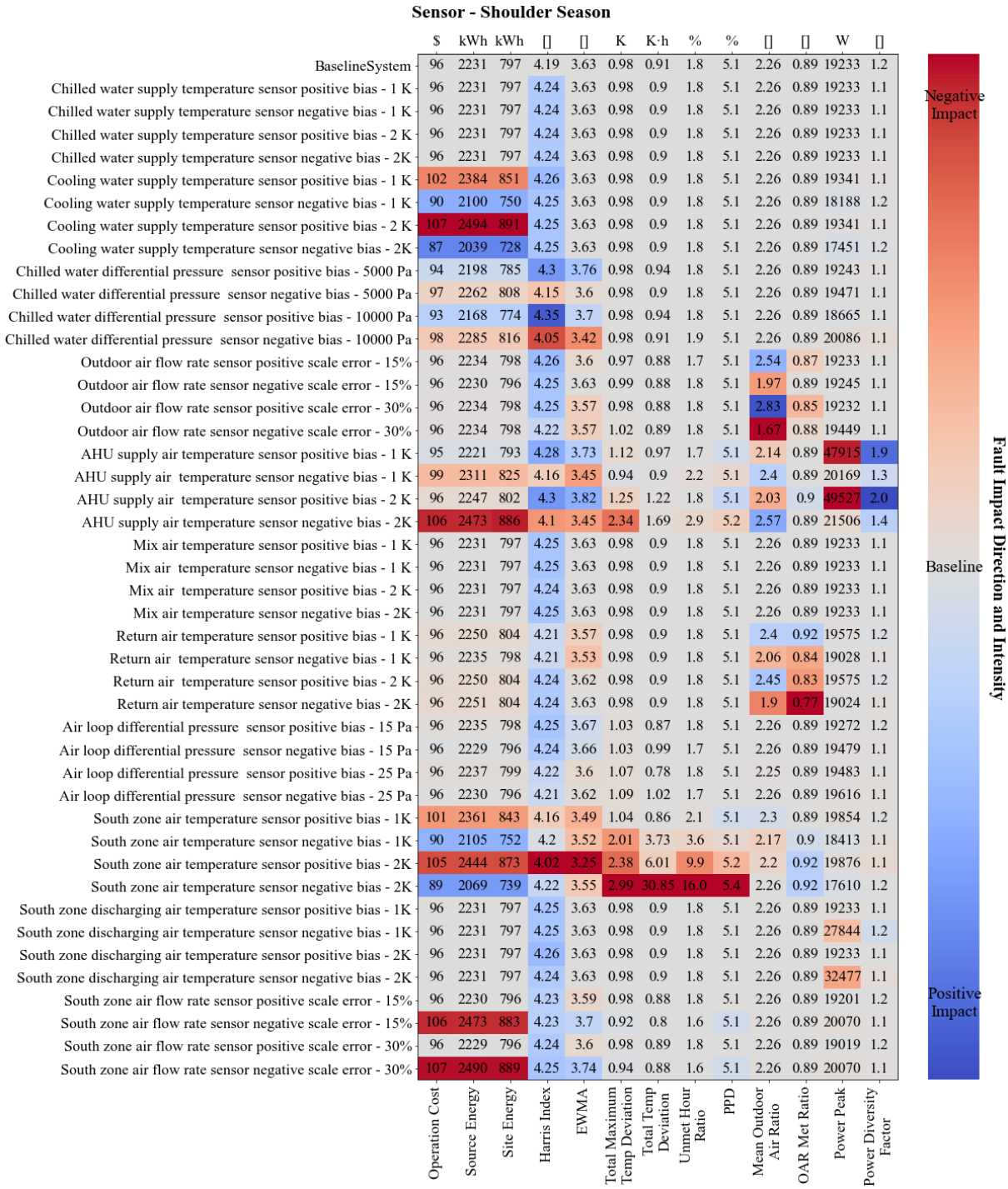

Figure B-1 Fault impact over key KPIs of sensor faults in the shoulder season

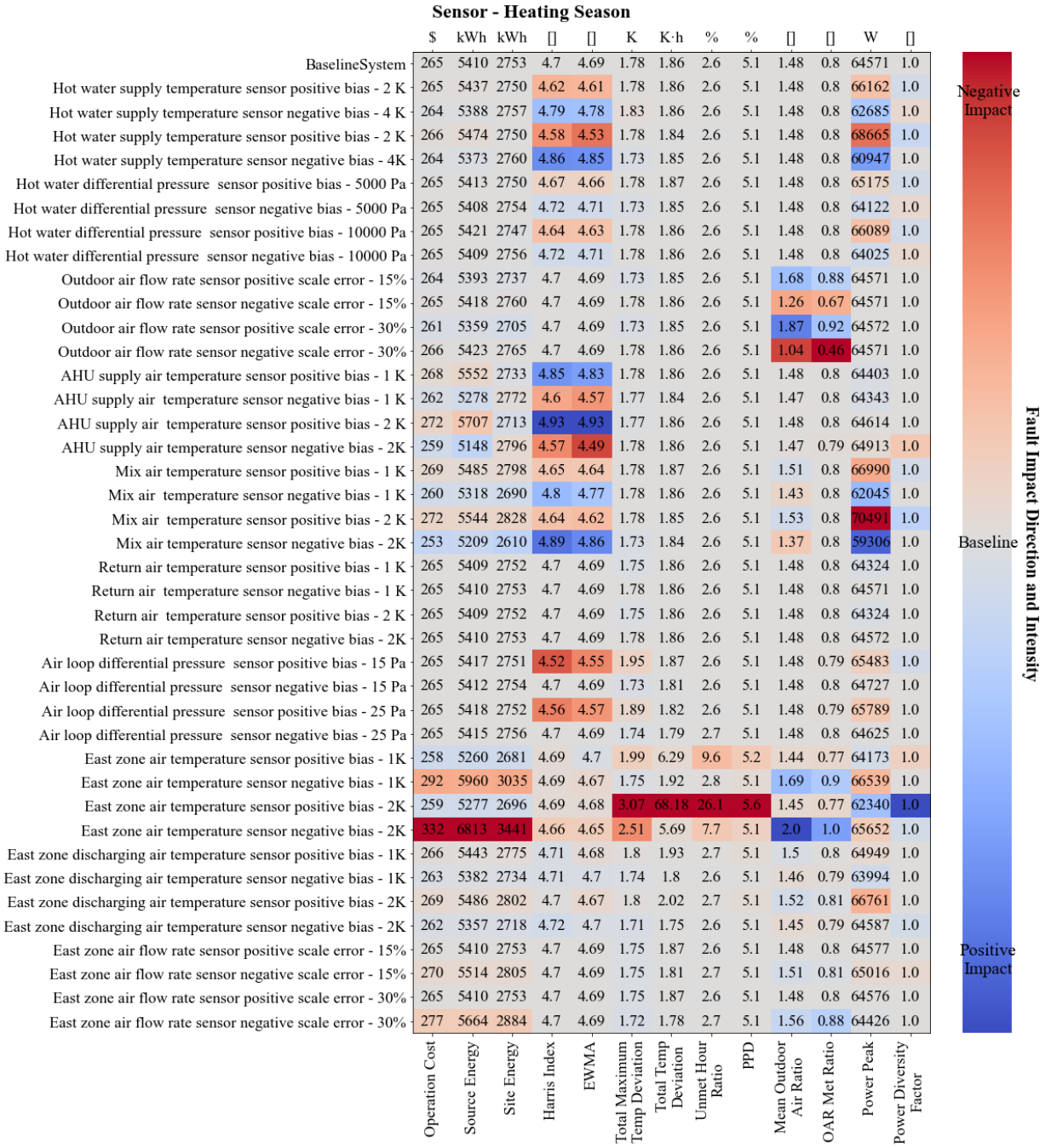

Figure B-2 Fault impact over key KPIs of sensor faults in the heating season

Figure B-2 shows the fault impacts over key KPIs of sensor faults in the heating season week. Different from the cooling season and heating season, the most fault-sensitive sensor is the zone air temperature sensor rather than the system-level sensors for the high-performance SOO.

The negative bias will cause to the overheating in the zone and the more terminal reheat. Due to the interaction between the zone and system in the SOO through the zone requests, the energy consumption of the system-level equipment such as the boiler, pump, and fan will also be increased. For the supply air temperature control loop, its control quality will not be heavily impacted by the sensor faults in the heating season. Like the cooling and heating season, the zone air temperature has large variations only for the zone air temperature sensor bias and the PPD metric does not have an obvious impact. For the ventilation performance, the baseline case in the heating season is not as good as the cooling and heating season because the heating coil freezing protection and seldom onset of the economizer mode. The outdoor air flow rate sensor negative bias directly worsens the ventilation performance while the return air temperature sensor bias has no bearing on the ventilation. For the peak power and power diversity, the results show that the sensor faults will not have an apparent impact. The severe sensor bias of the mixed air temperature, as a worst scenario, only increased 9% of the peak power.

B.2.2. HVAC Equipment

Figure B-3 shows the fault impacts over key KPIs of HVAC mechanical equipment faults in the shoulder season week. Likewise, the severe cooling coil fouling has the most negative impact on the multiple KPIs including the energy, operational cost and peak power. The impacts on the zone air temperature variations and thermal comfort are not as apparent as those in the cooling season. The other HVAC mechanical equipment faults all have a FIR less than 10% on the energy and cost performance. The HVAC mechanical equipment faults in the shoulder season also have little impact on the ventilation performance.

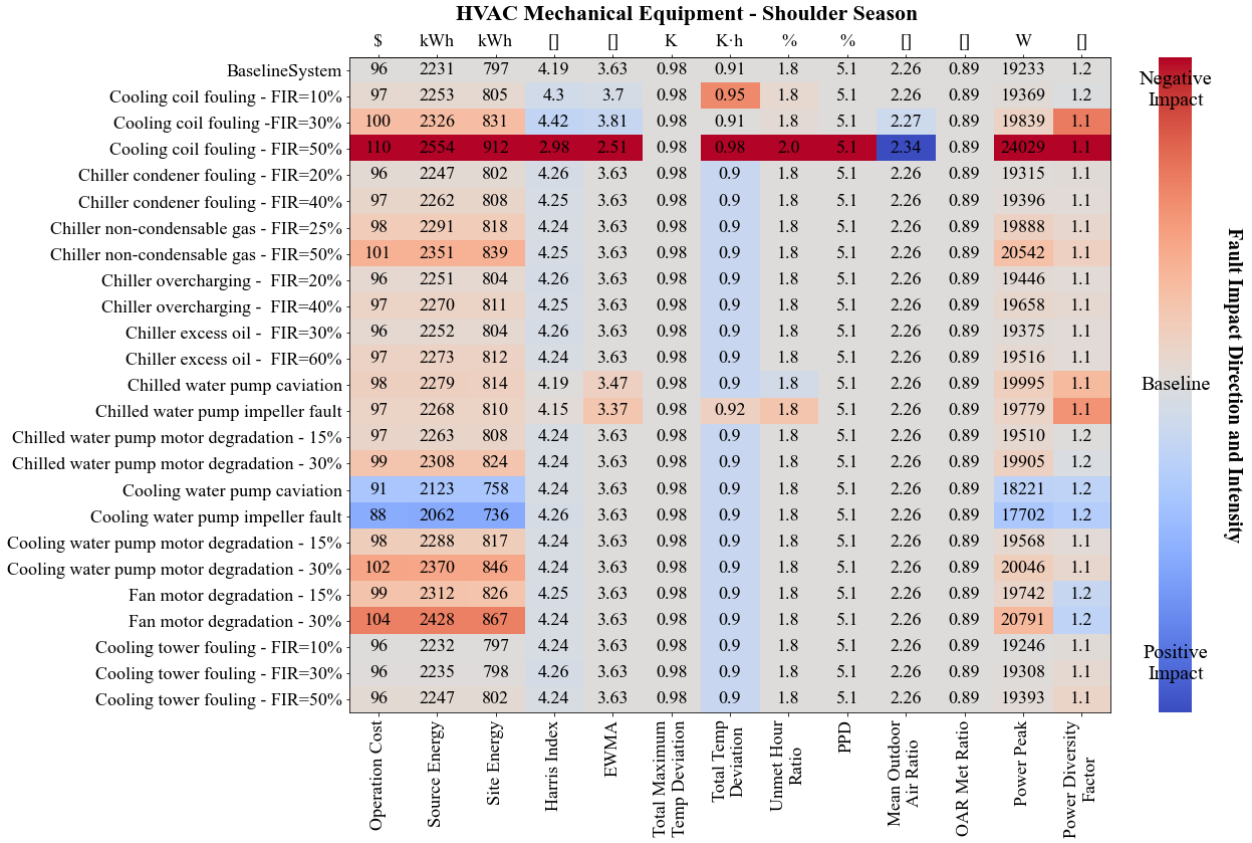

Figure B-3 Fault impact over key KPIs of HVAC equipment faults in the shoulder season

Figure B-4 shows the fault impacts over key KPIs of HVAC mechanical equipment faults in the heating season week. The severe boiler fouling, and the severe heating coil fouling are the top two most negative impact on the energy and cost. The latter also causes the degradation of the supply air temperature control loop and the increase of the peak power. The HVAC mechanical equipment faults in the heating season have little impact on the KPIs such as the zone air temperature variations, thermal comfort, ventilation performance, and the power diversity.

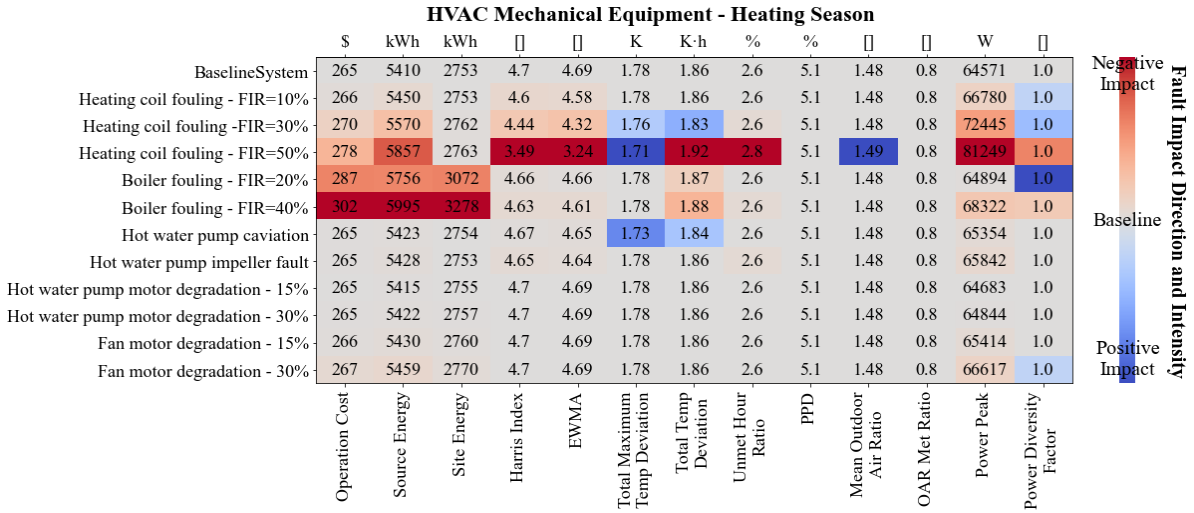

Figure B-4 Fault impact over key KPIs of HVAC equipment faults in the heating season

B.2.3. Control

Figure B-5 shows the fault impacts over key KPIs of control faults in the heating season week. All the studied control faults do not strongly influence on the cost and energy performance and the maximum FIR is 2.6%. One noticeable fault is the supply fan speed PID loop fault with P value equal to 0.01. There are more thermal unmet hours, and this fault leads to a higher peak power due to the triggering of the electric reheat.

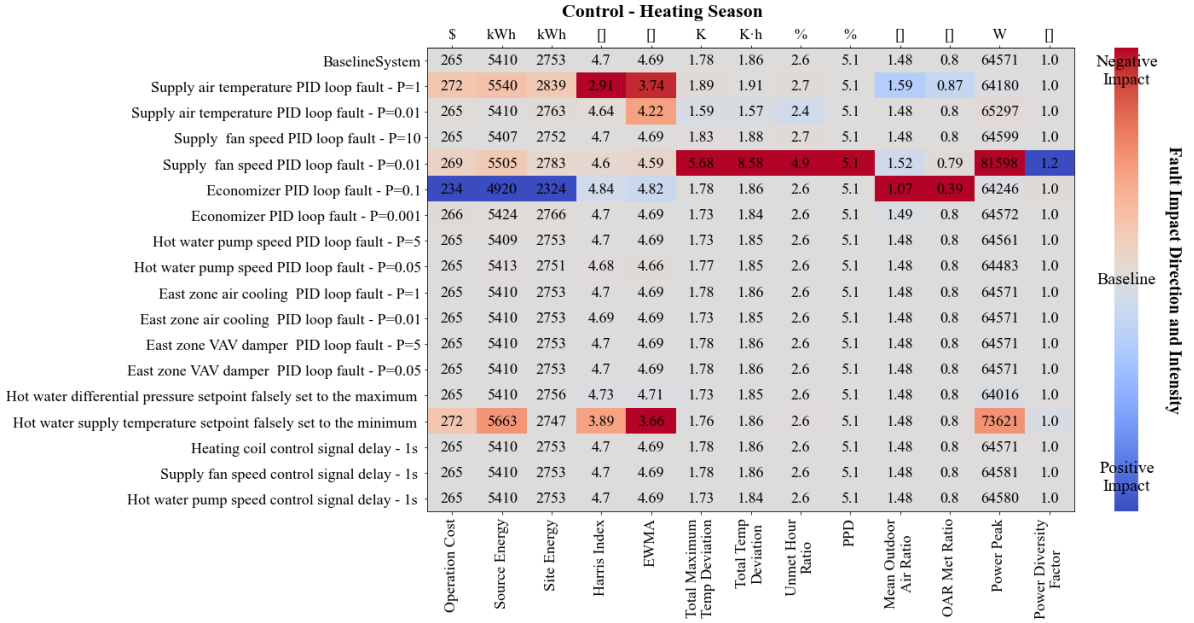

Figure B-5 Fault impact over key KPIs of control faults in the heating season